STUDY OF CHARACTERISTICS AND CATALYTIC ACTIVITIES OF Ga- AND Ag-MODIFIED ZEOLITES FOR TRANSFORMATION OF BIOMASS-DERIVED COMPOUNDS

ARTIT AUSAVASUKHI

A THESIS SUBMITTED IN PARTIAL FULFILLMENT
OF THE REQUIREMENT FOR THE DEGREE OF
DOCTOR OF PHILOSOPHY IN APPLIED CHEMISTRY
FACULTY OF SCIENCE
KING MONGKUT'S INSTITUTE OF TECHNOLOGY LADKRABANG
2009

KMITL-2009-SC-D-010-042

หัวข้อวิทยานิพนธ์	การศึกษาคุณลักษณะและความสามารถในการเร่งปฏิกิริยาของซีโอไลต์ที่ปรับปรุงด้วยโลหะแกลเลียมและเงินเพื่อใช้ในการเปลี่ยนสารอนุพันธ์ชีวมวล
นักศึกษา	นายอาทิตย์ อัศวสุขี
รหัสประจำตัว	47063503
ปริญญา	ปรัชญาดุษฎีบัณฑิต
สาขาวิชา	เคมีประยุกต์
พ.ศ.	2552
อาจารย์ผู้ควบคุมวิทยานิพนธ์	รศ.ดร. ตะวัน สุขน้อย

บทคัดย่อ

งานวิจัยนี้ทำการศึกษาการเปลี่ยนแปลงโลหะสปีชีส์ต่าง ๆ ของแกลเลียม และเงินในซีโอไลต์ในระหว่างการเร่งปฏิกิริยา และขั้นตอนการเตรียม ซึ่งส่งผลต่อสมบัติ และประสิทธิภาพในการเร่งปฏิกิริยา โลหะที่ได้รับการเติมแต่งในซีโอไลต์จะถูกประยุกต์ และออกแบบให้เหมาะสมสำหรับการใช้ในการเปลี่ยนสารอนุพันธ์ชีวมวลซึ่งเป็นทรัพยากรที่มีมากในประเทศไทยให้เป็นผลิตภัณฑ์ปิโตรเลียมที่มีค่าสูง โดยทำการศึกษาแบบจำลองการเร่งปฏิกิริยา (1) ดีไฮโดรจิเนชันของอีเทนเป็นเอททิลีน (2) อะโรมาไทเซชันของเอทานอลเป็นเบนซีน โทลูอีน เอทิลเบนซีน และไซลีน และ (3) การกำจัดออกซิเจนของเบนซัลดีไฮด์ และ*เมตา*-ครีซอลเป็นสารอะโรมาติกส์ที่ไม่มีออกซิเจน

ตัวเร่งปฏิกิริยาโลหะในซีโอไลต์ถูกเตรียมขึ้นโดยวิธีการแลกเปลี่ยนไอออน และการฝังตัวในซีโอไลต์ชนิด ZSM-5 และ Beta ตัวเร่งปฏิกิริยาที่เตรียมได้นี้จะนำมาทำการปรับสภาพด้วยไฮโดรเจน หรือไอน้ำ เพื่อตรวจสอบการเปลี่ยนแปลงสปีชีส์ของโลหะ จากนั้นจะนำตัวเร่งปฏิกิริยาก่อนและหลังการปรับสภาพมาทดสอบในเครื่องปฏิกรณ์แบบพัลส์ (Pulsed Reactor) และแบบเบดนิ่ง (Fixed bed Reactor) เพื่อศึกษาประสิทธิภาพในการเร่งปฏิกิริยาที่สภาวะเริ่มต้น และสภาวะคงที่ตามลำดับ

ในกรณีของ AgHZSM-5 พบว่าอัตราส่วนของซิลิกอนต่ออลูมิเนียมของซีโอไลต์มีผลต่อความสามารถในการรีดักชันและการเกิดขึ้นของสปีชีส์เงิน เมื่อทำการรีดักชันด้วยไฮโดรเจนที่อุณหภูมิ 425 องศาเซลเซียส พบว่าคลัสเตอร์ของโลหะเงิน จะเกิดขึ้นกับตัวเร่งปฏิกิริยา AgHZSM-5(11) ที่มีซิลิกอนต่ำ สำหรับตัวเร่งปฏิกิริยา AgHZSM-5(28) ที่มีซิลิกอนสูง จะพบแคตไอออนิคคลัสเตอร์ของเงินเป็นส่วนใหญ่ และมีคลัสเตอร์ของโลหะเงินเป็นส่วนน้อย ในบรรยากาศของแก๊สเฉื่อย แคตไอออนิคคลัสเตอร์ของเงินสามารถเกิดปฏิกิริยาย้อนกลับได้ที่อุณหภูมิต่ำกว่า 425

องศาเซลเซียส ให้เงินไอออน ปฏิกิริยาย้อนกลับที่เกิดขึ้นนี้จะส่งผลถึงประสิทธิภาพในการเร่งปฏิกิริยาของ AgHZSM-5 เพื่อให้เกิดผลิตภัณฑ์เป็นอะโรมาติกส์ในกรณีที่มีและไม่มีไฮโดรเจน

ในกรณีของ [Ga]HZSM-5 พบว่าการเกิดสปีชีส์ที่แตกต่างกันถูกกำหนดโดยอุณหภูมิ การปรับสภาพด้วยไอน้ำและไฮโดรเจน การเติมแต่งแกลเลียมใน HZSM-5 ทำให้เกิดสปีชีส์ GaO^+ ซึ่งสามารถเกิดการดูดซับทางเคมีกับน้ำเกิดเป็น GaO(OH) ซึ่งสามารถทำปฏิกิริยากับโครงผลึกซีโอไลต์ที่ไม่สมบูรณ์เกิดตำแหน่งกรดของแกลเลียมในซีโอไลต์ ตำแหน่งกรดนี้เกิดขึ้นได้ที่อุณหภูมิต่ำกว่า 425 องศาเซลเซียส และสามารถทำให้เกิดปฏิกิริยาโอลิโกเมอไรเซชันของเอททิลีน ปฏิกิริยารีฟอร์มมิงของสารไฮโดรคาร์บอนที่มีน้ำหนักโมเลกุลสูง และปฏิกิริยาการดีคาร์บอนิเลชันของเบนซัลดีไฮด์ เช่นเดียวกับในกรณีของการเร่งปฏิกิริยาด้วยตำแหน่งกรด เมื่อเพิ่มความร้อน GaO(OH) สามารถทำปฏิกิริยาดีไฮดรอกซิเลชันให้ GaO^+ กลับคืนมา ที่อุณหภูมิ 300 องศาเซลเซียส ในสภาวะที่ไม่มีน้ำ หรือเกิดปฏิกิริยาดีไฮเดรชันเป็น Ga_2O_3 ที่อุณหภูมิสูงกว่า 450 องศาเซลเซียส ภายใต้สภาวะนี้ตัวเร่งปฏิกิริยาสามารถเร่งปฏิกิริยาอะโรมาไทเซชันของโอเลฟินส์ขนาดเล็กได้ โดยเฉพาะอย่างยิ่งในสภาวะของการรีดักชันด้วยไฮโดรเจนที่อุณหภูมิ 550 องศาเซลเซียส สปีชีส์ที่เกิดจากการรีดักชันเป็น Ga^+ และ GaH_2^+ สามารถเร่งปฏิกิริยาดีไฮโดรจิเนชันของอีเทน ไฮโดรจิเนชัน และไฮโดรจิโนไลซีสของเบนซัลดีไฮด์ และ*เมตา*-ครีซอลที่อุณหภูมิสูงได้

Thesis Title	Study of Characteristics and Catalytic Activities of Ga- and Ag-Modified Zeolites for Transformation of Biomass-Derived Compounds
Student	Mr. Artit Ausavasukhi
Student ID	47063503
Degree	Doctor of Philosophy (Ph. D.)
Program	Applied Chemistry
Year	2009
Thesis Advisor	Assoc. Prof. Dr. Tawan Sooknoi

ABSTRACT

This thesis has studied the alteration of various metal species of Ga- and Ag-incorporated zeolite during the reaction and preparation which can readily influence with their catalytic activity and selectivity. Metal-incorporated zeolite should be applied and designed for converting biomass-derived compounds which is a rich hydrocarbon resource of Thailand to more valuable petrochemical products. The model reactions, (i) ethane dehydrogenation to ethylene, (ii) aromatization of ethanol to benzene, toluene, ethylbenzene, and xylene, and (iii) deoxygenation of benzaldehyde and *m*-cresol to oxygen-free aromatics are focused on this study.

The metal-incorporated zeolites are prepared by ion-exchange and impregnation method over ZSM-5 and Beta zeolites. These modified zeolites are treated with hydrogen or steam in order to investigate the alteration of metal species. Catalytic testing over the fresh and treated metal-modified zeolites are performed using pulsed and continuous fixed bed reactors in order to investigate activity at initial and steady state, respectively.

In AgHZSM-5, the Si/Al ratio of the host zeolite strongly influences the reducibility of the Ag species and the types of the reduced Ag species formed. Upon reduction with H_2 at 425 °C, metallic Ag clusters (Ag^0) are readily formed in a low silica sample, AgHZSM-5(11). For a higher silica sample, AgHZSM-5(28), most of the reduced Ag species, formed at 425 °C, are cationic Ag clusters (Ag_m^{n+}) with small amounts of the metallic ones. Under inert atmosphere, the cationic Ag clusters can readily undergo reversible interconversion at relatively low temperature (< 425 °C) and give back charge-balancing Ag cations (Ag^+). This phenomenon is suggested to play a decisive role in the catalytic activity of AgHZSM-5 towards BTX formation in the presence / absence of hydrogen.

In [Ga]HZSM-5, the formation of different Ga species is regulated by the temperature, the presence of water and H_2. Incorporation of Ga species into HZSM-5 leads to the formation of active GaO^+ which readily reacts with the chemisorbed water to form GaO(OH). The dispersed GaO(OH) can further react with the defect framework of zeolite, forming additional Brønsted acid sites associated with Ga in the framework (≡GaOHSi≡). The additional acid site could be obtained only at lower temperature (< 425 °C). Such acid sites can promote ethylene oligomerization, reforming of higher hydrocarbons, and benzaldehyde decarbonylation in a manner similar to that exhibited by conventional Brønsted acid sites. Upon heating, GaO(OH) can be dehydroxylated back to GaO^+ (~300 °C) in the absence of water or dehydrated to form Ga_2O_3 at high temperature (> 450 °C). Under such reaction condition, the activity for small olefin aromatization can be recovered. Particularly, in the H_2 reduction at 550 °C, the reduced Ga species, Ga^+, GaH_2^+ are readily formed. Such reduced Ga species would facilitate the ethane dehydrogenation, benzaldehyde and *m*-cresol hydrogenation and hydrogenolysis activity at high temperature.

ACKNOWLEDGEMENTS

The author wishes to express his sincere thanks to his advisor, Assoc. Prof. Dr. Tawan Sooknoi for his supervisions, helpful suggestions, caring, understanding and encouragements throughout this research.

Also, he wishes to thank Prof. Dr. Daniel E. Resasco for his stimulating suggestions and encouragement in research in the United States.

He is also grateful to Asst. Prof. Dr. Vanchat Chuenchom, Assoc. Prof. Dr. Sakda Trisak, Assoc. Prof. Dr. Thirasak Rirksomboon and Asst. Prof. Dr. Piboon Pantu for serving as the chairperson and the committee, and valuable comments.

He wishes to thank Prof. Dr. Jumras Limtrakul and Asst. Prof. Dr. Piboon Pantu for their suggestions and help in temperature-programmed hydrogen evolution, Dr. Wantana Klysubun for her help in X-ray absorption spectroscopy, and Dr. Chanchana Thanachayanont for her help in transmission electron microscope.

He would like to extend his sincere appreciation to all of his teachers, and his friends for their constant guidance advice, support and encouragement.

Sincere thanks are due to Rayong Olefins Co., Ltd. and Thailand Research Funds (TRF) through the Royal Golden Jubilee Ph.D. Program (Grant No. PHD/0213/2548) for financial support. He acknowledges the Department of Chemistry, Faculty of Science, King Mongkut's Institute of Technology Ladkrabang and School of Chemical, Biological and Materials Engineering, University of Oklahoma for the equipment, chemicals and facilities.

He deeply appreciates and thanks his parents and his family for their constant supports and encouragements.

Finally, the author dedicates this thesis to His Majesty the King for Royal Opinion to make him think about the good of the community.

Artit Ausavasukhi

CONTENTS

	Page
Thai Abstract	I
English Abstract	III
Acknowledgements	V
Contents	VI
List of tables	X
List of figures	XI
Chapter 1 Introduction	1
1.1 Statement and significance of the problems	1
1.2 Goal and objectives	5
1.3 Scope of the study	5
1.4 Expected results	6
References	7
Chapter 2 Zeolite Catalysts	8
2.1 Zeolite	8
2.1.1 Zeolite composition and structure	8
2.1.2 Zeolite catalysis	9
2.1.3 ZSM-5 zeolite	9
2.1.4 Beta zeolite	12
2.1.5 Shape selectivity of zeolites	13
2.1.6 Modification technique for metal-loading zeolite catalyst	14
2.1.7 Metal-modified zeolite	15
2.2 Hydrocarbon resource for Thailand	16
2.2.1 Natural gas	17
2.2.2 Biomass	18
References	20

CONTENTS (continued)

Chapter 3 Experimental Details..... 22

3.1 Reagents..... 22

3.2 Apparatus..... 23

3.3 Process of study..... 24

3.3.1 Modification of zeolites..... 24

3.3.2 Characterization of modified zeolites..... 24

3.3.3 Catalytic testing..... 25

3.3.4 Analysis of products..... 25

3.4 Modification of zeolites..... 25

3.4.1 Preparation of gallium-impregnated zeolite..... 25

3.4.2 Preparation of silver ion-exchanged zeolite..... 26

3.5 Characterization of catalysts..... 26

3.5.1 Inductively coupled plasma/Atomic emission spectroscopy.. 26

3.5.2 X-ray fluorescence..... 26

3.5.3 Scanning electron microscopy..... 26

3.5.4 X-ray diffraction..... 27

3.5.5 Gas adsorption analysis..... 27

3.5.6 Solid state magic angle spinning nuclear magnetic resonance..... 27

3.5.7 Fourier transform infrared spectroscopy..... 28

3.5.8 Ammonia-temperature-programmed desorption..... 28

3.5.9 *i*-propylamine-temperature-programmed desorption..... 28

3.5.10 Diffused reflectance ultraviolet spectroscopy..... 29

3.5.11 X-ray absorption near edge structure..... 29

3.5.12 Temperature-programmed reduction..... 29

3.5.13 Temperature-programmed hydrogen evolution..... 30

3.5.14 Transmission electron microscopy..... 30

3.5.15 Isotopic exchange of hydrogen/deuterium..... 30

3.5.16 Adsorbed reactant temperature-programmed desorption..... 30

CONTENTS (continued)

3.6 Catalytic testing..... 31

3.7 Analysis product..... 33

References..... 34

Chapter 4 Ag Species in AgHZSM-5 and Their Reversible Interconversion Behavior..... 36

4.1. Introduction..... 36

4.2. Experimental details..... 37

4.3. Results and discussion..... 39

4.4. Conclusions..... 59

References..... 61

Chapter 5 Additional Brønsted Acid Sites in [Ga]HZSM-5 Formed by the Presence of Water..... 67

5.1. Introduction..... 67

5.2. Experimental details..... 68

5.3. Results and discussion..... 69

5.4. Conclusions..... 81

References..... 82

Chapter 6 Tunable Ga Species in [Ga]HZSM-5 by H_2 Treatment: A Pulsed Study on Ethane Dehydrogenation..... 86

6.1. Introduction..... 86

6.2. Experimental details..... 88

6.3. Results and discussion..... 89

6.4. Conclusions..... 103

References..... 105

CONTENTS (continued)

Chapter 7 Catalytic Deoxygenation of Benzaldehyde and *m*-Cresol over Ga Modified Zeolite..... 108

7.1. Introduction..... 108

Part I: Catalytic deoxygenation of benzaldehyde over Ga-modified zeolite..... 109

7.2. Experimental details..... 109

7.3. Results and discussion..... 111

7.4. Conclusions..... 136

Part II: Catalytic deoxygenation of *m*-cresol over Ga-modified zeolite..... 137

7.5. Experimental details..... 137

7.6. Results and discussion..... 138

7.7. Conclusions..... 156

References..... 158

Chapter 8 Conclusions and Suggestions..... 164

8.1 Conclusions..... 164

8.2 Suggestions..... 167

Appendix A..... 168

Appendix B..... 173

Author biography..... 176

LIST OF TABLES

Table		Page
2.1	Composition of natural gas in Thailand.....	17
2.2	Gas chromatographic analysis of liquid fraction (wt%) in bio-pyrolysis oil (Bio-oil).....	19
4.1	Chemical composition and surface area of zeolite samples.....	39
4.2	Product distribution of ethanol conversion over modified ZSM-5 catalysts.....	55
5.1	Chemical composition and surface area of zeolite samples.....	68
5.2	Effect of water co-feeding over Ga-modified HZSM-5.....	78
5.3	Effect of temperature on ethanol conversion over [Ga]HZSM-5.....	80
6.1	Chemical composition and surface area of zeolite samples.....	89
6.2	% Conversion of ethane to ethylene over HZSM-5(28) and [Ga]HZSM-5(28).....	93
7.1	Chemical composition and surface area of catalyst samples.....	111
7.2	Summary of the temperature reduction and H_2 consumption.....	112
7.3	Acidity of various catalysts.....	115
7.4	Activity of H_2/D_2 exchange of various catalysts.....	119
7.5	Effect of Ga and type of carrier gas.....	122
7.6	The effect of support.....	132
7.7	Effect of water co-feeding.....	133
7.8	Chemical composition and surface area of catalyst samples.....	138
7.9	Effect of carrier gas.....	143
7.10	Effect of Ga content.....	145
7.11	Acidity of various catalysts.....	151
7.12	Activity of H_2/D_2 exchange of various catalysts	151
7.13	Effect of supporting material.....	153

LIST OF FIGURES

Figure		Page
2.1	Characteristic configuration (a) and its linkage within chains (b) in ZSM-5.....	10
2.2	Skeletal diagram of the [010]-plane of the ZSM-5 unit cell.....	10
2.3	Skeletal diagram of the [100]-plane of the ZSM-5 unit cell.....	11
2.4	Illustration of the channel structure in ZSM-5.....	11
2.5	Channel intersection viewed normal to [001]-plane of zeolite Beta.....	12
2.6	Skeletal diagram of the [100]-plane of the Beta unit cell.....	13
3.1	Flow diagrams of (a) pulsed reactor and (b) fixed bed flow reactor.....	32
4.1	XRD patterns of (a) HZSM-5(11), (b) 3AgHZSM-5(11), (c) red-3AgHZSM-5(11), (d) HZSM-5(28), (e) 3AgHZSM-5(28), and (f) red-3AgHZSM-5(28).....	40
4.2	^{1}H spin-echo MAS NMR spectra of (a) HZSM-5(11), (b) 3AgHZSM-5(11), (c) red-3AgHZSM-5(11), (d) HZSM-5(28), (e) 3AgHZSM-5(28), and (f) red-3AgHZSM-5(28).....	41
4.3	H_2-TPR profiles of 3AgHZSM-5(11) and 3AgHZSM-5(28).....	42
4.4	Primary and secondary H_2-TPR profiles of (a) 3AgHZSM-5(11) and (b) 3AgHZSM-5(28).....	44
4.5	TEM micrograph of (a) red-3AgHZSM-5(11) and (b) red-3AgHZSM-5(28).....	45
4.6	Primary and secondary H_2-TPR profiles of (a) 5AgHZSM-5(11) and (b) 5AgHZSM-5(28).....	46
4.7	TEM micrograph of (a) red-5AgHZSM-5(11) and (b) red-5AgHZSM-5(28).....	47
4.8	NH_3-TPD profiles of (a) comparison data of 3AgHZSM-5(11) and 3AgHZSM-5(28) catalysts. Gaussian deconvolution of the NH_3-TPD signal of (b) 3AgHZSM-5(11) and (c) 3AgHZSM-5(28).....	48
4.9	TPHE of 3AgHZSM-5(28).....	50
4.10	Primary (a) and secondary (b) H_2-TPR profiles of 3AgHZSM-5(28).....	51
4.11	DR-UV of (a) 3AgHZSM-5(11), (b) 3AgHZSM-5(28), (c) 1st-red-3AgHZSM-5(11), (d) 1st-red-3AgHZSM-5(28), (e) 2nd-red-3AgHZSM-5(11), and (f) 2nd-3AgHZSM-5(28).....	52

LIST OF FIGURES (continued)

Figure		Page
4.12	Ag L_3-edge XANES spectra of (a) 3AgHZSM-5(11), (b) 3AgHZSM-5(28), (c) red-3AgHZSM-5(11), (d) red-3AgHZSM-5(28), (e) $AgNO_3$, and (f) silver foil.....	53
4.13	*In situ* ^{13}C MAS NMR spectra of Ag-modified HZSM-5 zeolite (a) HZSM-5(11), (b) 3AgHZSM-5(11), (c) HZSM-5(28), and (d) 3AgHZSM-5(28).....	56
4.14	TPHE of 3AgHZSM-5(28) kept in H_2 stream after reduction.....	57
4.15	^1H spin-echo MAS NMR spectra of (a) 3AgHZSM-5(28),(b) 3AgHZSM-5(28) reduced at 350 °C for 2 hours, then cooled and kept under H_2, and (c) red-3AgHZSM-5(28).....	58
5.1	^1H MAS NMR spectra of (a) HZSM-5, (b) [Ga]HZSM-5, (c) st-[Ga]HZSM-5 treat at 270 °C and (d) HZSM-5, (e) [Ga]HZSM-5, and (f) st-[Ga]HZSM-5 treat at 360 °C.....	69
5.2	FTIR spectra of (a) st-[Ga]HZSM-5, (b) [Ga]HZSM-5, and (c) HZSM-5.....	70
5.3	NH_3-TPD profiles of (a) HZSM-5(28), (b) [Ga]HZSM-5(28), and (c) st-[Ga]HZSM-5(28).....	72
5.4	Thermograms of (a) HZSM-5, (b) [Ga]HZSM-5, and (c) st-[Ga]HZSM-5.....	74
5.5	TEM of (a) [Ga]HZSM-5 and (b) st-[Ga]HZSM-5.....	76
5.6	The TPR curves of b-[Ga]HZSM-5(28) and st-b-[Ga]HZSM-5(28) treated with steam at 425 °C.....	77
5.7	% Carbon yield of remaining ethylene and BTX from the reaction of 95 % ethanol, absolute ethanol, and ethylene using (a) HZSM-5(28) and (b) [Ga]HZSM-5(28) as a catalyst as a function of time on stream.....	79
6.1	The TPR profiles of (a) comparison data of [Ga]HZSM-5(28), (b) the primary H_2-TPR of [Ga]HZSM-5(28), (c) the secondary H_2-TPR of [Ga]HZSM-5(28), and (d) the tertiary H_2-TPR of [Ga]HZSM-5(28).....	91

LIST OF FIGURES (continued)

Figure		Page
6.2	NH_3-TPD profiles of (a) HZSM-5(28), (b) [Ga]HZSM-5(28), and (c) [Ga]HZSM-5(28) reduced with H_2 at 550 °C	92
6.3	Ethane pulsed reaction over [Ga]HZSM-5(28) catalyst with different reaction condition	95
6.4	Effect of Ga cluster and their treatment	97
6.5	The TPR profiles of (a) b-[Ga]HZSM-5(28) and (b) st-b-[Ga]HZSM-5(28) treated with steam at 425 °C	98
6.6	Effect of Si/Al ratio and treatment (a) treated with air at 550 °C, (b) treated with steam at 425 °C for 2 hours, and (c) treated with H_2 at 750 °C for 1 hour	100
6.7	The TPR profiles of (a) various [Ga]HZSM-5 different Si/Al ratio, (b) 3[Ga]HZSM-5(11), (c) 3[Ga]HZSM-5(28), and (d) 3[Ga]HZSM-5(165)	103
7.1	TPR profiles of (a) 1[Ga]HZSM-5, (b) 3[Ga]HZSM-5, (c) 6[Ga]HZSM-5, (d) 3[Ga]silica, and (e) comparison data of Ga supported catalyst	112
7.2	IPA-TPD of (a) HZSM-5, (b) red-1[Ga]HZSM-5, (c) red-3[Ga]HZSM-5, (d) 3[Ga]HZSM-5, and (e) st-3[Ga]HZSM-5	114
7.3	The effect of W/F	117
7.4	H_2/D_2 exchange over (a) HZSM-5 and (b) 3[Ga]HZSM-5 at 550 °C	119
7.5	Benzaldehyde-TPD of 3[Ga]HZSM-5 treated with H_2 and run TPD under H_2	121
7.6	Benzaldehyde-TPD of 3[Ga]HZSM-5 treated with H_2 and run TPD under He	121
7.7	The effect of Ga content	123
7.8	Benzaldehyde-TPD of 3[Ga]HZSM-5 treated with He and run TPD under He	125
7.9	The effect of pre-treatment	126
7.10	Plot of rate of benzene formation versus number of acid sites	127
7.11	The effect of temperature with selectivity of product over (a) HZSM-5 and (b) 3[Ga]HZSM-5	128

LIST OF FIGURES (continued)

Figure		Page
7.12	Benzaldehyde-pulsed reaction over 3[Ga]HZSM-5 under H_2 at (a) 450 °C, (b) 500 °C, and (c) 550 °C	130
7.13	Benzaldehyde-pulsed reaction over reduced 3[Ga]HZSM-5 under He at (a) 450 °C, (b) 500 °C, and (c) 550 °C	131
7.14	The effect of water co-feeding (a) without water and (b) with and without water	135
7.15	Effect of W/F on *m*-cresol conversion over 3[Ga]HBeta	138
7.16	Effect of W/F on phenol conversion over 3[Ga]HBeta	141
7.17	TPD of 3[Ga]HBeta after *m*-cresol conversion at 400 °C	142
7.18	Effect of carrier gas	144
7.19	TPR profiles of (a) 1[Ga]HBeta, (b) 3[Ga]HBeta, (c) 6[Ga]HBeta, (d) 3[Ga]HZSM-5, (e) 3[Ga]Silica, and (f) comparison data of Ga supported catalyst	148
7.20	IPA-TPD of (a) HBeta, (b) red-1[Ga]HBeta, (c) red-3[Ga]HBeta, and (d) 6[Ga]HBeta	150
7.21	Effect of temperature	152
7.22	Conversion of *m*-cresol over 3[Ga]HZSM-5	155

Chapter 1

Introduction

Zeolites are extensively used as catalysts for various industrial applications, due mainly to their selectivity and tunability. Especially, the catalysis by heteroatom-substituted zeolites have been received increasing interest recently [1-10]. The incorporated metals within zeolite micropores make them possible for the catalysts designed for Thailand development. This is in particular for converting biomass-derived compounds, natural gas and pyrolyzed biomass, which are a rich hydrocarbon resource of Thailand to more valuable petrochemical products. As most of our petrochemicals and energy needs today are met by crude oils, it is better if all the requirements of chemical industries and portions of other needs can be shared by natural gas and biomass. This can be achieved by using such metal-modified zeolite catalysts for the conversion of light hydrocarbons contained in natural gas and the conversion of oxygenates contained in pyrolyzed biomass to more valuable products, such as ethylene, propylene, and aromatics. These transformations require both dehydrogenation, hydrogenation, and hydrogenolysis activity from metal phase and acidic function for oligomerization, isomerization, cracking, and decarbonylation from zeolite [11].

Silver- and gallium-incorporated into a zeolite by ion-exchange or impregnation has been found to be an efficient catalyst for these catalytic processes [12]. It is known that in metal-modified zeolite catalyst, zeolite can serve as a supporting material with tunable pore size, acidity and site proximity. Therefore, the exchangeable cation or metal nanoparticles within micropore of zeolite is controlled by the framework charge and pore size which also regulate type of metal species. All these features provide an opportunity to potentially design catalysts at a molecular level with specificity and activity for catalytic system.

1.1 Statement and significance of the problems

Although the catalytic role of metal species within micropore of zeolite has been studied for over 20 years, the understanding of the altering of metal species during the reaction and also preparation are rather limited. It has been shown that different catalytic activities and the reaction pathway, and hence product selectivity are pronounced when different metal species (metal cation, cationic cluster, metallic cluster or oxide formed) are introduced. The micropore of zeolite

can exert a strong, localized electrostatic field that can alter the chemistry of the cations in the exchangeble site and the impregnated metal nanoparticles. Thus, the incorporated metal or metal oxide are not necessarily the same as cations adsorbed, precipitated or exchanged into other microporous solids.

This thesis has studied the alteration of various metal species of Ag- and Ga-incorporated zeolite during the preparation and reaction which can readily influence on their catalytic activity and selectivity. The modification by addition of these metal species has focused on improving the dehydrogenation, hydrogenation and hydrogenolysis activity of this catalyst. Metal-incorporated zeolite can be applied for converting biomass-derived compounds, natural gas and pyrolyzed biomass, to more valuable fuels and petrochemical products. The model reactions namely, (i) ethane dehydrogenation to ethylene, (ii) aromatization of ethanol to benzene, toluene, xylene and ethylbenze, and (iii) deoxygenation of benzaldehyde and *m*-cresol to oxygen-free aromatics are focused on this study.

The Ag- and Ga-incorporated zeolites are prepared by ion-exchange and impregnation methods over HZSM-5 and HBeta zeolites. These modified zeolites are treated with hydrogen or steam at various temperatures in order to investigate the alteration of metal species. Conventional techniques, such as X-ray fluorescence spectroscopy (XRF), inductively coupled plasma/atomic emission spectroscopy (ICP/AES), scanning electron microscopy (SEM), X-ray diffraction (XRD) and gas adsorption analysis are employed to determine the physical properties of the modified zeolite. Advanced techniques, such as ^{1}H and ^{13}C nuclear magnetic resonance (NMR), Fourier transform infrared spectroscopy (FTIR), temperature-programmed desorption of ammonia (NH_3-TPD), temperature-programmed desorption of *i*-propylamine (IPA-TPD), diffused reflectance ultraviolet spectroscopy (DR-UV), X-ray absorption near edge structure (XANES), temperature-programmed reduction (TPR), temperature-programmed hydrogen evolution (TPHE), transmission electron microscopy (TEM), and isotopic exchange of hydrogen/deuterium (H_2/D_2 exchange) are employed to determine the alteration of metal species and determine the nature of the acid and metal sites. In addition, catalytic testing over the fresh and treated metal-modified zeolites are performed using pulsed and continuous fixed bed reactors in order to investigate the activity at initial and steady state, respectively.

In **chapter 4**, the "reversible interconversion", which can be observed over zeolites modified by silver are mentioned. It was suggested that the Ag species formed will depend largely on the reducibility of the hydrocarbon species in the reaction stream. Consequently, the alteration of Ag species during the reaction may largely affect the catalyst activity and stability. The metallic or ionic clusters of Ag metal, formed by the reduction of charge-balancing cations, are usually stable and well-dispersed. However, in some cases, the reduced metals can reversibly react with the neighboring Brønsted acid sites, liberating H_2 and give back charge-balancing metal cations. If the reversible interconversion can readily take place at the reaction temperature (> 300 °C), one could not expect only a single form of Ag species are responsible for the activity. In addition, the Si/Al ratio of the zeolites would play a marked role in hosting, retaining and even altering the incorporated Ag species. Therefore, in this chapter, we provide further evidence for the influence of the zeolite Si/Al ratio on the reducibility and reversible interconversion of the incorporated Ag species. ^{1}H MAS NMR, together with temperature-programmed reduction (TPR) and temperature-programmed hydrogen evolution (TPHE) techniques, are mainly employed for determining the behavior of Ag species hosted by zeolites with different Si/Al ratios. Diffused reflectance ultraviolet spectroscopy (DR-UV) and X-ray absorption near edge structure (XANES) are employed to determine the nature of metal species. The suggestion that the incorporated Ag species can readily influence their catalytic behavior towards BTX is tested by ethanol and ethylene conversion. The effect of H_2, a readily reducing species, on the activity of AgZSM-5 will also be highlighted.

In Ga-incorporated zeolite, the formation of different Ga species is regulated by the temperature and treatment with steam or H_2. Despite the fact that the type of Ga species have been studied for many years, doubts still persist on its catalytic activity, mainly related to the nature of the active sites. In other words, the question is that which gallium species is responsible for the observed catalytic activity. This work is part of a project that aims to elucidate this question.

An increase in aromatic yield can be obtained for the conversion of methanol over GaHZSM-5 despite large amount of water is present, as co-product, in the reaction stream. This marked behaviour of Ga-containing zeolites leads to the question for the effect of water on the incorporated Ga species and their catalytic activity. In **chapter 5**, it was suggested the change in acid sites when water (that is present in the feed) interacts with the Ga species in [Ga]HZSM-5.

^{1}H MAS NMR, together with Fourier transform infrared spectroscopy (FTIR), temperature-programmed reduction (TPR) and thermogravimetric/differential thermogravimetric (TGA/DTG) techniques, are mainly employed to determine such phenomena over the acid sites. The effect of steam treatment of [Ga]HZSM-5 on its acidity/acid strength and the reducing ability of Ga species is also investigated. These additional acid sites may well affect the aromatization activity of this catalyst in the presence of water. Hence, aromatization of ethanol and ethylene will be compared and the effect of water on the reaction over [Ga]HZSM-5 will be discussed.

Various gallium species (Ga_2O_3, GaO^+, Ga^+, and GaH_2^+) in [Ga]ZSM-5 are believed to be active sites for alkane dehydrogenation. In **chapter 6**, the possible type of Ga species, which is formed *in situ*, under the effects of the different pre-treatments was investigated using pulsed reaction and temperature-programmed reduction. The oxide Ga species, Ga_2O_3 and GaO^+, obtained after pre-treatment with air was preliminary tested using ethane as a model feed. Subsequently, such oxide species were reduced by H_2 to form Ga^+ and GaH_2^+. The ethane dehydrogenation was repeated to obtain the catalytic activity of the reduced Ga species. However, it is reported that the Ga^+ species are the most stable species at high reaction temperature. While GaH_2^+ cannot be stabilized in the high reaction temperature without H_2. To obtain the catalytic activity of GaH_2^+, therefore, the ethane dehydrogenation was performed using H_2 as a carrier gas. It is suggested that GaH_2^+ species are predominant in [Ga]HZSM-5 under H_2 system. The obtained activity of various Ga species were compared. In addition, this chapter discusses the relative activity of the Ga species and its cluster size, together with acidity in HZSM-5 zeolite.

Ga based catalyst is also proposed for the deoxygenation of bio-oils to produce oxygen-free products. Reduced Ga cationic species are expected to be active for hydrogenation/ hydrogenolysis. In **chapter 7**, the deoxygenation reactions on supported gallium HZSM-5 and HBeta zeolites catalysts using benzaldehyde, and *m*-cresol as model feeds were studied. It is suggested that the catalytic activity and product selectivity are strongly influenced by the types and amounts of active sites. Hence, the catalytic testing was investigated over acid zeolites modified by various Ga content. In addition, the treatment condition would play a marked role for the alteration of Ga species. The effect of H_2 (providing reducing Ga species) and effect of steam (providing the change in acid sites) on the activity of Ga-modified zeolites will be discussed. Moreover, the variation of W/F and temperature-programmed techniques are performed to elucidate the possible reaction pathway for deoxygenation of benzaldehyde and *m*-cresol.

1.2 Goal and objectives

The specific objectives of the study are as follows:

1.2.1 To understand the characteristics of metal species and their catalytic activities and selectivity.

1.2.2 To understand the effect of metal and zeolite determined type of metal species for the change in dehydrogenation, hydrogenation, hydrogenolysis and aromatization activities and selectivity.

1.3 Scope of the study

1.3.1 Modification of ZSM-5 and Beta zeolite with gallium and silver.

1.3.1.1 Modify the silver-incorporated ZSM-5 by ion exchange method.

1.3.1.2 Modify the gallium-incorporated ZSM-5 and Beta by impregnation method.

1.3.2 Characterization of metal-modified ZSM-5 and Beta zeolites.

1.3.2.1 Investigate the physical properties of fresh metal-modified zeolite using conventional techniques, such as X-ray powder diffraction (XRD), scanning electron microscopy (SEM), X-ray fluorescence (XRF), inductively coupled plasma-atomic emission spectroscopy (ICP-AES), gas adsorption analyzer, transmission electron microscopy (TEM), ^{1}H and ^{13}C nuclear magnetic resonance (NMR) and Fourier transform infrared spectroscopy (FT-IR).

1.3.2.2 Investigate the change of active species over metal-modified zeolite under *in situ* treatment (hydrogen or steam) and after treatment or reaction using temperature-programmed reduction (TPR), temperature-programmed hydrogen evolution (TPHE), diffused reflectance ultraviolet spectroscopy (DR-UV), transmission electron microscopy (TEM), and X-ray absorption near edge spectroscopy (XANES).

1.3.3 Catalytic testing of modified ZSM-5 and Beta zeolites

1.3.3.1 Investigate their catalytic activity and selectivity of modified zeolite towards dehydrogenation of ethane to ethylene at initial, and after treatment with a pulsed reactor.

1.3.3.2 Investigate their catalytic activity and deactivation of modified zeolite towards aromatization of ethanol, deoxygenation of benzaldehyde and deoxygenation of *m*-cresol to light aromatic with a continuous fixed bed reactor.

1.4 Expected results

- 1.4.1 This research would lead to understanding in the activity of various metal species, namely gallium- and silver-incorporated with ZSM-5 and Beta for light hydrocarbon and oxygenates conversion.

1.4.2 This research would provide not only a potential to develop a technology for producing ethylene, propylene, and aromatics from light hydrocarbon and oxygenates, but also a guide for converting natural resource of Thailand to high value product.

References

[1] Weitkamp J., Puppe L. Editors. **Catalysis and Zeolites: Fundamentals and Applications.** Berlin : Springer-Verlag. 1999.

[2] Jansen J.C., Stocker M., Karge H.G. and Weitkamp J. Editors. **Advanced Zeolite Science and Applications.** Amsterdam : Elsevier Science. 1994.Bekkum H.V., Flanigen E.M., Jacobs P.A., Jansen J.C. Editors. **Introduction to Zeolite Science and Practice.** 3rd Ed. Amsterdam : Elsevier Science. 2001.

[3] Scott M.A., Kathleen A.C. and Prabir K.D. Editors. **Handbook of Zeolite Science and Technology**. New York : Marcel Dekker. 2003.

[4] Bekkum H.V., Flanigen E.M., Jacobs P.A. and Jansen J.C. Editors. **Introduction to Zeolite Science and Practice.** 3rd Ed. Amsterdam : Elsevier Science. 2001.

[5] Bruce C.G. **Catalytic Chemistry**. New York : John Wiley & Sons. 1992.

[6] Ian M.C. **Biomass, Catalysis and Liquid Fuels**. Pennsylvania : Technomic. 1983.

[7] Chen N.Y., Willium E.G. and Francis G.D. **Shape Selective Catalysis in Industrial Applications**. 2nd Ed. New York : Marcel Dekker. 1996.

[8] Subhash B. **Zeolite Catalysis: Principles and Applications.** Florida : CRC Press. 1990.

[9] Hegedus L.L. Editor. **Catalyst Design Progress and Perspectives.** New York : John Wiley & Sons. 1987.

[10] Jacobs P.A. Editor. **Zeolite Chemistry and Catalysis.** Amsterdam : Elsevier Science. 1991.

[11] Robert A.M. Editor. **Handbook of Petroleum Refining Processes.** 2nd Ed. New York : McGraw-Hill. 1997.

[12] Ausavasukhi A. **"The Production of Gasoline and Aromatics from Ethanol"** Master degree of science, Petrochemical and hydrocarbon chemistry, Faculty of Science, King Mongkut's Institute of Technology Ladkrabang. 2002.

Chapter 2

Zeolite Catalysts

Zeolites are crystalline aluminosilicates demonstrating unique properties due to the presence of shape selectivity. Moreover, zeolite frameworks are made of silicate and aluminate tetrahedral connected by corners. The negatively charged aluminium sites are neutralized by the charge balancing cations, such as sodium ion, proton. Duè to their shape selectivity and Brønsted acid sites, zeolites are used in many industrial processes such as xylene isomerization, toluene disproportionation, benzene and toluene ethylation, and methanol to gasoline conversion. Moreover, zeolites can be modified for dramatic activity by way of their cation-exchange capability. It is known that the charge balancing cations and incorporated metal cluster play an important role in controlling the catalytic activity of zeolites. Cations or metal clusters are located within specific sites in each zeolite topologies. Thus, in each type of zeolite with different silicon/aluminium ratio, differences in coordination around the cations or metal could be modified its own unique catalytic activity. All these features provide an opportunity to design a catalyst at a molecular level with high specificity and activity.

In recent years, development of renewable sources of energy and petrochemicals have been given to the conversion of biomass-derived compounds. Natural gas and biomass offer a potential to replace the reducing reserves of non-renewable fossil fuels. Moreover, natural gas and biomass provide significant promises as alternative power sources to increase energy efficiency, reduce pollution, and minimize our dependence on imported oil.

In this chapter, background knowledge of zeolite, natural gas, biomass, the influence of various metal species formation and role of such incorporated metal for dehydrogenation, hydrogenation, and hydrogenolysis of light hydrocarbon and oxygenates over metal-modified zeolite catalyst are reviewed.

2.1 Zeolite

2.1.1 Zeolite composition and structure

Zeolites can be described as a rigid three-dimensional network of silicate (SiO_4) and aluminate (AlO_4^-) in which the tetrahedra cross-linked by the sharing of oxygen atoms [1-3]. The electrovalence of the tetrahedral-containing aluminium is balanced by the positive charge of

cations such as an alkaline metal or an alkaline earth. One type of cation has been exchanged either in entirely or partially by another type of cation utilizing ion-exchange techniques in a conventional manner.

The silica and alumina tetrahedra are combined into more complicated secondary units, which form the building blocks of the framework zeolite crystal structures. The silica and alumina tetrahedral are geometrically arranged so that the zeolites possess an open framework structure, which defines a pore structure with a high surface area.

The properties of a zeolite are dependent on the topology of its framework, the size, shape, and accessibility of its free channels, the location charge and size of the cations within the framework, the presence of faults and occluded materials, the ordering of T-atoms, and the local environment of T-atoms. Such unique properties of zeolite make it especially interesting for heterogeneous catalysis.

2.1.2 Zeolite catalysis

Zeolite has been proved to be an efficient catalyst for many industrial processes [3-6]. In zeolites, catalysis takes place preferentially within the intracrystalline voids affected by aperture size and type of pore system, through which reactants and products must diffuse. Modification techniques including ion-exchange, introduction of acidic groups such as bridging ≡Si–OH–Al≡ (which impart Brønsted acidity), hydrothermal dealumination or stabilization (which produces Lewis acidity) and introduction of dispersed metal phases such as noble metals species, can be increase catalytic activity. The preferred zeolites of this thesis are selected from a class of zeolites which is generally highly effective in alkylation, isomerization, disproportionation and other reactions involving aromatic hydrocarbons and induced profound transformations of aliphatic hydrocarbons to aromatic hydrocarbons in commercially desirable yields.

2.1.3 ZSM-5 zeolite

Zeolite ZSM-5 [3-10] is a member of a new class of shape selective catalysts with unique channel structures. The framework of ZSM-5 contains a novel configuration of linked tetrahedra shown in Figure 2.1a, consisting of 8 and 5-membered rings. These secondary building units join through the edge to form chains as shown in Figure 2.1b.

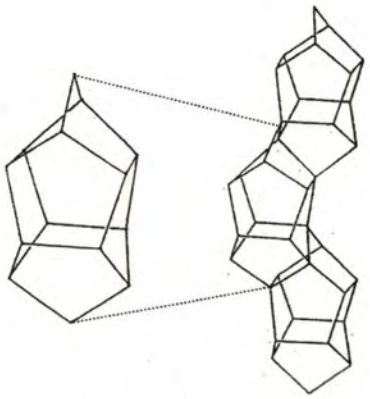

Figure 2.1 Characteristic configuration (a) and its linkage within chains (b) in ZSM-5.

The chains can be connected to form sheets and the linking of the sheets lead to a three dimensional framework structure. The chains extend along the *z*-axis. The sheets parallel to [010] and [100] are shown in Figure 2.2 and 2.3. Figure 2.2 shows that the *x*-axis is horizontal and the *z*-axis vertical and the 10-membered ring apertures shown are the entrances to the straight channels which run parallel to [010] plane. While, Figure 2.3 shows that the *y*-axis is horizontal and the *z*-axis vertical and the nearly circular 10-membered ring apertures shown are the entrances to the sinusoidal channels which run parallel to [100] plane.

The ZSM-5 framework can be generated by linking the sheets of Figure 2.2 across mirror planes forming four and 6-membered ring.

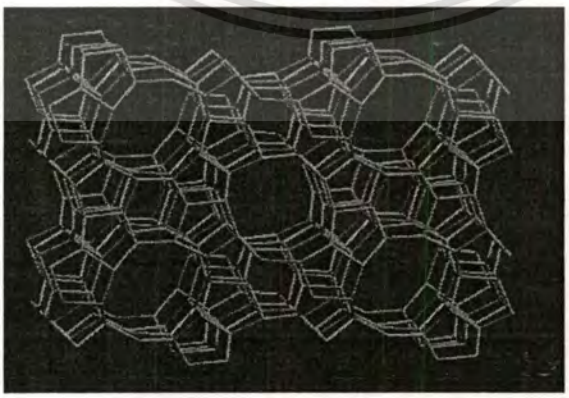

Figure 2.2 Skeletal diagram of the [010]-plane of the ZSM-5 unit cell.

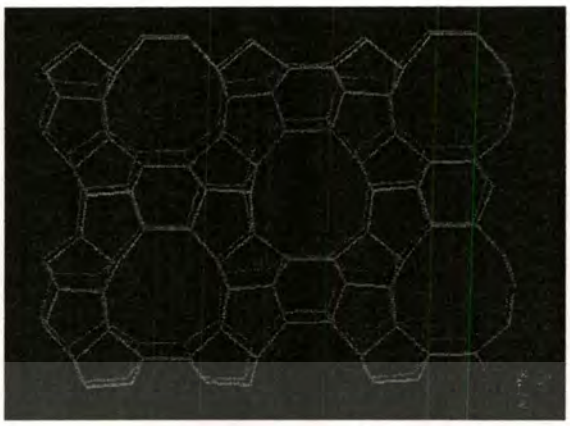

Figure 2.3 Skeletal diagram of the [100]-plane of the ZSM-5 unit cell.

ZSM-5 crystallizes in the idealized orthorhombic system with a space group Pnma and lattice constants; a = 20.1, b = 19.9, and c = 13.4 angstroms; monoclinic symmetry has also been observed. The unit cell composition of the sodium form are $Na_nAl_nSi_{96-n}O_{192}$ ~16 H_2O, where n is less than 27 and typically about 3.

The ZSM-5 framework contains two types of intersecting channels: one type is straight, has elliptical (0.51 to 0.58 nm) openings and runs parallel to the y-axis of the orthorhombic unit cell, while the other has near circular (0.54 to 0.56 nm) opening, is sinusoidal (zig-zag), and directed along the x-axis as illustrated in Figure 2.4.

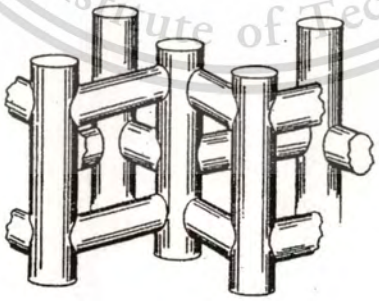

Figure 2.4 Illustration of the channel structure in ZSM-5.

ZSM-5 are used in many catalytic reactions of industrial interest such as xylene isomerization, toluene disproportionation, benzene and toluene ethylation, and methanol to gasoline conversion. Their individual catalytic properties are mainly due to their regular framework with a pore size which is intermediate to the large pore sized zeolites (for instance, zeolites X and Y) and the small pore sized zeolites (for instance, zeolite A).

2.1.4 Beta zeolite

Zeolite Beta [3-6] is an old zeolite discovered before Mobil began the "ZSM" naming sequence. The zeolite Beta has a 12-membered ring structure with intersected porous channels, wherein the pore diameter of the 12-membered ring is 0.57-0.75 nm for one-dimension porous channel parallel to the [001] crystal plane (Figure 2.5), while the pore diameter of the 12-membered ring is 0.56-0.65 nm for the two-dimension porous channel parallel to the [100] crystal plane (Figure 2.6).

Figure 2.5 Channel intersection viewed normal to [001]-plane of zeolite Beta.

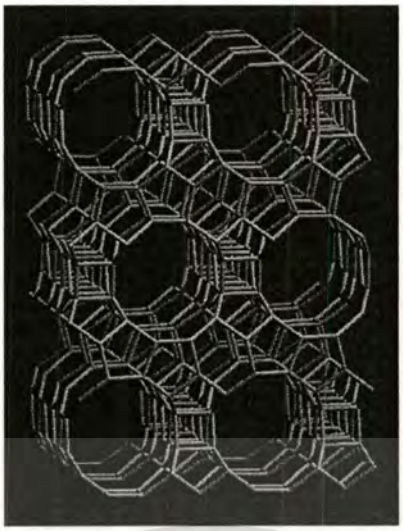

Figure 2.6 Skeletal diagram of the [100]-plane of the Beta unit cell.

Zeolite Beta was first synthesized by Wadlinger *et al.* (1967). Zeolite Beta represents the first high silica zeolite (Si/Al = 10-100) synthesized from a gel with alkali metal and organic template, tetraethylammonium cations. Zeolite Beta can be described by the general formula: $Na_nAl_nSi_{64-n}O_{128}$, where n = 7.

The zeolite Beta is a high silica zeolite with larger pores and a three-dimension structure that is only one discovered up to now, and has both acid catalytic property and structural selectivity due to its structural particularity, and further has very high thermostability (the failure temperature of the crystal lattice is higher than 1200 °C), hydrothermal stability and wear-resistant property. Due to the unique structural feature, the zeolite Beta has acid resistance, anti-coking property and show high catalytic activity for a series of reactions, and excellent performance in aspects of adsorption. Therefore it has broad prospects in applications and has been developed rapidly into a new-type of catalytic materials in recent years. After modified or supported with some metal components, the zeolite Beta can be widely used for petroleum refining and petrochemical processes such as hydrocracking, hydroisomerization, and hydration of olefins.

2.1.5 Shape selectivity of zeolites

The shape selectivity of the zeolites is the catalytic expression of many factors such as:

1. The sieving effect, i.e. the capability of the zeolite to admit into its pores or to reject reactive molecules having a critical diameter falling within a well defined range;

2. The (reverse) sieving effect, i.e. the capability of the zeolite to allow product molecules having a certain critical diameter to diffuse out of its pores. Thus, in the case of a product molecule having a diameter exceeding the pore size of the zeolite, this molecule will have to undergo additional cracking or rearrangement into a smaller molecule before diffusing out of the zeolite;
3. The effect on the reaction intermediates, i.e. the capability of certain active sites to determine the length and geometry of reaction intermediate species.

The unique catalytic properties of zeolite ZSM-5 and Beta are attributed to both the three-dimensional system of intersecting channels and its strong acid sites. ZSM-5 and Beta zeolites have pore system which is believed to be significant for their unusually low coke formation. These features make it sterically difficult for the formation of the large polynuclear hydrocarbons.

The acid sites in zeolites are mainly located at the zeolite channel intersections and originates in the Brønsted centers created by the tetrahedral aluminium sites. Moreover, Lewis acid sites are also formed by dehydroxylation of the zeolite surface by activating the zeolite at high temperature. Although acid zeolite possesses excellent acid properties such as, dehydration and oligomerization, it is a poor dehydrogenation catalyst for ethylene, propylene, and aromatics selectivity and hence the catalyst requires modification by the addition of various promoters.

While most industrial application of zeolite catalyst make use of these in acid form, zeolite are also excellent support for metals species. Zeolite supported metal species, a bifunctional zeolite catalyst, is an acid zeolite on which a metal species phase is deposited. The function of the metal is to catalyze dehydrogenation and hydrogenation reactions. The word "metal species" is used in the non-restrictive sense to describe species in its, not yet fully understood their valency. The advantage of bifunctional catalysis over the monofunctional acid catalysis is that the metal dehydrogenates the alkanes into alkenes which can further undergo a variety of acid catalyzed reactions to form desirable products.

2.1.6 Modification technique for metal-loading zeolite catalyst

Metal-containing zeolites can be used as catalysts for different purposes and under various conditions [1,2,5-8,11]. The various techniques which can be employed are ion-exchange,

impregnation, codeposition, adsorption from the gaseous phase, adsorption of metal vapor, comulling, and introduction of compounds during zeolite synthesis (crystallization). However, ion-exchange and impregnation are techniques commonly used in this thesis.

2.1.6.1 Ion-exchange

Zeolites possess tetrahedral-containing Al providing the electrovalence which is balanced by positive charge of cations. The ability of zeolites to cation-exchange therefore offers great opportunities for introducing the metal cation or proton into zeolite cavities for active site preparation. The exchangeable cation should result in uniform dispersion depending on the Al framework. Moreover, this metal cation containing zeolite is often used to prepare metal containing zeolite catalysts by reduction treatment. For example, by treating a zeolite containing Ag^{+} ions with hydrogen, metallic silver (Ag^{o}) or cationic cluster (Ag_n^{+}) can be formed [12,13]. This depends largely on the reduction condition, type of cation, type of zeolite, its Al content and the metal content. This preparation is usually designed to introduce the metal into the zeolite pore system. However, some metal is formed as a cluster on external surface of zeolite. This can also be achieved by impregnating the zeolite with metal particles or metal compounds.

2.1.6.2 Impregnation

Impregnation is a method of introduction the metal component to zeolites which possess the low or without exchangeable site, or hardly ion-exchange, or requires the larger metal content. In this method, the metal or metal oxide are present largely on external surface of the zeolite. Moreover, the appropriate treatment condition is required for obtaining well-dispersed catalyst, and also the size of cluster influencing the catalytic activity.

2.1.7 Metal-modified zeolite

The metal-incorporated zeolite, especially those with ZSM-5 and Beta zeolites have been received increasing interest [1,2,5-8]. It has been shown that different catalytic properties are presented when different metal atoms are introduced, for example, titanium-silicate is efficient for ammoximation of cyclohexane, whereas Fe-zeolite is a good catalyst for redox reaction. However, in this research the incorporated of gallium, and silver were found to be the efficient

catalyst for ethylene, propylene, and aromatic production from a light hydrocarbon and oxygenates.

2.1.7.1 Gallium-incorporated zeolite

The preferred catalyst for alkane aromatization is gallium-incorporated acid zeolite [14-17]. The incorporation of gallium can be achieved either by ion-exchange or impregnation. Moreover, it can be incorporated into the zeolite structure during the zeolite synthesis. The weight of gallium-incorporated is typically between 1 and 5%. In light alkane aromatization, activity is attributed to the presence of bifunctional sites of non-framework gallium species and zeolitic protons, located closely to each other in the zeolite channels. A commercial effective aromatization process called the Cyclar process employs this catalyst to transform liquefied petroleum gas (LPG) to aromatics.

2.1.7.2 Silver-incorporated zeolite

Silver-incorporated acid zeolite catalyst is also an active catalyst for light alkane aromatization and it sharply enhances the C-H bond cleavage of starting alkane. Thus, silver-incorporated HZSM-5 catalysts produce less methane and ethane than Ga- or Zn-acid zeolite which enhanced both C-H and C-C cleavage [15,18,19]. Moreover, it is interesting to use this metal for dehydrogenation of light hydrocarbon to produce light olefins.

2.2 Hydrocarbon resource for Thailand

Thailand has limited domestic oil production and reserves, and imports make up a significant portion of the country's oil consumption. It is better if all the requirements of chemical industry and portions of other needs can be shared by natural gas and biomass. Our country is rich in these resources and we have been designated to become an economic power. The production of fuel and petrochemicals from natural gas and biomass is one of the alternative ways of fostering the development of liquid energy and petrochemical for Thailand.

2.2.1 Natural gas

Natural gas is a naturally occurring mixture of light hydrocarbons accompanied by some non-hydrocarbon compounds [20-22]. The principal component of most natural gas is methane. Higher molecular weight paraffinic hydrocarbons (C2-C7) are usually present in smaller amounts with the natural gas mixture, and their ratios vary considerably from one gas field to another.

At the end of 1981, natural gas was first produced from Erawan gas field of Unocal Thailand Ltd., at the capacity of 130 MMCFD, marking the new era of energy resources in Thailand. During the initial stages of gas production, the natural gas produced was delivered, by pipeline, to power plants and cement plants for use as fuel in substitution for fuel oil. As natural gas discovered in Thailand (Table 2.1) is composed of various valuable hydrocarbon components which can be separated for use as feedstock in the petrochemical industry, efforts have been made by the government to optimize its value.

Table 2.1 Composition of natural gas in Thailand [23].

Composition	Erawan	Bongkoch	Yanada	Yaetagoon
CH_4	63.565	62.315	69.099	79.110
C_2H_6	8.285	7.318	0.915	7.360
C_3H_8	4.900	4.466	0.167	2.550
i-C_4H_{10}	1.225	1.002	0.018	0.550
n-C_4H_{10}	1.095	0.990	0.028	0.640
i-C_5H_{12}	0.370	0.333	0.008	0.240
n-C_5H_{12}	0.250	0.219	0.003	0.140
C_{6+}	0.455	0.340	0.020	0.150
CO_2	15.995	22.287	4.144	6.970
N_2	3.860	0.730	25.598	2.290

Compared to other types of fuel, natural gas is cheaper, cleaner, and of higher quality. Therefore, the level of natural gas consumption has been continually increasing each year. While concessionaires in gas exploration and production have been striving to search for new gas sources and to produce the most from existing sources; public and private sectors have continued

to search for new uses of natural gas - not only as fuel in power plants, industrial factories, and vehicles.

2.2.2 Biomass

Biomass, as a renewable energy source, refers to living and recently dead biological materials that can be used as fuel or for industrial production. In this context, biomass refers to plant matter grown to generate electricity or produce bio-fuel, and it also includes plant or animal matter used for production of fibers, chemicals or heat. Biomass may also include biodegradable wastes that can be burnt as fuel. It excludes organic material which has been transformed by geological processes into substances such as coal or petroleum. Although fossil fuels have their origin in ancient biomass, they are not considered biomass by the generally accepted definition because they contain carbon that has been "out" of the carbon cycle for a very long time. Their combustion therefore disturbs the carbon dioxide content in the atmosphere.

Biomass is part of the carbon cycle. Carbon from the atmosphere is converted into biological matter by photosynthesis. On death or combustion the carbon goes back into the atmosphere as carbon dioxide (CO_2). This happens over a relatively short timescale and plant matter used as a fuel can be constantly replaced by planting for new growth. Therefore a reasonably stable level of atmospheric carbon results from its use as a fuel. It is accepted that the amount of carbon stored in dry wood is approximately 50 % by weight.

A wide variety of technologies are available to produce energy from biomass. Biomass is the only renewable resource that can be directly converted into liquid fuel, thus providing a competitively priced fuel for transport, heat and power production. Fast pyrolysis of biomass for liquids production is of particular interest, as it is the only thermal process that directly produces useable liquid product from lignocellulosic biomass [24]. Literally, pyrolysis corresponds to the thermal conversion occurring in the absence of oxygen. Biomass pyrolysis results in the production of three products: gas, pyrolysis oil and charcoal [24].

Table 2.2 Gas chromatographic analysis of liquid fraction (wt%) in bio-pyrolysis oil (Bio-oil).

Composition	Wood [25]	Corncob [26]
Acids and ester	10.4	6.0
Alcohols	5.3	4.1
Aldehydes	10.9	8.6
Aliphatic hydrocarbons	0.4	0.2
Amines	0.5	-
Aromatic hydrocarbons	5.6	7.6
Ethers	2.2	-
Furans	2.5	-
Ketones	36.6	16.9
Phenols	10.9	38.6
Unidentified fraction	14.7	18.0

The relative proportions of these products depend very much on the pyrolysis method, the characteristics of the biomass and the reaction parameters (Table 2.2). Temperature, heating rate and vapour residence time can be adjusted to favor charcoal or bio-oil productions [27]. However, the high oxygen content of the oil induces instability within the oil through polymerization reactions, which then increases the viscosity of the oil. Furthermore, the oil is highly odorous. It has a tarry odor reminiscent of stale cigarettes, making it uncomfortable to work with, thus reducing the probability of promoting the oil commercially.

References

[1] Scott M.A., Kathleen A.C. and Prabir K.D. Editors. **Handbook of Zeolite Science and Technology**. New York : Marcel Dekker. 2003.

[2] Bekkum H.V., Flanigen E.M. and Jansen J.C. Editors. **Introduction to Zeolite Science and Practice**. Amsterdam : Elsevier. 1991.

[3] Bruce C.G. **Catalytic Chemistry**. New York : John Wiley & Sons. 1992.

[4] Ian M.C. **Biomass, Catalysis and Liquid Fuels**. Pennsylvania : Technomic. 1983.

[5] Chen N.Y., Willium E.G. and Francis G.D. **Shape Selective Catalysis in Industrial Applications**. 2nd Ed. New York : Marcel Dekker. 1996.

[6] Subhash B. **Zeolite Catalysis: Principles and Applications**. Florida : CRC Press. 1990.

[7] Hegedus L.L. Editor. **Catalyst Design Progress and Perspectives**. New York : John Wiley & Sons. 1987.

[8] Jacobs P.A. Editor. **Zeolite Chemistry and Catalysis**. Amsterdam : Elsevier Science. 1991.

[9] Kokotailo G.T., Lawton S.L. and Olson D.H. "Structure of Synthetic Zeolite ZSM-5" **Nature**. vol. 272, 1978. pp. 437-438.

[10] Robert J.A., Kansington M., George R.L. and Audbon N.J. **"Crystalline Zeolite ZSM-5 and Method of Preparing the Same"** U.S patent no. 3702886, November 1972.

[11] Armor J.N. "Metal-Exchanged Zeolite as Catalysts" **Microporous and Mesoporous Materials**. vol. 22, 1998. pp. 451-456.

[12] Toshihide B., Hidenori S., Toshiaki. T. and Muneyoshi A. "Chemisorption Study of Hydrogen and Methane by ^{1}H MAS NMR and Conversion of Methane in the Presence of Ethylene on Ag-Y Zeolite" **Applied Catalysis A: General**. vol. 231, 2002. pp. 55-63.

[13] Junji S., Yuu T., Akira S., Shigeo S., Atsushi S. and Tahashi H. "Influence of Zeolite Support on Activity Enhancement by Addition of Hydrogen for SCR of NO by Propane over Ag-zeolites" **Applied Catalysis B: Environmental**. vol. 54, 2004. pp. 137-144.

[14] Cynthia T.C. **"Aromatization of Aliphatics over a Zeolite Containing Framework Gallium"** U.S patent no. 4891463, January 1990.

[15] Laurent P., Jean P.B., Jean L.G., Francis R. and Alain S. **"Catalyst of the Gallosilicate Type and Its Utilization for the Aromatization of Light C2-C4 Gases"** U.S patent no. 5073672, December 1991.

[16] Choudhary V.R., Devadas P. "Regenerability of Coked H-GaMFI Propane Aromatization Catalyst, Activity/Selectivity and Deactivation" **Applied Catalysis A: General.** vol. 168, 1998. pp. 187-200.

[17] Vasant R.C, Kshudiram M. and Chinta S. "Influence of Zeolite Factors Affecting Zeolite Acidity on the Propane Aromatization Activity and Selectivity of Ga/H-ZSM-5" **Microporous and Mesoporous Materials.** vol. 37, 2000. pp. 1-8.

[18] Wei Q.L., Lin Z., Gui D.S. and En Z.M. "Saturation of Aromatics and Aromatization of C3 and C4 Hydrocarbons over Metal Loaded Pillared Clay Catalysts" **Catalysis Today.** vol. 51, 1999. pp. 135-140.

[19] Weitkamp J. Editor. **Zeolite and Related Microporous Materials: State of the Art 1994.** Amsterdam : Elsevier Science. 1994.

[20] Sami M., Lewis F.H. **Chemistry of Petrochemical Processes.** Houston : Gulf. 1994.

[21] Nelson W.L. **Petroleum Refinery Engineering.** 4th Ed. Auckland : McGraw-Hill. 1985.

[22] Robert A.M. Editor. **Handbook of Petroleum Refining Processes.** 2nd Ed. New York : McGraw-Hill. 1997.

[23] PTT Public Company Limited. **"Natural Gas Information"** [Online]. Available : http://pttinternet.pttplc.com/csc_gas/csc_ind/information/ngi_04.asp. 2001.

[24] Basak B.U., Ayse E.P. and Ersan P. "Composition of Products Obtained via Fast Pyrolysis of Olive-Oil Residue: Effect of Pyrolysis Temperature" **Journal of Analytical and Applied Pyrolysis.** vol.79, 2007. pp. 147-153.

[25] Adjaye J.D., Bakhshi N.N. "Production of Hydrocarbons by Catalytic Upgrading of a Fast Pyrolysis Bio-Oil. Part I: Conversion over Various Catalsyts" **Fuel Processing Technology.** vol. 45, 1995. pp. 161-183.

[26] Zhang H., Xiao R., Huang H. and Xiao G. "Comparison of non-Catalytic and Catalytic Fast Pyrolysis of Corncob in a Fluidized Bed Reactor" **Bioresource Technology.** vol. 100, 2009. pp. 1428-1434.

[27] Horne P.A., Williams P.T. "Influence of Temperature on the Products from the Flash Pyrolysis of Biomass" **Fuel.** vol. 75, 1996. pp.1051-1059.

Chapter 3

Experimental Details

3.1 Reagents

	Chemicals	Grade of purity	Manufacturers
3.1.1	Air zero	HP	TIG
3.1.2	Ammonia/He	10 %	TIG
3.1.3	Benzaldehyde	Analytical	Fluka Chemika
3.1.4	Benzene	Analytical	CARLO ERBA REAGENTI
3.1.5	Deuterium	HP	BOC
3.1.6	Distilled water		
3.1.7	Ethane gas	HP	TIG
3.1.8	Ethyl alcohol (absolute)	Analytical	CARLO ERBA REAGENTI
3.1.9	Ethylbenzene	GC	Fluka Chemika
3.1.10	Ethylene gas	CP	BOC GASES
3.1.11	Gallium nitrate	99.9 %	ALDRICH
3.1.12	Gallium oxide	Analytical	Fluka Chemika
3.1.13	Helium gas	HP	TIG
3.1.14	Hydrogen gas	HP	TIG
3.1.15	Hydrogen/Argon	10 %	TIG
3.1.16	*i*-Propylamine	GC	Fluka Chemika
3.1.17	Liquefied petroleum gas	Commercial	SIAM GAS
3.1.18	Liquid nitrogen		TIG
3.1.19	*m*-Cresol	Analytical	Fluka Chemika
3.1.20	*n*-Heptane	GLC	CARLO ERBA REAGENTI
3.1.21	*n*-Hexane	Analytical	Mallinckrodt
3.1.22	Nitrogen gas	High purity	TIG
3.1.23	*n*-Nonane	GC	MERCK
3.1.24	*n*-Pentane	Analytical	LAB-SCAN

	Chemicals	Grade of purity	Manufacturers
3.1.25	Silver nitrate	Analytical	Fluka Chemika
3.1.26	Toluene	GC	Fluka Chemika
3.1.27	Xylene	GC	Fluka Chemika
3.1.28	Zeolite Beta (SuD Chem)		SuD Chem
3.1.29	Zeolite CBV2314		Zeolyst
3.1.30	Zeolite CBV5524G		Zeolyst
3.1.31	Zeolite ZSM-5 (SuD Chem)		SuD Chem

3.2 Apparatus

3.2.1 Beaker

3.2.2 Buchner flask

3.2.3 Clamp

3.2.4 Diffused reflectance ultraviolet spectrometer

3.2.5 Erlenmeyer flask

3.2.6 Fourier transform infrared spectrometer

3.2.7 Gas adsorption analyzer

3.2.8 Gas chromatograph

3.2.9 Graduated cylinder

3.2.10 Graduated pipette

3.2.11 Heating bath

3.2.12 Heating mantle

3.2.13 Metal rings

3.2.14 Pasteur pipette

3.2.15 Scanning electron microscope

3.2.16 Supporting stand

3.2.17 Temperature-programmed apparatus

3.2.18 Transmission electron microscope

3.2.19 Vial

3.2.20 Wash bottle

3.2.21 Water circulator

3.2.22 X-ray absorption near edge spectrometer

3.2.23 X-ray diffractometer

3.2.24 X-ray fluorescence spectrometer

3.3 Process of study

A process of the study on the conversion of light hydrocarbons and biomass models to ethylene, propylene, and aromatics over zeolite catalyst comprises the following stages:

3.3.1 Modification of zeolites

3.3.1.1 Modify ZSM-5 and Beta obtained from several suppliers by impregnation and/or ion-exchange with gallium, silver and proton.

3.3.1.2 Activate the materials obtained in 3.3.1.1.

3.3.2 Characterization of modified zeolites

3.3.2.1 Determine the silicon/aluminium ratio by inductively coupled plasma/atomic emission spectroscopy and X-ray fluorescence spectroscopy.

3.3.2.2 Determine the crystal morphology by scanning electron microscopy.

3.3.2.3 Investigate the zeolite structure by X-ray diffractometer.

3.3.2.4 Determine the metal content in zeolite by inductively coupled plasma/atomic emission spectroscopy and X-ray fluorescence spectroscopy.

3.3.2.5 Determine the surface area by gas adsorption analysis.

3.3.2.6 Determine the acidity of zeolite by ^{1}H nuclear magnetic resonance, Fourier transform infrared spectroscopy, ammonia-temperature-programmed desorption and *i*-propylamine temperature-programmed desorption.

3.3.2.7 Investigate the species type of metal-modified acid zeolite by diffuse reflectance ultraviolet spectroscopy and X-ray absorption near edge structure.

3.3.2.8 Investigate the reduction ability of metal-modified acid zeolite by temperature-programmed reduction.

3.3.2.9 Investigate the solid state reaction that produced hydrogen gas by temperature-programmed hydrogen evolution.

3.3.2.10 Investigate the cluster size and size distribution of metal-modified acid zeolite by transmission electron microscope.

3.3.2.11 Investigate the H_2/D_2 dissociation of acid zeolite and metal-modified acid zeolite by mass spectrometer.

3.3.3 Catalytic testing

3.3.3.1 Investigate the effect of temperature.

3.3.3.2 Investigate the effect of space time

3.3.3.3 Investigate the effect of carrier gas

3.3.3.4 Investigate the type of feed.

3.3.3.5 Investigate the effect of water co-feeding

3.3.3.6 Investigate the effect of metal loading and method of incorporation.

3.3.4 Analysis of products

3.3.4.1 Determine the amount of hydrocarbon and oxygenated products by FID-gas chromatography.

3.4 Modification of zeolites

3.4.1 Preparation of gallium-impregnated zeolite

The loading of gallium onto the zeolite was done according to the following procedure [1]: 0.0754 grams of gallium nitrate were dissolved in small amount of water. This solution was added to 4 grams of zeolite, and the resulting mixture was stirred for few minutes. Then water was gently evaporated to dryness on a hotplate. The resulting solid was further dried at 120 °C for 3 hours and activated in air 550 °C for 5 hours. This catalyst will be referred to as 1[Ga]HZeolite. The content of gallium of the resulting catalyst was approximately 1 wt%.

In the 3[Ga]HZeolite and 6[Ga]HZeolite, 0.2262 and 0.6786 grams of gallium nitrate were impregnated on acid zeolite, respectively. Then, the impregnated solid were then activated by air at 550 °C for 5 hours. The content of gallium was determined by inductively coupled plasma/atomic emission spectroscopy and X-ray fluorescence spectrometer.

3.4.2 Preparation of silver ion-exchanged zeolite

Silver-incorporated zeolite was carried out by ion-exchange of proton form by silver cation solution [1]. 2 grams of zeolite were ion-exchanged in 125 mL of 0.05-0.50 M silver nitrate solution and stirred at room temperature for 6-24 hours (The variation of silver content loaded in zeolite were prepared by different of silver nitrate concentration and time). This mixture was then filtered and washed 1 time with 50 mL of distilled water at room temperature. Finally the zeolite was dried at 120 °C for 3 hours and activated in air 550 °C for 5 hours. This catalyst will be referred to as AgHZeolite. The content of silver was determined by inductively coupled plasma/atomic emission spectroscopy and X-ray fluorescence spectrometer. In the case of reduction, this catalyst was either further activated by hydrogen at 350 °C for 2 hours (mild-red-AgHZeolite) or at 425 °C for 4 hours (red-AgHZeolite). Hereafter, the catalysts will be designated as % weight of Ag-AgHZeolite(Si/Al ratio), e.g., 3AgHZSM-5(11).

3.5 Characterization of catalysts

3.5.1 Inductively coupled plasma/Atomic emission spectroscopy

Elemental analysis of the metal-modified zeolite is also performed by inductively coupled plasma/atomic emission spectroscopy (ICP/AES). An accurate 50 mg of zeolite sample was weighed and then digested with hydrofluoric acid [2]. This solution was diluted to 100 mL in a volumetric plastic flask. Then, the diluted sample solution was measured against a blank. Finally, the silicon, aluminium, and metal content were calculated using calibration curves.

3.5.2 X-ray fluorescence

The conventional technique to check the chemical composition of zeolite is by X-ray fluorescence spectroscopy [2,3]. This method was done according to the following procedure: the sample was finely grinded and mixed with boric acid. Then, it was transferred and placed into the XRF sample holder. The X-ray emitted from the sample was detected by wavelength dispersive method.

3.5.3 Scanning electron microscopy

Scanning electron microscopy (SEM) is the most versatile technique for studying morphology and crystallite size [2,3]. This technique was done according to the following

procedure: the sample was finely dispersed on an SEM stub. The sample surface was then coated with gold thin film. After that the sample holder was left in sample chamber, and evacuated from ambient pressure to below 10^{-4} Torr. Then, the holding sample can be adjusted, tilted and moved in the X, Y and Z directions. As a consequence, sample surface can be viewed from almost any perspective.

3.5.4 X-ray diffraction

The best way to check the zeolite structure is by X-ray diffraction [4]. This method was done according to the following procedure: the sample was finely grinded to permit packing of the sample into an XRD sample holder. The XRD pattern was obtained by scanning over the angle range from 2-theta = 5 to 60 with 30 mA, 45.0 kV, step angle 0.040 degree, and detection time 1.50 seconds/step. The X-ray source was Cu-Kα.

3.5.5 Gas adsorption analysis

Gas adsorption analysis is the technique generally used for determining surface area of solid catalyst [5]. This technique was done according to the following procedure: the zeolite sample was weighed about 20 mg and transferred to a clean, dry empty sample cell. This sample cell was attached to the outgassing station. Then, a heating mantle was installed with the sample cell and the temperature was raised to 350 $^{\circ}$C for 24 hours. After the residual adsorbate was removed by heating under vacuum, nitrogen adsorbate was filled by opening the gas inlet valve. The sample cell was attached to the sample station. Initially, a dewar flask of liquid nitrogen was placed around the sample cell. Nitrogen adsorbate pressure can be regulated by 1 torr transducer with 3 minutes equilibration time and 0 scaled tolerance. When the adsorption was complete, the sample cell was removed from the sample station, dried throughly and reweighed.

3.5.6 Solid state magic angle spinning nuclear magnetic resonance

Nuclear magnetic resonance (NMR) has been widely used to characterized zeolite acidity and catalytic reaction [3,6,7]. ^{1}H MAS NMR spectra were recorded at 300 MHz on a Brüker spectrometer with an MAS probe with 5 mm ZrO_2 rotor. Prior to the measurement, a sample was filled into an NMR rotor and heated up to 270 and 360 $^{\circ}$C under high vacuum (3.0×10^{-5} Torr) using a home-made vacuum manifold equipped with a turbomolecular pump. After treatment, the

sample was filled with helium and transferred into the spectrometer. A spin-echo pulse program was used to acquire ^{1}H spectra with 64 scans. Samples were spun at 5 kHz, and the chemical shifts were referenced to TMS standard. For the probe analysis of ethylene, ^{13}C MAS NMR spectra were recorded by cross-polarization pulse program, using adamentane as a reference.

3.5.7 Fourier transform infrared spectroscopy

Fourier transform infrared spectroscopy (FTIR) is frequently used to study the zeolite acidity [6,8]. The infrared spectra were recorded on a Brüker series spectrometer. Thin zeolite wafer of 10 mm in diameter were made by pressing approximately 10 mg of fine zeolite powder under 5 tons of pressure for 2 minutes. The thin wafer was placed in a home-made type sample holder and transferred into the IR cell equipped with heating rod. This equipment specially designed to allow *in situ* high temperature treatments and gas dosage, was attached in the vacuum system (3×10^{-5} Torr). A zeolite sample was dehydrated at 350 °C under vacuum for 2 hours. An IR spectrum was acquired in the transmission mode at room temperature over the wave number of 4000-1300 cm^{-1}.

3.5.8 Ammonia-temperature-programmed desorption

Ammonia is probably the most frequently used probe molecule for acidity assessment. Its small molecular size allows one to probe almost all acid sites of both micro- and mesoporous materials [6,9]. NH_3-temperature-programmed desorption (NH_3-TPD) experiments were carried out using a TCD detector. Before adsorption, the samples (0.05 g) were dried in a flow of He at 550 °C for 2 hours. Adsorption of 10% NH_3/He was performed at 50 °C. After saturation, the samples were flushed with He at this temperature for 2 hours. TPD measurements were done from 50 to 700 °C with a heating rate of 10 °C/min, using He as a carrier gas.

3.5.9 *i*-propylamine-temperature-programmed desorption

Temperature-programmed desorption of *i*-propylamine (IPA-TPD) is used to determine the Brønsted acidity [10]. First, 25 mg of sample was pretreated at 550 °C in a flow of He or H_2. After the treatment, the sample was cooled in He to room temperature and then *i*-propylamine (IPA) was injected to the sample until saturation. The excess IPA was removed by flowing He. When a constant signal was achieved, the sample was heated to 900 °C at a rate of 10 °C/min. The

masses used to identify various desorption products in IPA-TPD were m/z = 44 (*i*-propylamine), m/z = 41 (propylene), and m/z = 17 (ammonia). The amount of desorbed propylene was simultaneously calibrated with 2 mL pulses of 2% propylene in He and the Brønsted acidity was then calculated.

3.5.10 Diffused reflectance ultraviolet spectroscopy

Zeolite samples usually exhibit low transparency, hence, measurements in reflection mode are performed [3]. Diffused reflectance ultraviolet spectra of metal-modified zeolite were measured with Shimadzu spectrometer. The sample was packed into the sample holder. A UV spectrum was acquired in the reflectance mode at room temperature with wavelength 1000-600 nm.

3.5.11 X-ray absorption near edge structure

The energy of the X-ray absorption edge can often determine the oxidation state of the metal species [11]. X-ray absorption near edge structure were measured at NSRC (National Synchrotron Research Center) using a Si (111) double crystal monochromator. The storage ring was operated at 1.2 GeV. Data were collected in the transmission mode on self-supporting sample wafers using gas-filled ionization chambers as detectors.

3.5.12 Temperature-programmed reduction

Temperature-programmed reduction (TPR) provides information on the nature of the catalyst by monitoring their reducibility [12]. Temperature-programmed reduction were measured using thermal conductivity detector (TCD). The sample weighed 0.15 g was placed into a tube reactor, which was located inside a temperature-regulated furnace. The heating rate of 10 $^{\circ}$C/min, the 2-7% H_2 in Ar flow of 30 mL/min was applied for TPR analysis. Water produced during the reduction process was removed in a U-shape glass trap at -70 $^{\circ}$C (vapor of liquid N_2) before entering the TCD.

Double TPR reaction was performed for checking reversible reduction-oxidation cycle. After the first TPR analysis was finished, the sample was cooled to 50 $^{\circ}$C under a flow of N_2. Then, the TPR analysis was repeated by monitoring the H_2 consumption with TCD.

3.5.13 Temperature-programmed hydrogen evolution

Temperature-programmed hydrogen evolution (TPHE) study is carried out to observe hydrogen evolution that is connected with the solid-state redox reaction [13]. Temperature-programmed hydrogen evolution experiments were performed in a temperature-programmed apparatus. After catalyst was reduced at 425 °C, a sample was cool down to 50 °C under Ar flow (30 mL/min). Then, metal-modified zeolite was heated in an Ar flow (30 mL/min) to 800 °C with a heating rate of 10 °C/min. The quadrapole detector was used to analyze hydrogen gas generated.

3.5.14 Transmission electron microscopy

Transmission electron microscopy (TEM) is directly interpretable, and the technique is tailor-made for detecting clusters of catalytically active metal on zeolite [14]. For characterization by transmission electron microscopy, the wet sample was crushed in a mortar, and the suspended powder was subjected to disperse on a carbon-coated copper TEM grid. Electron micrographs were acquired with a Philips Jeol transmission electron microscope.

3.5.15 Isotopic exchange of hydrogen/deuterium

The isotopic exchange of hydrogen (H_2) with deuterium (D_2) is a typical metal/acid-catalyzed reaction. During H_2/D_2 exchange, hydrogen atoms are replaced by deuterium atom. Its product distribution gives direct information about the hydrogenation/dehydrogenation, hydrogenolysis and hydrogen transfer depending on the electronic properties of the metal species and Brønsted acid sites [15,16]. H_2/D_2 exchange was studied using an MS detector. The catalyst sample was heated in a flow of H_2 (m/z = 2) at 450-550 °C and then consecutive 2 mL pulses of pure deuterium, D_2 (m/z =4) were injected to the sample. The masses were monitored to determine the reactant feed and the product formation (H-D, m/z = 3).

3.5.16 Adsorbed reactant temperature-programmed desorption

Temperature-programmed desorption (TPD) is one of the most widely used and flexible techniques for characterizing surface catalysis. By monitoring gas phase concentration of the species desorbed, due to a linear increase in surface temperature, key information can be obtained. These include the amount and number of different kinds of surface species, the kinetics of the desorption process, the enthalpy of desorption, and differentiation between simple

desorption and chemical reaction-desorption [17,18]. Before adsorption, the sample (50 mg) was dried in a flow of He (or H_2) at 550 °C for 2 hours. Adsorption of reactant until saturation was performed at its boiling temperature, the sample was then flushed with He (or H_2) at such temperature for 3 hours. TPD measurements were done from its boiling temperature to 900 °C with a heating rate of 10 °C/min using He (or H_2) as a carrier gas. The masses (m/z) of the expected products were monitored using mass spectrometer. The evolution of the retained product over modified acid zeolite catalysts was also followed by TPD. After the reaction, the catalyst sample was flushed in a flow of He at reaction temperature and then cooled to 100 °C. TPD measurements were done from 100 to 900 °C with a heating rate of 10 °C/min using H_2 as the carrier gas. The masses (m/z) of the expected products were monitored.

3.6 Catalytic testing

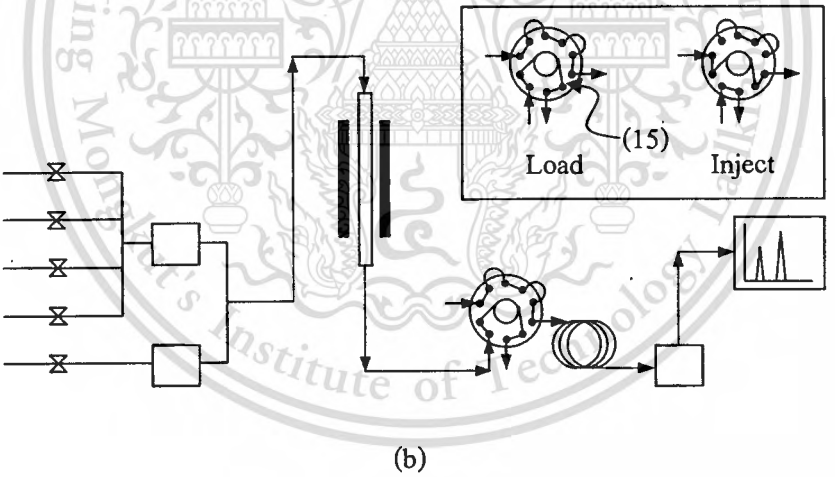

(b)

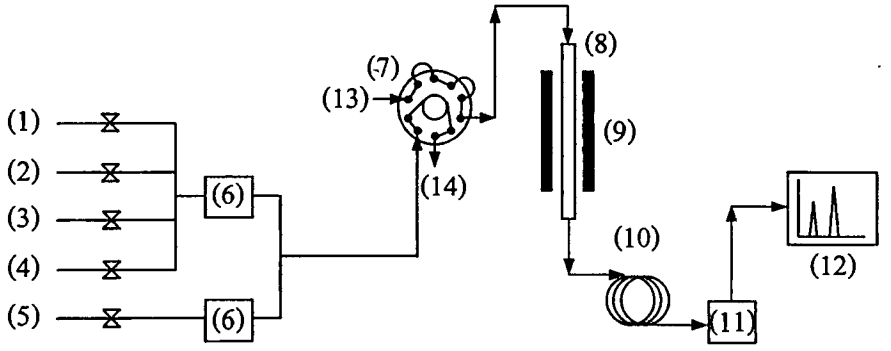

(a)

Figure 3.1 Flow diagrams of (a) pulsed reactor and (b) fixed bed flow reactor.
(1) Air/O_2, (2) N_2, (3) He, (4) H_2, (5) Hydrocarbon feed, (6) Mass flow controller, (7) 10-way valve, (8) Quartz tube reactor, (9) Furnace, (10) GC column, (11) Detector (FID or MS detector), (12) Monitor, (13) GC carrier gas, (14) Vent, (15) Gas sampling loop (25 microliters)

The pulse reaction technique allows us to study an initial state of a flow reaction. Characteristic behaviors of non-equilibrium state can also be observed [19]. Two kinds of pulsed reactions were employed in this study: gas and liquid phase injection.

A simple pulsed reactor device (Figure 3.1(a)) was obtained when a gas chromatograph column was directly connected with the end of the reactor. In this catalytic testing unit, a quartz tube reactor was located inside a temperature-regulated furnace. Therefore, the reaction preferred at the high temperature (450-800 °C), such as dehydrogenation can be carried out. Reactants (light hydrocarbon) and/or treating gas were regulated by mass flow controllers and passed to a 25 microliter sampling loop of GC. Pulse of gas was then fed to the catalyst bed under chromatographic flow. The preferred reaction conditions used in a pulsed reactor testing unit were as follows: 12.5 mg catalyst; 5 v/v% dilution of reactant feed with inert or H_2.

In the case of liquid injection, 50 mg of the catalyst was pretreated in a flow of He or H_2 (30 mL/min). After the pretreatment, 1 microliter of pure liquid reactant was injected to the pretreated catalyst. This procedure was repeated at different reaction temperatures. The products of the pulse reaction were on-line analyzed by an MS detector.

The catalytic activity and deactivation behavior of the modified zeolite were investigated with a fixed bed flow reactor (Figure 3.2(b)). The reactant feed was carried by N_2 (or He, H_2) through a catalyst bed set in a catalytic reactor, which was located inside a temperature-regulated furnace. The gaseous mixture flowing out of the reactor passed to a gas sampling loop. The products were periodically collected and analyzed by online gas chromatography (GC).

3.7 Analysis product

The product analysis was generally performed using an on-line gas chromatography. The gas sample was collected in gas sampling loop, then periodically injected into GC column (HP-PLOT for light hydrocarbon gas, VA-1 for heavier hydrocarbon, DB-5 for hydrocarbon and oxygenated compounds) connected to flame ionized detectors. The components were separated as they pass through the column with an inert carrier gas and their presence in the effluent was detected and recorded as a chromatogram.

The peak area from the chromatogram was measured and calculated as the peak area percent value. Then the unknown peak can be identified by GC-MS technique and quantified using ethylene, ethane, LPG, *n*-pentane, *n*-hexane, *n*-heptane, benzene, toluene, ethyl benzene, xylene, benzaldehyde, *m*-cresol and phenol as standard for calibration. The composition of the hydrocarbon samples were determined by the normalization method.

References

[1] Raymond L.M. "Hybrid Catalyst Containing a Microporous Zeolite and a Mesoporous Cocatalyst Forming a Pore Continuum for a Better Desorption of Reaction Products" **Microporous and Mesoporous Materials.** vol. 28, 1999. pp. 9-17.

[2] Ausavasukhi A. **"The Production of Gasoline and Aromatics from Ethanol"** Master degree of science, Petrochemical and hydrocarbon chemistry, Faculty of Science, King Mongkut's Institute of Technology Ladkrabang. 2002.

[3] Bekkum H.V., Flanigen E.M. and Jansen J.C. Editors. **Introduction to Zeolite Science and Practice.** Amsterdam : Elsevier. 1991.

[4] Cullity B.D. **Elements of X-ray Diffraction.** 2nd Ed. Reading : Addison-Wesley. 1978.

[5] Schwarz J.A., Contescu C.I. **Surfaces of Nanopaticles and Porous Materials.** New York : CRC Press. 1999.

[6] Scott M.A., Kathleen A.C. and Prabir K.D. Editors. **Handbook of Zeolite Science and Technology.** New York : Marcel Dekker. 2003.

[7] Melinda J.D. Editor. **Solid State NMR Spectroscopy: Principles and Applications.** New York : John Wiley & Sons. 2002.

[8] Smith B.C. **Fundamentals of Fourier Transform Infrared Spectroscopy.** Boca Raton : CRC Press. 1996.

[9] Katada N., Niwa M. "Analysis of Acidic Properties of Zeolitic and Non-zeolitic Solid Acid Catalysts Using Temperature-Programmed Desorption of Ammonia" **Catalysis Surveys from Asia.** vol. 8, 2004. pp. 161-170.

[10] Gricus Kofke T. J., Gorte R.J. and Kokotailo G.T. "Stoichiometric Adsorption Complexes in H-ZSM-5, H-ZSM-12, and H-Mordenite Zeolites" **Journal of Catalysis.** vol. 115, 1989. pp. 265-272.

[11] Lippard S. J., Berg J.M. **Principles of Bioinorganic Chemistry.** California : University Science Books. 1994.

[12] Subhash B. **Zeolite Catalysis: Principles and Applications.** Florida : CRC Press. 1990.

[13] Hagen A., Schneider E., Kleinert A. and Roessner F. "Modification of Acid Supports by Solid-State Redox Reaction Part I. Preparation and Characterization" **Journal of Catalysis.** vol. 222, 2004. pp. 227-237.

[14] Thomas J.M., Gai P.L. "Electron Microscopy and the Materials Chemistry of Solid Catalysts" **Advances in Catalysis**. vol. 48, 2004. pp. 171-227.

[15] Oudenhuijzen M.K., Bokhoven van J. A. and Koningsberger D,C. "Supported-Induced Compensation Effects in H/D Exchange of Cyclopentane" **Journal of Catalysis**. vol. 219, 2003. pp. 134-145.

[16] Wen B., Sachtler W.M.H. "H/D Exchange of Methane over Transition Metal/MFI Catalysts" **Applied Catalysis A: General**. vol. 229, 2002. pp. 11-22.

[17] Kolasinski K. **Surface Science: Foundations of Catalysis and Nanoscience**. Chichester : John Wiley and Sons. 2002.

[18] Shengfu J., Jian Y., Cigang X., Jiaxin W. and Jinzhen X. "Temperature-Programmed Desorption/Pulse Surface Reaction (TPD/TPSR) Studies of CH_4, C_2H_6, C_2H_4, and CO over a Cobalt/MWNTS Catalyst" **Reaction Kinetics and Catalysis Letters**. vol. 89, 2006. pp. 209-217.

[19] Matsuhashi H. "Catalytic Characterization: Utilization of Pulse Reaction Technique" **Catalysts & Catalysis**. vol. 44, 2002. pp. 39-43.

Chapter 4

Ag Species in AgHZSM-5 and Their Reversible Interconversion Behavior

4.1 Introduction

The behavior of metallic and ionic clusters incorporated into zeolites is of great interest for their catalytic activity. Among the metal clusters, many efforts have been devoted to study the formation and characterization of Ag clusters, and the various types of Ag clusters [1-6]. This is due to the fact that Ag-modified zeolites show high activity in many catalytic processes. There are several reports demonstrating a specified catalysis of Ag-modified zeolites for the various types of reactions such as photo-dimerization of alkane [7], photocatalytic degradation of malathion [8], methane activation with ethylene to form propylene [9] and selective catalytic reduction of NO by alkane in the presence of hydrogen [10,11]. Moreover, the isolated silver cation was believed to be an active center for the dehydrogenation of light alkanes for aromatic production [12].

It is known that the charge-balancing Ag cation (Ag^+) in zeolites can be readily reduced with hydrogen or hydrocarbon to form silver metal (Ag^0) and the framework Brønsted acid site [13,14]

$$ZO^- Ag^+ + \tfrac{1}{2} H_2 \longrightarrow Ag^0 + ZO^- H^+ \qquad \text{Eq. (1)}$$

where ZO^- represents the negative framework charge of zeolite.

The subsequent aggregation of the reduced Ag metal, either its own species or even with the Ag cations, can be expected, forming various types of silver nanoparticles including Ag cationic clusters (Ag_n^+) [15,16]:

$$(n-1)Ag^0 + ZO^- Ag^+ \longrightarrow ZO^- Ag_n^+ \qquad \text{Eq. (2)}$$

In zeolites, the metallic or ionic clusters of noble metal, formed by the reduction of charge-balancing cations, are usually stable and well-dispersed. They may agglomerate to form relatively larger clusters, so-called "sintering", upon heating at high temperature. However, in

some cases, the reduced metals can reversibly react with the neighboring Brønsted acid sites, liberating H_2 and give back charge-balancing metal cations. This process is the so-called "reversible interconversion", which can be observed over zeolites modified by various metals, such as Zn [17] and Ag [9,18,19]. For example, Baba *et al.* [9] have observed the dissociation of hydrogen and methane over Ag_n^+ and these reactions (Eqs. (3)-(4)) are reversible upon reduction-evacuation cycles at low temperature (< 100 °C), providing different types of Ag species.

$$ZO^- Ag_n^+ + H_2 \rightleftharpoons Ag_n\text{-}H + ZO\text{-}H \qquad \text{Eq. (3)}$$

$$ZO^- Ag_n^+ + CH_4 \rightleftharpoons Ag_n\text{-}H + ZO^{\delta-}\text{-}CH_3^{\delta+} \qquad \text{Eq. (4)}$$

If the above reactions, so-called "the reversible interconversions" can readily take place at the reaction temperature (> 300 °C), one could not expect only a single form of Ag species for all cases. This is because the Ag species formed will depend largely on the reducibility of the hydrocarbon species in the reaction stream. Accordingly, the alteration of Ag species during the reaction would be the usual case and may largely affect the catalyst activity and stability. This could be an explanation for the observed differences in catalytic activity of Ag-modified zeolites over various types of reactions, as mentioned earlier.

According to the above speculation, one could expect that the Si/Al ratio of the zeolites would play a marked role in hosting, retaining and even altering the incorporated Ag species. Therefore, in this work, we provide further evidence for the influence of the zeolite Si/Al ratio on the reducibility and reversible interconversion of the incorporated Ag species. ^{1}H MAS NMR, together with temperature-programmed reduction (TPR) and temperature-programmed hydrogen evolution (TPHE) techniques, are mainly employed for determining the behavior of Ag species hosted by zeolites with different Si/Al ratios. The suggestion that the incorporated Ag species can readily influence their catalytic behavior towards BTX is tested by ethanol conversion. The effect of H_2, a readily reducing species, on the activity of AgZSM-5 will also be highlighted.

4.2 Experimental details

NH_4ZSM-5 (Si/Al ~11 and 28) samples were commercially obtained from Zeolyst International. Conventional ion-exchange of NH_4ZSM-5 with $AgNO_3$ solution, using different concentrations and conditions, was employed to obtain approximately 3 and 5 wt% Ag loading

for both HZSM-5 with Si/Al ~11 and 28 [20-22]. The samples were washed, dried and then calcined at 550 °C for 5 hours. Hereafter, the catalysts will be designated as %loading-AgHZSM-5(11) and AgHZSM-5(28) according to their Si/Al ratios. In the case of the sample that was reduced at 425 °C for 4 hours, the prefix "red-" will be used to refer to it, such as red-AgHZSM-5(11). Powder X-ray diffraction (XRD) was employed for determining zeolite crystallinity and the Ag metal phase.

^{1}H MAS NMR spectra were recorded at 300 MHz on a Brüker spectrometer with a BBI MAS probe using a 5 mm ZrO_2 rotor. Prior to the measurements, a home-made apparatus was used, by which the sample can be filled into an NMR rotor and heated to 350 °C in high vacuum (3.0×10^{-5} Torr) for dehydration. After the treatment, the sample container can be filled with He (or H_2), sealed and transferred into the spectrometer. A spin-echo pulsing sequence was used to acquire ^{1}H spectra with 64 scans each. Samples were spun at 5 kHz, and chemical shifts were referenced to tetramethylsilane (TMS). For the probe analysis of ethylene reaction, ^{13}C MAS NMR spectra were recorded by cross-polarization pulse program. After the treatment, the sample can be filled with ethylene gas and sealed. The rotor was heated to 60 °C in order to activate the adsorbed ethylene. Samples were spun at 3 kHz, and chemical shifts were referenced to adamentane.

TEM was performed on a Philips Jeol microscope. The samples were crushed in a mortar, and the powders were dispersed on a carbon-coated copper TEM grid. As a consequence, the cluster size of Ag species can be viewed from almost any perspective.

NH_3-temperature-programmed desorption (NH_3-TPD) experiments were carried out using a TCD detector. Before adsorption, the samples (0.05 g) were dried in a flow of He at 550 °C for 2 hours. Adsorption of 10 % NH_3/He until saturation took place at 50 °C, then the samples were flushed with He at the same temperature for 2 hours. TPD measurements were done from 50 to 700 °C with a heating rate of 10 °C/min, with He as the carrier gas.

Temperature-programmed reduction (TPR) experiments were carried out using a TCD detector. The H_2 consumption was recorded with temperature, when the catalyst samples were heated in a flow of 2% H_2/Ar (30 mL/min) with a heating rate of 10 °C/min, and then cooled to 50 °C in a flow of He. Same conditions for secondary TPR experiments were used for all samples.

Temperature-programmed hydrogen evolution (TPHE) experiments were recorded using a selective quadrupole detector (QMS 422, QuadStar™) for m/z = 2. Catalyst samples were

reduced in a flow of 2% H_2/Ar (30 mL/min) at a heating rate of 10 °C/min and held at 425 °C for 4 hours, and then cooled to 50 °C under the flow of either 2% H_2/Ar or pure Ar. These samples were flushed with Ar at room temperature for 2 hours and then heated to 900 °C under Ar stream.

Diffused reflectance ultraviolet spectra of Ag-modified zeolite were measured with Shimadzu spectrometer. The sample was packed into the sample holder. A UV spectrum was acquired in a reflectance mode at room temperature over the wavelength of 1000-600 nm for Ag species absorption.

X-ray absorption near edge structure (XANES) were measured at NSRC (National Synchrotron Research Center) using a Si (111) double crystal monochromator. The storage ring was operated at 1.2 GeV. Data are collected in a transmission mode on self-supporting sample wafers using gas-filled ionization chambers as detectors.

Catalytic testing on ethanol aromatization was performed with a continuous fixed bed reactor as described in section 3.6. The vaporized ethanol was carried by N_2 gas through a catalyst bed set inside a temperature-regulated furnace. The preferred reaction conditions used in the experiments were as follows: temperature, 425 °C; total pressure, 1 atm; carrier gas, N_2 or H_2; W/F, 6.75 g·h/mol. The products are analyzed by an on-line gas chromatograph equipped with a flame ionization detector (FID) and VA-1 capillary column (Appendix B).

4.3 Results and discussion

The characteristics of the zeolite samples are shown in Table 4.1.

Table 4.1 Chemical composition and surface area of zeolite samples.

Catalyst	Si/Al[a]	Degree of Ag ion-exchange (%)	Ag content[a] (wt%)	Surface area (m^2/g)
HZSM-5(11)	11	-	-	644
3AgHZSM-5(11)	11	20	2.3	481
5AgHZSM-5(11)	11	30	4.5	465
HZSM-5(28)	28	-	-	560
3AgHZSM-5(28)	28	50	2.3	493
5AgHZSM-5(28)	28	80	4.5	480

[a] Elemental analysis for Si, Al, and Ag were performed using ICP.

Although the extent of Ag ion-exchange are different for AgHZSM-5(11) and AgHZSM-5(28), the total Ag loadings on both samples are the same. As an incomplete Ag ion-exchange is obtained for both AgHZSM-5(11) and AgHZSM-5(28), some acid sites shall remain after calcinations. No metallic Ag is observed by XRD (Figure 4.1).

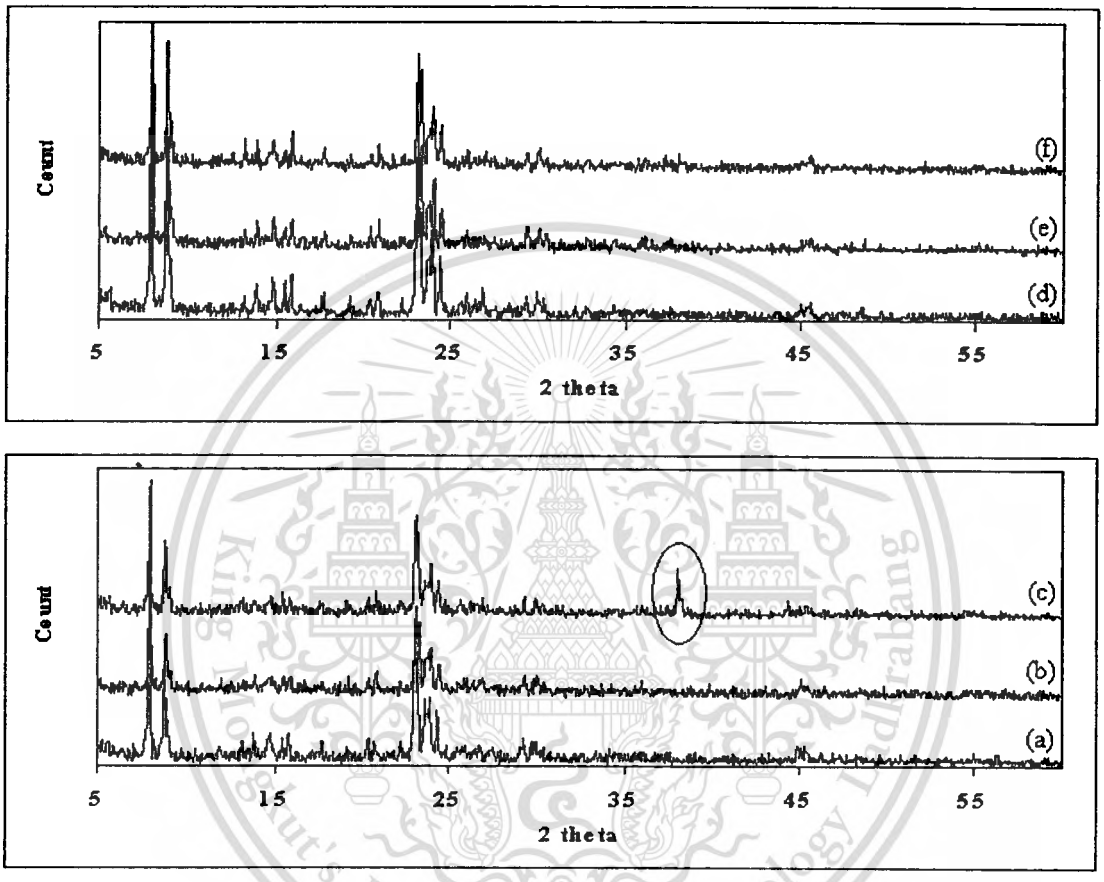

Figure 4.1 XRD patterns of (a) HZSM-5(11), (b) 3AgHZSM-5(11), (c) red-3AgHZSM-5(11), (d) HZSM-5(28), (e) 3AgHZSM-5(28), and (f) red-3AgHZSM-5(28).

It is presumed that incorporated Ag species are well-dispersed as charge-balancing Ag cations. After H_2 reduction at 425 °C, metallic Ag can be observed at 2-theta 38° only for the red-3AgHZSM-5(11) sample (Figure 4.1c). This result is confirmed by the ^1H MAS NMR experiment.

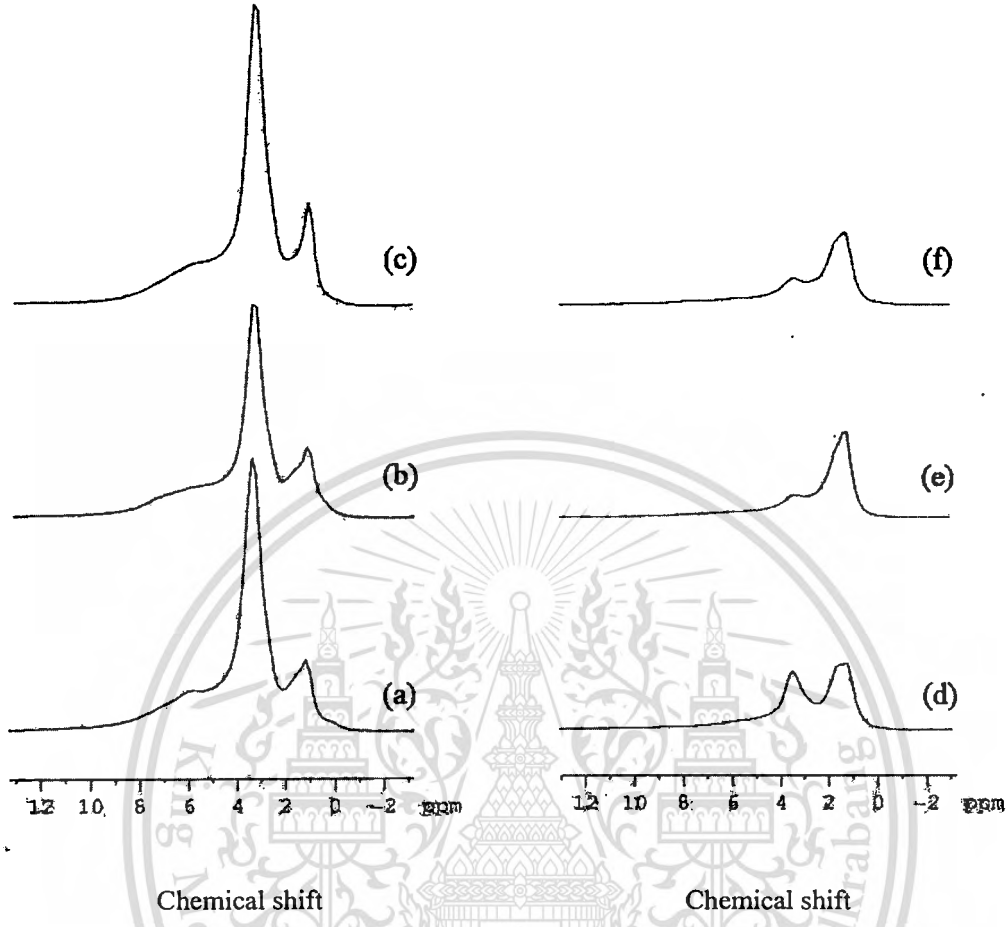

Figure 4.2 ^{1}H spin-echo MAS NMR spectra of (a) HZSM-5(11), (b) 3AgHZSM-5(11), (c) red-3AgHZSM-5(11), (d) HZSM-5(28), (e) 3AgHZSM-5(28), and (f) red-3AgHZSM-5(28).

All the spectra were recorded at room temperature, resonance frequency of 300 MHz, a sample spinning rate of 5 kHz with 64 scans.

From Figure 4.2, it is found that the Brønsted acid sites (signal at ~3.9 ppm) [23-26] of both 3AgHZSM-5(11) and 3AgHZSM-5(28) are markedly reduced, as compared to the parent HZSM-5. This is due to the replacement of Ag cations onto the Brønsted acid sites. When 3AgHZSM-5(11) was reduced under H_2 atmosphere at 425 °C, Brønsted acid sites almost recovered (red-3AgHZSM-5(11)). It is obvious that silver cations in 3AgHZSM-5(11) can be readily reduced, forming Ag metal, bearing consecutive Brønsted acid sites (Eq. (1)). On the other hand, no recovery of Brønsted acid site was found for red-3AgHZSM-5(28) when it was reduced

at the same condition. This result is consistent with XRD results of red-3AgHZSM-5(28) where no metallic Ag phase can be observed (Figure 4.1f).

The fact that there is no recovery of Brønsted acid sites and Ag metallic phase of 3AgHZSM-5(28) may be derived from two possibilities: (i) the charge-balancing Ag cations in 3AgZSM-5(28) may not be reduced to Ag metals at 425 °C or (ii) the charge-balancing Ag cations in 3AgZSM-5(28) could be reduced, but the metallic Ag species may not be stable. Such metallic Ag species could reversibly react with Brønsted to form charge-balancing Ag cations, liberating H_2 gas (Eq. (5)), in a manner similar to that observed over ZnZSM-5 [17]. This is, in other words, "the reversible interconversion".

$$Ag_n + nZO\text{-}H \longrightarrow nZO\text{-}Ag^{+} + \frac{n}{2}H_2 \qquad \text{Eq. (5)}$$

The two hypotheses were tested by H_2-TPR experiment.

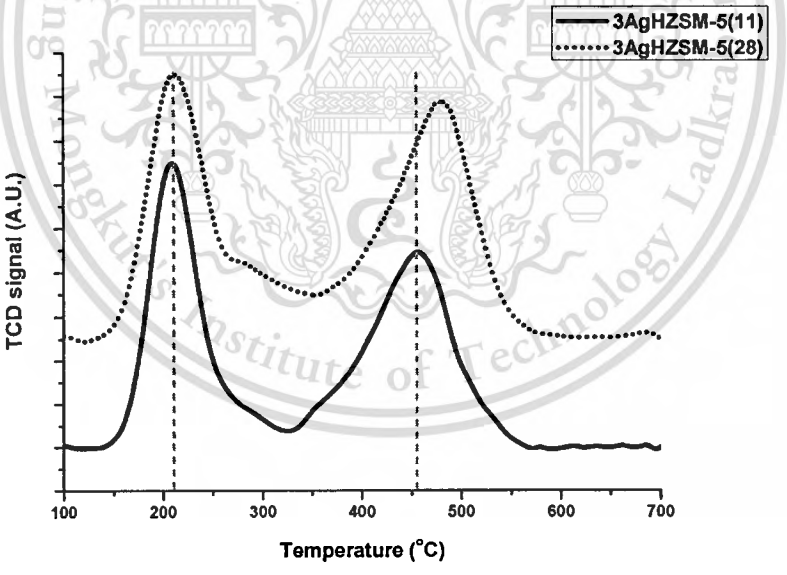

Figure 4.3 H_2-TPR profiles of 3AgHZSM-5(11) and 3AgHZSM-5(28).

In Figure 4.3, the thermogram clearly shows two H_2 consumption peaks over both 3AgHZSM-5(11) and 3AgHZSM-5(28) samples, indicating that they can indeed be reduced. The first peak appears in a temperature range from 150 °C to 270 °C and the second peak is pronounced from 350 °C to 550 °C. This is consistent with an observation made by Junji Shibata

and *et al.* [27]. They suggested that all of the Ag cations were readily reduced to "Ag cationic clusters (Ag_n^+)" at the first peak, and that the cationic clusters were further reduced to Ag metal particles at the second peak.

The above observation also suggests that the Ag species in 3AgHZSM-5(11) and 3AgHZSM-5(28) are not really the same. Comparing TPR (Figure 4.3) of 3AgHZSM-5(11) and 3AgHZSM-5(28), one can see that the first H_2 consumption peak of both samples appears at the same temperature (220 °C). This suggests that the reductions of the charge-balancing Ag cations into Ag cationic clusters (Ag_n^+) for both 3AgHZSM-5(11) and 3AgHZSM-5(28) occur in a similar manner. However, the second H_2 consumption peak of 3AgHZSM-5(11) appears at relatively lower temperature (457 °C), as compared with that of 3AgHZSM-5(28) (485 °C). This indicates a relatively lower stability of the Ag cationic clusters in 3AgHZSM-5(11), as compared with those in 3AgHZSM-5(28). In other words, it is likely that "Ag cationic clusters" can be retained in a silica rich 3AgHZSM-5(28), while such species are easily reduced into a "metallic form" in a lower silica sample: 3AgHZSM-5(11).

This strongly supports the observation by XRD that Ag metallic phase can be readily formed in 3AgHZSM-5(11), even though the reduction temperature (425 °C) is lower than that observed by TPR (457 °C). However, this still leads to the uncertainty about whether the cationic Ag clusters in 3AgHZSM-5(28) can or cannot be reduced into metallic phase (i), or whether the reversible interconversion (ii) of Ag species in AgHZSM-5(28) is responsible for non-recoverable Brønsted acid sites and missing Ag metallic phase in this sample. Therefore, further investigation on TPR was performed in order to verify the cause of such ambiguity.

Immediately after the primary TPR, both samples were then subjected to a repeat reduction even though they were not exposed to an oxidizing atmosphere (Figure 4.4).

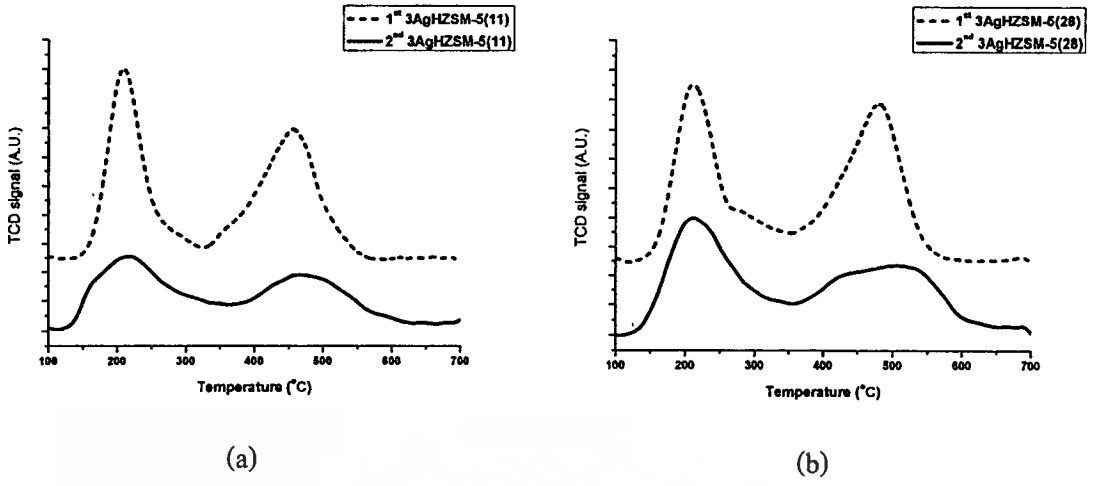

(a) (b)

Figure 4.4 Primary and secondary H_2-TPR profiles of (a) 3AgHZSM-5(11) and (b) 3AgHZSM-5(28).

It is shown that exactly two H_2 consumption peaks are repeatedly obtained. This result suggests that some of the Ag metal species in both samples (after the first severe reduction up to 700 °C) must have been reversely converted to Ag cations, possibly during the cooling period under He stream. Otherwise, a secondary reduction should not be observed. Therefore, it can be concluded at this stage that the reversible interconversion of the reduced Ag metal species can readily take place in both 3AgHZSM-5(11) and 3AgHZSM-5(28). In addition, this is likely to be the cause of non-recoverable Brønsted acid sites and missing Ag metallic phase in red-3AgHZSM-5(28).

This experiment also reveals that the ability of the reduced Ag metal species to undergo reversible interconversion are not truly the same for 3AgHZSM-5(11) and 3AgHZSM-5(28). It can be seen from Figure 4.4 that the secondary TPR of 3AgHZSM-5(28) shows a higher H_2 consumption, as compared with that of 3AgHZSM-5(11). This indicates that the reversible interconversion of the reduced Ag metal species in 3AgHZSM-5(28) is more feasible, as compared to that in 3AgHZSM-5(11). Since the reversible interconversion requires Brønsted acid sites, one could expect that 3AgHZSM-5(11), the sample with higher acid-site density, would provide a better opportunity for its incorporated Ag metal species to reversely convert into charge-balancing Ag cations. However, that is not the case. In turn, the reduced Ag species 3AgHZSM-5(11) is relatively less active for reversible interconversion. This is presumably because, in 3AgHZSM-5(11), the site proximity is relatively closed, the reduced Ag metals can be

easily agglomerated into a large Ag metal clusters, as clearly seen by XRD (Figure 4.1) and TEM (Figure 4.5).

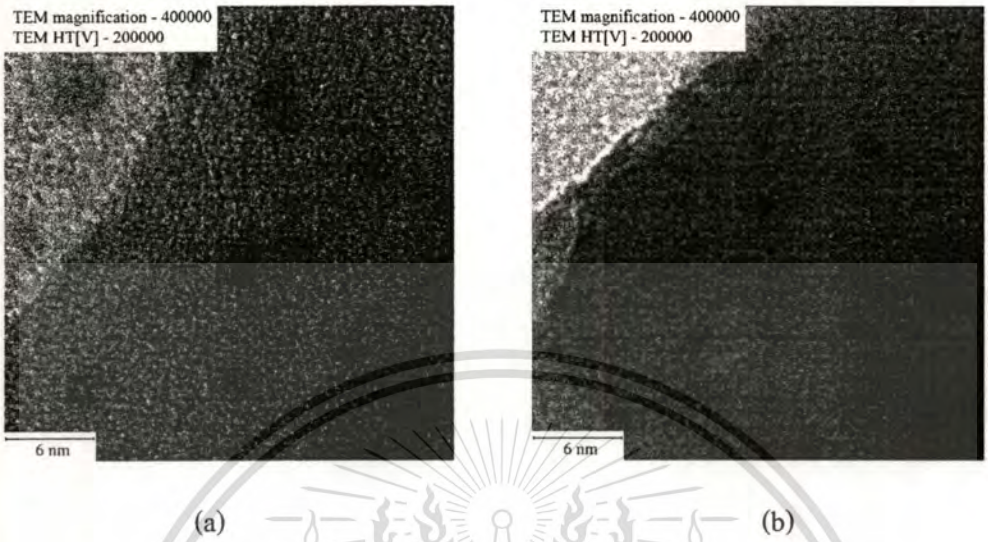

Figure 4.5 TEM micrograph of (a) red-3AgHZSM-5(11) and (b) red-3AgHZSM-5(28). The Ag crystals are distinguishable on the surface of the zeolite.

It can be seen that Ag-metal particle sizes of 3-4 nm were obtained over 3AgHZSM-5(11), which those of 1-2 nm were evenly dispersed on the outer surface of 3AgHZSM-5(28). Hence, it would be difficult for such large Ag metal clusters to undergo reversible interconversion, due to its relatively high stability, as discussed earlier. On the other hand, it is expected that the Ag metal species in 3AgHZSM-5(28) should be primarily dispersed upon reduction (Figure 4.5) and may not be quite stable due to a weak interaction with the higher silica framework. This would allow a reversible interconversion of such Ag metal species with neighboring Brønsted acid sites. Consistent with this view, no Ag metallic phase and no recoverable Brønsted acid sites can be observed in red-3AgHZSM-5(28) by XRD or NMR, respectively.

In order to validate the effect of Ag cluster size on reversible interconversion, samples with high Ag content, 5AgHZSM-5(11) and 5AgHZSM-5(28), were subjected to be interested for double H_2-TPR. It is expected that a higher Ag content lead to formation of relatively larger Ag metallic cluster after reduction.

In Figure 4.6, the primary H_2-TPR clearly shows two H_2 consumption peaks over 5AgHZSM-5 in manner similar to that observed over 3AgHZSM-5 samples except with a high

extent of H_2 consumption (Figure 4.3). Immediately after the primary TPR, both samples were also subjected to a repeat reduction without exposing to an oxidizing atmosphere (Figure 4.6).

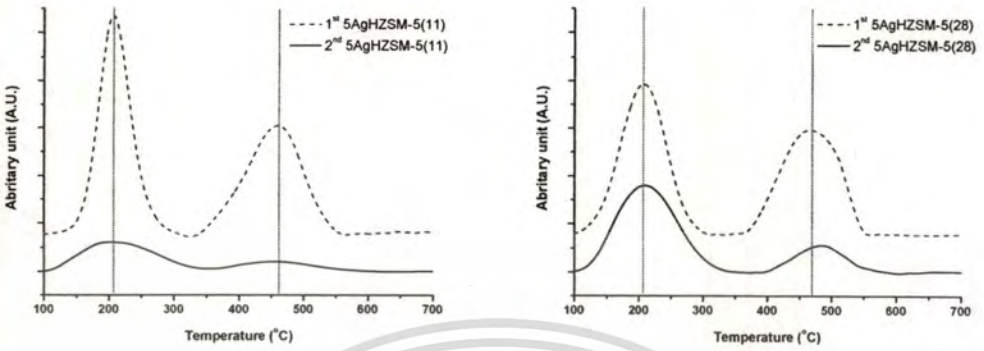

(a) (b)

Figure 4.6 Primary and secondary H_2-TPR profiles of (a) 5AgHZSM-5(11) and (b) 5AgHZSM-5(28).

It can be seen that some of the Ag metal species in both samples were also reversely converted to Ag cations. However, the reversible interconversion of the reduced Ag metal species in 5AgHZSM-5(11) is less feasible, as compared to that in 3AgHZSM-5(11) (Figure 4.4). This is clearly because, 5AgHZSM-5(11) possesses a higher Ag contents, thus the reduced Ag metals can be easily agglomerated into a larger Ag metal clusters. This suggestion was confirmed by TEM, as shown in Figure 4.7.

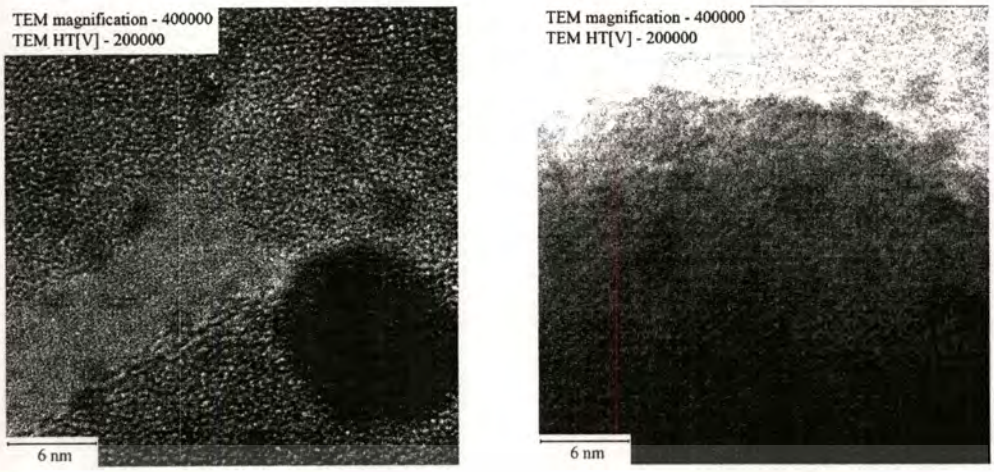

(a) (b)

Figure 4.7 TEM micrograph of (a) red-5AgHZSM-5(11) and (b) red-5AgHZSM-5(28). The Ag crystals are distinguishable on the surface of the zeolite.

It can be seen that Ag metal particle sizes of ~ 3 nm and ~ 15 nm were obtained over 5AgHZSM-5(11), whilst those of ~ 3 nm were evenly dispersed on the outer surface of 5AgHZSM-5(28). Hence, it confirms that such large Ag metal clusters cannot readily undergo reversible interconversion, due to its relatively higher stability, as discussed earlier.

The NH_3-TPD profiles of the 3AgHZSM-5(11) and 3AgHZSM-5(28) samples also suggests the effect of acid sites for the reversible interconversion, as shown in Figure 4.8.

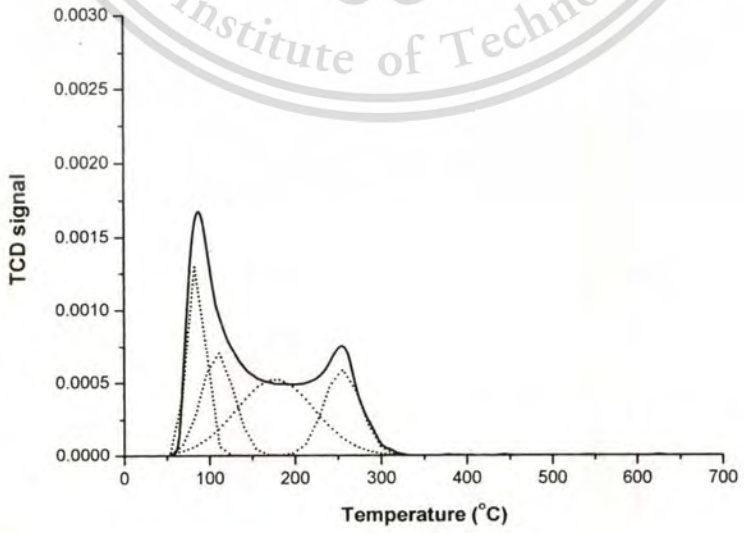

(c)

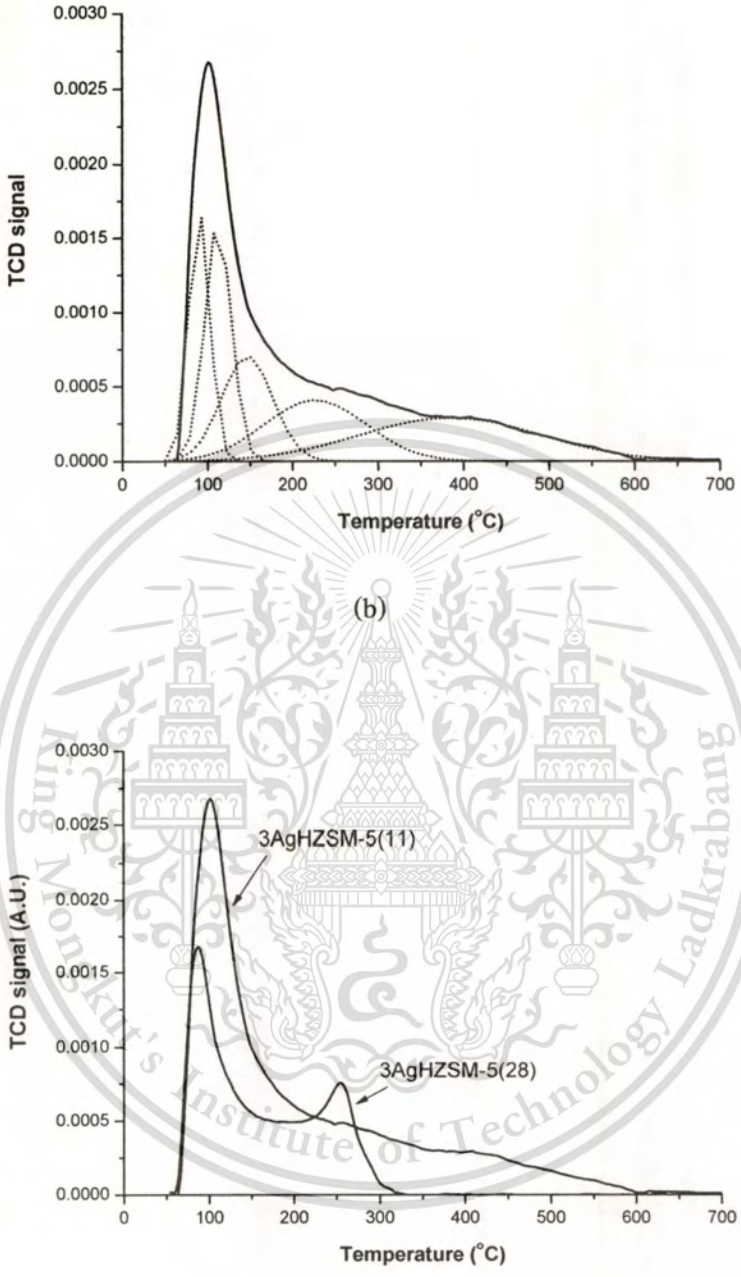

Figure 4.8 NH_3-TPD profiles of (a) comparison data of 3AgHZSM-5(11) and 3AgHZSM-5(28) catalysts. Gaussian deconvolution of the NH_3-TPD signal of (b) 3AgHZSM-5(11) and (c) 3AgHZSM-5(28).

Typically, the spectra of HZSM-5 exhibits two characteristic peaks [28,29]; (i) from the NH_3 adsorbed on Si–OH or from non-zeolitic impurity (~50-200 °C), and (ii) from the NH_3 adsorbed on the acidic hydroxide group ≡Si–OH–Al≡ (~300-450 °C). However, the peak position can be shifted when the metal was incorporated [30]. The TPD profiles of both 3AgHZSM-5(11) and 3AgHZSM-5(28) were deconvoluted by the Gaussian curve-fitting method; hence, several desorption peaks are revealed. These are suggested to derive form additional NH_3 adsorbed on the Ag cationic sites. Consistent with the suggestion that Ag cations are retained in the 3AgHZSM-5(28), a distinct desorption, observed particularly in this sample at ~250 °C, is believed to be the NH_3 adsorbed on the Ag cations.

It is also obvious that 3AgHZSM-5(28) possesses no significant amount of strong acid sites (~300-450 °C), which this can be observed as a broad peak in 3AgHZSM-5(11). The difference in the amount and strength of Brønsted sites in these two samples may well influence their reversible interconversion, in addition to the effect of the Ag-cluster size as discussed earlier.

Together with the observed higher reduction temperature (Figure 4.3) for Ag cationic clusters in 3AgHZSM-5(28), it is now certain that, after reduction at 425 °C, the charge-balancing Ag cations in this particular sample, are indeed reduced into Ag cationic clusters, and some may well be further reduced to Ag metal clusters. During a slow cooling down from 425 °C under inert atmosphere, the Ag cationic clusters can undergo reversible interconversion into charge-balancing Ag cations, liberating H_2 as shown in Eq. (6).

$$ZO\text{-}Ag_n^+ + (n\text{-}1)ZO\text{-}H \longrightarrow nZO\text{-}Ag^+ + \left(\frac{n-1}{2}\right)H_2 \qquad \text{Eq. (6)}$$

The Ag metallic clusters would require a higher temperature for the reversible interconversion. This hypothesis is readily illustrated by TPHE experiment. It can be clearly seen from Figure 4.9 that H_2 gas is evolved at ~700 °C from the primarily reduced 3AgHZSM-5(28) upon re-heating under an inert Ar stream.

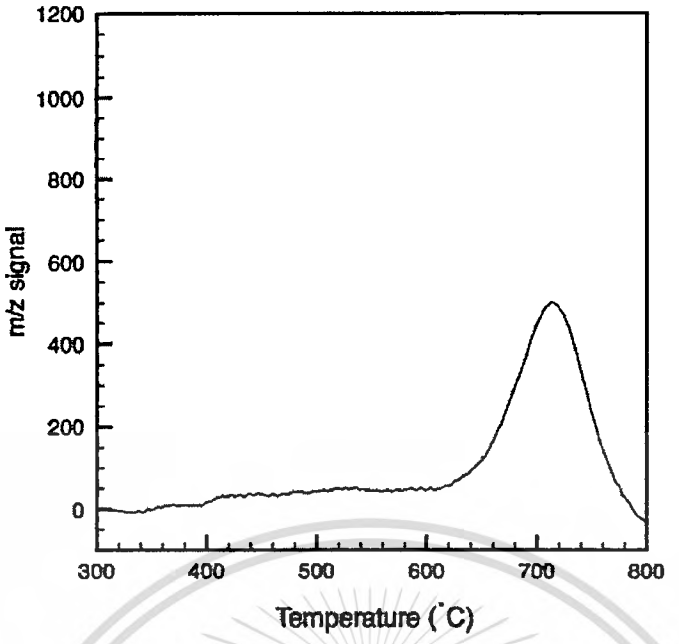

Figure 4.9 TPHE of 3AgHZSM-5(28).

The only explanation for such observations is that the remaining Ag metallic clusters can readily react with Brønsted acid, as suggested earlier (Eq. (5)). This is because most of the Ag cationic clusters, formed at 425 °C, would readily react with Brønsted acid sites forming charge-balancing Ag cations after cooling in inert He stream, as demonstrated by another low temperature TPR experiment (Figure 4.10).

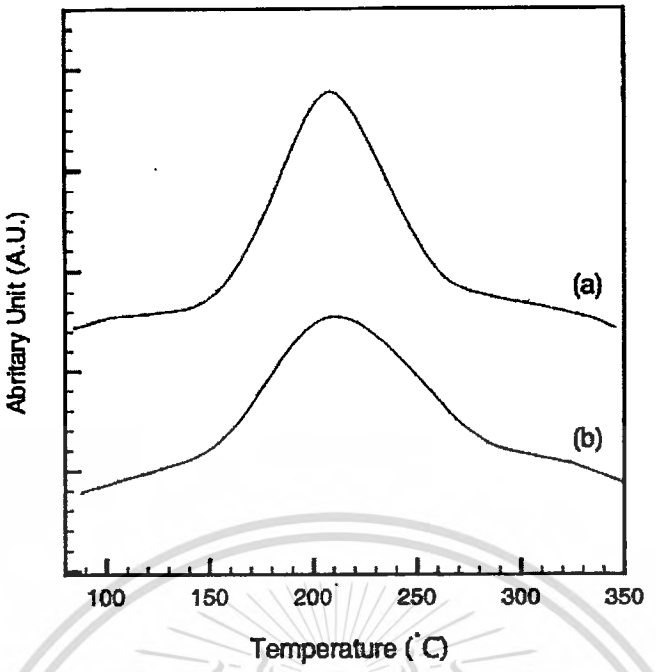

Figure 4.10 Primary (a) and secondary (b) H_2-TPR profiles of 3AgHZSM-5(28).

[a] *In a TCD detector, the samples were heated in a flow of 2% H_2/Ar (30 mL/min) with a heating rate of 10 °C/min to 350 °C.*

[b] *After primary TPR experiments, the samples were then cooled to 50 °C in a flow of He and the experiments were repeated under the same condition.*

In this test, TPRs of 3AgHZSM-5(28) were just completed up to 350 °C, to ensure that only cationic Ag clusters were formed. It can be seen from Figure 4.10 that a repeat H_2 consumption is obtained in secondary TPR, indicating a readily reversible interconversion of cationic Ag clusters in this sample. Accordingly, the reduced species that exhibit TPHE at 700 °C (Figure 4.9), would only be the relatively stable metallic Ag clusters that have withstood the reversible interconversion at lower temperature.

To investigate the existence of various Ag species, the DR-UV and XANES were performed.

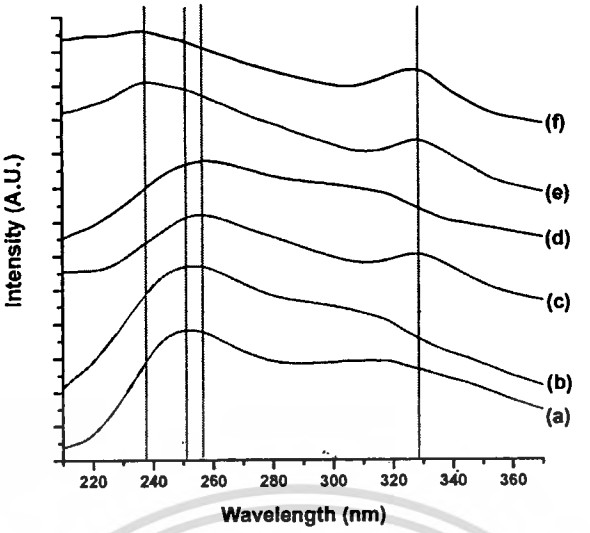

Figure 4.11 DR-UV of (a) 3AgHZSM-5(11), (b) 3AgHZSM-5(28), (c) 1st-red-3AgHZSM-5(11), (d) 1st-red-3AgHZSM-5(28), (e) 2nd-red-3AgHZSM-5(11), and (f) 2nd-3AgHZSM-5(28).

Figure 4.11 shows UV-vis spectra of 3AgHZSM-5 zeolite before and after the H_2-TPR experiment. The bands at 252 nm assignable to the $4d^{10}$ to $4d^9 5s^1$ transition of Ag^+ ion [31-34] were observed over both 3AgHZSM-5(11) (Figure 4.11a) and 3AgHZSM-5(28) (Figure 4.11b). After the primary H_2-TPR experiment, strong bands around 257 nm were observed (Figure 4.11c and d). As the H_2-TPR result suggesting the formation of the Ag cationic cluster, the bands at 257 nm can be tentatively assigned to the electronic transition of Ag cationic cluster. The positions of these bands are close to those reported by Gachard *et. al.* assigning a UV absorption band at 265 nm to Ag cationic cluster [35]. In addition, the band around 329 nm possibly due to the electronic transition of small Ag metal particles [31-35] was observed only the 3AgHZSM-5(11) samples (Figure 4.11c). Consistent with the result that X-ray diffraction lines of the metallic Ag crystallites appear in the 3AgHZSM-5(11) treated under H_2 gas (Figure 4.11c), it is obvious that Ag metal particles are the major species in this sample. Note that bands around 329 nm were also observed over the secondary H_2-TPR samples (Figure 4.11e and f). It is confirmed that after the severe H_2 reduction, the Ag metallic phase can be formed. Such metallic Ag clusters are resistant to the reversible interconversion, hence, the metallic Ag species can be dominantly obtained in both samples. This result indicates that the Ag species in 3AgHZSM-5(11) and 3AgHZSM-5(28) are not really the same only after the primary reduction. The charge-balancing Ag cations in

3AgHZSM-5(11) can be readily reduced into Ag cationic and consecutive Ag metallic species. In contrast, most of the primarily reduced Ag species in the 3AgHZSM-5(28) sample are Ag cationic clusters. Only under the severe H_2 reduction, the reduced Ag species in 3AgHZSM-5(28) would then agglomerate into larger and more stable Ag metal clusters.

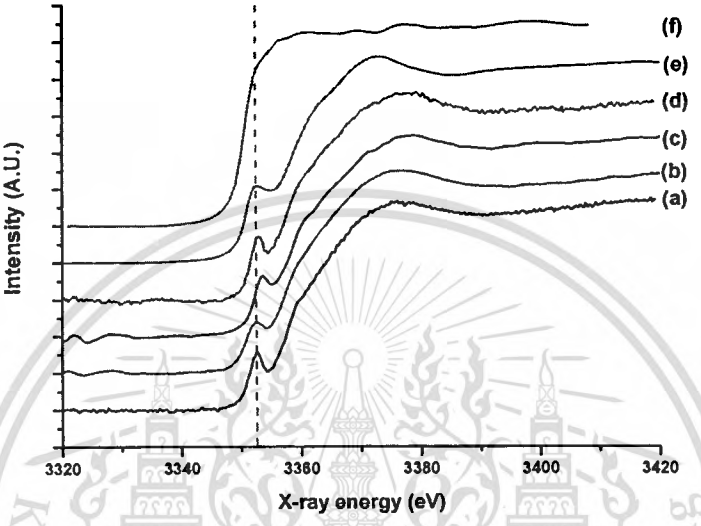

Figure 4.12 Ag L_3-edge XANES spectra of (a) 3AgHZSM-5(11), (b) 3AgHZSM-5(28), (c) red-3AgHZSM-5(11), (d) red-3AgHZSM-5(28), (e) $AgNO_3$, and (f) silver foil.

Further evidence supporting above discussion is XANES. Figure 4.12 shows L_3-edge XANES spectrum of 3AgHZSM-5 before and after the H_2 treatment at 425 °C, together with those of Ag metal and $AgNO_3$ as references. It can be seen that the XANES spectrum of both 3AgHZSM-5(11) and 3AgHZSM-5(28) were close to that of $AgNO_3$ (~ 3352 eV), suggesting that Ag species in this sample are present as Ag cations [36,37]. After H_2 treatment at 425 °C, the XANES spectrum of 3AgHZSM-5(11) slightly shifts toward high energy (Figure 4.12c). This is presumably due to the formation of Ag metallic species in 3AgHZSM-5(11) as primarily observed by XRD (Figure 4.1c) when treated with H_2 under the same condition. However, the different XANES spectrum characteristic as compared to that of Ag foil is presumably due to the smaller Ag cluster size of Ag metal formed over in this sample [34,37-39]. In contrast, XANES spectrum of the reduced 3AgHZSM-5(28) (Figure 4.12d) was similar to that prior to reduction and to $AgNO_3$ sample suggesting that the cationic species is retained in this sample.

It can be primarily concluded at this state that, the double H_2-TPR and the TPHE does not only confirm the reversible interconversion of Ag species in AgHZSM-5, but also give evidence for the existence of some different Ag species retaining after primarily reduction and surviving from the reversible interconversion at 425 °C, as supported by DR-UV and XANES. This clearly depicts the difference in Ag species in AgHZSM-5(11) and AgHZSM-5(28) after reduction at 425 °C. As TPR (Figure 4.3) shows that the charge-balancing Ag cations in AgHZSM-5(11) can be easily reduced into Ag metallic species, this sample is resistant to reversible interconversion at 425 °C. Hence, a stable metallic phase is retained (by XRD). The sample also reveals recoverable acid sites (by NMR) and relatively less H_2 consumption in secondary TPR (Figure 4.4a). In contrast, AgHZSM-5(28) founds it somewhat difficult to be completely reduced at this temperature. Most of the reduced Ag species in this sample are Ag cationic clusters, with small amounts of the metallic ones. Therefore, the reduced Ag species in AgHZSM-5(28) can readily undergo reversible interconversion at 425 °C, showing no metal phase (by XRD), non-recoverable acid sites and again a relatively higher H_2 consumption in secondary TPR (Figure 4.4b). The small amounts of metallic Ag clusters formed in AgHZSM-5(28), can survive the reversible interconversion at 425 °C and can evolve H_2 at higher temperatures as evidenced by TPHE experiments (Figure 4.9).

In the catalytic point of view, a complete reversible interconversion would not be preferred for acid-catalyzed reactions because it leads to the decrease in active Brønsted acid sites. This is indeed observed by the ethanol conversion over 3AgHZSM-5(28).

Table 4.2 Product distribution of ethanol conversion over modified ZSM-5 catalysts[a].

Catalyst	Product distribution (% carbon yield)[b]					
	C2	C3	C4	C5-C8	BTX[c]	C9+
HZSM-5(11)	13.3	29.4	27.7	1.9	17.8	9.8
3AgHZSM-5(11)	19.8	15.7	16.7	1.9	27.4	18.5
HZSM-5(28)	21.6	25.0	23.9	4.3	13.0	12.2
3AgHZSM-5(28)	96.2	0.0	1.3	0.1	0.7	1.7
3AgHZSM-5(28)/H_2	36.2	23.0	24.6	4.0	6.1	6.2

[a] Reaction conditions: Temperature = 425 °C, Pressure = 1 atm, Carrier gas = N_2 or H_2, W/F = 6.75 g·h/mol.

[b] Product distribution at 1 hour on stream.

[c] BTX = benzene, toluene, ethylbenzene and xylenes.

It can be seen in Table 4.2 that the activity and the BTX selectivity obtained from 3AgHZSM-5(28) are exceedingly low, as compared to those of HZSM-5(28). While an increase in the catalytic activity towards aromatization is observed over 3AgHZSM-11, as compared to HZSM-5(11). This is clearly because Brønsted acid sites cannot be recovered in 3AgHZSM-5(28), due to the reversible interconversion of the reduced Ag species. The decrease in acid sites would leave ethylene mainly unreacted since the protonation of ethylene is a rate-determining step and the dehydration of ethanol to ethylene is virtual completely. Hence, such a decrease in Brønsted acid site results in a complete conversion of ethanol to ethylene but with lower BTX.

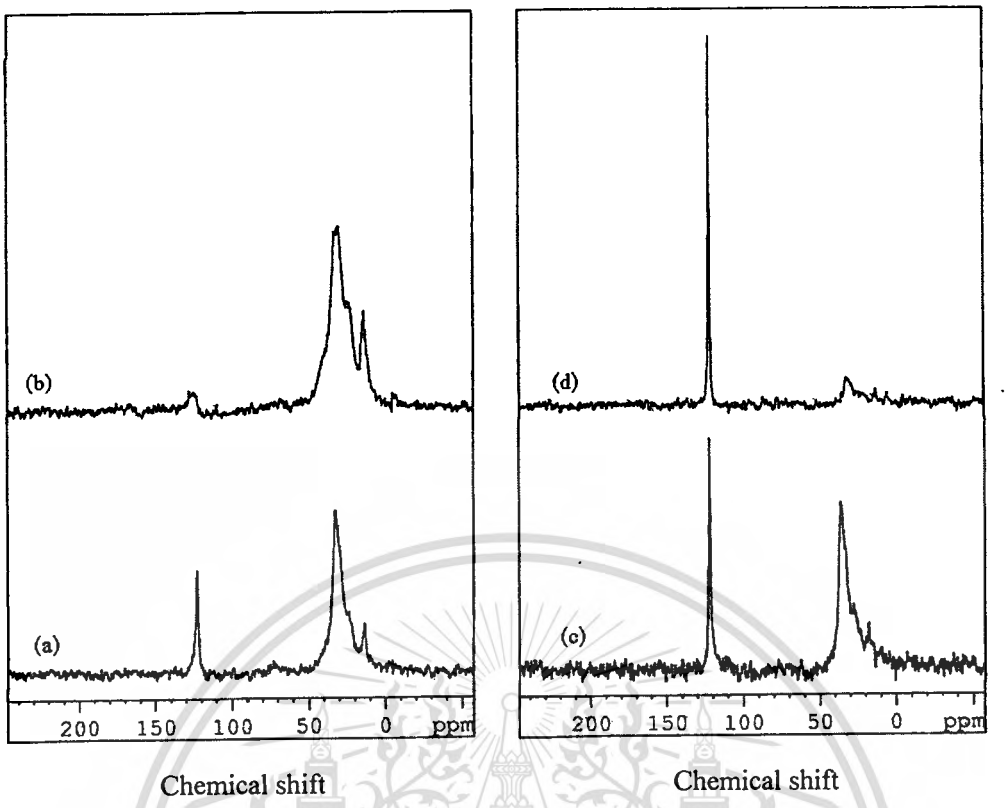

Figure 4.13 *In situ* ^{13}C MAS NMR spectra of Ag-modified HZSM-5 zeolite (a) HZSM-5(11), (b) 3AgHZSM-5(11), (c) HZSM-5(28), and (d) 3AgHZSM-5(28).

In support with this view their catalytic behavior of 3AgHZSM-5, Figure 4.13 shows the ^{13}C MAS NMR spectra recorded on the conversion of ethylene at 60 °C over Ag-modified zeolite. As compared with the HZSM-5(11), the spectrum of 3AgHZSM-5(11) (Figure 4.13b) shows a marked increase in the signals at 10-50 ppm due to the oligomerized products of ethylene [40-43]. This result is consistent with the observed high catalytic activity of 3AgHZSM-5(11) for the ethanol conversion (Table 4.2). However, small amounts of ethylene (125 ppm) [43,44] can be converted to oligomerized products (10-50 ppm) for over 3AgHZSM-5(28), as compared to that in HZSM-5(28). This supports the suggestion that Brønsted acid sites cannot be recovered in 3AgHZSM-5(28), due to the reversible interconversion of the reduced Ag species.

Since the reversible interconversion would be thermodynamically favored in the absence of H_2, preventing this reaction may well be achieved by keeping the reduced Ag species in a H_2 stream. This was actually tested by another TPHE experiment, in which 3AgHZSM-5(28) was subjected to be reduced at 425 °C and cooled down in a H_2 flow, instead a flow of the inert gas. This is intended to keep all the reduced Ag species in its forms, and to prevent the reversible

interconversion that might have taken place during the cooling period. The sample was then flushed with Ar at 50 °C to ensure that no physisorbed hydrogen was on the surface. From this TPHE experiment (Figure 4.14), it can be clearly seen again that H_2 evolves, at relatively low temperature, from the primarily reduced 3AgHZSM-5(28).

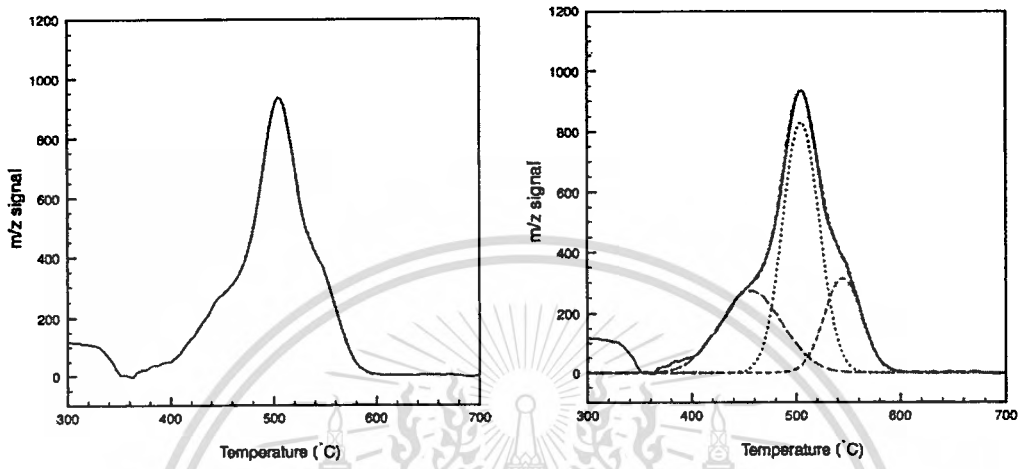

Figure 4.14 TPHE of 3AgHZSM-5(28) kept in H_2 stream after reduction. Gaussian deconvolution of the TPHE signal is presented on the right.

With the Gaussian deconvolution, there appear to be three different H_2 evolutions at 447 °C, 505 °C and 545 °C. Since excessive amounts of H_2 are evolved in this experiment, as compared to that cooled in He (Figure 4.9), one of these signals would arise from desorption of the chemisorbed hydrogen on the reduced Ag species. The other two signals would have been contributed from the reversible interconversion of two different reduced Ag species. If one compares the signal intensity with that of the previous TPHE (Figure 4.9), it is reasonable to presume that the signal at 505 °C may be referred to as chemisored H_2 and the signals at 447 °C and 545 °C are due to the cationic and metallic Ag clusters, respectively. It is believed that in the presence of chemisorbed H_2 the metallic Ag clusters may be formed as small clusters. This would lead to a relatively lower temperature for the reversible interconversion in this experiment. Nevertheless, this TPHE result indicates that the reduced Ag species, particularly the Ag cationic clusters, are indeed preserved during the cooling period and undergo reversible interconversion as a prove of its existence.

Accordingly, it is expected that using H_2 as carrier gas in the reaction would keep the Ag species in a reduced form and hold the acid sites on the framework. Consistent with this view, when the ethanol conversion was tested under a flow of H_2, it was found that a relatively higher activity and BTX selectivity were obtained from 3AgHZSM-5(28), as compared with that using N_2 as a carrier gas (Table 4.2). As the acidity is pronounced upon the reduction of Ag cations, the acid-catalyzed reactions, such as alkylation, cyclization, aromatization, are therefore facilitated.

The recoverable acid sites are indeed observed by another ^{1}H-NMR experiment (Figure 4.15), in which 3AgHZSM-5(28) is reduced at relatively mild reduction temperature (350 °C) for 2 hours, then cooled and kept under H_2.

Figure 4.15 ^{1}H spin-echo MAS NMR spectra of (a) 3AgHZSM-5(28), (b) 3AgHZSM-5(28) reduced at 350 °C for 2 hours, then cooled and kept under H_2, and (c) red-3AgHZSM-5(28).

Unlike the sample cooled in He (Figure 4.2), this reduced 3AgHZSM-5(28) truly reveals recoverable Brønsted acid sites. This again confirms that the presence of H_2 can readily prevent reversible interconversion of the reduced Ag species and that the Brønsted acid sites can be conserved. The ^{1}H-NMR of this particular sample (Figure 4.15) also reveals an additional obscure peak at -0.5 ppm. Since it appears at an extraordinarily high field, this species must have experienced a highly electron-rich environment. Due to the fact that it is only pronounced when 3AgHZSM-5(28) is reduced and kept in hydrogen, the signal at -0.5 ppm can be plausibly referred to the "hydride" species associated with cationic or metallic Ag clusters [9,45]. It is believed that H_2 not only keeps Ag species in its reduced forms but H_2 can also chemisorb on such reduced Ag species and consecutively dissociate to form silver hydride (Ag-H) (Eq. (3)). In addition, the existence of the silver hydride species is in good agreement with the proposed chemisorbed H_2 that evolved at 505 °C in the previous TPHE experiment (Figure 4.14).

From the above, it is very interesting that, in a catalyst, both acidic protons (~3.9 ppm) and hydrides (~ -0.5 ppm) can readily exist and be observed at the same time. This is another beautiful example of locally catalytic sites generated within the micropores of zeolite, and may well support the explanation for the enhanced catalytic activity for BTX production when silver is incorporated. Since the hydride transfer play an important role in the aromatization of hydrocarbons over acid catalysts [46-49], the presence of the reduced Ag species that form and stabilize hydride species without interfering with the acid function would allow a rapid hydrogen transfer from the carbocation intermediates. This would readily facilitate the formation of aromatics [50,51] from light hydrocarbons. Although this cannot be clearly demonstrated by 3AgHZSM-5(28), due to its low acidity (high Si/Al), the enhanced activity due to incorporated Ag is clearly shown by its higher acidity counterpart, the 3AgHZSM-5(11). In Table 4.2, higher BTX selectivity is readily obtained from 3AgHZSM-5(11), as compared with HZSM-5(11) which also well agrees with the previous reports [12,52].

4.4 Conclusions

In AgHZSM-5, the Si/Al ratio of the host zeolite strongly influences the reducibility of the Ag species and the types of the reduced Ag species formed. Upon reduction with H_2 at 425 °C, metallic Ag clusters are readily formed in a low silica sample, AgHZSM-5(11). This is due to the closely proximate sites that allow the reduced Ag species to agglomerate into larger and more

stable Ag metal clusters. TPR and TPHE experiments also evidence that the metallic Ag clusters are resistant to the reversible interconversion up to ~700 °C. It is presumed that the larger the metal clusters, the less easily it can react with the neighboring Brønsted acid sites. For AgHZSM-5(28), a higher silica sample, most of the reduced Ag species, formed at 425 °C, are cationic Ag clusters with small amounts of the metallic ones. This may well be due to a better interaction of the softer cationic Ag clusters with the soft framework of high silica zeolites. Under inert atmosphere, the cationic Ag clusters can readily undergo reversible interconversion at relatively low temperature (<425 °C). This leads to no observation of recoverable acid sites and Ag metal phases (by XRD, DR-UV and XANES) in this sample after reduction at 425 °C. ^{1}H MAS NMR results show that by keeping the sample under a flow of H_2, the reduced Ag species and Brønsted acid sites can be preserved. In addition, a hydride species was evidenced, suggesting a possibility for the catalyst to promote hydride transfer. This is consistent with the observed increase in catalytic activity when hydrogen is present in the reaction.

References

[1] Kim Y., Seff K. "The Octahedral Hexasilver Molecule. Seven Crystal Structures of Variously Vacuum-Dehydrated Fully Ag^{+}-Exchanged Zeolite A" **Journal of the American Chemical Society**. vol. 100, 1978. pp. 6989-6997.

[2] Xu B., Kevan L. "Formation of Silver Ionic Clusters and Silver Metal Particles in Zeolite Rho Studied by Electron Spin Resonance and Far-Infrared Spectroscopies" **The Journal of Physical Chemistry**. vol. 95, 1991. pp. 1147-1151.

[3] Lee S.H., Kim Y. and Seff K. "Weak Ag^{+}-Ag^{+} Bonding in Zeolite X. Crystal Structure of $Ag_{92}Si_{100}Al_{92}O_{384}$ Hydrated and Fully Dehydrated in Flowing Oxygen" **Microporous and Mesoporous Materials**. vol. 41, 2000. pp. 49-59.

[4] Lamberti C., Prestipino C., Bordiga S., Fitch A.N. and Marra C.L. "Characterization of Isolated Ag Cations in Homoionic Ag-Y Zeolites: A Combined Anomalous XRPD and EXAFS Study" **Nuclear Instruments and Methods in Physics Research B**. vol. 200, 2003. pp. 155-159.

[5] Lins J.O.M.A, Nascimento M.A.C. "A Density Functional Study of Some Silver Cluster Hydrides" **Chemical Physics Letters**. vol. 391, 2004. pp. 9-15.

[6] Suzuki Y., Matsumoto N., Ainai T., Miyanaga T. and Hoshino H. "*In situ* Infrared and EXAFS Studies of an Ag Cluster in Zeolite X" **Polyhedron**. vol. 24, 2005. pp. 685-691.

[7] Yoshida H., Hamajima T., Kato Y., Shibata J., Satsuma A. and Hattori T. "Active Ag Species in MFI Zeolite for Direct Methane Conversion in the Light and Dark" **Research on Chemical Intermediates**. vol. 29, 2003. pp. 897-910.

[8] Kanan S.M., Kanan M.C. and Patterson H.H. "Photophysical Properties of Ag(I)-exchanged Zeolite A and the Photoassisted Degradation of Malathion" **The Journal of Physical Chemistry B**. vol. 105, 2001. pp. 7508-7516.

[9] Baba T., Sawada H., Takahashi T. and Abe M. "Chemisorption Study of Hydrogen and Methane by ^{1}H MAS NMR and Conversion of Methane in the Presence of Ethylene on Ag-Y Zeolite" **Applied Catalysis A: General**. vol. 231, 2002. pp. 55-63.

[10] Shibata J., Takada Y., Shichi A., Satokawa S., Satsuma A. and Hattori T. "Influence of Zeolite Support on Activity Enhancement by Addition of Hydrogen for SCR of NO by

Propane over Ag-Zeolites" **Applied Catalysis B: Environmental.** vol. 54, 2004. pp. 137-144.

[11] Shibata J., Takada Y., Shichi A., Satokawa S., Satsuma A. and Hattori T. "Ag Cluster as Active Species for SCR of NO by Propane in the Presence of Hydrogen over Ag-MFI" **Journal of Catalysis.** vol. 222, 2004. pp. 368-376.

[12] Inoue Y., Nakashiro K. and Ono Y. "Selective Conversion of Methanol into Aromatic Hydrocarbons over Silver-Exchanged ZSM-5 Zeolites" **Microporous Materials.** vol. 4, 1995. pp. 379-383.

[13] Konova P., Arve K., Klingstedt F., Nikolov P., Naydenov A., Kumar N. and Murzin D.Y. "A Combination of Ag/Alumina and Ag-Modified ZSM-5 to Remove NO_x and CO During Lean Conditions" **Applied Catalysis B: Environmental.** vol. 70, 2007. pp. 138-145.

[14] Beyer H., Jacobs P.A. and Uytterhoeven J.B. "Redox Behavior of Transition Metal Ions in Zeolites. Part 2.-Kinetic Study of the Reduction and Reoxidation of Silver-Y Zeolites" **Journal of the Chemical Society, Faraday Transaction 1: Physical Chemistry in Condensed Phase.** vol. 72, 1976. pp. 674-685.

[15] Gellens L.R., Mortier W.J. and Uytterhoeven J.B. "Oxidation and Reduction of Silver in Zeolite Y: A Structural Study" **Zeolites.** vol. 1, 1981. pp. 85-90.

[16] Gellens L.R, Mortier W.J., Schoonheydt R.A. and Uytterhoeven J.B. "The Nature of the Charged Silver Clusters in Dehydrated Zeolites of Type A" **The Journal of Physical Chemistry.** vol. 85, 1981. pp. 2783-2788.

[17] Heemsoth J., Tegeler E., Roessner F. and Hagen A. "Generation of Active Sites for Ethane Aromatization in ZSM-5 Zeolites by a Solid-State Reaction of Zinc Metal with Brønsted Acid Sites of the Zeolite" **Microporous and Mesoporous Materials.** vol. 46, 2001. pp. 185-190.

[18] Baker M.D., Ozin G.A. and Godber J. "Far-Infrared Studies of Silver Atoms, Silver Ions, and Silver Clusters in Zeolites A and Y" **The Journal of Physical Chemistry.** vol. 89, 1985. pp. 305-311.

[19] Berndt H., Richter M., Gerlach T. and Barerns M. "Influence of Brønsted Acidity on the Redox Properties of Silver Species in Zeolite Mordenite" **Journal of the Chemical Society, Faraday Transaction.** vol. 94, 1998. pp. 2043-2046.

[20] Li Z., Flytzani-Sterhanopoulos M. "Selective Catalytic Reduction of Nitric Oxide by Methane over Cerium and Silver Ion-Exchanged ZSM-5 Zeolites" **Applied Catalysis A: General**. vol. 165, 1997. pp. 15-34.

[21] Li Z., Flytzani-Sterhanopoulos M. "On the Promotion of Ag-ZSM-5 by Cerium for the SCR of NO by Methane" **Journal of Catalysis**. vol. 182, 1999. pp. 313-327.

[22] Shichi A., Kawamura Y., Satsuma A. and Hattori T. "30-O-03-Effect of Carbon Number in Hydrocarbon Reductant on the Selective Catalytic Rduction of NO over Cation-Exchanged MFI Zeolites" **Studies in Surface Science and Catalysis**. vol. 135, 2001. pp. 172.

[23] Anderson M.W., Barrie P.J. and Klinowski J. "^{1}H Magic-Angle-Spinning NMR Studies of the Adsorption of Alcohols on Molecular Sieve Catalysts" **The Journal of Physical Chemistry**. vol. 95, 1991. pp. 235-239.

[24] Beck L.W., White J.L. and Haw J.F. "^{1}H {^{27}Al} Double-Resonance Experiments in Solids: An Unexpected Observation in the ^{1}H MAS NMR Spectrum of Zeolite HZSM-5" **Journal of the American Chemical Society**. vol. 116, 1994. pp. 9657-9661.

[25] Hunger M., Freude D. and Pfeifer H. "Magic-Angle Spinning Nuclear Magnetic Resonance Studies of Water Molecules Adsorbed on Brønsted- and Lewis-acid Sites in Zeolites and Amorphous Silic-Aluminas" **Journal of the Chemical Society, Faraday Transactions**. vol. 87, 1991. pp. 657-662.

[26] Hunger M. "Brønsted Acid Sites in Zeolites Characterized by Multinuclear Solid-State NMR Spectroscopy" **Catalysis Reviews Science and Engineering**. vol. 39, 1997. pp. 345-393.

[27] Shibata J., Shimizu K., Takada Y., Shichi A., Yoshida H., Satokawa S., Satsuma A. and Hattori T. "Structural of Active Ag Clusters in Ag Zeolites for SCR of NO by Propane in the Presence of Hydrogen" **Journal of Catalysis**. vol. 227, 2004. pp. 367-374.

[28] Hidalgo C.V., Itoh H., Hattori T., Niwa M. and Murakami Y. "Measurement of the Acidity of Various Zeolites by Temperature-Programmed Desorption of Ammonia. **Journal of Catalysis**. vol. 85, 1984. pp. 362-369.

[29] Post J.G., van Hoff J.H.C. "Acidity and Activity of H-ZSM-5 Measured with NH_3-t.p.d. and *n*-Hexane Cracking" **Zeolites**. vol. 4, 1984. pp. 9-14.

[30] Ma D., Zhang W., Shu Y., Liu X., Xu Y. and Bao X. "MAS NMR, ESR and TPD Studies of Mo/HZSM-5 Catalysts: Evidence for the Migration of Molybdenum Species into the Zeolitic Channels" **Catalysis Letter**. vol. 66, 2000. pp. 155–160.

[31] Shibata J., Takada Y., Shichi A., Satokawa S., Satsuma A. and Hattori T., "Ag Cluster as Active Species for SCR of NO by Propane in the Presence of Hydrogen over Ag-MFI" **Journal of Catalysis**. vol. 222, 2004. pp. 368-376.

[32] Shibata J., Takada Y., Shichi A., Satokawa S., Satsuma A. and Hattori T., "Influence of Zeolite Support on Activity Enhancement by Addition of Hydrogen for SCR of NO by Propane over Ag-Zeolites" **Applied Catalysis B: Environmental**. vol. 54, 2004. pp. 137-144.

[33] Li Z., Flytzani-Sterhanopoulos M., "On the Promotion of Ag-ZSM-5 by Cerium for the SCR of NO by Methane" **Journal of Catalysis**. vol. 182, 1999. pp. 313-327.

[34] Shibata J., Shimizu K., Takada Y., Shichi A., Yoshida H., Satokawa S., Satsuma A. and Hattori T., "Structure of Active Ag Clusters in Ag Zeolites for SCR of NO by Propane in the Presence of Hydrogen" **Journal of Catalysis**. vol. 227, 2004. pp. 367-374.

[35] Gachard E., Belloni J. and Subramanian M.A., "Optical and EPR Spectroscopic Studies of Silver Clusters in Ag, Na-Y Zeolite by γ-irradiation" **Journals of Materials Chemistry**. vol. 6, 1996. pp. 867-870.

[36] Behrens P., "Bonding in Silver-Oxygen Compounds from Ag L3 XANES Spectroscopy" **Solid State Communications**. vol. 81. 1992. pp. 235-239.

[37] Bernieri E., Burattini E., Dalba G., Fornasini P. and Rocca F., "X-ray Absorption Measurements at the L3 Edge on Silver Borate Glasses with Synchrotron Radiation" **Solid State Communications**. vol. 48, 1983. pp. 421-425.

[38] Matsuoka M., Matsuda E., Tsuji K., Yamashita H. and Anpo M., "The Photocatalytic Decomposition of Nitric Oxide on Ag+/ZSM-5 Catalyst Prepared by Ion-Exchange" **Journal of Molecular Catalysis A: General**. vol. 107, 1996. pp. 399-403.

[39] Shimizu K., Shibata J., Yoshida H. Satsuma A. and Hattori T., "Silver-Alumina Catalysts for Selective Reduction of NO by Higher Hydrocarbons: Structure of Active Sites and Reaction Mechanism" **Applied Catalysis B: Environmental**. vol. 30, 2001. pp. 151-162.

[40] Hunger M., "*In situ* Flow MAS NMR Spectroscopy: State of the Art and Applications in Heterogeneous Catalysis" **Progress in Nuclear Magnetic Resonance Spectroscopy**. vol. 53, 2008. pp. 105-127.

[41] Derouane E.G., Heyong H., Hamid S.B.D. and Ivanova I.I., "*In situ* MAS NMR Investigations of Molecular Sieves and Zeolite-Catalyzed Reactions" **Catalysis Letters.** vol. 58, 1999. pp. 1-19.

[42] Ivanova I.I., Nesterenko N.S. and Fernandez C., "*In situ* MAS NMR Studies of Alkylaromatics Transformations over Acidic Zeolites" **Catalysis Today**. vol. 113, 2006. pp. 115-125.

[43] Hunger M., "*In situ* NMR Spectroscopy in Heterogeneous Catalysis" **Catalysis Today.** vol. 97, 2004. pp. 3-12.

[44] Wang W., Jiang Y. and Hunger M., "Mechanistic Investigations of the Methanol-to-Olefin (MTO) Process on Acidic Zeolite Catalysts by *In situ* Solid-State NMR Spectroscopy" **Catalysis Today**. vol. 113, 2006. pp. 102-114.

[45] Baba T., Tohjo Y., Takahashi T., Sawada H. and Ono Y. "Properties of Chemisorbed Hydrogen Species on Ag-A Zeolite Partially Reduced with Hydrogen as Studied by 1H MAS NMR" **Catalysis Today**. vol. 66, 2001. pp. 81-89.

[46] Kitagawa H., Sendoda Y. and Ono Y. "Transformation of Propane into Aromatic Hydrocarbons over ZSM-5 Zeolites" **Journal of Catalysis**. vol. 101, 1986. pp. 12-18.

[47] Gnep N.S., Doyemet J.Y., Seco A.M., Ribeiro F.R. and Guisnet M. "Conversion of Light Alkanes into Aromatic Hydrocarbons: 1-Dehydrocyclodimerization of Propane on PtHZSM-5 Catalysts" **Applied Catalysis**. vol. 35, 1987. pp. 93-108.

[48] Iglesia E., Baumgartner J.E. "Hydrogen Transfer and Activation of Propane and Methane on ZSM5-Based Catalysts. **Catalysis Letters.** vol. 21, 1993. pp. 55-70.

[49] Liu C., Deng Y., Pan Y., Gu Y., Qiao B. and Gao X. "Effect of ZSM-5 on the Aromatization Performance in Cracking Catalyst" **Journal of Molecular Catalysis A: Chemical**. vol. 215, 2004. pp. 195-199.

[50] Huang M., Kaliaguine S. "Propene Aromatization over Alkali-Exchanged ZSM-5 Zeolites" **Journal of Molecular Catalysis.** vol. 81, 1993. pp. 37-49.

[51] Bayense C.R., van der Pol A.J.H.P. and van Hooff J.H.C. "Aromatization of Propane over MFI-Gallosilicates" **Applied Catalysis.** vol. 72, 1991. pp. 81-98.

[52] Ono Y., Osako M., Kim G.J. and Inoue Y. "Ag-ZSM-5 as a Catalyst for Aromatization of Alkanes, Alkenes, and Methanol" **Studies in Surface Science and Catalysis**. vol. 84, 1994. pp. 1773-1780.

Chapter 5

Additional Brønsted Acid Sites in [Ga]HZSM-5 Formed by the Presence of Water

5.1 Introduction

Gallium-containing zeolites have been extensively investigated due to their unique catalytic performances in light hydrocarbon aromatization [1-8]. The active Ga species were suggested to be the non-framework Ga species present in the zeolite under reducing atmosphere (either by H_2 or the hydrocarbon feeds). Such species including Ga^{3+}, GaO^+, Ga_2O, and Ga^+, were believed to be responsible for dehydrocyclization activity [9-12]. The synergetic effect by Ga species and the acid sites of zeolite was also derived from the facilitated adsorption of hydrocarbons and desorption of H_2 over acid sites, respectively [13-15]. Accordingly, the concentration of acid sites and Ga dispersion would play significant roles in the aromatization activity of gallium-containing zeolites [16].

It is worth noting that all the proposed Ga species are high in Lewis acid character [17]. Thus, in the presence of water, the interaction of hydrocarbon feed with the above Ga species could be modified. With this view, one could expect that a competitive adsorption of water against the hydrocarbon feed and hydrogen on such Ga species would lead to a drop in the activity, as generally observed over other metal loaded catalysts [18-20]. However, an increase in aromatic yield can be obtained for the conversion of methanol over [Ga]HZSM-5 [21,22] even though a large amount of water is present, as co-product, in the reaction stream. This marked behaviour of Ga-containing zeolite leads to the question for the effect of water on the incorporated Ga species and their catalytic activity.

In this work, we provide further evidence for additional acid sites formed by an interaction of water and the Ga species present in [Ga]HZSM-5. ^{1}H MAS NMR, together with Fourier transform infrared spectroscopy (FTIR), temperature-programmed reduction (TPR) and thermogravimetric/differential thermogravimetric (TGA/DTG) techniques, were mainly employed to determine such additional acid sites. The effects of steam treatment of [Ga]HZSM-5 on its acidity/acid strength and reducing ability of Ga species were also investigated. These additional acid sites may affect the aromatization activity of this catalyst in the presence of water.

Hence, aromatization of ethanol and of ethylene is compared and the effect of water on the reaction over [Ga]HZSM-5 is highlighted.

5.2 Experimental details

HZSM-5 (Si/Al ~ 28) was prepared by calcining NH_4ZSM-5 (Zeolyst International) at 550 °C for 4 hours in air. Ga-modified HZSM-5 (3 wt% Ga, as shown in Table 5.1) was prepared by impregnation of NH_4ZSM-5 with $Ga(NO_3)_3$. The sample was then activated by air at 550 °C for 4 hours ([Ga]HZSM-5), while st-[Ga]HZSM-5 was prepared by heating of [Ga]HZSM-5 at 425 °C under ~1 % H_2O/N_2 (30 mL/min) for 3 hours. In addition, the b-[Ga]HZSM-5 (3 wt% Ga loading) was prepared by HZSM-5 support with bulk Ga_2O_3 (particle size ~ 50-200 nm).

Table 5.1 Chemical composition and surface area of zeolite samples.

Catalyst	Ga content (wt%)	Surface area (m^2/g)
HZSM-5	-	560
[Ga]HZSM-5	2.9	525
b-[Ga]HZSM-5	2.8	533

^{1}H MAS NMR spectra were recorded at 300 MHz on a Brüker spectrometer with a BBI MAS probe using a 5 mm ZrO_2 rotor. Prior to the measurement, the sample was packed into an NMR rotor and heated to 270 °C and 360 °C under high vacuum (3.0×10^{-5} Torr) in a homemade apparatus for dehydration. After the treatment, the sample can be filled with He, sealed and transferred into the spectrometer. The samples were spun at 5 kHz. A spin-echo pulsing sequence was used to acquire ^{1}H spectra with 64 scans. The chemical shifts were referenced to TMS.

FTIR spectra were recorded on a Brüker series spectrometer. A thin zeolite wafer 10 mm in diameter was placed in a homemade sample holder and then transferred into the IR cell equipped with heating rod. The zeolite sample was dehydrated at 350 °C under vacuum (3×10^{-5} Torr) for 5 hours. After cooling, IR spectra were acquired in the transmission mode at room temperature over the wave number range of 4000-1300 cm^{-1}. For TGA/DTG, the sample (10-15 mg) was heated from 40 to 900 °C under a flow of N_2 with a heating rate of 10 °C/min.

NH_3-temperature-programmed desorption (NH_3-TPD) experiments were carried out using a TCD detector. Before adsorption, the samples (0.05 g) were dried in a flow of He at 425 °C for 2 hours. Adsorption of 10 % NH_3/He took place at 50 °C until saturation, then the samples were flushed with He at the same temperature for 2 hours. TPD measurements were carried out from 50 to 800 °C with a heating rate of 10 °C/min using He as a carrier gas.

Temperature-programmed reduction (TPR) was performed using a TCD as detector. H_2 consumption was recorded with temperature as the sample (0.05 g) was heated in a flow of 7 % H_2/Ar (30 mL/min) with a heating rate of 10 °C/min. Water produced during the reduction process was removed in a U-shaped glass trap at -70 °C before entering the TCD.

Catalytic study on aromatization of ethylene/ethanol was performed in a fixed bed flow reactor. The feed (ethylene gas/vaporized ethanol) was carried by N_2 through a catalyst bed of [Ga]HZSM-5 (0.15 g) at 425-525 °C. The products are analyzed by an on-line gas chromatograph equipped with a flame ionization detector (FID) and VA-1 capillary column (Appendix B).

5.3 Results and discussion

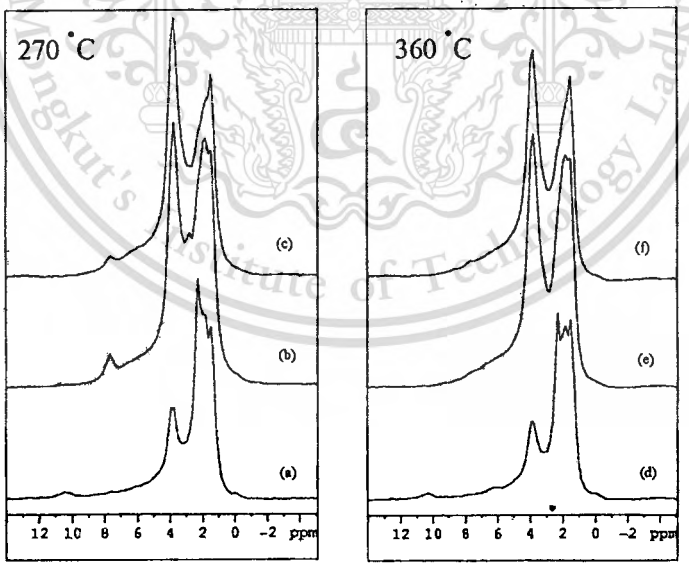

Figure 5.1 ^{1}H MAS NMR spectra of (a) HZSM-5, (b) [Ga]HZSM-5, and (c) st-[Ga]HZSM-5 treated at 270 °C and (d) HZSM-5, (e) [Ga]HZSM-5, and (f) st-[Ga]HZSM-5 treated at 360 °C.

Figure 5.1 shows that ^{1}H MAS NMR spectra of HZSM-5 exhibited two major characteristic resonance lines. The signals at lower chemical shift (1.5-2.3 ppm) can be referred to the defect hydroxyls of the zeolite framework. It was suggested that [23] the signal at 1.5 ppm arises from silanol protons, whilst the signals at 1.8 and 2.3 ppm are assigned to the non–acidic hydroxyls which are bounded to the Al extra-framework and the defect Al framework sites (Al-OH), respectively. The signal at higher chemical shift (3.9 ppm) can be ascribed to the bridging hydroxyl groups (≡Si–OH–Al≡, Brønsted acid site) [24]. Omegna *et al.* [23] also reported a signal at ~ 6.4 ppm, attributed either to (i) another kind of Brønsted acid site, influenced by additional electrostatic interaction of the zeolite framework, or (ii) the residual ammonium ions. However, it is believed that such species can also be observed as an obscure peak at 10.4 ppm in this experiment.

It can be clearly seen that the intensity of Brønsted acid site of [Ga]HZSM-5 (Figure 5.1b) is markedly increased and shifts towards a higher field (3.7 ppm), as compared to that of HZSM-5 (3.9 ppm). In addition a new signal at 7.7 ppm (Figure 5.1b) became pronounced when Ga is incorporated. This indicates that the incorporation of Ga into HZSM-5 increases the total acidity of the catalyst. Such additional acidity is consistent with the increase in the intensity of FTIR band at ~ 3600 cm^{-1} (Figure 5.2), assigned to Brønsted acid sites [25-27], for [Ga]HZSM-5 and st-[Ga]HZSM-5, as compared with the value for HZSM-5.

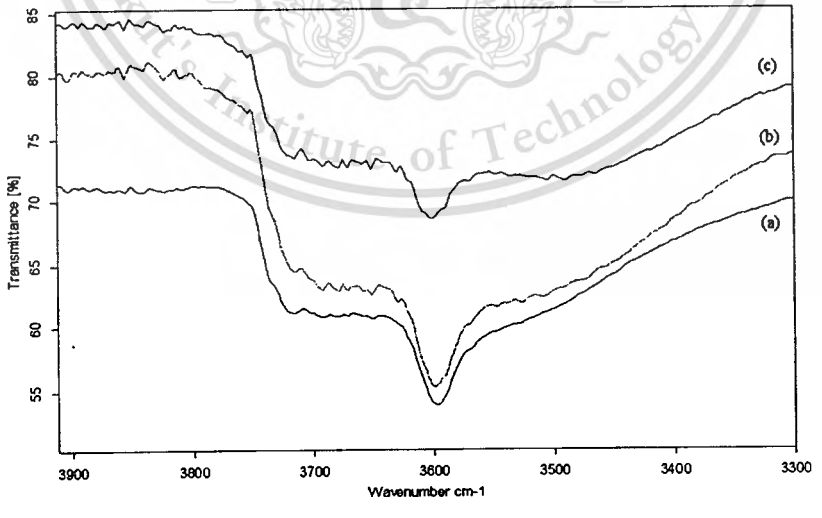

Figure 5.2 FTIR spectra of (a) st-[Ga]HZSM-5, (b) [Ga]HZSM-5, and (c) HZSM-5.

Several reports [5, 28-30] suggest that, when soluble Ga species is incorporated into HZSM-5, $Ga(OH)_2^+$ is primarily exchanged into the negative framework of ZSM-5. Such species can dehydrate to form GaO^+ at high temperature [5,31].

$$Ga(OH)_2^+ \longrightarrow GaO^+ + H_2O \qquad \text{Eq. (1)}$$

The GaO^+ would be dispersed over the exchangeable sites in the framework and can readily react with water when re-exposed to the atmosphere, forming the extra-framework GaO(OH) and Brønsted acid sites [32].

$$GaO^+ + H_2O \longrightarrow GaO(OH) + H_z^+ \qquad \text{Eq. (2)}$$

It is proposed in this work that this extra-framework GaO(OH) species exhibits an additional signal at 7.7 ppm of [Ga]HZSM-5 (Figure 5.1b). It should also be noted that the observed higher chemical shift for this signal may not be necessarily due to a higher acid strength of the GaO(OH). The interaction of high spin-state Ga may well affect the observed chemical shift in various manners.

Unlike GaO^+ species, such extra-framework GaO(OH) would not be localized at the exchangeable sites, but would rather be *mobile* upon heating. Accordingly, it is reasonable to speculate that such GaO(OH) species can be incorporated into the framework by the reaction with available defect silanols, forming additional Brønsted acid sites (≡Ga–OH–Si≡).

$$GaO(OH) + n(\equiv Si–OH) \longrightarrow [\equiv Ga–OH–Si\equiv] + H_2O \qquad \text{Eq. (3)}$$

Corresponding with this, an increase in the Brønsted acid signal at 3.7 ppm is observed, together with a decrease in non-acidic hydroxyl signals at 1.5-2.3 ppm (Figure 5.1b). Such additional acid sites (≡Ga–OH–Si≡) would exhibit a lower acid strength, as compared to that of the typical framework Al (≡Al–OH–Si≡). This is presumably due to the lower electronegativity of the larger, softer Ga cation, as compared with the value of the smaller, harder Al cation. Indeed, a relatively lower chemical shift for the signal of Brønsted acid site in [Ga]HZSM-5 was evidenced (~3.7 ppm, as compared to ~3.9 ppm for HZSM-5).

Upon further heating, the remaining GaO(OH) species can be dehydrated by a reaction with any Brønsted acid sites forming back GaO^+, and the chemisorbed water is practically removed. In support with this view, heating the sample up to ~360 °C under vacuum can readily diminish the GaO(OH) signal (Figure 5.1e). Further investigation (not shown) reveals that this signal (~7.7 ppm) can be recovered when the sample was re-exposed to the atmosphere and the process can be virtually repetitive. Some additional Ga insertion was also expected when [Ga]HZSM-5 is heated to 360 °C. This is observed by a further reduction of signals at 1.5-2.3 ppm, together with an increase in the intensity of the signal at ~3.7 ppm (Figure 5.1e).

Further evidence supporting the insertion of Ga into the zeolite framework (the additional Brønsted acid site) is shown by NH_3-TPD profiles (Figure 5.3).

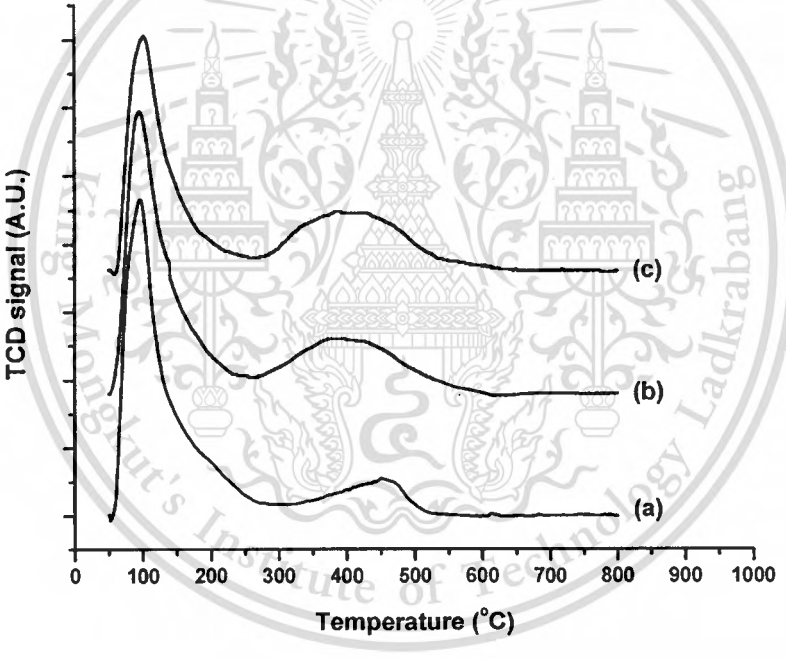

Figure 5.3 NH_3-TPD profiles of (a) HZSM-5(28), (b) [Ga]HZSM-5(28), and (c) st-[Ga]HZSM-5(28).

Typically, the spectrum of HZSM-5 exhibits two characteristic peaks [33,34]: (i) from the NH_3 adsorbed on Si–OH or from non-zeolitic impurity (~ 50-200 °C), and (ii) from the NH_3 adsorbed on the acidic hydroxide group ≡Si–OH–Al≡ (~ 300-500 °C). It can be clearly seen that, when the Ga was incorporated [35], a higher intensity of NH_3-acid site desorption was found, indicating an increase in acidity. This is presumably due to the insertion of Ga into the framework,

as observed earlier by NMR and FTIR. Moreover, the peak shifted towards lower temperature, suggesting a relatively weaker acid strength, as compared to the typical ≡Si–OH–Al≡ in HZSM-5. This is consistent with the above discussion that the additional acid site (≡Si–OH–Ga≡) formed by Ga incorporation would possess a weaker acid strength and, hence, a weaker interaction with NH_3.

From NMR results, it appears that the insertion of the incorporated Ga is preferred, as evidenced by a higher intensity of the signal at 3.7 ppm, as compared to that at 7.7 ppm. This is particularly the case at elevated temperature and when the defect hydroxyls are available. In contrast, GaO(OH) would be retained in the presence of water at relatively lower temperature (< 300 °C). This is deduced from the observed weight loss at 300 °C when [Ga]HZSM-5 was heated under N_2 (Figure 5.4b).

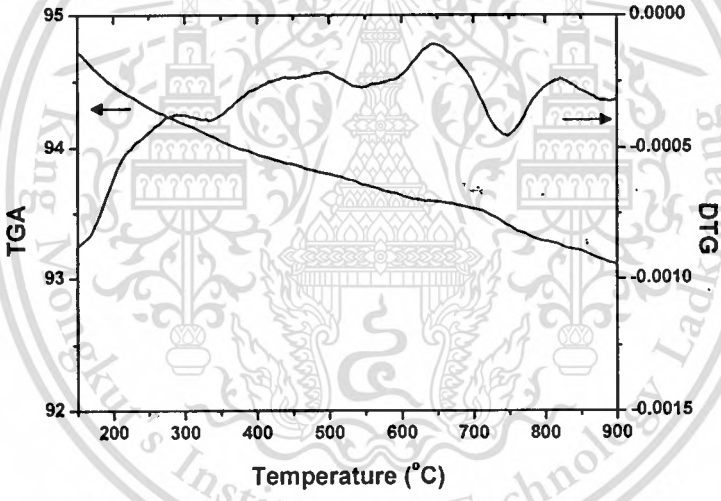

(c)

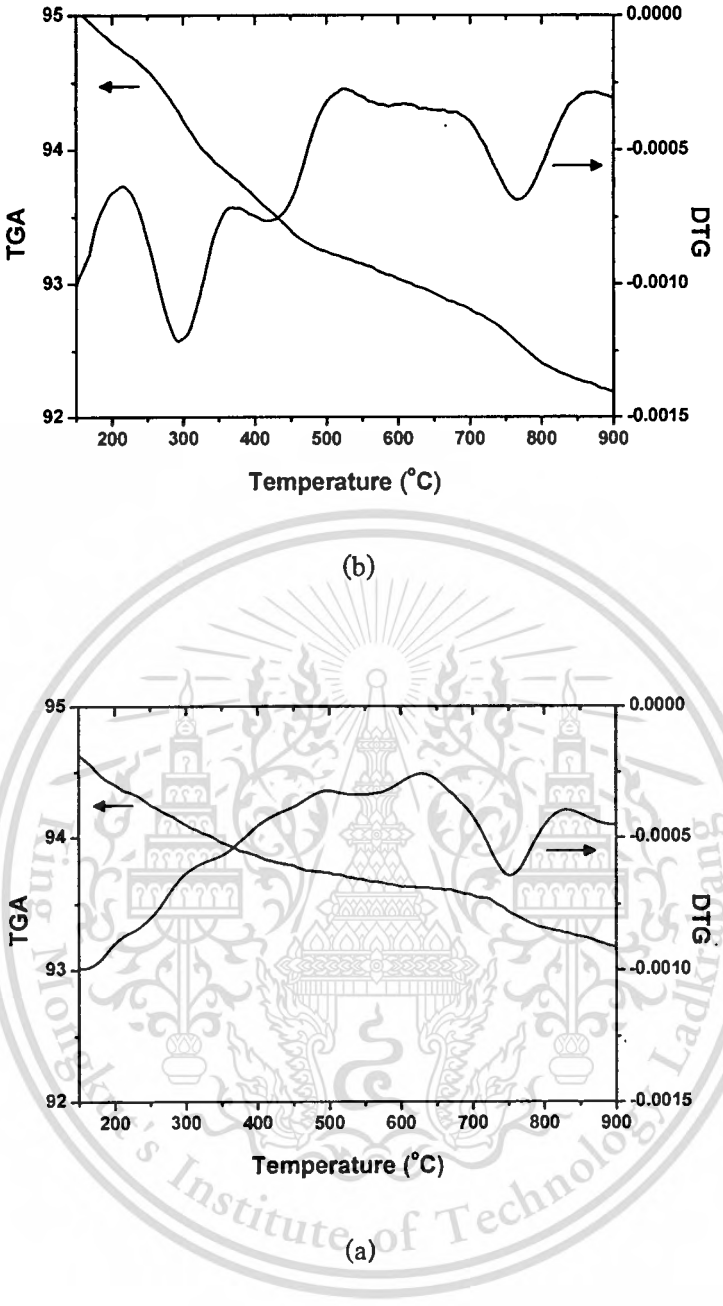

Figure 5.4 Thermograms of (a) HZSM-5, (b) [Ga]HZSM-5, and (c) st-[Ga]HZSM-5.

In support, this DTG signal can be described by the dehydroxylation of GaO(OH) to form GaO^+ species (Eq. (4) (or the reversed reaction of Eq. (2))

$$GaO(OH) + H_z^+ \longrightarrow GaO^+ + H_2O \qquad \text{Eq. (4)}$$

Another weight loss can be observed at ~ 450 °C for [Ga]HZSM-5. This signal is uniquely derived from the incorporated Ga species, since it was not observed in HZSM-5 (Figure 5.4a). This signal is likely to be associated with the dehydration of the extra-framework GaO(OH) to form Ga_2O_3 (Eq. (5)) [32].

$$2GaO(OH) \longrightarrow Ga_2O_3 + H_2O \qquad \text{Eq. (5)}$$

As mentioned earlier, the extra-framework GaO(OH) is rather *mobile*. It may well be readily agglomerated and subsequently dehydrated to form Ga_2O_3 at high temperature, in addition to the insertion into the framework (Eq. (3)), as suggested by NMR. Accordingly it appears that, upon heating, GaO(OH) can either react with Brønsted acid sites or with itself to form GaO^+ or Ga_2O_3, respectively. This observation suggests that GaO(OH) species can only be present in [Ga]HZSM-5 at <450 °C.

Under steam treatment at 425 °C, similar chemical shifts can be observed for st-[Ga]HZSM-5 (Figure 5.1c). However, the intensity of signals at ~3.7 ppm is slightly increased while those at 1.5-2.3 ppm and 7.7 ppm are decreased when compared to the values for [Ga]HZSM-5 (Figure 5.1b). This result indicates that the steam treatment may well promote an additional insertion of Ga species into the framework. As mild steaming usually increases the migration of impregnated metal or metal oxide extra-framework [18-20], a better dispersion/insertion of Ga species (GaO(OH)) to the lattice defects would be facilitated. This leads to an increase in Brønsted acid sites and to reduction of defect hydroxyls and GaO(OH) of the catalyst, as observed.

Further evidence supporting the insertion of Ga species after steaming was observed from DTG (Figure 5.4). While weight losses at 300 and 450 °C are clearly shown in [Ga]HZSM-5, only a tiny weight loss is observed over st-[Ga]HZSM-5 (Figure 5.4c). This again suggests that, under steaming, most of Ga extra-framework (GaO(OH)) can further react with the defect framework of zeolite. Consequently, small amounts of GaO(OH) remain in the sample after steaming and only trace of water can be liberated from the st-[Ga]HZSM-5. The reduced number of GaO(OH) species remaining in the catalyst is also consistent with the observed decrease in signal at 7.7 ppm in the st-[Ga]HZSM-5 (Figure 5.1c).

When the steamed sample (st-[Ga]HZSM-5) was further heated at 360 °C for 15 hours under high vacuum (3.0×10^{-5} Torr), the resonance signal at 7.7 ppm appears to be less (Figure

5.1f) suggesting that the remaining GaO(OH) can react with Brønsted acid sites to form GaO^+ species at a temperature higher than 300 °C. Unlike [Ga]HZSM-5, the additional insertion of the Ga species was not expected for the st-[Ga]HZSM-5 after heating. This is because Ga species would have already inserted into almost every available active defect framework location during the steam treatment at 425 °C. Consequently, the reduction of signal at 3.7 ppm is instead observed over st-[Ga]HZSM-5 after heating (Figure 5.1f). This indeed demonstrates the consumption of Brønsted acid sites (H_z^+) by the reaction with the remaining GaO(OH) without generating any additional acid sites. In support with this view, there is also no significant change in the signal at 1.5-2.3 ppm (defect hydroxyls) for this sample.

TEM also provides additional clues for a better dispersion of Ga species when the catalyst was treated with steam. It can be clearly seen in Figure 5.5a that Ga particles in [Ga]HZSM-5 locate principally on the external surface of the zeolite crystals with a cluster size ~ 12 nm. However, Ga particles cannot be observed on st-[Ga]HZSM-5 sample despite of the same Ga loading (~ 3 wt%).

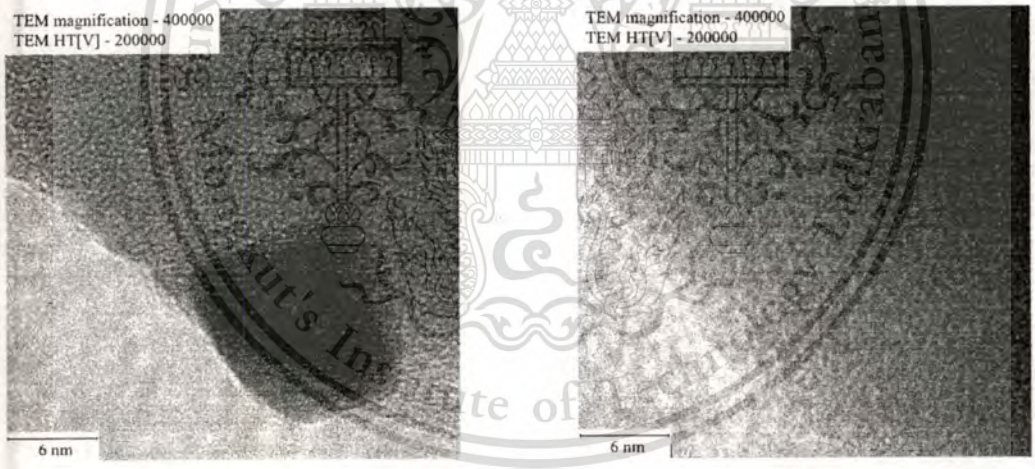

(a) (b)

Figure 5.5 TEM micrograph of (a) [Ga]HZSM-5 and (b) st-[Ga]HZSM-5.

This implies that steaming may well enhance the dispersion of nano-structured Ga particles. However, it may be a mistake to deduce from TEM that the consecutive insertion of Ga species into the zeolite framework is the only example of the better dispersion of Ga species in st-[Ga]HZSM-5. Formation of other species such as GaO^+ would also be highly dispersed and cannot be observed by TEM.

Further investigation on the effect of steaming was performed by H_2-TPR studies (Figure 5.6) of the physical mixing of Ga_2O_3 (particle size ~ 50-200 nm) with HZSM-5 zeolite (b-[Ga]HZSM-5) and their steamed sample (st-b-[Ga]HZSM-5).

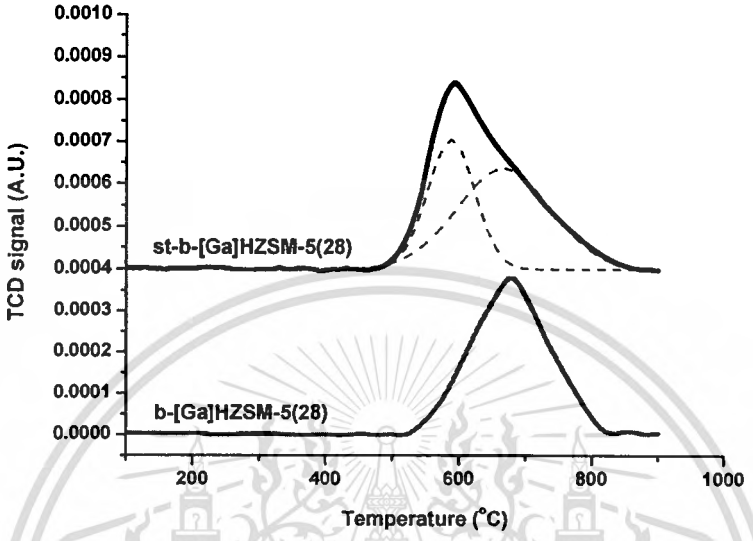

Figure 5.6 The TPR curves of b-[Ga]HZSM-5(28) and st-b-[Ga]HZSM-5(28) treated with steam at 425 °C.

It can be seen that a reduction peak of bulk Ga_2O_3 in b-[Ga]HZSM-5 appears at ~ 670 °C. As expected, a smaller signal was observed for the reduction of bulk Ga_2O_3 in st-b-[Ga]HZSM-5, indicating that less bulk Ga_2O_3 is retained in this sample. In other words, larger parts of the bulk Ga_2O_3 can be re-dispersed by reaction with steam, presumably forming GaO(OH) (Eq. (6)) and/or inserting into the framework (Eq. (3)), as discussed previously.

$$Ga_2O_3 + H_2O \longrightarrow 2GaO(OH) \qquad \text{Eq. (6)}$$

In agreement with this view, the reduction peak of Ga species in the steamed sample (st-b-[Ga]HZSM-5) shifts toward a lower temperature. This is because the highly dispersed Ga species would be more feasibly reduced, as compared to the bulk Ga_2O_3.

From the above results, we can conclude that the presence of water can promote the formation of GaO(OH), an additional acid site, by reactions both with GaO^+ and with bulk Ga_2O_3. Upon heating, this GaO(OH) species can either (i) be inserted into the framework by reaction

with defect hydroxyls (> 300 °C), (ii) react with Brønsted acid sites to form GaO^+ or (iii) become dehydrated to form smaller clusters of Ga_2O_3 (> 450 °C). Accordingly, the catalytic activity of [Ga]HZSM-5 at temperature higher than 450 °C shall not be affected by the presence of water. In contrast, the effect of water would be significant at temperatures lower than 450 °C, as shown by the conversion of ethanol and ethylene in Table 5.2.

Table 5.2 Effect of water co-feeding over Ga-modified HZSM-5[a].

Catalyst	Feed	Product distribution (% carbon yield)[b]				
		C2	C3	C4	C5+	BTX[c]
HZSM-5	95 wt% Ethanol	13.75	32.75	30.51	14.22	8.76
	Absolute ethanol	9.44	30.02	30.46	15.57	14.50
	Ethylene	7.46	32.23	31.75	14.33	14.22
[Ga] HZSM-5	95 wt% Ethanol	9.50	27.34	30.64	17.04	15.47
	Absolute ethanol	9.80	27.95	31.52	18.05	12.68
	Ethylene	19.66	18.73	26.94	14.60	20.07

[a] Pressure = 1 atm, Temperature = 425 °C, W/F = 15.97 g·h/mol.

[b] Product distributions were averaged over 1-3 hours on stream.

[c] BTX = benzene, toluene, ethylbenzene and xylenes.

In the reactions using 95 % ethanol, absolute ethanol and ethylene as feed at 425 °C, slightly deactivations of both the catalysts: HZSM-5(28) and [Ga]HZSM-5(28) were observed (Figure 5.7).

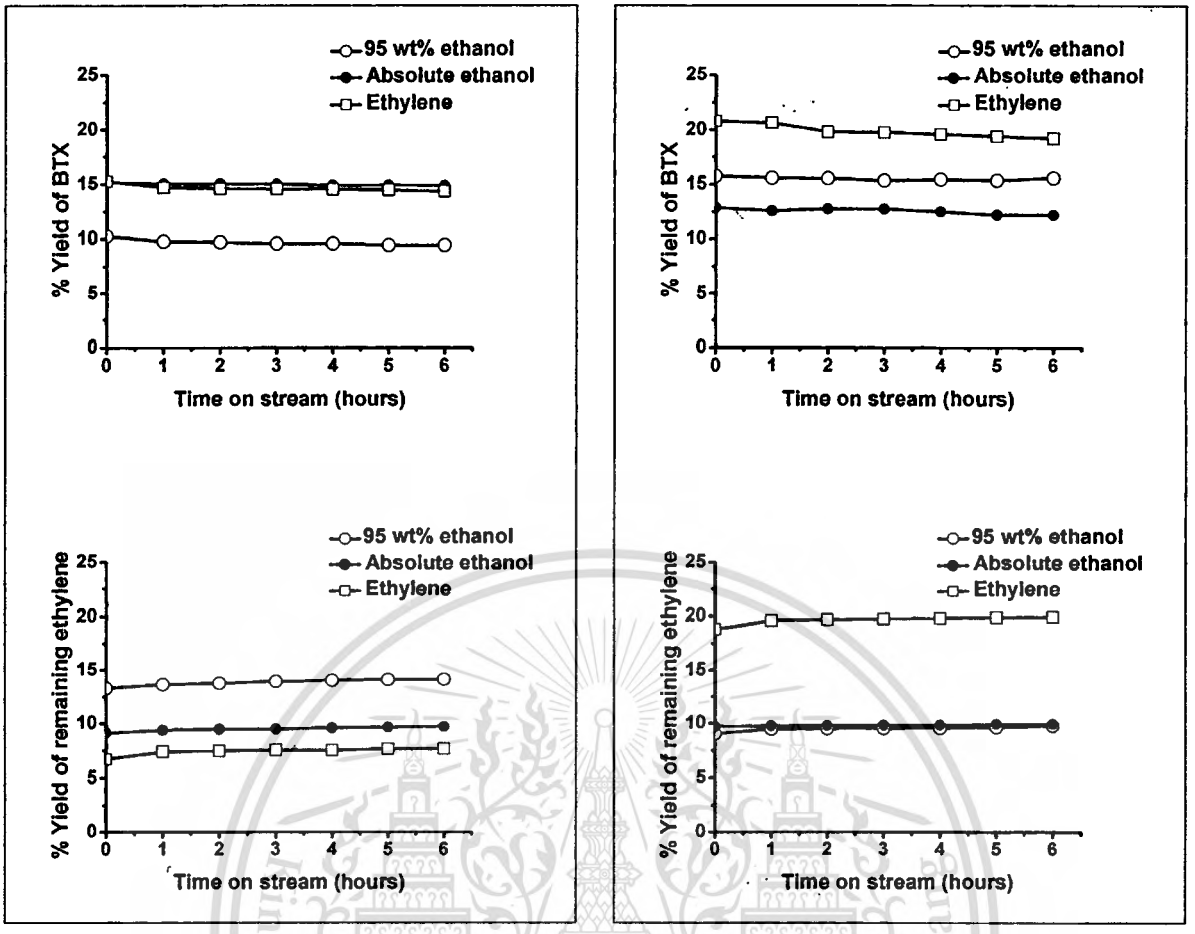

Figure 5.7 % Carbon yield of remaining ethylene and BTX[a] from the reaction of 95 % ethanol, absolute ethanol, and ethylene using (a) HZSM-5(28) and (b) [Ga]HZSM-5(28) as a catalyst as a function of time on stream.

[a] *BTX = benzene, toluene, ethylbenzene and xylenes.*

For the reactions using ethanol as feed, ethanol is virtually completely converted to ethylene over acid catalyst (HZSM-5). The conversion of the primarily formed ethylene to higher hydrocarbons decreases with a rise in water content (as seen by the amount of ethylene retained in the product stream, Table 5.2). It indicates that water, either produced by ethanol dehydration (absolute ethanol) or present as co-feed (95 % ethanol), can inhibit oligomerization of the ethylene by competitive adsorption over the acid sites.

Surprisingly, in the case of [Ga]HZSM-5, selectivity of C_4^+ hydrocarbons increases with rise in water content. This supports the above observation that the presence of water can produce additional acid sites in [Ga]HZSM-5 (Eq. (2)) which can remain at the reaction temperature (425

°C). The enhanced acidity of [Ga]HZSM-5 can promote ethylene oligomerization and the subsequent aromatization of higher hydrocarbons. It is believed that GaO^+ is not present under such reaction conditions as it would be react with water to form GaO(OH). Only GaO(OH) and the additional acid sites generated by insertion of Ga species are responsible for the observed activity.

In a different manner, BTX selectivity is also high for the reaction using ethylene as feed at 425 °C, although the fraction of ethylene converted is relatively low. Researchers suggest that the increase of BTX selectivity would be predominantly derived from the aromatization of small olefins. Since there is no water present in the reaction, GaO^+ and its reduced species can be retained and can readily promote the aromatization reaction.

Table 5.3 Effect of temperature on ethanol conversion over [Ga]HZSM-5[a].

Catalyst	Temperature (°C)	Product distribution (% carbon yield)[b]				
		C2	C3	C4	C5+	BTX[c]
[Ga]HZSM-5	425	9.80	27.95	31.52	18.05	12.68
	450	13.16	33.49	30.03	14.15	9.17
	525	42.46	23.61	11.56	7.07	15.30

[a] Pressure = 1 atm, Temperature = 425-525 °C, W/F = 15.97 g·h/mol.

[b] Product distributions were averaged over 1-3 hours on stream.

[c] BTX = benzene, toluene, ethylbenzene and xylenes.

As the chemisorbed water plays a marked role in the formation of additional acid sites and the active species, the catalytic behaviour of [Ga]HZSM-5 would be readily regulated by temperature. This can be seen by a lower fraction of ethylene converted and a lower BTX selectivity at 450 °C, as shown in Table 5.3. As the temperature was increased, relatively less chemisorbed water could be retained in [Ga]HZSM-5. Hence, smaller number of acid sites would be expected, as compared to the reaction at 425 °C. This leads to a lower selectivity to produce the higher hydrocarbon. In turn, small olefin aromatization is then promoted in ethanol

conversion over [Ga]HZSM-5 at 525 °C. This is because, at high temperature (525 °C), chemisorption of water on GaO^+ to form GaO(OH) is prohibited, although water is always present in the feed. Consequently, the GaO^+ and its reduced species would be responsible for the observed activity (namely aromatization [1-8]), as seen by an increase in BTX selectivity, even though the fraction of ethylene converted was exceedingly decreased.

5.4 Conclusions

The formation of different Ga species is regulated by the temperature and the presence of water. Incorporation of Ga species into HZSM-5 leads to the formation of active GaO^+, which can readily react with the chemisorbed water to form GaO(OH). The dispersed GaO(OH) can further react with the defect framework of zeolite, forming additional Brønsted acid sites associated with Ga in the framework. As new acid sites can be generated in Ga-modified HZSM-5 upon water chemisorption, we suggest that the additional acid sites could be obtained only at lower temperature (< 425 °C). Such acid sites can promote ethylene olgomerization and reforming of higher hydrocarbons, in a manner similar to that exhibited by conventional Brønsted acid sites. Upon heating, GaO(OH) can be dehydroxylated back to GaO^+ (~300 °C) in the absence of water or dehydrated to form Ga_2O_3 at high temperature (> 450 °C). Under such reaction conditions, the activity for small olefin aromatization can be recovered.

References

[1] Choudhary V.R., Mantri K. and Sivadinarayana C. "Influence of Zeolite Factors Affecting Zeolitic Acidity on the Propane Aromatization Activity and Selectivity of Ga/H-ZSM-5" **Microporous and Mesoporous Materials.** vol. 37, 2000. pp. 1-8.

[2] Choudhary T.V., Kinage A.K., Banerjee S. and Choudhary V.R. "Effect of Temperature on the Product Selectivity and Aromatics Distribution in Aromatization of Propane over H-GaAlMFI Zeolite" **Microporous and Mesoporous Materials.** vol. 70, 2004. pp. 37-42.

[3] Ono Y., Kanae K., "Transformation of Butanes over ZSM-5 Zeolites" **Journal of the Chemical Society, Faraday Transactions.** vol. 87, 1991. pp. 663-667.

[4] Kanazirev V., Price G.L. and Dooley K.M. "Preparation of Ga-Doped Zeolites via Hydrogen Induced Solid State Interaction Between Ga_2O_3 and HZSM-5 Zeolite" **Studies in Surface Science and Catalysis.** vol. 69, 1991. pp. 277-285.

[5] Dooley K.M., Chang C. and Price G.L. "Effects of Pretreatments on State of Gallium and Aromatization Activity of Gallium/ZSM-5 Catalysts" **Applied Catalysis A: General.** vol. 84, 1992. pp. 17-30.

[6] Kwak B.S., Sachtler W.M.H. "Effect of Ga/Proton Balance in Ga/HZSM-5 Catalysts on C_3 Conversion to Aromatics" **Journal of Catalysis.** vol. 145, 1994. pp. 456-463.

[7] Choudhary V.R., Kinage A.K., Sivadinarayana C. and Guisnet M. "Pulse Reaction Studies on Variations of Initial Activity/Selectivity of O_2 and H_2 Pretreated Ga-Modified ZSM-5 Type Zeolite Catalysts in Propane Aromatization" **Journal of Catalysis.** vol. 158, 1996. pp. 23-33.

[8] Joly J.F., Ajot H., Merlen E., Raatz F. and Alario F. "Parameters Affecting the Dispersion of the Gallium Phase of Gallium H-MFI Aromatization Catalysts" **Applied Catalysis A: General.** vol. 79, 1991. pp. 249-263.

[9] Meriaudeau P., Naccache C. "Further Evidence on the Change of Acid Properties of H-ZSM-5 by Ga and Pt" **Journal of Catalysis.** vol. 157, 1995. pp. 283-288.

[10] Meriaudeau P., Sapaly G., Wicker G. and Naccache C. "Revisiting Ga_2O_3/H-ZSM-5 Propane Aromatization Catalysts" **Catalysis Letter.** vol. 27, 1994. pp. 143-148.

[11] Price G.L., Kanazirev V. "Ga_2O_3/HZSM-5 Propane Aromatization Catalysts: Formation of Active Centers via Solid-State Reaction" **Journal of Catalysis.** vol. 126, 1990. pp. 267-278.

[12] Kanazirev V., Price G.L. and Dooley K.M. "Preparation of Ga-Doped Zeolite Catalysts via Hydrogen Induced Solid State Interaction Between Ga_2O_3 and HZSM-5 Zeolite" **Studies in Surface Science and Catalysis**. vol. 69, 1991. pp. 277-285.

[13] Meriaudeau P., Naccache C. "The Role of Ga_2O_3 and Proton Acidity on the Dehydrogenating Activity of Ga_2O_3-HZSM-5 Catalysts: Evidence of a Bifunctional Mechanism" **Journal of Molecular Catalysis Letter**. vol. 59, 1990. pp. L31-L36.

[14] Bayense C.R., van der Pol A.J.H.P. and van Hoof J.H.C. "Aromatization of Propane over MFI-Gallosilicates" **Applied Catalysis**. vol. 72, 1991. pp. 81-98.

[15] Ono Y. "Transformation of Lower Alkanes into Aromatic Hydrocarbons over ZSM-5 Zeolites" **Catalysis Reviews Science and Engineering**. vol. 34, 1992. pp. 179-226.

[16] Guisnet M., Gnep N.S. "Aromatization of Propane over GaHMFI Catalysts. Reaction Scheme, Nature of the Dehydrogenating Species and Mode of Coke Formation" **Catalysis Today**. vol. 31, 1996. pp. 275-292.

[17] Rane N., Kersbulck M., van Santen R.A. and Hensen E.J.M. "Cracking of *n*-Heptane over Brønsted Acid Sites and Lewis Acid Ga Sites in ZSM-5 Zeolite" **Microporous and Mesoporous Materials**. vol. 110, 2008. pp. 279-291.

[18] Martin M.A., Pajares J.A. and Tejuca L.G. "Sintering of Supported Palladium" **Reaction Kinetics and Catalysis Letters**. vol. 30, 1986. pp. 105-111.

[19] Ruckenstein E., Hu X.D. "The Effect of Steam on Supported Metal Catalysts" **Journal of Catalysis**. vol. 100, 1986. pp. 1-16.

[20] Zhang Y., Zhou Y., Yang K., Li Y., Wang Y. and Wu Y. X. P. "Effect of Hydrothermal Treatment on Catalytic Properties of PtSnNa/ZSM-5 Catalyst for Propane Dehydrogenation" **Microporous and Mesoporous Materials**. vol. 96, 2006. pp. 245-254.

[21] Ono Y., Adachi H. and Sendoda Y. "Selective Conversion of Methanol into Aromatic Hydrocarbons over Zinc-Exchanged ZSM-5 Zeolites" **Journal of the Chemical Society, Faraday Transaction I: Physical Chemistry in Condensed Phases**. vol. 84, 1988. pp. 1091-1099.

[22] Freeman D., Wells R.P.K. and Hutchings G.J. "Conversion of Methanol to Hydrocarbons over Ga_2O_3/H-ZSM-5 and Ga_2O_3/WO_3 Catalysts" **Journal of Catalysis**. vol. 205, 2002. pp. 358-365.

[23] Omegna A., Haouas M., Kogelbauer A. and Prins R. "Realumination of Dealuminated HZSM-5 Zeolites by Acid Treatment: A Reexamination" **Microporous and Mesoporous Materials**. vol. 46, 2001. pp. 177-184.

[24] Hunger M. "Brønsted Acid Sites in Zeolites Characterized by Multinuclear Solid-State NMR Spectroscopy" **Catalysis Reviews Science and Engineering**. vol. 39, 1997. pp. 345-393.

[25] Qin G., Zheng L., Xie Y. and Wu C. "On the Framework Hydroxyl Groups of H-ZSM-5 zeolites" **Journal of Catalysis**. vol. 95, 1985. pp. 609-612.

[26] Zecchina A., Bordiga S., Spoto G., Scarano D., Petrini G., Leofanti G., Padovan M. and Otero Arean C. "Low-Temperature Fourier-Transform Infrared Investigation of the Interaction of CO with Nanosized ZSM5 and Silicalite" **Journal of the Chemical Society, Faraday Transactions**. vol. 88, 1992. pp. 2959-2969.

[27] Knozinger H., Huber S. "IR Spectroscopy of Small and Weakly Interacting Molecular Probes for Acidic and Basic Zeolites" **Journal of the Chemical Society, Faraday Transaction**. vol. 94, 1998. pp. 2047-2059.

[28] Pokrovski G.S., Schott J., Hazemann J.L., Farges F. and Pokrovsky O.S. "An X-ray Absorption Fine Structure and Nuclear Magnetic Resonance Spectroscopy Study of Gallium-Silica Complexes in Aqueous Solution" **Geo Chimica et Cosmochimica Acta**. vol. 66, 2002. pp. 4203-4220.

[29] Shpiro E.S., Shevchenko D.P., Tkachenko O.P. and Dmitriev R.V. "Platinum Promoting Effects in Pt/Ga Zeolite Catalysts of Lower Alkane Aromatization. I. Ga and Pt Electronic States, Dispersion and Distribution in Zeolite Crystals in Dependence of Preparation Techniques. Dynamic Effects Caused by Reaction Mixture" **Applied Catalysis A: General**. vol. 107, 1994. pp. 147-164.

[30] Nowak I., Quartararo J., Derouane E.G. and Vedrine J.C. "Effect of H_2-O_2 Pre-Teatments on the State of Gallium in Ga/H-ZSM-5 Propane Aromatisation Catalysts" **Applied Catalysis A: General**. vol. 251, 2003. pp. 107-120.

[31] Kazansky V.B., Subbotina I.R., van Santen R.A. and Hensen E.J.M. "DRIFTS Study of the Nature and Chemical Reactivity of Gallium Ions in Ga/ZSM-5: II. Oxidation of Reduced Ga Species in ZSM-5 by Nitrous Oxide or Water" **Journal of Catalysis**. vol. 233, 2005. pp. 351-358.

[32] Garcia Sanchez M., Magusin P.C.M.M., Hensen E.J.M. and Thune P.C., **Journal of Catalysis**. vol. 219, 2003. pp. 352-361.

[33] Hidalgo C.V., Itoh H., Hattori T., Niwa M. and Murakami Y. "Measurement of the Acidity of Various Zeolites by Temperature-Programmed Desorption of Ammonia. **Journal of Catalysis**. vol. 85, 1984. pp. 362-369.

[34] Post J.G., van Hoff J.H.C. "Acidity and Activity of H-ZSM-5 Measured with NH_3-t.p.d. and *n*-Hexane Cracking" **Zeolites**. vol. 4, 1984. pp. 9-14.

[35] Ma D., Zhang W., Shu Y., Liu X., Xu Y. and Bao X. "MAS NMR, ESR and TPD Studies of Mo/HZSM-5 Catalysts: Evidence for the Migration of Molybdenum Species into the Zeolitic Channels" **Catalysis Letter**. vol. 66, 2000. pp. 155–160.

Chapter 6

Tunable Ga Species in [Ga]HZSM-5 by H_2 Treatment : A Pulsed Study on Ethane Dehydrogenation

6.1 Introduction

Gallium-incorporated HZSM-5 zeolites ([Ga]HZSM-5) are recognized as being effective catalysts for converting light alkanes to aromatics [1-8]. Key roles are played by modified Ga in the dehydrogenation of paraffins [1-3], whereas Brønsted acid catalyzes the oligomerization of the olefins thus produced and possibly their subsequent aromatization. While the study of the type of Ga species has spanned many years, controversy remains as to its catalytic activity, which relates mainly to the nature of the active sites which gallium species is responsible for the catalytic activity [1,9-12].

It was first believed that the Ga_2O_3 obtained after calcination, was the active catalytic species, because it was capable of dehydrocyclization [9,13] and H_2 dissociations [14]. However, it was found subsequently that the intrinsic dehydrogenation activity of Ga_2O_3/HZSM-5 was better than that of Ga_2O_3 alone. Since this discovery, there have been many experimental investigations that have attempted to elucidate the structure of the Ga species which was carried out under the reducing atmosphere of H_2 (either by feeding or *in situ* to produce it from dehydrogenation of hydrocarbons) and its interaction with Brønsted acid. Researchers have reported that the Ga_2O_3 species are readily reduced during pretreatment with hydrogen or with the hydrocarbon feed to Ga_2O species that migrate into the zeolite channels [3,10,15,16].

$$Ga_2O_3 + 2H_2 \longrightarrow Ga_2O + 2H_2O \qquad \text{Eq. (1)}$$

These mobile species react with the zeolitic Brønsted acid, resulting in the formation of reduced cationic, Ga^+ species bound to a negative framework charge of the zeolites [3,10,15,16].

$$Ga_2O + 2H^+ \longrightarrow 2Ga^+ + H_2O \qquad \text{Eq. (2)}$$

Alternatively, several reports [3,17-19] suggest that $Ga(OH)_2^+$ is primarily exchanged into the negative framework of HZSM-5. Such species can dehydrate to form GaO^+ at high temperature [3,20].

$$Ga(OH)_2^+ \longrightarrow GaO^+ + H_2O \qquad \text{Eq. (3)}$$

The GaO^+ would be dispersed over the exchangeable sites in the framework, however, such Ga species can readily react with H_2, finally forming the Ga^+ species [21,22].

$$GaO^+ + H_2 \longrightarrow Ga^+ + H_2O \qquad \text{Eq. (4)}$$

It is also believed that H_2 not only keeps Ga species in its reduced forms but can also chemisorb on Ga^+ species and consecutively dissociate to form gallium dihydride (GaH_2^+) [23].

$$Ga^+ + H_2 \longrightarrow GaH_2^+ \qquad \text{Eq. (5)}$$

The existence of the gallium dihydride species is in good agreement with the observed adsorption band at ~ 2040 cm^{-1} [23]. Kazansky *et al.* [20,23] reported that such Ga species are relatively stable and decompose only partially in a reductive hydrogen atmosphere at elevated temperatures.

The resulting material may contain several types of reduced Ga species and also gallium oxide particles if the reduction process is not complete. The oxide species may include bulkier aggregates on the external surface or smaller ones in the micropore space of the zeolite. Consequently, the Ga active species promoted alkane dehydrogenation has not been fully understood yet due to the wide variety of Ga species (Ga_2O_3, GaO^+, Ga^+, and GaH_2^+).

Recently, this research has attempted to determine the catalytic activity of various Ga species based on the ethane dehydrogenation. The possible type of Ga species, which is formed *in situ*, can be achieved according to the different pre-treatments. For example, the isolated Ga_2O_3 and the exchangeble GaO^+ species can be obtained after calcination with air. While the Ga^+ cationic species would result from the reduction of Ga oxide. Finally, GaH_2^+ can be stabilized under the H_2 system. The catalytic activity of such Ga species was investigated using a pulsed

reactor. In addition, the hydrogen or steam treatment and the Si/Al ratio of the host zeolite influencing its catalytic activity were also highlighted.

6.2 Experimental details

HZSM-5 samples were commercially obtained from Zeolyst International (Si/Al ~ 11 and 28) and Sud-Chemie (Si/Al ~ 165). Conventional impregnation of HZSM-5 with $Ga(NO_3)_3$ was employed to obtain 3 wt% Ga loading. The sample was then calcined at 550 °C for 4 hours in a flow of dry air. Hereafter, the catalysts were designated as [Ga]HZSM-5(Si/Al) according to their Si/Al ratio. In addition, the b-[Ga]HZSM-5 (3 wt% Ga loading) was prepared by HZSM-5 support with bulk Ga_2O_3 (particle size ~ 50-200 nm) in order to study the catalytic activity of Ga oxide species and the influence of the cluster size on the formation of various Ga species.

Temperature-programmed reduction (TPR) experiments were carried out using a TCD detector. Prior to the H_2-TPR, the sample was heated to 550 °C in dry air for 1 hour (30 mL/min). Subsequently, the sample was cooled to 50 °C. The H_2 consumption was recorded with the temperature, when the catalyst samples were heated in a flow of 2 % H_2/Ar (30 mL/min) with a heating rate of 10 °C/min.

NH_3-temperature-programmed desorption (NH_3-TPD) experiments were carried out using a TCD detector. Before adsorption, the samples (0.05 g) were treated in a flow of He or H_2 at 550 °C for 2 hours. Adsorption of 10 % NH_3/He until saturation took place at 50 °C, then the samples were flushed with He at the same temperature for 2 hours. TPD measurements were taken from 50 to 700 °C with a heating rate of 10 °C/min, with He as the carrier gas.

The procedure for the ethane pulse reaction studies was as follows. The 15 mg of catalyst was pretreated in a flow of He or H_2 (60 mL/min). After the pretreatment, 25 microliter of 5 v/v% ethane in He or H_2 gas was injected into the pretreated catalyst to obtain its initial activity. This procedure was repeated to obtain the ethane pulse reaction data at the different reaction conditions: exp1 = 5 % ethane/He was fed using He as carrier gas, exp 2 = the 10 pulses of pure H_2 was injected to the catalyst, and then 5 % ethane/He was fed using He as carrier gas, exp 3, 4 = the exp 2 was re-operated, exp 5 = 5 % ethane/H_2 was fed using H_2 as carrier gas, exp 6 = the exp 2 was re-operated, exp 7 = the exp 5 was re-operated, and exp 8 = the exp 2 was re-operated. The products of the ethane pulse reaction were analyzed by an on-line gas chromatograph equipped with a flame ionization detector (FID) and HP-Plot capillary column (Appendix B).

6.3. Results and discussion

6.3.1 Catalyst characterization

The characteristics of the zeolite samples including Si/Al ratio of the host zeolite, % Ga loading, and BET surface area are shown in Table 6.1.

Table 6.1 Chemical composition and surface area of zeolite samples.

Catalyst	Si/Al	Ga content[a] (wt%)	Surface area (m^2/g)
HZSM-5(11)	11	-	645
HZSM-5(28)	28	-	560
HZSM-5(165)	165	-	540
[Ga]HZSM-5(11)	11	2.8	590
[Ga]HZSM-5(28)	28	2.8	525
[Ga]HZSM-5(165)	165	2.8	520
b-[Ga]HZSM-5(28)	28	2.7	530
b-[Ga]HZSM-5(165)	165	2.7	510

[a] Elemental analysis for Si, Al, and Ga were performed using ICP.

The Ga content on the impregnated and physical mixed catalyst is the same.

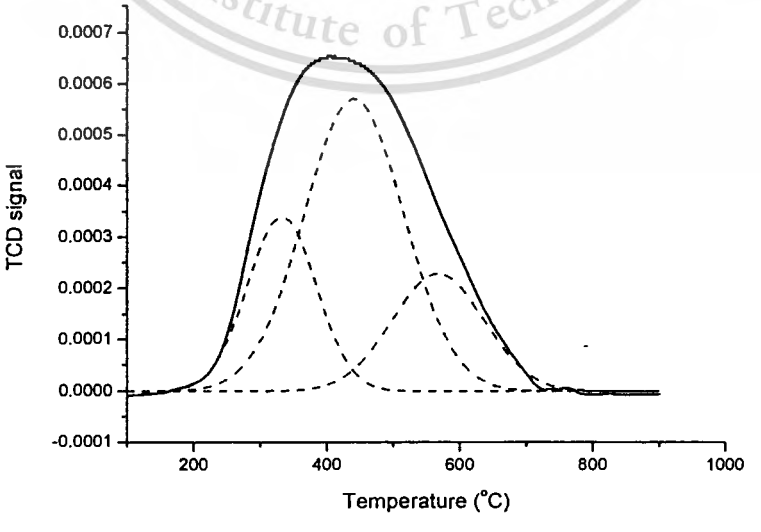

(d)

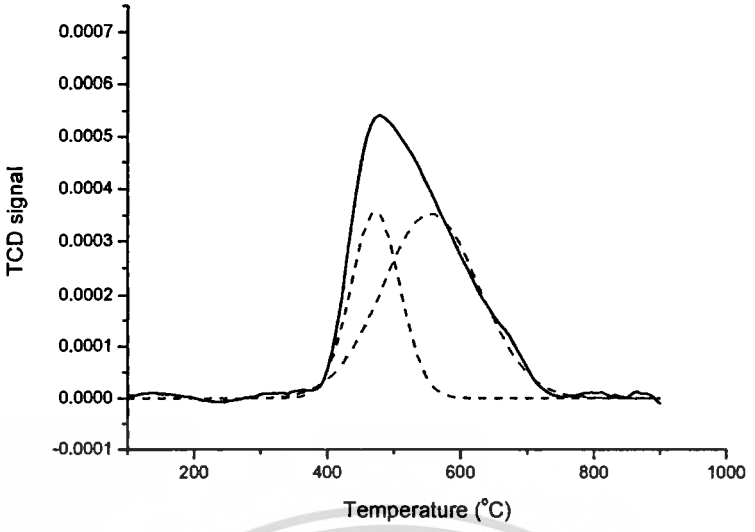

(c)

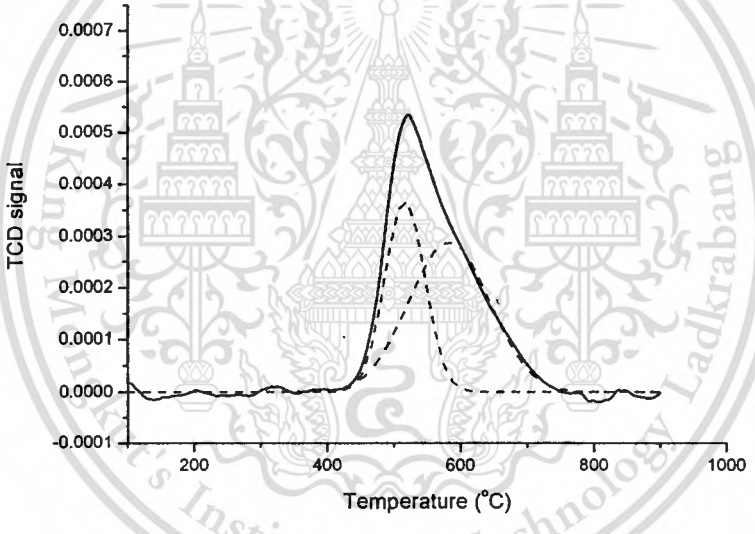

(b)

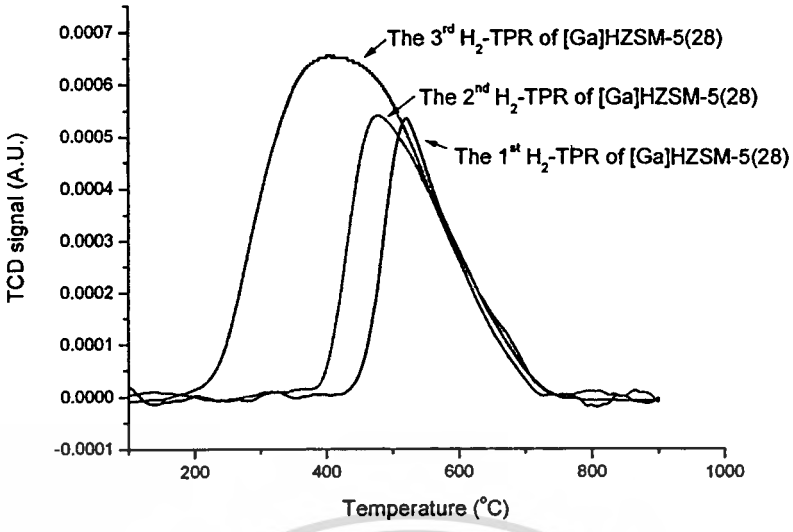

(a)

Figure 6.1. The TPR profiles of (a) comparison data of [Ga]HZSM-5(28), (b) the primary H_2-TPR of [Ga]HZSM-5(28), (c) the secondary H_2-TPR of [Ga]HZSM-5(28), and (d) the tertiary H_2-TPR of [Ga]HZSM-5(28).

Figure 6.1 shows the TPR profile of the Ga-modified HZSM-5(28) zeolite samples. With the Gaussian deconvolution, it can be seen that there are two major peaks for the calcined [Ga]HZSM-5(28) (Figure 6.1b). In this case, the T_1 peak (~ 510 °C) was assigned to the reduction of well-dispersed Ga species such as small Ga_2O_3 particles and/or GaO^+ species interacting with the zeolite framework. While, the T_2 peak (~ 600 °C) was attributed to larger, bulk Ga_2O_3 particles separated from or loosely supported on the zeolite matrix [19]. It is evidenced that the calcined [Ga]HZSM-5(28) contains several types of Ga species.

After the primary H_2-TPR, the sample was slowly cooled down to 100 °C under H_2 and then readily switched to He. Subsequently, the sample was purged with air for 2 hours in order to recover the Ga oxide species. To investigate the change in the nature and number of Ga species caused by reduction/oxidation by the secondary H_2-TPR was performed (Figure 6.1c). It shows the two major peaks, as were observed previously. Interestingly, the peaks were shifted to the lower reduction temperature. It is suggested that this derives from a better-dispersion of Ga species after the reduction/oxidation process. Supported with this suggestion, the process was repeated. The tertiary H_2-TPR (Figure 6.1d) shows the new peak at lower reduction temperatures

observed at ~ 320 °C. It is suggested that the Ga_2O_3 particles can be reduced and consequently migrated to the negative Al tetrahedral framework. When this species was re-oxidized with air, the smaller particle of Ga species was generated resulting in the shift to a lower reduction temperature. From the above results, it is worthy noting that the H_2 reduction can improve the dispersion of the Ga species and subsequently modify their reducing ability. Moreover, a relatively higher extent of H_2 consumption (H_2/Ga_2O_3) can be obtained over the tertiary H_2-TPR. This is due to the well-dispersed Ga species being able to be readily reduced. In contrast, a lower % H_2 consumption can be obtained over the bulk Ga_2O_3 cluster due to an incomplete reduction.

Further evidence to support the reduction of the Ga oxide species to the Ga cationic species (Ga^+ and GaH_2^+) is shown in the NH_3-TPD profiles (Figure 6.2).

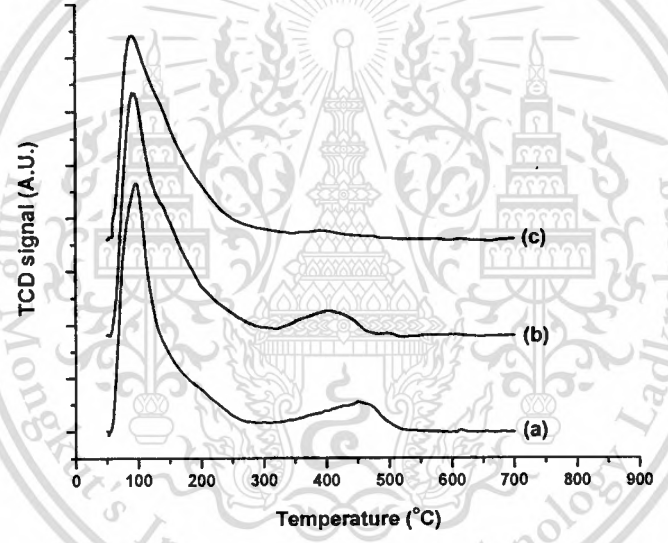

Figure 6.2. NH_3-TPD profiles of (a) HZSM-5(28), (b) [Ga]HZSM-5(28), and (c) [Ga]HZSM-5(28) reduced with H_2 at 550 °C.

Typically, the spectra of HZSM-5(28) exhibits two characteristic peaks [24,25]; (i) from the NH_3 adsorbed on Si–OH or from non-zeolitic impurity (~ 50-200 °C), and (ii) from the NH_3 adsorbed on the acidic hydroxide group ≡Si–OH–Al≡ (~ 300-500 °C). It can be seen that when the Ga species was introduced into zeolite, only a slight decrease in bridging Brønsted acid site can be observed. This suggests that, as the catalyst was calcined and only treated with He, the incorporated Ga are mostly retained as isolated oxide (Ga_2O_3) and exchangeable (GaO^+) forms. Such GaO^+ can replace onto the Brønsted acid site. Accordingly, the acidity of the [Ga]HZSM-5

can be diminished as compared to that of HZSM-5 (Figure 6.2). However, a dramatic decrease in the Brønsted acid site could be seen when the catalyst was treated with H_2. This is due to the replacement of Ga cationic species (Ga^+ and GaH_2^+) onto the Brønsted acid sites. It is evidenced that the exchangeable Ga cationic species are predominant in [Ga]HZSM-5 when the catalyst is reduced.

6.3.2 Effect of Ga-incorporated HZSM-5

Table 6.2 % Conversion of ethane to ethylene over HZSM-5(28) and [Ga]HZSM-5(28).

Reaction temperature (°C)	HZSM-5(28)		[Ga]HZSM-5(28)	
	He	H_2	He	H_2
550	0.00	0.00	4.87	19.35
600	0.73	0.00	18.52	42.29
650	2.56	0.90	25.84	53.36
700	6.13	2.16	55.89	62.40
				(94.89, 5.11)[a]
750	12.55	3.39	67.75	69.13
				(82.41, 17.59)[a]

Reaction conditions: Catalysts = HZSM-5(28) and [Ga]HZSM-5(28), Reaction temperature = 550-750 °C, Carrier gas = He and H_2, Reactant = ethane.

[a] The selectivity of ethylene was 100 % except these results that ethylene and methane selectivity were shown in blanket.

From Table 6.2, it can be clearly seen that the conversion of ethane to ethylene is increased with reaction temperature for all experiments. This is due to an increase in the dehydrogenation rate which is favored at a high reaction temperature. Regarding to the activity of HZSM-5(28), a low conversion of ethane can be obtained when using both H_2 and He as carrier gas. While the introduction of Ga in zeolite ([Ga]HZSM-5(28)) can promote a higher dehydrogenation activity leading to a high ethylene yield. This is consistent with the previous work [1-3] that Ga-modified zeolite is of great interest for light paraffin aromatization via

dehydrogenation activity of the incorporated Ga. It is interesting that the higher ethane conversion can be obtained over such Ga-modified catalyst under H_2. This confirms that the reduced Ga species (Ga^+, GaH_2^+) possesses a high dehydrogenation activity as compared to the Ga oxide species (Ga_2O_3, GaO^+). However, the question as to why the reduced Ga species possess the relatively high dehydrogenation activity remains unclear. Such reduced Ga species may be present as Ga^+ and/or GaH_2^+ depending on the treatment. Accordingly, the study of pulsed reaction aimed to compare the catalytic activity of such reduced Ga species was carried out. For instance, the Ga^+ can be achieved by the reduction of Ga oxide and such Ga species can readily chemisorb H_2, forming GaH_2^+. However, the GaH_2^+ species was only preserved by keeping it in the H_2 system. Without H_2, the GaH_2^+ can decompose mainly to Ga^+ at high temperature.

6.3.3 Effect of Ga species type

The reaction temperature of 650 °C was chosen to investigate ethane dehydrogenation. This is because, according to the TPR (Figure 6.1), it could provide the predominant reduced Ga species when Ga oxide was reduced. Moreover, the GaH_2^+ can also decompose to Ga^+ at this reaction temperature under the non-reducing atmosphere [20,23].

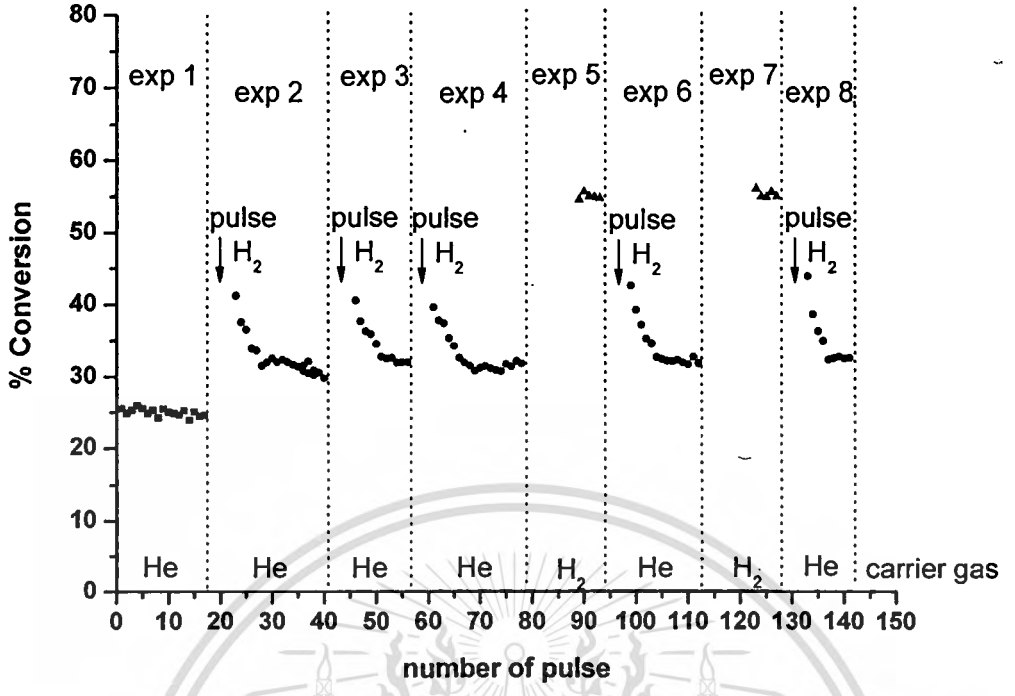

Figure 6.3 Ethane pulsed reaction over [Ga]HZSM-5(28) catalyst with different reaction condition.

Reaction conditions: Catalyst = [Ga]HZSM-5(28), Reaction temperature = 650 °C, Pulsed volume = 25 microliters.

From Figure 6.3, it is interesting to note that the dehydrogenation activity of Ga-modified ZSM-5 depends largely on the Ga species which can be regulated by the H_2 concentration. It was found that ~ 25 % conversion of ethane can be obtained at the reaction using He as the carrier gas (Exp. 1). The small Ga_2O_3 particles generated after calcination and/or GaO^+ generated by the dehydration of $Ga(OH)_2^+$ ((Eq. (3)) were suggested to be the active species under this reaction condition. As the catalyst was calcined and only treated with He, the incorporated Ga are mostly retained as isolated Ga_2O_3 and exchangeable GaO^+. Such Ga oxide species in [Ga]HZSM-5(28) can provide a relatively higher activity of ethane dehydrogenation, as compared to HZSM-5 (~ 2 % conversion). Again, it is interesting to note that there is no change of activity with the number of ethane pulses, despite the H_2 also being produced from the ethane dehydrogenation. This clearly shows that there is an excess of Ga active sites and the initial activity can be obtained from every single pulse.

When the catalyst was *in situ* reduced with pure H_2 (Exp. 2), a reproducible activity for ethane dehydrogenation to ethylene (~ 30% conversion) can be obtained. This evidences that, by reduction with H_2, a reduced Ga species can be generated and that possess a higher activity, as compared to the oxide forms. As H_2 can reduce Ga_2O_3 ((Eq. (1-2)) and/or GaO^+ ((Eq. (4)) to form Ga^+ and the Ga^+ formed can chemisorb H_2 to form GaH_2^+ ((Eq. (5)), it is likely that such GaH_2^+ species provide the catalytic activity higher than Ga^+ and Ga oxide. This is concluded from the high activity observed initially after H_2 is withdrawn. However, the GaH_2^+ cannot be stabilized in the absence of H_2. Hence, H_2 can readily desorb, particularly at high reaction temperatures to Ga^+ and a decrease in catalytic activity can be observed (~ 40 % to ~ 30 % conversion) in Exp. 2. Kazansky *et al.* [20,23] reported that at elevated temperatures GaH_2^+ species can consistently be stabilized only in a reductive hydrogen atmosphere. If the decomposition of GaH_2^+ can readily take place at the reaction temperature, this may well support the explanation for the change in catalytic activity for dehydrogenation in Exp. 2. However, the reduced Ga^+ species can be reserved after the H_2 desorption, consequently they can still promote a higher yield of ethylene, as compared to the Ga oxide species. To confirm the above suggestion, the same operating condition was performed with pulsed ethane dehydrogenation (Exps. 3 and 4). As expected, a similar result can be observed. It is, therefore, clear that the observed decrease in catalytic activity of [Ga]HZSM-5(28) (Exps. 2-4) is influenced by the decomposition of GaH_2^+ to Ga^+ species.

Since the decomposition of GaH_2^+ to Ga^+ would be favored in the absence of H_2, preventing this reaction may well be achieved by keeping the catalyst in a H_2 stream. Therefore, H_2 mixed with ethane was pulsed in the reaction (Exp. 5) under the H_2 carrier. It was found that a relative increase in activity was obtained (~ 55 % conversion) and there is no change in catalytic activity observed under the reaction using H_2 as the carrier gas. Accordingly, it is believed that the GaH_2^+ species is kept and that possesses the highest dehydrogenation activity among the other Ga species mentioned.

After switching to He (Exp. 6), the change in catalytic activity can be observed. It is evidenced that the GaH_2^+ could only be preserved when it was kept in the reducing stream. In contrast, the active GaH_2^+ can be decomposed to Ga^+ at a high reaction temperature under a non-reducing gas stream. Hence, the result observed in Exp. 6 is similar to those that were observed in Exps. 2-4. To confirm the above suggestion, Exps. 7 and 8 were tested and apparently such phenomenon can be reproduced. From the above results, it can be concluded that under the H_2 stream, GaH_2^+ cations are the predominant species in [Ga]HZSM-5 and provide the high catalytic

activity for ethane dehydrogenation to ethylene. The decrease in catalytic activity observed in Exps. 2-4, 6, and 8, is attributed to the decomposition of such GaH_2^+ cations to Ga^+.

6.3.4 Effect of Ga clusters and their treatment

Although Ga oxide is less active than the reduced Ga species, it is worthwhile investigating which Ga oxide species (Ga_2O_3 and GaO^+) is responsible for the observed activity in Exp. 1. Hence, the bulk Ga_2O_3 on HZSM-5(28) ((b-[Ga]HZSM-5(28)) was prepared and its catalytic activity tested.

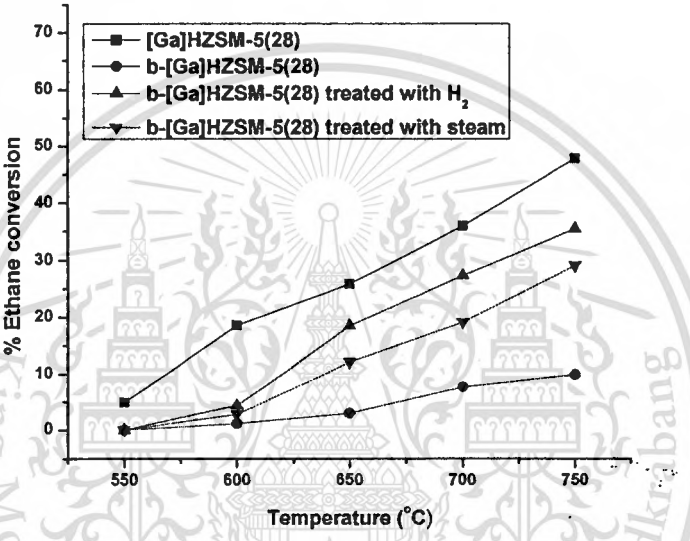

Figure 6.4 Effect of Ga cluster and their treatment.

Reaction conditions: Catalysts = [Ga]HZSM-5(28), b-[Ga]HZSM-5(28), and st-b-[Ga]HZSM-5(28), Reaction temperature = 550-750 °C, Carrier gas = He, Reactant = ethane.

From the Figure 6.4, it was clearly seen that a relatively lower ethane conversion can be obtained over b-[Ga]HZSM-5(28) (Ga particle size ~ 50-200 nm), as compared to [Ga]HZSM-5(28) in which Ga particles locate principally on the external surface of the zeolite crystals with a cluster size ~ 12 nm (not shown). A lower yield of ethylene can be derived by a small number of Ga_2O_3 sites on the surface, due mainly to the non-dispersion of the bulky Ga cluster.

After H_2 reduction at 750 °C, the bulky Ga oxide species would presumably be reduced and dispersed in the zeolite support, consequently, high ethane conversion can be pronounced. This is consistent with the H_2-TPR (Figure 6.1d) that the observed change in the nature and number of Ga species is caused by H_2 reduction. However, the dispersion of Ga_2O_3 upon

reduction in H_2 mainly produces Ga^+. To obtain the GaO^+ species, the solid-state reaction of Ga_2O_3 and steam was performed. It is suggested that water can react with the bulk Ga_2O_3 to form the well-dispersed GaO(OH) species and such species can consecutively react with Brønsted acid sites to form the exchangeable GaO^+.

$$Ga_2O_3 + H_2O \longrightarrow 2GaO(OH) \qquad \text{Eq. (6)}$$

$$GaO(OH) + H^+ \longrightarrow GaO^+ + H_2O \qquad \text{Eq. (7)}$$

The catalytic activity of b-[Ga]HZSM-5(28) treated with steam (st-b-[Ga]HZSM-5(28)) was investigated over ethane conversion and compared with that of Ga-containing HZSM-5(28) zeolite prepared by impregnation and solid-state redox reaction using H_2. From the Figure 6.4, it is worth noting that treating the bulk Ga_2O_3 with steam at 425 °C for 2 hours ((st-b-[Ga]HZSM-5(28)) can enhance the dehydrogenation activity of the b-[Ga]HZSM-5(28) catalyst. After the formation of GaO^+ due to the steaming, the relatively higher dehydrogenation activity can be observed, despite the sample not being reduced.

Further evidence to support this observation can be obtained by the TPR of b-[Ga]HZSM-5(28) and st-b-[Ga]HZSM-5(28) as shown in Figure 6.5.

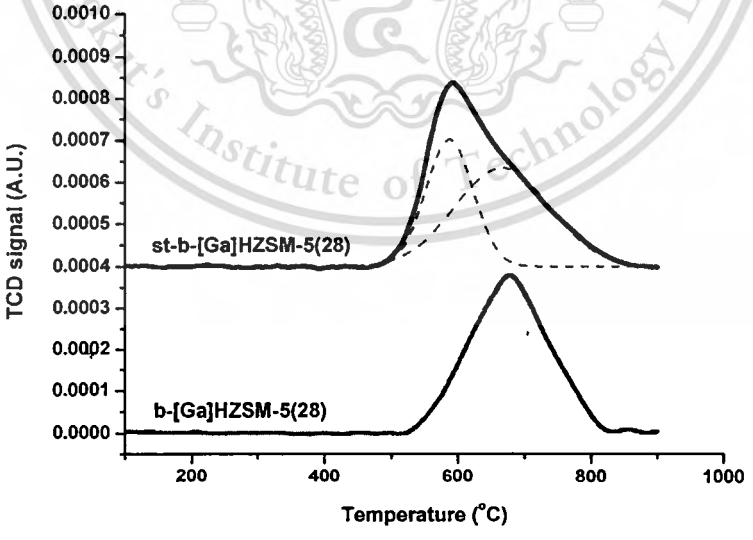

Figure 6.5 The TPR profiles of (a) b-[Ga]HZSM-5(28) and (b) st-b-[Ga]HZSM-5(28) treated with steam at 425 °C.

It can be seen that a reduction peak of bulk Ga_2O_3 in b-[Ga]HZSM-5(28) appears at ~ 670 °C. As expected, a H_2 consumption peak of the Ga species in the steamed sample (st-b-[Ga]HZSM-5(28)) is shifted toward a lower temperature. This is because the highly dispersed Ga species obtained from the steam treatment would be more feasibly reduced, as compared to the bulk Ga_2O_3. With the Gaussian deconvolution, a smaller signal at ~ 670 °C was observed over the st-b-[Ga]HZSM-5(28), indicating that less bulk Ga_2O_3 is retained in this sample. In other words, larger parts of the bulk Ga_2O_3 can be re-dispersed by reaction with steam ((Eq. (6-7)) to form GaO^+. Such Ga species possess the higher dehydrogenation activity, as compared to the bulk Ga_2O_3 (Figure 6.4).

6.3.5 Effect of the Si/Al ratio of zeolite

To study the effect of the Si/Al ratio of zeolite support, a ZSM-5 zeolite possessing a different Si/Al ratio (ZSM-5(165)) was prepared. The results are shown in Figure 6.6.

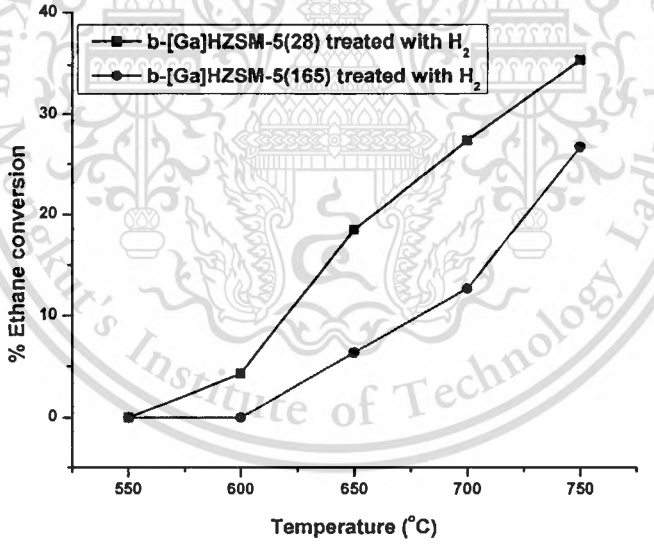

(c)

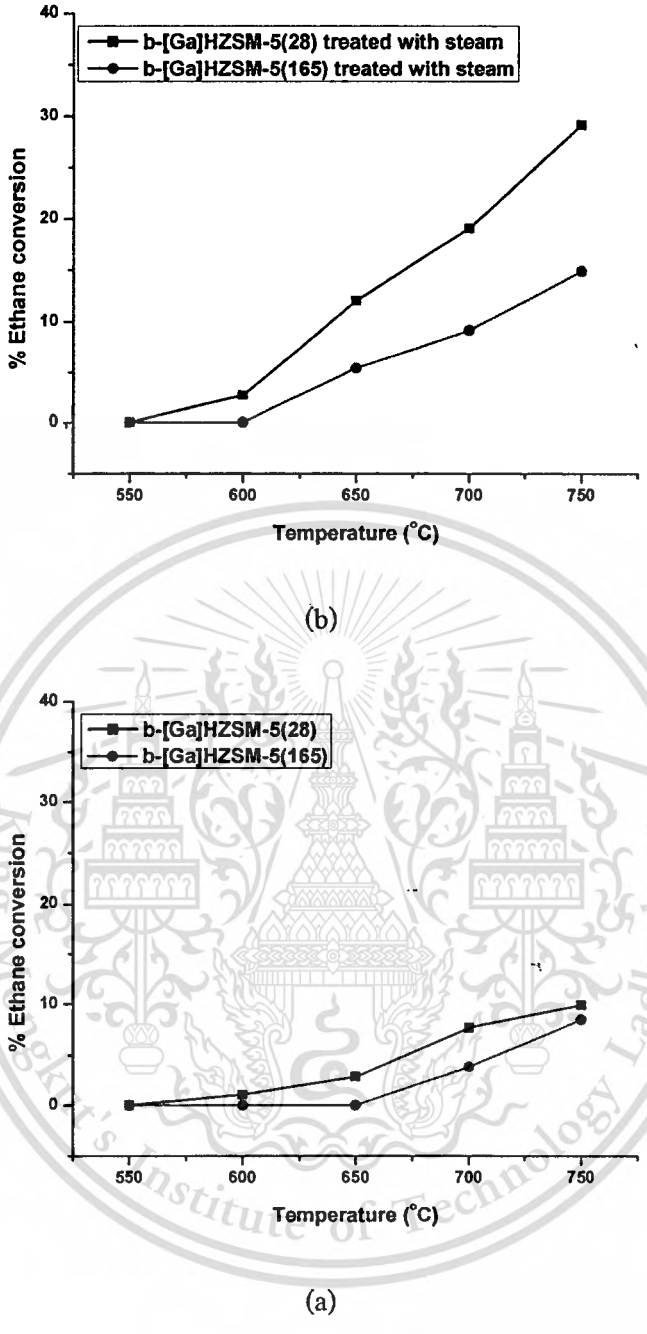

Figure 6.6 Effect of Si/Al ratio and treatment (a) treated with air at 550 °C, (b) treated with steam at 425 °C for 2 hours, and (c) treated with H_2 at 750 °C for 1 hour.

Reaction conditions: Catalysts = b-[Ga]HZSM-5(28), st-b-[Ga]HZSM-5(28), red-b-[Ga]HZSM-5(28), b-[Ga]HZSM-5(165), st-b-[Ga]HZSM-5(165), and red-b-[Ga]HZSM-5(165), Reaction temperature = 550-750 °C, Carrier gas = He, Reactant = ethane.

It is certain that the H_2 reduction and steaming can enhance the dehydrogenation activity by generating the Ga cationic species (Ga^+ and GaO^+). Although the same Ga content was loaded into the b-[Ga]HZSM-5(165), the lower dehydrogenation activity can be obtained, as compared to that b-[Ga]HZSM-5(28).

This is presumably explained by the number of Brønsted acid sites that play an important role in determining the number of reduced Ga cationic species formed into zeolite. The high acidity of zeolite can promote the high number of reduced Ga cationic species resulting in the high dehydrogenation activity ((Eqs. (2) and (7)).

To support with this view, the TPR of Ga-incorporated ZSM-5 with different Si/Al were determined.

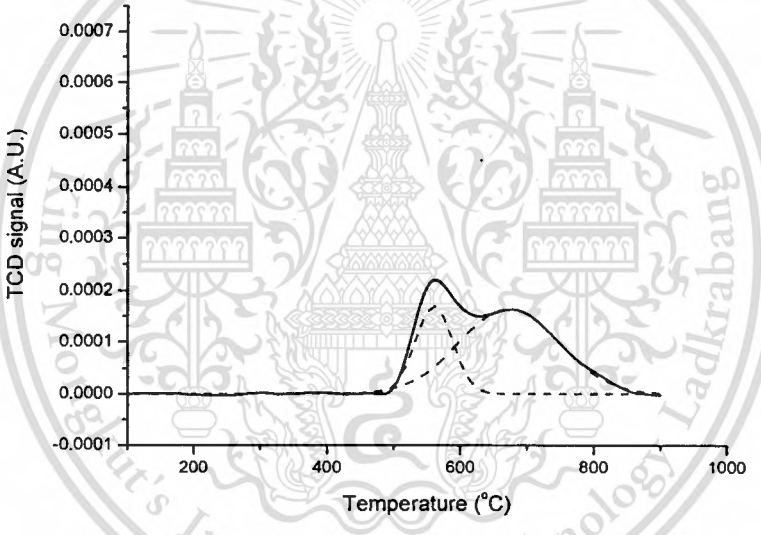

(d)

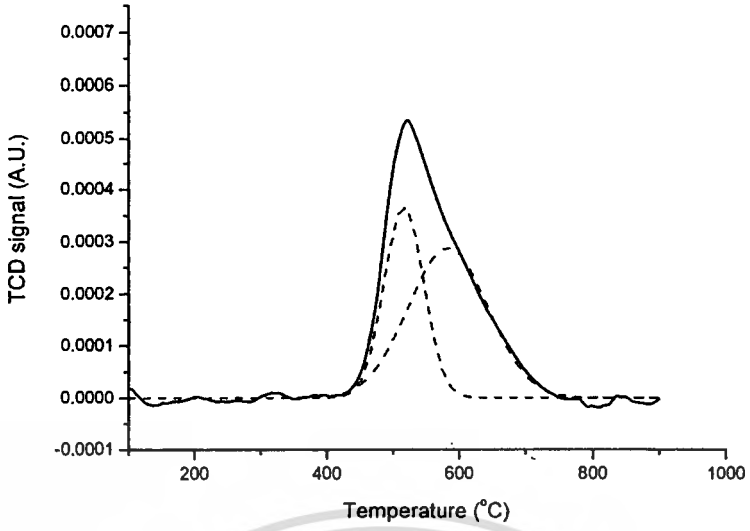

(c)

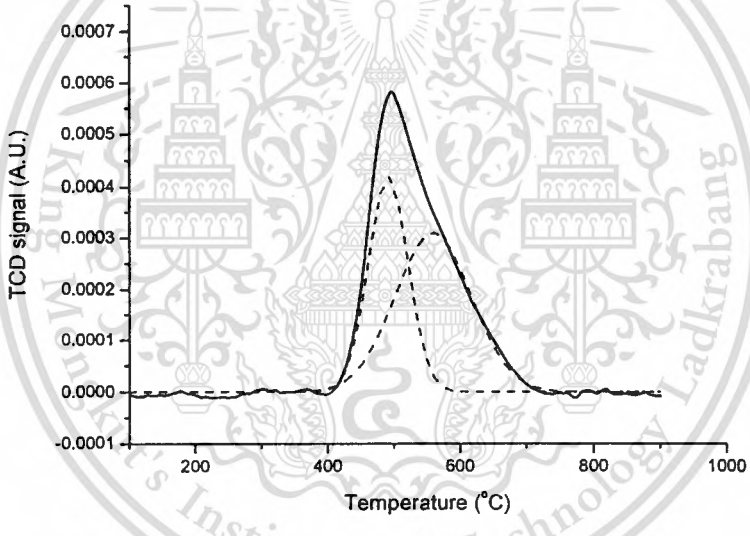

(b)

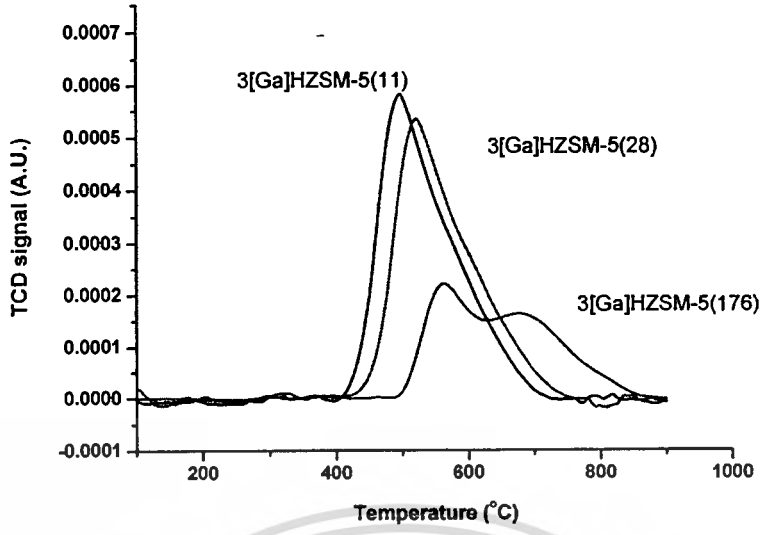

(a)

Figure 6.7 The TPR profiles of (a) various [Ga]HZSM-5 different Si/Al ratio, (b) 3[Ga]HZSM-5(11), (c) 3[Ga]HZSM-5(28), and (d) 3[Ga]HZSM-5(165).

With increasing the Si/Al ratio, the peak at the higher reduction temperature can be pronounced (Figure 6.7). This indicates that the high silica framework of the host zeolite, Ga_2O_3 particles can be aggregated outer the pore size of ZSM-5. This is due to the limitation of negative Al tetrahedral. From the above results, it is interesting to note that the acidity of zeolite can also control the dispersion of the Ga species and readily reduce their ability during the H_2 pretreatment or even in the reaction.

6.4. Conclusions

As the catalyst was calcined and only treated with He, the incorporated Ga are mostly retained as oxide forms, possibly Ga_2O_3, and GaO^+. Under the reaction condition studied, such Ga oxide species provide ~ 25 % ethane conversion. The Ga^+ generated under H_2 reduction, can further chemisorb H_2 to form active GaH_2^+. However, the decrease in catalytic activity was observed due to the decomposition of GaH_2^+ in He leading to the formation of Ga^+ which provides ~ 30 % ethane conversion. Preventing this decomposition reaction may well be achieved by keeping the GaH_2^+ species in a H_2 stream. Such GaH_2^+ species provide the highest catalytic activity (~ 55 % conversion) among the other Ga species mentioned. In addition, the hydrogen or

steam treatment can disperse the bulky Ga oxide species leading to the higher active cationic Ga species of Ga^{+} and GaO^{+}. While, Ga supported on the high aluminum zeolite (Si/Al ~ 28) displays the higher dehydrogenation, as compared to that high silica framework zeolite (Si/Al ~ 165). This is because the Brønsted acid of zeolite can control the dispersion resulting in the increase in the higher active sites.

References

[1] Choudhary V.R., Mantri K. and Sivadinarayana C., "Influence of Zeolite Factors Affecting Zeolitic on the Propane Aromatization Activity and Selectivity of Ga/H-ZSM-5" **Microporous and Mesoporous Materials.** vol. 37, 2000. pp. 1-8.

[2] Choudhary T.V., Kinage A.K., Banerjee S. and Choudhary V.R., "Effect of Temperature on the Product Selectivity and Aromatics Distribution in Aromatization of Propane over H-GaAlMFI Zeolite" **Microporous and Mesoporous Materials.** vol. 70, 2004. pp. 37-42.

[3] Dooley K.M., Chang C. and Price G.L., "Effects of Pretreatments on State of Gallium and Aromatization Activity of Gallium/ZSM-5 Catalysts" **Applied Catalysis A: General.** vol. 84, 1992. pp. 17-30.

[4] Kanazirev V., Price G.L. and Dooley K.M. "Preparation of Ga-Doped Zeolites via Hydrogen Induced Solid State Interaction Between Ga_2O_3 and HZSM-5 Zeolite" **Studies in Surface Science and Catalysis.** vol. 69, 1991. pp. 277-285.

[5] Ono Y., Kanae K., "Transformation of Butanes over ZSM-5 Zeolites" **Journal of the Chemical Society, Faraday Transactions.** vol. 87, 1991. pp. 663-667.

[6] Kwak B.S., Sachtler W.M.H. "Effect of Ga/Proton Balance in Ga/HZSM-5 Catalysts on C_3 Conversion to Aromatics" **Journal of Catalysis.** vol. 145, 1994. pp. 456-463.

[7] Choudhary V.R., Kinage A.K., Sivadinarayana C. and Guisnet M. "Pulse Reaction Studies on Variations of Initial Activity/Selectivity of O_2 and H_2 Pretreated Ga-Modified ZSM-5 Type Zeolite Catalysts in Propane Aromatization" **Journal of Catalysis.** vol. 158, 1996. pp. 23-33.

[8] Joly J.F., Ajot H., Merlen E., Raatz F. and Alario F. "Parameters Affecting the Dispersion of the Gallium Phase of Gallium H-MFI Aromatization Catalysts" **Applied Catalysis A: General.** vol. 79, 1991. pp. 249-263.

[9] Guisnet M., Gnep N.S. and Alario F., "Aromatization of Short Chain Alkanes on Zeolite Catalysts" **Applied Catalysis A: General.** vol. 89, 1992. pp. 1-30.

[10] Meitzner G.D., Iglesia E., Baumgartner J.E. and Huang E.S., "The Chemical State of Gallium in Working Alkane Dehydrocyclodimerization Catalysts. *In situ* Gallium *K*-Edge X-Ray Absorption Spectroscopy" **Journal of Catalysis.** vol. 140, 1993. pp. 209-225.

[11] Abdul Hamid S.B., Derouane E.G., Meriaudeau P. and Naccache C., "Effect of Reductive and Oxidative Atmospheres on the Propane Aromatisation Activity and Selectivity of Ga/H-ZSM-5 Catalysts" **Catalysis Today**. vol. 31, 1996. pp. 327-334.

[12] Fricke R., Kosslick H., Lischke G. and Richter M., "Incorporation of Gallium into Zeolites: Syntheses, Properties and Catalytic Application" **Chemical Reviews**. vol. 100, 2000. pp. 2303-2405.

[13] Meriaudeau P., Naccache C.. "Dehydrogenation and Dehydrocyclization Catalytic Properties of Gallium Oxide" **Journal of Molecular Catalysis**. vol. 50, 1989. pp. L7-L10.

[14] Meriaudeau P., Primet M., "FTIR Study of Hydrogen Adsorption on α-Ga_2O_3" **Journal of Molecular Catalysis**. 61 (1990) 227-234.

[15] Biscardi J.A., Iglesia E., "Structure and Function of Metal Cations in Light Alkane Reactions Catalyzed by Modified H-ZSM5" **Catalysis Today**. vol. 31, 1996. pp. 207-231.

[16] Price G.L., Kanazirev V. "Ga_2O_3/HZSM-5 Propane Aromatization Catalysts: Formation of Active Centers via Solid-State Reaction" **Journal of Catalysis**. vol. 126, 1990. pp. 267-278.

[17] Pokrovski G.S., Schott J., Hazemann J.L., Farges F. and Pokrovsky O.S. "An X-ray Absorption Fine Structure and Nuclear Magnetic Resonance Spectroscopy Study of Gallium-Silica Complexes in Aqueous Solution" **Geo Chimica et Cosmochimica Acta**. vol. 66, 2002. pp. 4203-4220.

[18] Shpiro E.S., Shevchenko D.P., Tkachenko O.P. and Dmitriev R.V. "Platinum Promoting Effects in Pt/Ga Zeolite Catalysts of Lower Alkane Aromatization. I. Ga and Pt Electronic States, Dispersion and Distribution in Zeolite Crystals in Dependence of Preparation Techniques. Dynamic Effects Caused by Reaction Mixture" **Applied Catalysis A: General**. vol. 107, 1994. pp. 147-164.

[19] Nowak I., Quartararo J., Derouane E.G. and Vedrine J.C. "Effect of H_2-O_2 Pre-Teatments on the State of Gallium in Ga/H-ZSM-5 Propane Aromatisation Catalysts" **Applied Catalysis A: General**. vol. 251, 2003. pp. 107-120.

[20] Kazansky V.B., Subbotina I.R., van Santen R.A. and Hensen E.J.M. "DRIFTS Study of the Nature and Chemical Reactivity of Gallium Ions in Ga/ZSM-5: II. Oxidation of Reduced Ga Species in ZSM-5 by Nitrous Oxide or Water" **Journal of Catalysis**. vol. 233, 2005. pp. 351-358.

[21] Gonzales N.O., Chakraborty A.K. and Bell A.T. "A Density Functional Theory Study of Hydrogen Recombination and Hydrogen-Deuterium Exchange on Ga/H-ZSM-5" **Topics in Catalysis**. vol. 9, 1999. pp. 207-213.

[22] Rane N., Overweg A.R., Kazansky V.B., van Santen R.A. and Hensen E.J.M., "Characterization and Reactivity of Ga^+ and GaO^+ Cations in Zeolite ZSM-5" **Journal of Catalysis**. vol. 239, 2006. pp. 478-485.

[23] Kazansky V.B., Subbotina I.R., van Santen R.A. and Hensen E.J.M. "DRIFTS Study of the Chemical State of Modifying Gallium Ions in Reduced Ga/ZSM-5 Prepared by Impregnation I. Observation of Gallium Hydrides and Application of CO Adsorption as a Molecular Probe for Reduced Gallium Ions" **Journal of Catalysis**. vol. 227, 2004. pp. 263-269.

[24] Hidalgo C.V., Itoh H., Hattori T., Niwa M. and Murakami Y., "Measurement of the Acidity of Various Zeolites by Temperature-Programmed Desorption of Ammonia" **Journal of Catalysis**. vol. 85, 1984. pp. 362-369.

[25] Post J.G., van Hoff J.H.C., "Acidity and activity of H-ZSM-5 measured with NH_3-t.p.d. and *n*-hexane cracking" **Zeolites**. vol. 4, 1984. pp. 9-14.

Chapter 7

Catalytic Deoxygenation of Benzaldehyde and *m*-Cresol over Ga-Modified Zeolite

7.1 Introduction

In addition to the observed high ethane dehydrogenation activity in **Chapter 6**, Ga supported zeolites catalysts have been found to exhibit relatively high activity towards reactions involving dehydrogenation of light alkanes, namely aromatization [1-6]. Various gallium species reported in literatures [7-11] are well agreed with earlier observation in this thesis, i.e. as gallium oxide, in aggregated form on the external zeolite surface or as small particles in the zeolite micropore space, or in cationic form as oxidic GaO^+ or reduced Ga^+ or GaH_2^+ species. Among these, reduced Ga cationic species appears to be the most active center for hydrogenation/ hydrogenolysis. This can be applied for the rare noble metal, Ga based catalyst is proposed for the deoxygenation of oxygenated compounds in bio-oils to produce oxygen-free aromatics.

Bio-oils derived from biomass have been increasingly attractive as alternative sources of fuels and chemicals [12-16]. This is due to an increase in petroleum prices, government regulations on alternative energy, and commitments to greenhouse gas reduction [14,17,18]. However, the bio-oils contains various types of oxygenates that can cause problems when used as fuels. Among these, aldehyde and carboxylic are the most unwanted components [19-21]. Deoxygenation of bio-oils not only improves its fuel properties, but also provides alternative sources of petrochemicals [22-25].

This chapter deals with the conversion of benzaldehyde and *m*-cresol, the model compounds representing aromatic aldehydes and phenolic compound in bio-oil, to oxygen-free compounds. The deoxygenation reaction on supported gallium HZSM-5 and HBeta zeolite catalysts using benzaldehyde and *m*-cresol as the model feed were highlighted. The effects of reaction conditions such as H_2, reaction temperature, and water co-feeding were investigated in a continuous flow system. Moreover, the temperature-programmed techniques were performed to investigate the possible reaction pathway.

Part I : Catalytic deoxygenation of benzaldehyde over Ga-modified zeolite

7.2 Experimental details

7.2.1 Catalyst preparation and characterization

HZSM-5 (Si/Al ~ 45) samples were commercially obtained from Sud-Chemie. Conventional impregnate of HZSM-5 with $Ga(NO_3)_3$ were employed to obtain 1-6 wt% Ga loading [26,27]. The samples were then calcined at 550 °C for 4 hours in a flow of dry air. Hereafter, the catalysts were designated as %loading-[Ga]HZSM-5 according to their %Ga loading. In addition, the 3[Ga]Silica (3 wt% Ga loading) was prepared by silica (Hi-Sil from PPG) support with $Ga(NO_3)_3$ in order to study the effect of support influencing the formation of Ga species.

Temperature-programmed reduction (TPR) experiments were carried out using a TCD detector. Prior to the H_2-TPR, the sample was heated to 550 °C in a dry air for 1 hour (30 mL/min). Subsequently, the sample was cooled to 50 °C. The H_2 consumption was recorded with temperature, when the catalyst samples were heated in a flow of 2% H_2/Ar (30 mL/min) with a heating rate of 10 °C/min to 900 °C.

Temperature-programmed desorption of *i*-propylamine (IPA-TPD) were used to determine the Brønsted acidity. First, 50 mg of sample was pretreated at 550 °C in a flow of He. To study on the decrease in Brønsted acid site after [Ga]HZSM-5 reduction (red-[Ga]HZSM-5) and the additional of Brønsted acid site after [Ga]HZSM-5 steaming (st-[Ga]HZSM-5), the [Ga]HZSM-5 was pretreated at 550 °C in a flow of H_2 for 2 hours and at 450 °C in a flow of 0.6% H_2O/He for 2 hours, respectively. After the treatment, the sample was cooled in He to room temperature and then *i*-propylamine (IPA) was injected to the sample until saturation at 40 °C. The excess IPA was removed by flowing He. When the constant signal was achieved, the sample was heated to 900 °C at a rate of 10 °C/min. The mass peaks used to identify the various desorption products in IPA-TPD are as follows: *i*-propylamine (m/z = 44), propylene (m/z = 41), and ammonia (m/z = 17). The amount of desorbed IPA was simultaneously calibrated with 2 mL pulses of 2% propylene in He and the Brønsted acidity was then calculated [28].

H_2/D_2 exchange was studied using an MS detector. The catalyst sample was heated in a flow of H_2 (m/z = 2) at 450-550 °C and then consecutive 2 mL pulses of pure deuterium, D_2 (m/z =

4), were injected to the sample. The mass peaks were monitored to determine the reactant fed and the formation of H-D (*m/z* = 3).

7.2.2 Temperature-programmed desorption (TPD) of benzaldehyde

The evolution of pre-adsorbed benzaldehyde over modified HZSM-5 catalysts was followed by TPD. Before adsorption the sample (50 mg) were dried in a flow of He (or H_2) at 550 °C for 2 hours. Adsorption of benzaldehyde until saturation took place at 180 °C, the sample was flushed with He (or H_2) at the same temperature for 3 hours. TPD measurements were done from 180 to 900 °C with a heating rate of 10 °C/min using He (or H_2) as the carrier gas. The masses (*m/z*) of 15, 18, 28, 77, 91, and 105 were monitored to determine the methane, water, carbon monoxide, benzene, toluene, and benzaldehyde, respectively.

7.2.3 Benzaldehyde pulse reaction

The procedure for the benzaldehyde pulse reaction studies was as follows; 50 mg of catalyst was pretreated in a flow of He or H_2 (30 mL/min). After the pretreatment, 1 microliter of pure liquid benzaldehyde was injected to the pretreated catalyst to obtain its initial activity/selectivity. This procedure was repeated to obtain the benzaldehyde conversion at the different reaction temperature. The products of the pulse reaction were analyzed by the MS detector, in a manner similar to that benzaldehyde TPD section.

7.2.4 Catalytic activity measurements for the deoxygenation of benzaldehyde

Catalytic testing of benzaldehyde conversion was performed with a continuous fixed bed reactor. Saturated vapor of benzaldehyde at 20 °C was carried by He (or H_2) at 30 mL/min regulated by a mass flow controller. The catalyst bed was set in a quartz tube reactor that was located inside a temperature-regulated furnace. The products were periodically collected and analyzed by an on-line gas chromatograph equipped with a flame ionization detector (FID) and HP-5 capillary column (Appendix B). The preferred reaction conditions used in the experiments were as follows; temperature, 400-550 °C; total pressure, 1 atm; carrier gas, He or H_2; W/F, 25-150 g·h/mol. To investigate the effect of water co-feeding, water was continuously fed through the sample bed at a flow rate of 0.034 mL/min using a syringe pump then mixed with the benzaldehyde feed.

7.3 Results and discussion

7.3.1 Catalyst characterization

The characteristics of the catalyst samples including Si/Al ratio of the host zeolite, % Ga loading, and BET surface area are shown in Table 7.1.

Table 7.1 Chemical composition and surface area of catalyst samples.

Catalyst	Si/Al	Ga content[a] (wt%)	Surface area (m^2/g)
HZSM-5	45	-	545
1[Ga]HZSM-5	45	0.9	520
3[Ga]HZSM-5	45	2.8	510
6[Ga]HZSM-5	45	5.8	500
3[Ga]Silica	ND	2.9	370

[a] Elemental analysis for Si, Al, and Ga were performed using ICP.

Figure 7.1 shows the TPR curves observed for the calcined catalyst samples.

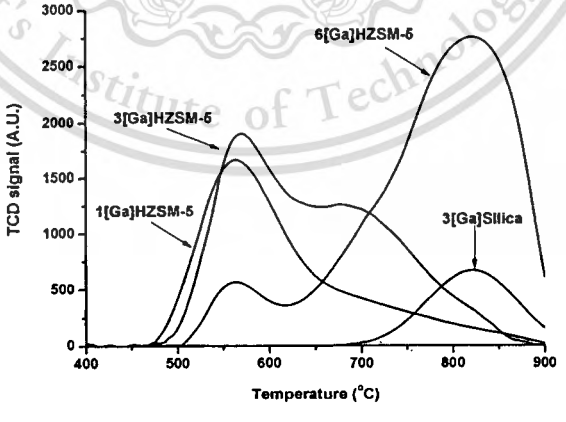

(e)

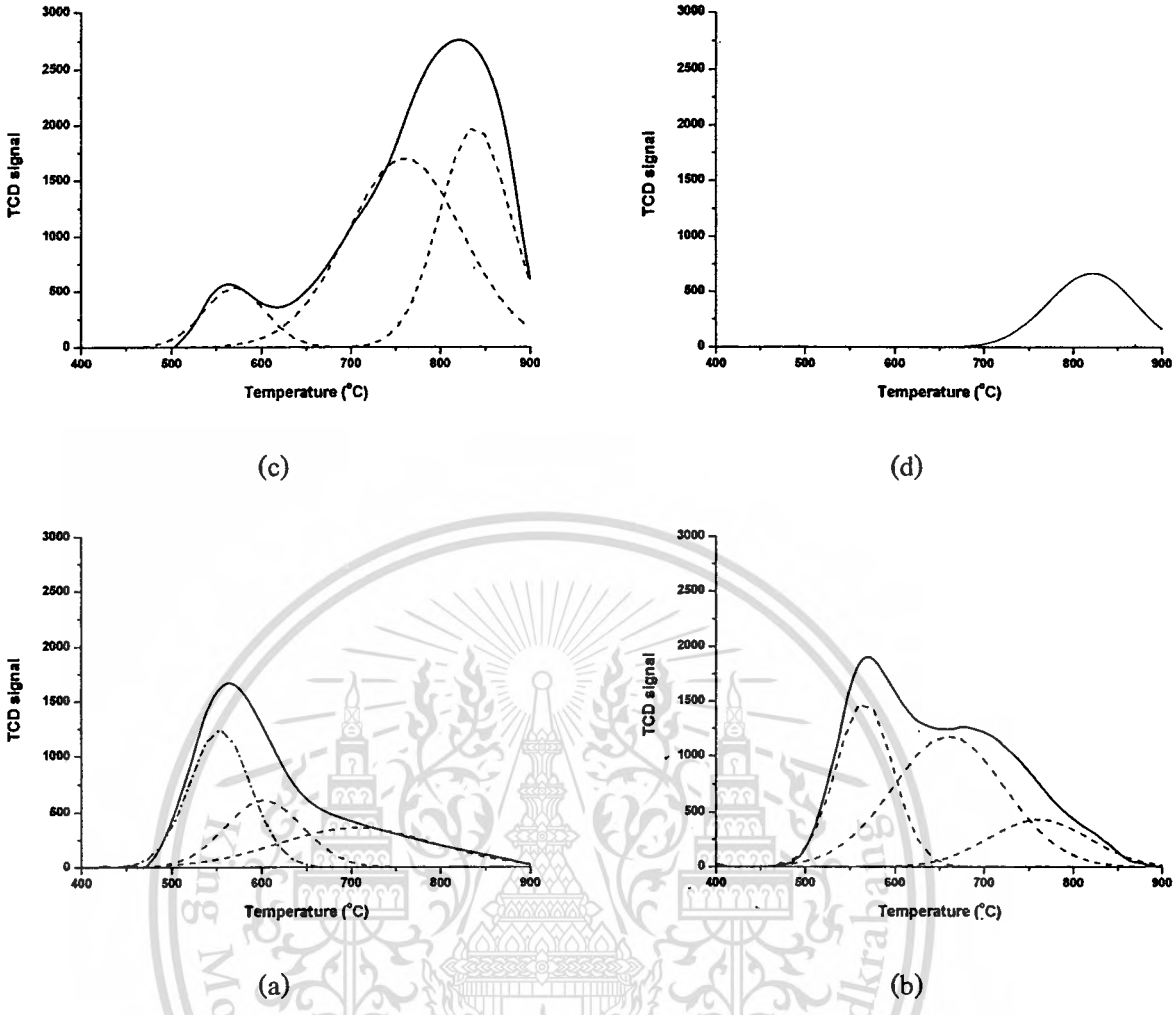

Figure 7.1 TPR profiles of (a) 1[Ga]HZSM-5, (b) 3[Ga]HZSM-5, (c) 6[Ga]HZSM-5, (d) 3[Ga]Silica, and e) comparison data of Ga supported catalyst.

With the Gaussian deconvolution, three major peaks are observed on the Ga supported zeolite and the H_2 consumption for each reduction peak are summarized in Table 7.2.

Table 7.2 Summary of the temperature reduction and H_2 consumption.

Catalyst	Temperature (°C)			% Area of H_2 consumption			H_2/Ga_2O_3
	T_1	T_2	T_3	A_1	A_2	A_3	(mol ratio)
1[Ga]HZSM-5	553	602	706	43	26	31	1.25
3[Ga]HZSM-5	566	660	761	32	51	17	0.61
6[Ga]HZSM-5	570	760	838	9	53	38	0.43
3[Ga]Silica	ND	ND	820	0	0	100	0.13

In the case of low % Ga loading (1 and 3[Ga]HZSM-5), the T_1 (~ 550-560 °C) and T_2 (~ 600-660 °C) peak were assigned to the reduction of well-dispersed Ga species such as small Ga_2O_3 particles or GaO^+ species interacting with the zeolite. While, the T_3 (~ 700-760 °C) peak was attributed to large, bulk Ga_2O_3 particles separated from or loosely support on the zeolite matrix [29]. By increasing Ga content up to 6 wt%, the T_2 and T_3 shift to higher temperatures. This indicates that the incorporated Ga species can be agglomerated into a larger Ga_2O_3 cluster, particularly on the outer surface of ZSM-5. This is due to a relatively weaker interaction of the incorporated Ga species with a framework having limited Al content (Si/Al = 45). This is consistent with the TPR curve of 3[Ga]Silica indicates that a well-dispersion cannot be obtained over the support without uniform pore system and adequate high activity acid site. Hence, the 3[Ga]Silica TPR curve displays only one peak of larger gallium oxide particles at relatively high reduction temperature (Figure 7.1d).

From Table 7.2, the highest extent of H_2 consumption (H_2/Ga_2O_3) can be obtained over 1[Ga]HZSM-5 and this decreases with an increase in Ga loading, in consistent with Kwak's report [5]. The relatively lower reduction extent can be explained by the incomplete reduction of bulk Ga_2O_3 cluster [30,31]. Accordingly, a high % H_2 consumption of well-dispersed Ga species in 1[Ga]HZSM-5 (A_1-A_2) was particularly observed for highly dispersed Ga species at low reduction temperature.

The acidity of Ga-modified HZSM-5 catalysts after H_2 reduction was determined by IPA-TPD method [28] and the results were shown in Figure 7.2.

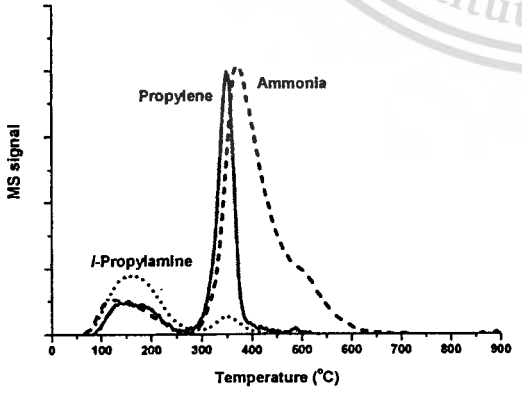

(d)

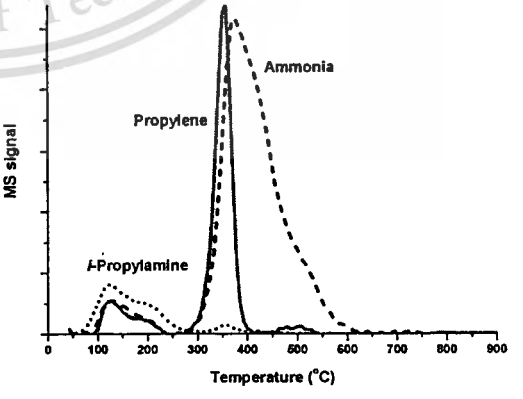

(e)

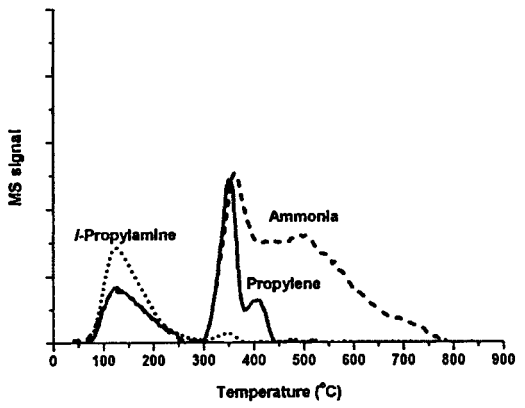

(b)

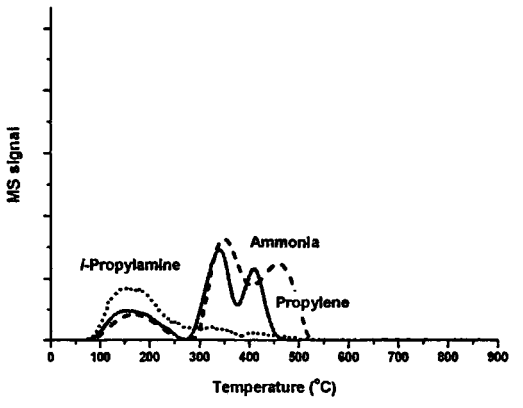

(c)

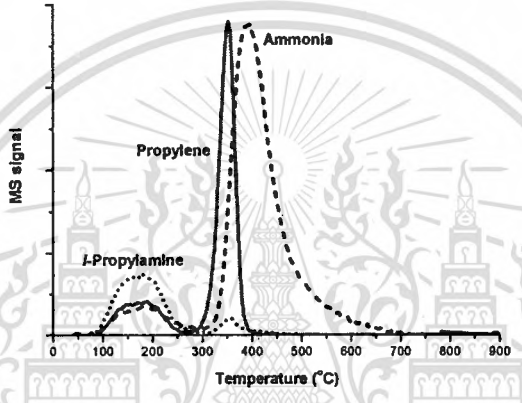

(a)

Figure 7.2 IPA-TPD of (a) HZSM-5, (b) red-1[Ga]HZSM-5[a], (c) red-3[Ga]HZSM-5[a], (d) 3[Ga]HZSM-5[b], and (e) st-3[Ga]HZSM-5[c].

[a] *The Ga supported zeolite was firstly reduced with H_2 at 550 °C for 2 hours.*

[b] *The Ga supported zeolite was firstly treated with He at 550 °C for 2 hours.*

[c] *The Ga supported zeolite was firstly treated with steam at 450 °C for 2 hours.*

It was found that the Hofmann degradation of *i*-propylamine to ammonia and propylene take places over HZSM-5 at ~350 °C. The number of bridgingly Brønsted acid site (≡Si-OH-Al≡) can be calculated and shown in Table 7.3.

Table 7.3 Acidity of various catalysts[a].

Catalyst	Acidity of catalyst (micromol/g)		
	High activity acid sites	Low activity acid sites	Total acidity
HZSM-5	315	0	315 (*330*[b])
3[Ga]HZSM-5	305	0	305
red-1[Ga]HZSM-5	149	31	180
red-3[Ga]HZSM-5	91	64	155
st-3[Ga]HZSM-5	377	0	377

[a] The data were summarized from IPA-TPD curves.

[b] Theoretical acidity calculated from Si/Al ratio.

The TPR and IPA-TPD studies (Figure 7.1 and 7.2) provide some insight into the chemistry of zeolite-Ga species for formation of the reduced Ga species under H_2 treatment. The reduction of octahedrally coordination Ga_2O_3 (Ga^{3+} ions) would lead to the formation of reduced univalent Ga^+ ions which can replace with acidic protons (Eq. (1)-(2)) [1, 9,32,33].

$$Ga_2O_3 + 2H_2 \longrightarrow Ga_2O + 2H_2O \qquad \text{Eq. (1)}$$

$$Ga_2O + 2Z^-H^+ \longrightarrow 2Z^-Ga^+ + H_2O \qquad \text{Eq. (2)}$$

where Z^- represents the negative framework charge of zeolite.

This suggestion is evidenced by the H_2 consumption (Figure 7.1 and Table 7.2) and decrease in Brønsted acid site in the order of 3[Ga]HZSM-5 < 1[Ga]HZSM-5 < HZSM-5 (Figure 7.2 and Table 7.3) when the [Ga]HZSM-5 is reduced. The Ga cationic species (Ga^+) would be formed over the exchangeable sites.

In addition to a decreased number of sites with high activity acid sites, an introduction of Ga content into zeolite can provide the additional acid sites with relatively lower activity (> 400 °C) when treatment with H_2. This signal may well be assigned to GaOH species which has been previously observed by FTIR after reduction of [Ga]HZSM-5 in H_2 [11,34]. Accordingly, no signal at > 400 °C can be observed over 3[Ga]HZSM-5 treated with He [35]. As the Ga content is

increased, such additional weak acid sites are also increased together with the reduction of strong acid sites.

However, only a slightly reduction of bridgingly Brønsted acid site can be observed (Figure 7.2 and Table 7.3), when the catalyst was calcined and only treated with He, This suggests that the incorporated Ga are mostly retained as isolated oxide forms (i.e. Ga_2O_3). Accordingly, the acidity of the 3[Ga]HZSM-5 can be pronounced with a similar extent as observed over HZSM-5 (Table 7.3). Alternatively, several reports [29,32] suggest that, when soluble Ga species is incorporated into HZSM-5, $Ga(OH)_2^+$ is primarily exchanged into the negative framework of ZSM-5. Such species can dehydrate to form GaO^+ at high temperature [36].

$$Ga(OH)_2^+ \longrightarrow GaO^+ + H_2O \qquad \text{Eq. (3)}$$

The GaO^+ would be dispersed over the exchangeable sites in the framework leading to the decrease in Brønsted acid.

When the Ga containing zeolite was subjected to steaming (st-3[Ga]HZSM-5), the Brønsted acid site is markedly increased (Figure 7.2e), as compared to that of HZSM-5. This is consistent with our previous works [37] that under hydrothermal treatment, the incorporated Ga species can be inserted into the framework possibly by reaction with the defect silanols of the framework. This would lead to an additional Brønsted acid sites, as evidenced by solid state ^{1}H-NMR and FTIR in **Chapter 5**.

$$GaO^+ + H_2O \longrightarrow GaO(OH) + H^+ \qquad \text{Eq. (4)}$$

It is suggested that such GaO(OH) species [38] can be incorporated in the framework by the reaction with available defect silanols, forming additional Brøsted acid sites (≡Ga-OH-Si≡) [37].

$$GaO(OH) + 4\ (\equiv Si\text{-}OH) \longrightarrow GaH(OSi\equiv)_4 + 2H_2O \qquad \text{Eq. (5)}$$

7.3.2 Effect of W/F

The product distribution from benzaldehyde conversion on 3[Ga]HZSM-5 at 500 °C is shown in Figure 7.3 as a function of space times (W/F).

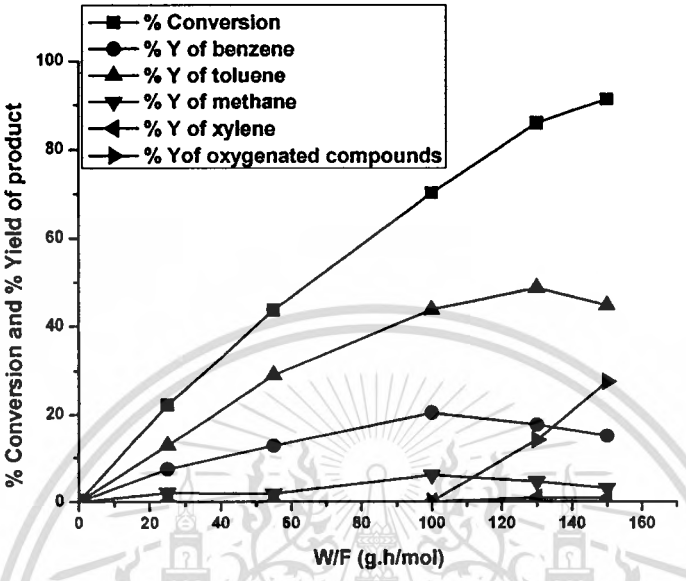

Figure 7.3 The effect of W/F.

Reaction conditions: Catalyst = 3[Ga]HZSM-5, W/F = 25-150 g·h/mol, Reaction temperature = 500 °C, Carrier gas = H_2, Pressure = 1 atm.

It is clearly seen from the Figure 7.3 that benzaldehyde can be converted to benzene, toluene, and methane over 3[Ga]HZSM-5 catalyst under H_2 stream. The major products, namely benzene and toluene are expected products from decarbonylation and hydrogenation/ hydrogenolysis of benzaldehyde, respectively. The observed increase in benzene and toluene with low space time (W/F) < 100 g·h/mol, suggests that the formation of benzene and toluene are in parallel. The fact that toluene is highly produced over this catalyst suggested that the hydrogenation/hydrogenolysis of benzaldehyde is preferably promoted over Ga containing zeolite. The formation of methane is derived by the side reaction of toluene hydrodealkylation. This is generally observed over the metal-modified acid zeolite [39,40].

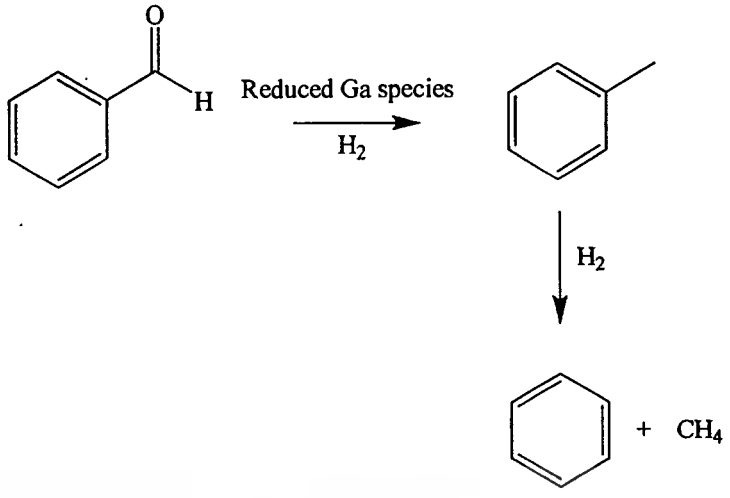

At relatively higher W/F (> 100 g·h/mol), xylenes and high molecular weight oxygenated compounds can also be observed (Figure 7.3). Xylenes were possibly derived from the toluene disproportionation. While the oxygenates can be generated from the secondary reaction of benzaldehyde with the decarbonylated/hydrogenolysed species.

It is suggested that the hydrogenation/hydrogenolysis activity is promoted over the reduced Ga species (Ga^+/GaH_2^+) generated after the H_2 treatment. After the formation of Ga^+ by H_2 reduction, such Ga^+ ions can further chemisorb molecular H_2 resulting in the formation of gallium dihydrides (GaH_2^+) [29, 32, 41, 42].

$$Z^-Ga^+ + H_2 \longrightarrow Z^-GaH_2^+ \qquad \text{Eq. (6)}$$

The existence of the GaH_2^+ species is in good agreement with the previously observed adsorption band at ~ 2040 cm^{-1} [11]. Since the hydride transfer play an important role in the formation of toluene. It is believed that H_2 not only keeps Ga species in its reduced forms but H_2 can also preserve GaH_2^+ species.

The evidence supported the hydrogenation/hydrogenolysis activity of GaH_2^+ was shown in Figure 7.4 and Table 7.4.

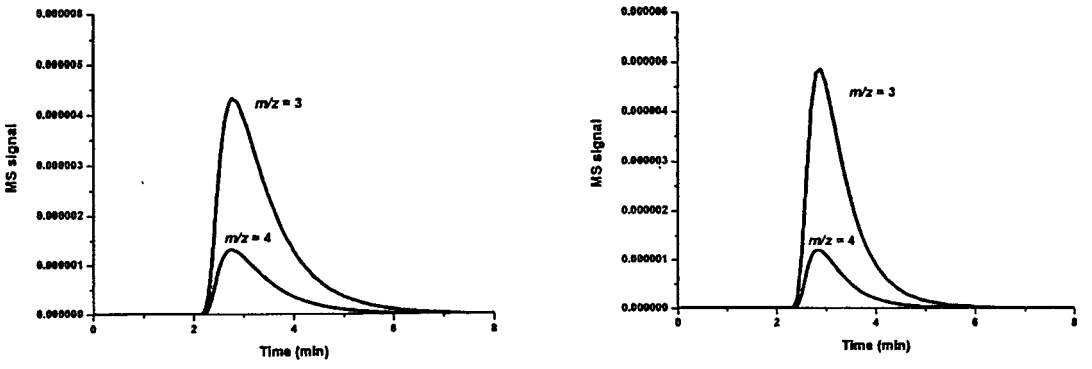

Figure 7.4 H_2/D_2 exchange over (a) HZSM-5 and (b) 3[Ga]HZSM-5 at 550 °C.

The signal of H-D and D-D were obtained by detect m/z = 3 and 4, respectively.

Table 7.4 Activity of H_2/D_2 exchange of various catalysts.

Type of catalyst	Temperature (°C)	Area ratio of H-D/D-D
HZSM-5	450	3.18
	500	3.33
	550	3.44
3[Ga]HZSM-5	450	3.52
	500	4.00
	550	4.22

H_2/D_2 exchange to form H-D (*m/z* = 3) can be promoted over both HZSM-5 and 3[Ga]HZSM-5. The activity was also increased with temperature. It is clearly seen that 3[Ga]HZSM-5 exhibits a higher activity for H_2/D_2 exchange for all temperature, as compared to HZSM-5. This suggests that, in addition to the acid-catalyzed H_2/D_2 exchange, hydrogenation/hydrogenolysis can be readily promoted over 3[Ga]HZSM-5.

The GaH_2^+ species which is presumably generated by the interaction of reduced Ga^+ species with H_2 (Eq. (6)), is suggested to be an active species for H_2/D_2 exchange process. This process involved the formation of the stable intermediate Z(D)(Ga(H_2)(D)) was proposed by Gonzales [43].

$$ZGa(H_2) + D_2 \rightleftharpoons Z(D)(Ga(H_2)(D)) \quad \text{Eq. (7)}$$

$$Z(D)(Ga(H_2)(D)) \longrightarrow ZGa(H)(D) + HD \quad \text{Eq. (8)}$$

D_2 molecule can dissociate to two D atoms; one interacts with the $Z^-GaH_2^+$ site, the other is bonded to an O atom in the zeolite framework.

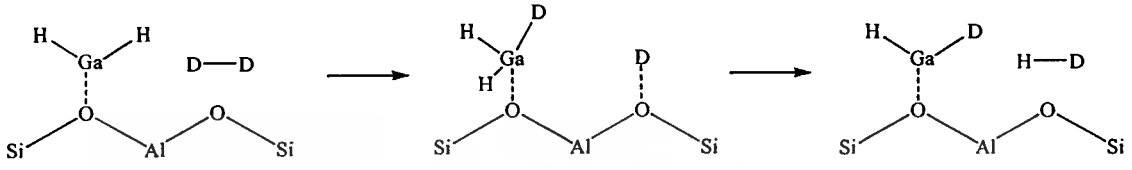

However, it is important to note that the observed H_2/D_2 exchanged activity over HZSM-5 does not derive from the dissociative adsorption of H_2/D_2 and consecutive recombination of the adsorbed H/D species. It is known that, over HZSM-5, the D_2 can adsorb on the Brønsted acid site by interacting with both acidic proton and the countered framework oxygen. The formation of H–D–D triad (three centers-two electrons) is proposed [43] for the transition state of H-D formation, in a manner similar to H_2 transfer mechanism.

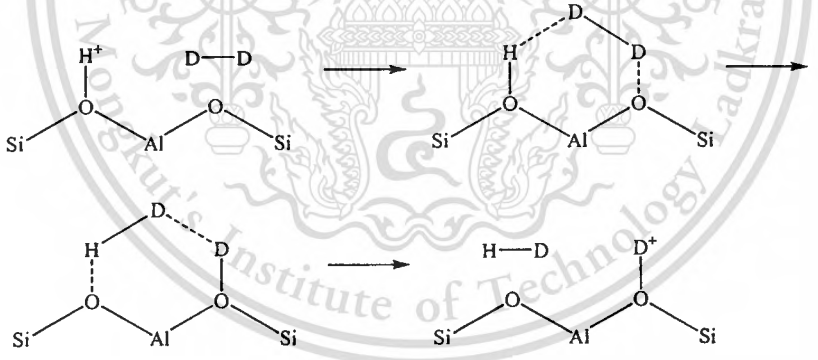

From the above results, it can be suggested that the GaH_2^+ formed by H_2 chemisorption can promote dihydride to the carbonyl group of benzaldehyde leading to the benzyl alcohol which can readily hydrogenolyse to form toluene and water.

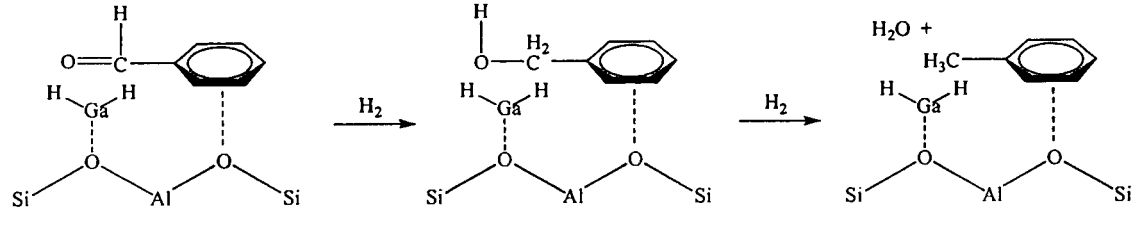

The formation of water together with toluene can be evidenced by the benzaldehyde-TPD (Figure 7.5).

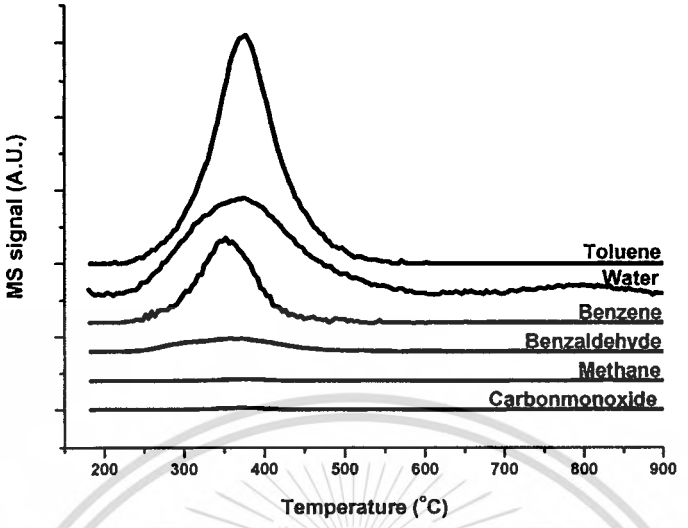

Figure 7.5 Benzaldehyde-TPD of 3[Ga]HZSM-5 treated with H_2 and run TPD under H_2.

7.3.3 Effect of Ga and type of carrier gas

When the Ga in 3[Ga]HZSM-5 is primarily reduced, the benzaldehyde conversion under He stream still provides small amount of toluene (15.89 % selectivity) at initial state. After that only 100 % selectivity of benzene is obtained for the rest of time on stream (41.72 % conversion).

This is consistent with the benzaldehyde-TPD over 3[Ga]HZSM-5 treated with H_2 and then carried out the TPD under He stream (Figure 7.6).

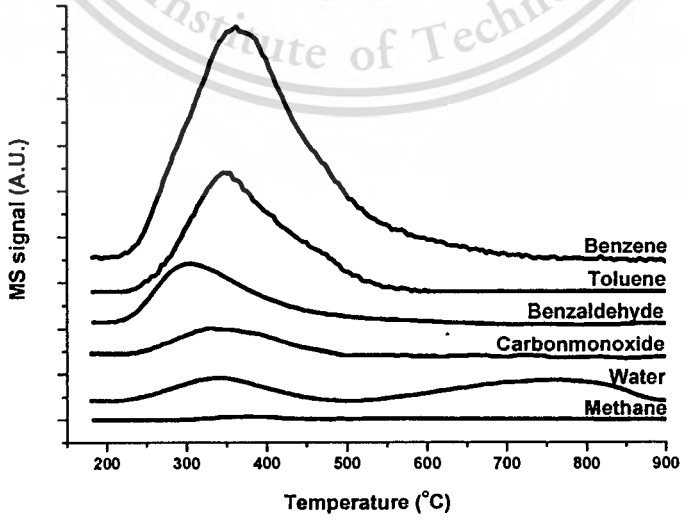

Figure 7.6 Benzaldehyde-TPD of 3[Ga]HZSM-5 treated with H_2 and run TPD under He.

It can be seen that benzene is mainly evolved in this test. Since the hydrogenation/ hydrogenolysis reaction require H_2 for toluene production, such reactions were diminished without H_2. Although the benzaldehyde conversion was carried out under He stream, the retained reduced Ga species still promote hydrogenation/hydrogenolysis giving toluene yield at initial state. It is suggested that the retained reduced Ga species can readily chemisorbed hydrogen, presumably GaH_2^+. Such Ga species can promote dihydride to carbonyl group of benzaldehyde, as discussed earlier. However, the lower toluene yield can be obtained over reduced 3[Ga]HZSM-5 under He stream, as compared to the reaction using H_2 gas. Consistent with Kazansky *et. al.* [11] reported that GaH_2^+ species are relatively stable and decompose only partially in the system without H_2. If the decomposition can readily take place at the reaction temperature, this is may well support the decrease in catalytic activity for hydrogenation/hydrogenolysis under He stream.

Supporting with this view, only benzene yield can be observed (Table 7.5) over non-reduced 3[Ga]HZSM-5 under He stream.

Table 7.5 Effect of Ga and type of carrier gas.

Type of catalysts	Temperature (°C)	Carrier gas	% Conversion	Product distribution (% yield)		
				Benzene	toluene	Methane
H ZSM-5	450	He	56.32	56.32	0.00	0.00
		H_2	54.23	54.23	0.00	0.00
3[Ga]H ZSM-5	450	He	55.80	55.80	0.00	0.00
		H_2	58.20	19.95	36.40	1.85
3[Ga]H ZSM-5	500	He	69.07	69.07	0.00	0.00
		H_2	70.22	20.42	43.71	6.09

Reaction conditions: Catalysts = HZSM-5 and 3[Ga]HZSM-5, W/F = 100 g·h/mol, Reaction temperature = 450 and 500 °C, Carrier gas = He and H_2, Pressure = 1 atm.

Although the Ga is present in the catalyst, the reaction of benzaldehyde over 3[Ga]HZSM-5 using He as a carrier gas, yields only benzene. This is presumably because the active Ga species, responsible for hydrogenation/hydrogenolysis activity may not exist in the [Ga]ZSM-5 treated with He. With the IPA-TPD results (Figure 7.2), 3[Ga]HZSM-5 treated with

He exhibits a similar acidity to HZSM-5 (Table 7.3). Accordingly, only decarbonylation activity can be obtained from this catalyst.

From the above results, it is concluded that the active species, which can promote the hydrogenation/hydrogenolysis forming toluene is the GaH_2^+ species. The lack of reducing gas (H_2), the Ga oxide species cannot promote the hydrogenation/hydrogenolysis. The Brønsted acid site plays important role to promote decarbonylation activity giving more benzene yield.

7.3.4 Effect of Ga content

To confirm the catalytic activity of the incorporated Ga species, the effect of Ga content was investigated (Figure 7.7).

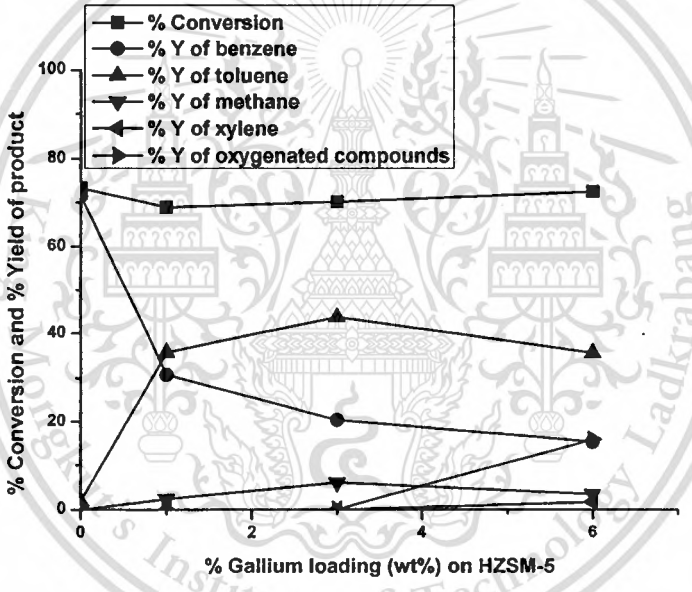

Figure 7.7 The effect of Ga content.

Reaction conditions: W/F = 100 g·h/mol, Reaction temperature = 500 °C, Carrier gas = H_2, Pressure = 1 atm.

From Figure 7.7, it is clearly seen that the increase in Ga content can especially convert benzaldehyde to form toluene. This is due to the increase in hydrogenation/hydrogenolysis activity provided by the incorporated Ga species. However, the decrease in toluene yield, along with an increase in high MW oxygenates can be observed over 6[Ga]HZSM-5. This is presumably explained that, as toluene would be largely produced, the catalyst can promote the secondary reaction of toluene with benzaldehyde to form high MW oxygenates.

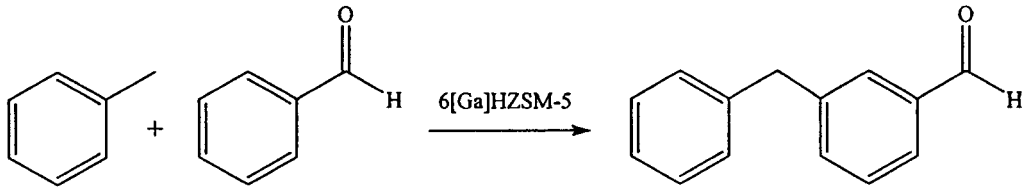

This suggestion is confirmed by the reaction of benzaldehyde/toluene, co-feeding over Ga-modified HZSM-5 catalyst (not shown). As expected, the relatively higher yield of high MW oxygenates was obtained. In addition, the xylene and oxygenated compounds generated at high W/F (Figure 7.3) and high Ga content (Figure 7.7) are presumably due to toluene disproportionation and alkylation of hydrogenolysed products, respectively.

From the above results (Table 7.5), benzene formation is derived not only from the toluene hydrodealkylation, but also from the benzaldehyde decarbonylation. This is evidenced by the benzene/methane ratio. It is suggested that the benzene formation is promoted over the Brønsted acid site of 3[Ga]HZSM-5 by decarbonylation.

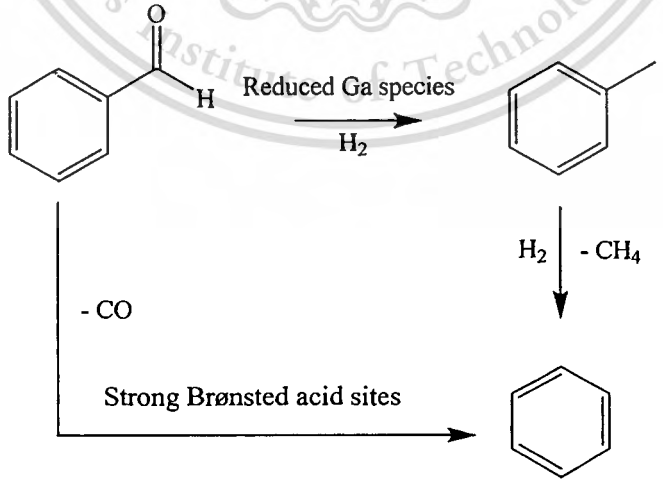

To confirm the decarbonylation activity promoted by Brønsted acid site, the benzaldehyde conversion over HZSM-5 was carried out. The Brønsted acid site of HZSM-5

provides the only yield of benzene (Table 7.5). Moreover, it can be seen that the presence of H_2 does not significantly affect the activity of HZSM-5. The result suggests that the decarbonylation does not require H_2 gas, as benzene can be largely produced in the reaction using He as carrier gas. It is likely that the Brønsted acid is responsible for decarbonylation of these catalysts, as no conversion of benzaldehyde can be obtained over NaZSM-5 (not shown).

Further evidences supporting the formation of benzene were studied using benzaldehyde-TPD (Figure 7.8).

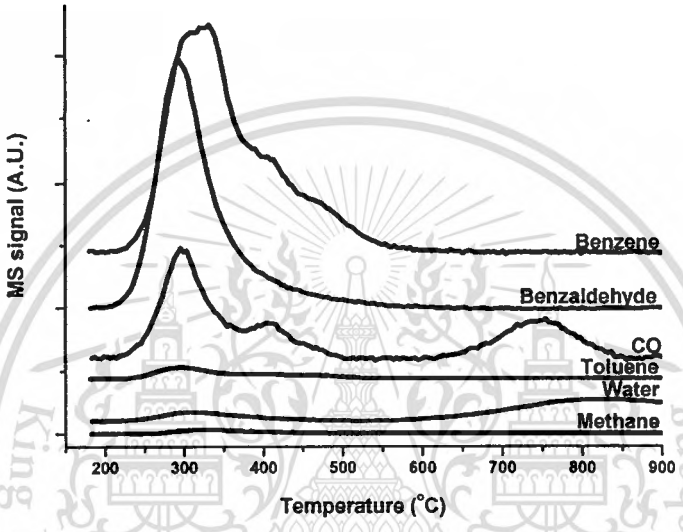

Figure 7.8 Benzaldehyde-TPD of 3[Ga]HZSM-5 treated with He and run TPD under He.

From Figure 7.8, it is clearly seen that benzaldehyde can be converted to benzene together with CO. It is proposed that benzaldehyde is strongly adsorbed on the Brønsted acid site leading to the protonation of the conjugated π-electron in aromatic. Consequently, the weakening of C-C bond of aromatic-carbonyl group results in the decarbonylation to form benzene and CO.

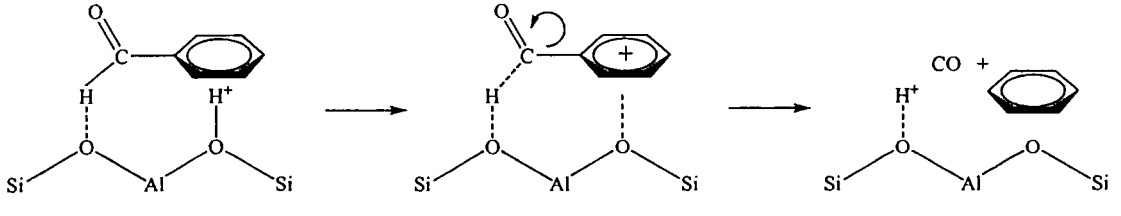

The role of Brønsted acid site on benzene formation was further supported by the benzaldehyde conversion over 3[Ga]HZSM-5 treated with H_2 and then run the benzaldehyde conversion under He stream (Figure 7.9).

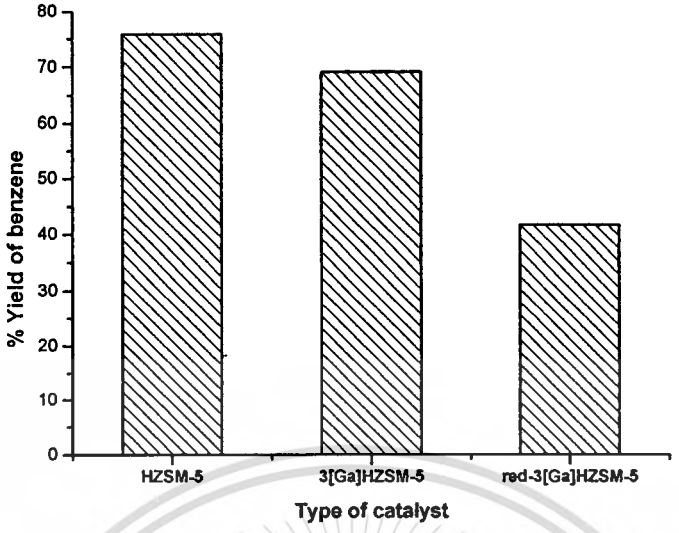

Figure 7.9 The effect of pre-treatment.

Reaction conditions: Catalysts = HZSM-5, 3[Ga]HZSM-5, and red-3[Ga]HZSM-5 (red-3[Ga]HZSM-5 was treated with H_2 at 550 °C for 2 hours and then cool down to 500 °C under He gas), W/F = 100 g·h/mol, Reaction temperature = 500 °C, Carrier gas = He, Pressure = 1 atm.

As expected, the relatively low yield of benzene over treated catalyst with H_2 (red-3[Ga]HZSM-5) was obtained, as compared to HZSM-5 and 3[Ga]HZSM-5 treated with He. This is because the reduction of Ga leads to the formation of Ga cationic species which can replace the Brønsted acid site resulting in the decrease in acidity, as discussed earlier.

From the above results, it can be concluded that the formation of benzene depends largely on the number of acid sites which promotes direct decarbonylation. To prove this suggestion, the rate of benzene formation was plot with both number of high activity acid sites and total acid sites (Figure 7.10), as calculated from IPA-TPD (Table 7.3).

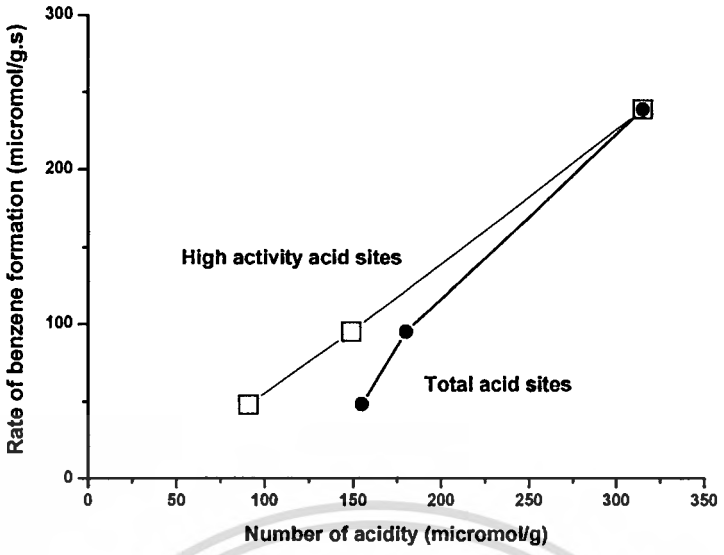

Figure 7.10 Plot of rate of benzene formation versus number of acid sites.
Reaction conditions: Catalysts = HZSM-5, 1[Ga]HZSM-5, and 3[Ga]HZSM-5, W/F = 100 g·h/mol, Reaction temperature = 500 °C, Carrier gas = H_2, Pressure = 1 atm.

It was also found that only the plot of benzene formation versus with high activity acid sites provide the linear graph. It is evidenced that the high activity of Brønsted acid site can promote direct decarbonylation of benzaldehyde to form benzene. This shall not be the case of lower activity acid sites of GaOH species. The obtained linear plot could be confirmed the rate of benzene formation is proportional with the concentration of high activity acid sites implying a direct decarbonylation mechanism.

Regarding to the benzaldehyde conversion under H_2 stream, HZSM-5 cannot generate the high toluene yield (Table 7.5) though HZSM-5 can facilitate H_2/D_2 exchange (Table 7.4). This is due to the fact that HZSM-5 cannot dissociate H_2 molecule to form 2 H atoms which readily hydrogenate to unsaturated bond [43]. But it can only provide H_2 exchange by adsorbed species on the Brønsted acid site and the O atoms of the zeolite framework. The formation of H–D–D triad is proposed for the transition state.

$$Z^-H^+ + D_2 \rightleftharpoons Z^-D^+ + HD \qquad \text{Eq. (9)}$$

7.3.5 Effect of temperature

It is known that the hydrogenolysis/decarbonylation activity is thermodynamically favored at high reaction temperature. Consequently, the increase in reaction temperature may largely affect the benzaldehyde conversion to toluene and benzene.

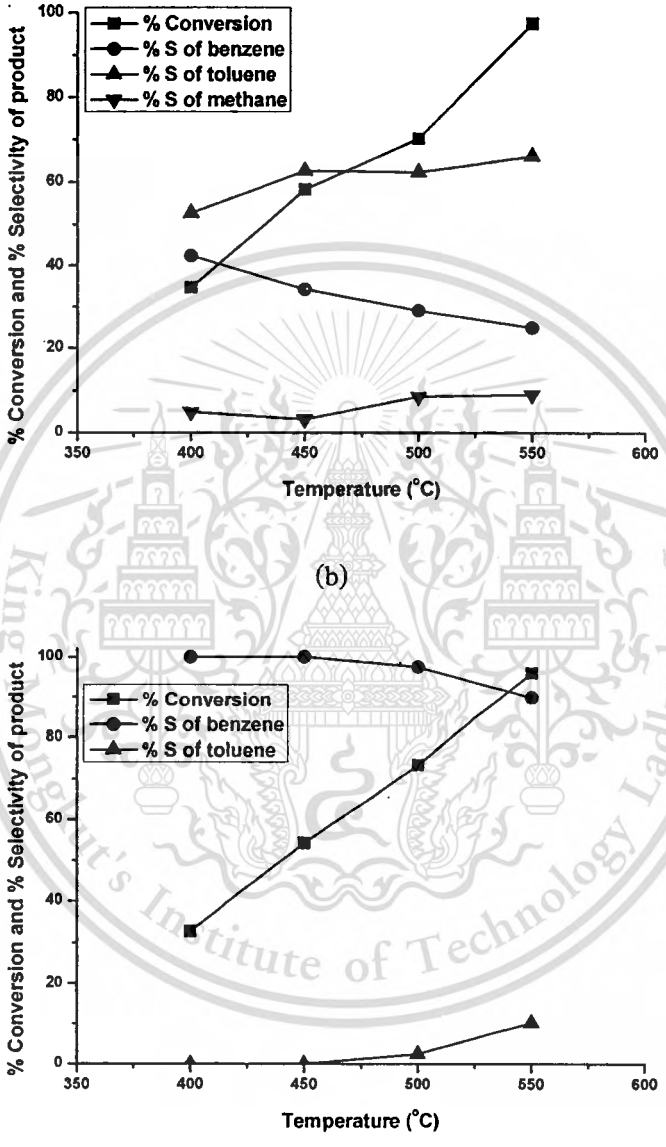

Figure 7.11 The effect of temperature with selectivity of product over (a) HZSM-5 and (b) 3[Ga]HZSM-5.

Reaction conditions: Catalysts = HZSM-5 and 3[Ga]HZSM-5, W/F = 100 g·h/mol, Reaction temperature = 400-550 °C, Carrier gas = H_2, Pressure = 1 atm.

From Figure 7.11, it was clearly observed that an increase in reaction temperature can dramatically increase the benzaldehyde conversion over 3[Ga]HZSM-5. It is also found that the selectivity of toluene and methane are especially increased with temperature and *vice versa* for the benzene. This is due to the increase in both rate of hydrogenolysis and hydrodealkylation which are favored at high reaction temperature. While, the small amount of toluene observed over HZSM-5 at the high reaction temperature is presumably due to H_2 transfer of the carbocation intermediates when the temperature was increased. This is consistent with an increase in H_2/D_2 exchange with temperature (Table 7.4).

In a support manner, benzaldehyde-pulsed reaction (Figure 7.12) reveals that an increase in reaction temperature can increase the hydrogenolysis/decarbonylation activity leading to the high yield of toluene and benzene. Moreover, the formation of water and CO can also be observed.

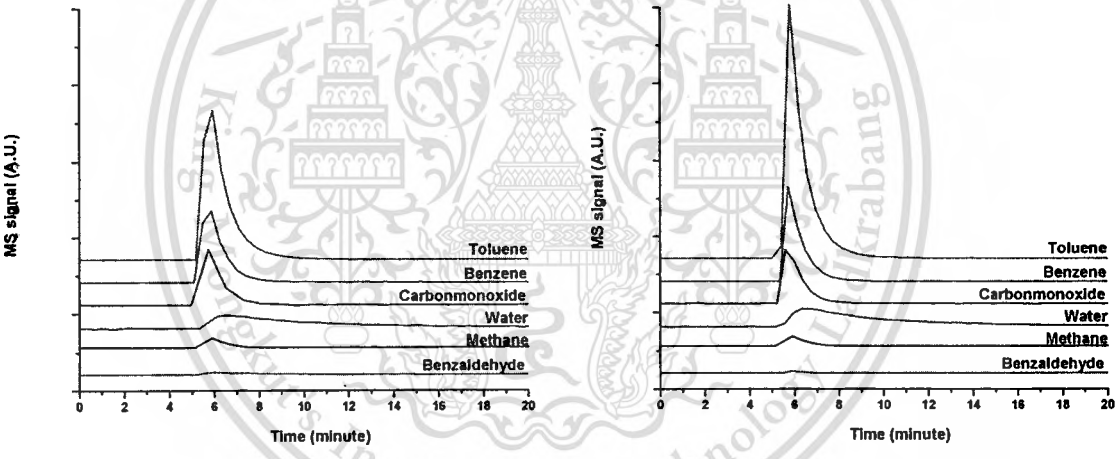

(b) (c)

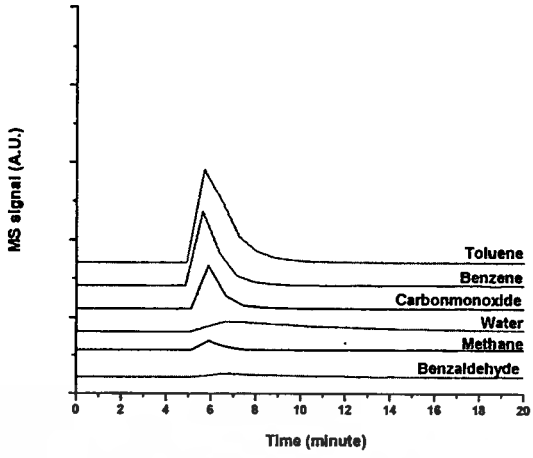

(a)

Figure 7.12 Benzaldehyde-pulsed reaction over 3[Ga]HZSM-5 under H_2 at (a) 450 °C, (b) 500 °C, and (c) 550 °C.

Although the benzaldehyde-pulsed reaction was carried out under He stream, the retained reduced Ga species (Ga^+/GaH_2^+) after reduction still promote hydrogenation/hydrogenolysis giving toluene as shown in Figure 7.13. However, the lower toluene yield can be obtained over reduced 3[Ga]HZSM-5 under He stream. While the Brønsted acid sites play important role for decarbonylation providing high benzene yield with rise in reaction temperature.

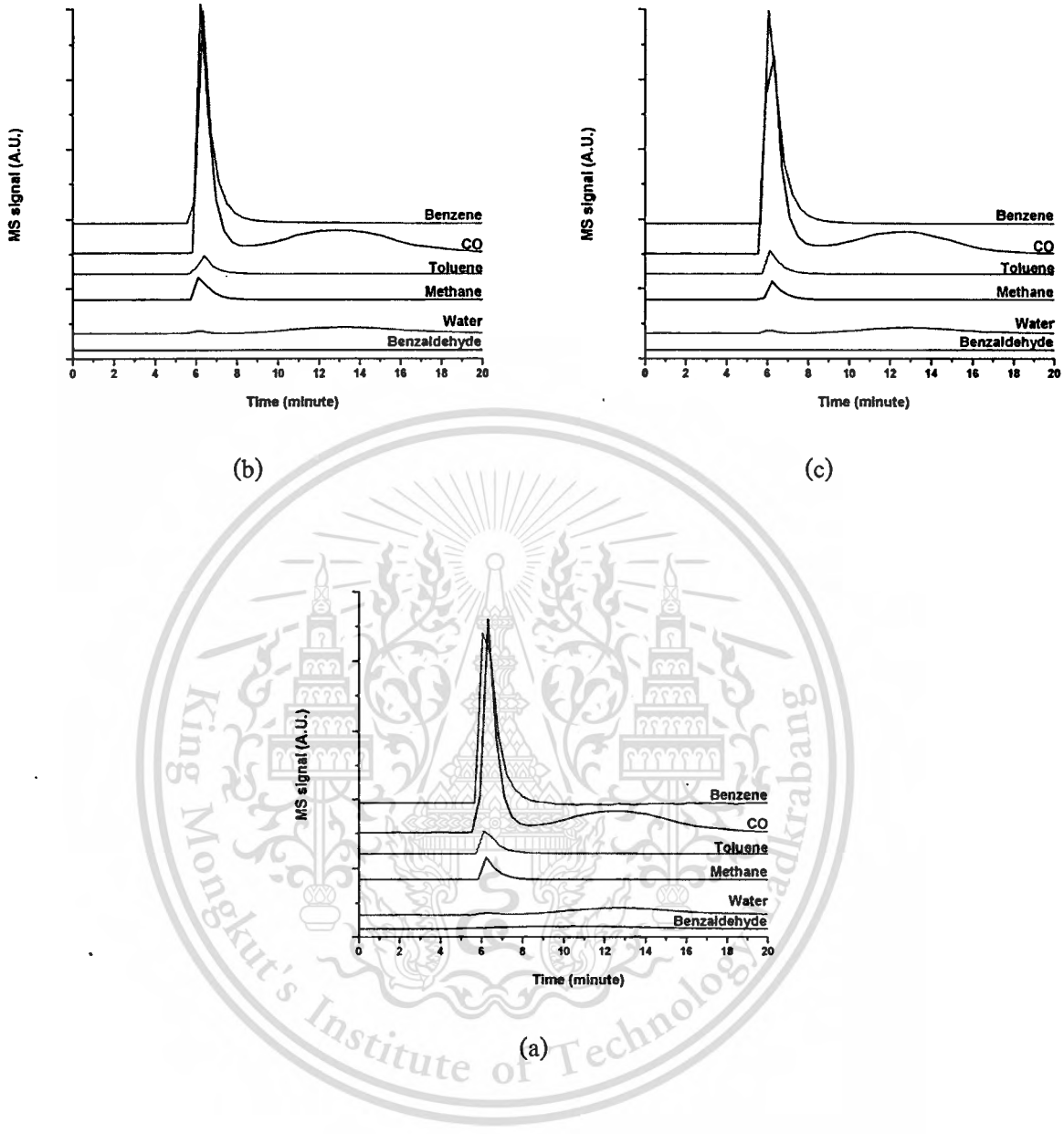

Figure 7.13 Benzaldehyde-pulsed reaction over reduced 3[Ga]HZSM-5 under He at (a) 450 °C, (b) 500 °C, and (c) 550 °C.

7.3.6 Effect of support

In addition, the zeolites support plays a marked role in preserve the incorporated reduced Ga species. Therefore, in this section, further evidence for the influence of the zeolite support on the catalytic activity of the incorporated Ga catalyst is provided.

Table 7.6 The effect of support.

Product distribution	Type of catalyst		
	3[Ga]Silica	3[Ga]HZSM-5	3[Ga]HZSM-5
W/F (g·h/mol)	100	100	20
Temperature (°C)	550	550	500
% Conversion	20.22	97.50	22.25
% Y of methane	0.00	8.91	2.00
% Y of benzene	6.10	24.21	7.46
% Y of toluene	14.12	64.37	12.79
% S of methane	0.00	9.14	8.99
% S of benzene	30.17	24.83	33.53
% S of toluene	69.83	66.03	57.48

Reaction conditions: Catalyst treated with H_2 at 500-550 °C for 2 hours, W/F = 20-100 g·h/mol, Reaction temperature = 550 °C, Carrier gas = H_2, Pressure = 1 atm.

From the Table 7.6, a low benzaldehyde conversion was obtained over 3[Ga]Silica, as compared to 3[Ga]HZSM-5 using the same reaction condition. This is presumably because silica support possesses much lower activity acid site, as compared to bridgingly Brønsted acid sites of zeolite. In addition, the non-uniform pore system of silica may not provide well-dispersed Ga active sites and inactive Ga species may well form over this catalyst. This is in consistent with the observed high reduction temperature of Ga species by TPR (Figure 7.1d).

The 3[Ga]Silica provides the relatively lower yield of toluene (Table 7.6). This is presumably because there is no the Ga cationic species in this catalyst. The silica support possesses the non-uniform pore size and no negatively framework charge. Consequently, such silica support cannot produce the well-dispersion of Ga species leading to the agglomeration of bulk Ga_2O_3, as evidenced by H_2-TPR (Figure 7.1d). It is presumably suggested that observed activity of 3[Ga]Silica derives from the interaction of H_2 with gallia surfaces. Two different types of dissociative H_2 species; (i) homolytic dissociative adsorption to form Ga-H species and (ii) heterolytic dissociative adsorption to form Ga-OH and Ga-H, have been reported [44-46].

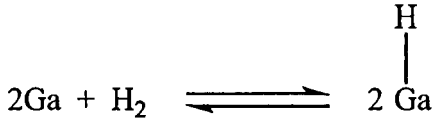

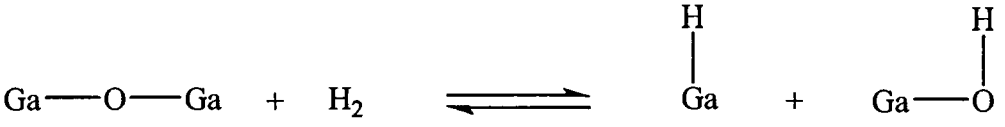

It is concluded that only some part of gallia can be reduced (Figure 7.1d), hence, the lower activity is obtained over this catalyst.

7.3.7 Effect of water co-feeding

Since water was always present in pyrolysis bio-oil [47,48], the effect of water co-feeding was studied and the results were shown in Table 7.7.

Table 7.7 Effect of water co-feeding.

Catalyst	Carrier gas	% Conversion	Product distribution (% yield)		
			Benzene	Toluene	Methane
HZSM-5	He	56.32	56.32	0.00	0.00
	He + water	51.14	51.14	0.00	0.00
3[Ga]HZSM-5	He	55.80	55.80	0.00	0.00
	He + water	67.52	67.52	0.00	0.00
3[Ga]HZSM-5	H_2	58.20	19.95	36.40	1.85
	H_2 + water	65.19	46.94	18.24	0.00

Reaction conditions: Catalysts = HZSM-5 and 3[Ga]HZSM-5, W/F = 100 g·h/mol, Reaction temperature = 450 °C, Carrier gas = He and H_2, Pressure = 1 atm.

It was found that the conversion of benzaldehyde over HZSM-5 slightly decreases with rise in water content. It indicates that water, which is present as co-feed, can inhibit decarbonylation of benzaldehyde presumably by competitive adsorption over the acid sites.

A significant change in catalytic activity of Ga-modified HZSM-5 can be observed in the reaction of benzaldehyde with water co-feeding (Table 7.7). An increase in benzene yield with

rise in water content can be observed over 3[Ga]HZSM-5 when using He as carrier (Table 7.7). This is presumably due to the enhanced acidity of 3[Ga]HZSM-5, as evidenced by IPA-TPD (Table 7.3). It expresses that the presence of water can generate the additional new acid sites in 3[Ga]HZSM-5 which can retain at high temperature.

This shall not be the case of HZSM-5. The water which is present as co-feed, can competitively adsorb over the acid sites leading to the low decarbonylation of benzaldehyde.

Using 3[Ga]HZSM-5 as catalyst under H_2 (Table 7.7), yield of toluene is relatively low when water is present in the feed (Figure 7.14). This suggests that water may well alter the Ga species, causing a reduced the hydrogenation/hydrogenolysis activity of 3[Ga]HZSM-5 [49,50].

$$Ga^{+} + H_2O \longrightarrow GaO^{+} + H_2 \qquad \text{Eq. (10)}$$

The incorporated Ga species can be interacted with water forming GaO(OH) (Eq. (5)). It is interesting to note that this activity can be recovered after water is withdrawn from the reaction stream (Figure 7.14), suggesting that the mediating effect of water is reversible.

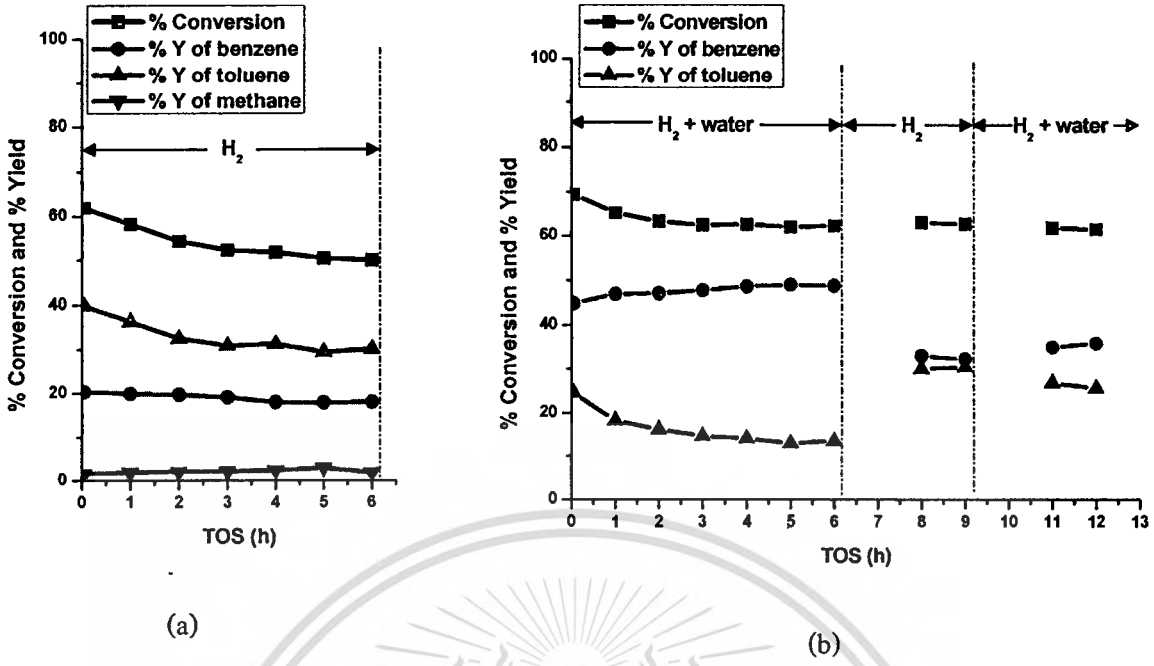

Figure 7.14 The effect of water co-feeding (a) without water and (b) with and without water. *Reaction conditions: Catalyst = 3[Ga]HZSM-5, W/F = 100 g·h/mol, Reaction temperature = 450 °C, Carrier gas = H_2, Pressure = 1 atm. Water was firstly injected for treating catalyst and running benzaldehyde conversion (initial-6 hours). Then the feeding of water was stopped until 9 hours on stream and feeding again.*

The water can interact with most of Ga cationic species to form the additional of Brønsted acid site, as discussed earlier. This leads to the high benzaldehyde conversion to benzene. It is suggested that the decrease in yield of toluene would be predominantly derived from the decrease in GaH_2^+ species. Since there is water in the reaction, reduced Ga species can be diminished. The observed hydrogenation/hydrogenolysis to produce toluene would be derived from the retained Ga^+ and GaH_2^+ in the catalyst. These results indicated very significantly that the catalytic behavior of 3[Ga]HZSM-5 can be regulated from hydrogenation/hydrogenolysis to decarbonylation activity by the presence of water.

Interestingly, the hydrogenation/hydrogenolysis activity of 3[Ga]HZSM-5 can be recovered when flow of water is withdrawn (Figure 7.14). This is presumably explained by the recovery of the Ga active site (i.e. Ga^+ and GaH_2^+), as shown in reversible Eq. (5) and Eq. (10).

7.4 Conclusions

The benzaldehyde conversion over [Ga]HZSM-5, the benzene formation was promoted by the decarbonylation activity over Brønsted acid site. While GaH_2^+ species generated during H_2 stream, can promote hydrogenation/hydrogenolysis properties leading to toluene formation. However, no observation of toluene yield can be obtained over [Ga]HZSM-5 under non-reducing atmosphere despite the catalyst is primarily reduced. This is due to the lack of GaH_2^+ species. The presence of water as co-feeding in the benzaldehyde conversion over [Ga]HZSM-5 under He stream, the relatively higher benzene yield can be obtained due to the pronounced Brønsted acid site. On the other hand, the relatively lower yield of benzene can be obtained over HZSM-5 when water is present. In the case of benzaldehyde conversion under H_2 stream, water co-feeding can diminish the GaH_2^+ species while the pronounced Brønsted acid site leading to the lower toluene, but higher benzene yield.

Part II : Catalytic deoxygenation of *m*-cresol over Ga-modified zeolite

7.5 Experimental details

7.5.1 Catalyst preparation and characterization

HBeta (Si/Al ~ 11) samples were commercially obtained from Zeolyst. Conventional impregnation with $Ga(NO_3)_3$ were employed to obtain 1-6 wt% Ga loading. The samples were then calcined at 550 °C for 4 hours in a flow of dry air. Hereafter, the catalysts were designated as %loading-[Ga]HBeta. 3[Ga]HZSM-5 and 3[Ga]Silica (3 wt% Ga loading) were also prepared by impregnation of HZSM-5 (Si/Al ~ 45) and silica (Hi-Sil), respectively.

Temperature-programmed reduction (TPR) experiments, temperature-programmed desorption of *i*-propylamine (IPA-TPD) and H_2/D_2 exchange were carried out, as discussed earlier in **section 7.2**.

7.5.2 Temperature-programmed desorption (TPD)

After the *m*-cresol conversion, the retained products on the catalyst surface were preserved by cooling down in a flow of He to 100 °C. TPD measurements were done from 100 to 900 °C with a heating rate of 10 °C/min using H_2 as a carrier gas. The masses (*m/z*) of 15 (methane), 18 (water), 27, 29, 41, 43, 56 (hydrocarbons), 78 (benzene), 91 (toluene), 94 (phenol) and 168, 184, 196 (bicyclic compounds) were monitored.

7.5.3 Catalytic activity measurements

Catalytic testing of *m*-cresol conversion was performed with a continuous fixed bed flow reactor. Saturated vapor of *m*-cresol at 20 °C was carried by He (or H_2) at 30 mL/min regulated by a mass flow controller. The catalyst bed was set in a quartz tube reactor that was located inside a temperature-regulated furnace. The products were periodically collected and analyzed by an on-line gas chromatograph equipped with a flame ionization detector (FID) and VA-1 capillary column (Appendix B). The preferred reaction conditions used in the experiments were as follows: temperature, 400-550 °C; total pressure, 1 atm; carrier gas, He or H_2; W/F, 1.9-21.9 h.

7.6 Results and discussions

The characteristics of the catalyst samples including Si/Al ratio of the host zeolite, % Ga loading, and BET surface area are shown in Table 7.8.

Table 7.8 Chemical composition and surface area of catalyst samples.

Catalyst	Si/Al	Ga content[a] (wt%)	Surface area (m^2/g)
HBeta	11	-	615
1[Ga]HBeta	11	1.0	590
3[Ga]HBeta	11	2.9	580
6[Ga]HBeta	11	5.9	570
3[Ga]Silica	ND	2.9	370
3[Ga]HZSM-5	45	2.8	510

[a] Elemental analysis for Si, Al, and Ga were performed using ICP.

The product distribution from the *m*-cresol conversion on 3[Ga]HBeta at 400 °C is shown in Figure 7.15.

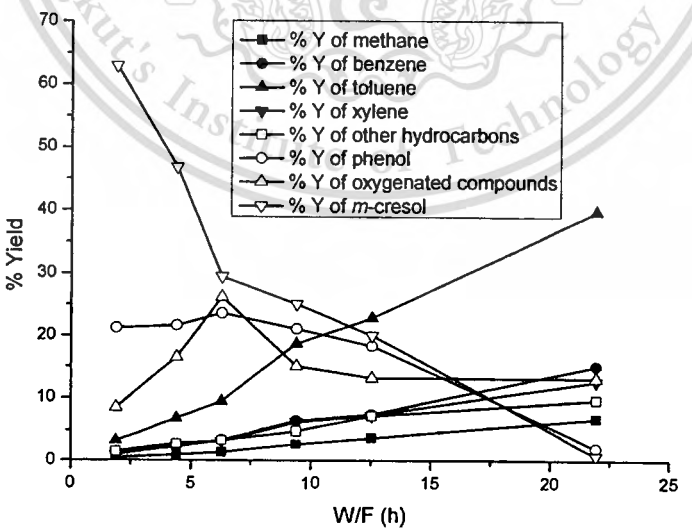

Figure 7.15 Effect of W/F on *m*-cresol conversion over 3[Ga]HBeta.

Reaction conditions: Catalyst = 3[Ga]HBeta, W/F = 1.9-21.9 h, Reaction temperature = 400 °C, Carrier gas = H_2, Pressure = 1 atm.

The increase in yield of phenol and oxygenated compounds can be initially observed when increase in W/F (1.9-6.3 h). After that (W/F = 6.3-21.9 h) the yield of phenol and oxygenated compounds are decreased. While, the methane, C2-C6 hydrocarbons, benzene, toluene, xylene are increased with W/F. This implies that toluene is not a primary product arising from the direct hydrogenolysis of *m*-cresol. By contrast, phenol and oxygenated compounds appears to be primarily formed in parallel. A marked drop of the oxygenated compounds as a function of W/F indicates that these heavier compounds tend to be hydrogenolysed/decomposed into lighter hydrocarbons as the catalyst bed increases.

Although, phenol is largely produced at low space time, the directly hydrogenolysis of *m*-cresol to phenol shall not be the case. This is because methane is not proportionally produced in this space time region (Figure 7.15). Hence, the "surface pool mechanism" is proposed. It is expected that the *m*-cresol would strongly adsorb on the surface of the catalyst, initially forming the high MW oxygenated intermediates. This is presumably proceeded by surface condensation of the adsorbed species, in a manner similar to the intermediates of aromatic disproportionation [51,52]. Only difference is that, in this case, oxygenated compounds are involved into the "surface pool intermediates". Such intermediates would be primary precursors for phenol and oxygenated compounds. The richer carbon surface pool intermediates would be hydrogenolysed to form light aromatics (benzene, toluene, xylene) and light hydrocarbons (C2-C6 hydrocarbons).

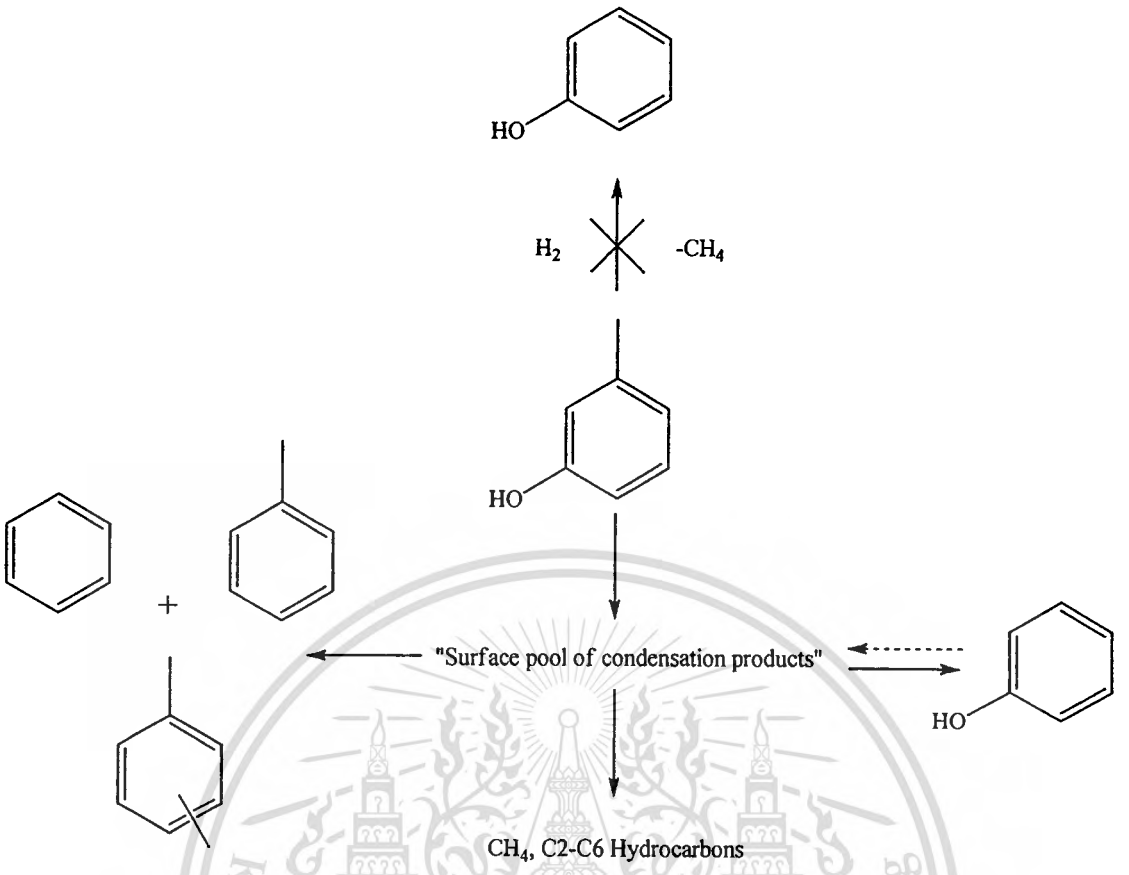

A gradual decline in phenol with space time suggests that phenol may well be consecutively converted to hydrocarbons at high W/F. Phenol may well re-adsorb in the surface pool intermediates. This is confirmed by the phenol conversion over 3[Ga]HBeta catalyst which gives products similar to that observed in *m*-cresol conversion (benzene, toluene, xylene and oxygenated compounds) (Figure 7.16).

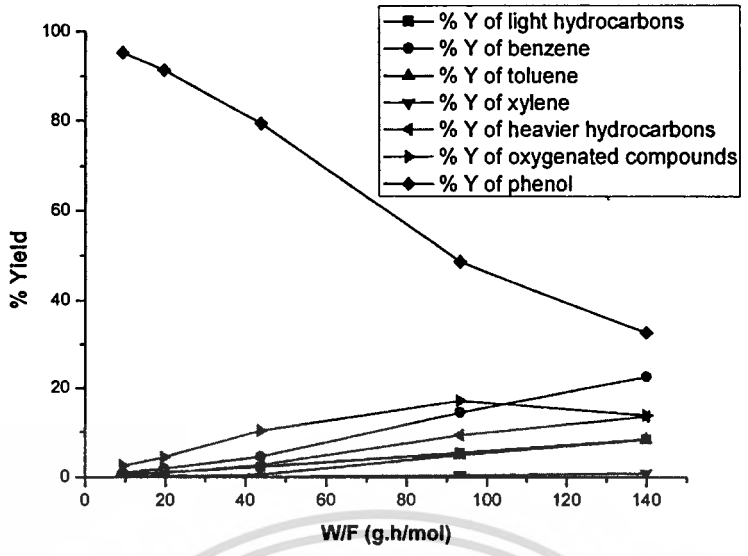

Figure 7.16 Effect of W/F on phenol conversion over 3[Ga]HBeta.

Reaction conditions: Catalyst = 3[Ga]HBeta, W/F = 9.3-139.9 g·h/mol, Reaction temperature = 400 °C, Carrier gas = H_2, Pressure = 1 atm.

Supporting this suggestion, the TPD in H_2, after the *m*-cresol conversion (Figure 7.17), shows that significant amounts of light aromatics, namely benzene (*m/z* = 78), toluene (*m/z* = 91) are desorbed from the 3[Ga]HBeta catalyst together with light hydrocarbons, namely methane (*m/z* = 15) and other hydrocarbons (*m/z* = 27, 29, 41, 43, 56) at 250-450 °C. Only small signal of high *m/z* fragment ion implying the bicyclic oxygenates (*m/z* = 168, 184, and 196) are exhibited at the desorption peaks at 500 °C.

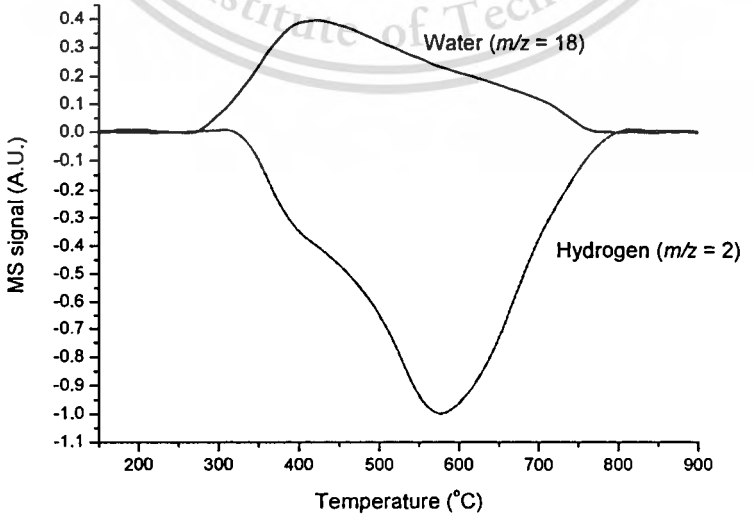

(b)

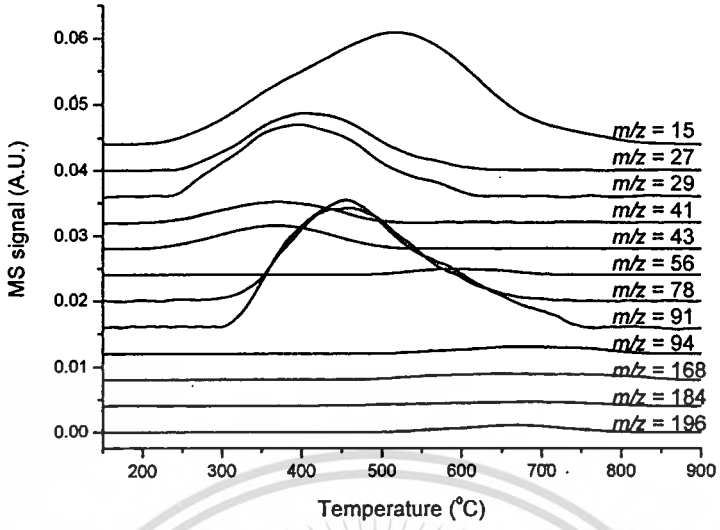

(a)

Figure 7.17 TPD of 3[Ga]HBeta after *m*-cresol conversion at 400 °C.

The masses (m/z) of 2 (hydrogen), 15 (methane), 18 (water), 27, 29, 41, 43, 56 (hydrocarbons), 78 (benzene), 91 (toluene), 94 (phenol) and 168, 184, 196 (bicyclic compounds) were monitored.

These signals were suggested to arise from the hydrogenolysed products of the surface pool intermediates. This is consistent with the observed H_2 consumption and water production, as shown in Figure 7.17b.

Further evidence supporting the surface pool mechanism was shown in Table 7.9.

Table 7.9 Effect of carrier gas.

Reaction condition	Initial		6 h on stream	
	H_2	He	H_2	He
% Conversion	84.52	74.25	79.08	37.84
% Yield				
Methane	2.30	0.36	1.67	0.11
Benzene	10.67	12.89	7.33	0.88
Toluene	23.54	14.03	16.44	1.82
Xylene	10.04	2.56	6.45	0.25
Other hydrocarbons	1.87	3.37	1.36	0.68
Phenol	14.07	22.55	15.72	12.33
Oxygenated compounds	22.03	18.49	30.09	21.78
Total yield	84.52	74.25	79.08	37.84
% Selectivity				
Methane	2.72	0.49	2.12	0.28
Benzene	12.62	17.36	9.27	2.32
Toluene	27.85	18.90	20.80	4.80
Xylene	11.88	3.45	8.16	0.67
Other hydrocarbons	2.22	4.54	1.72	1.79
Phenol	16.65	30.36	19.88	32.58
Oxygenated compounds	26.06	24.90	38.06	57.56
Total selectivity	100.00	100.00	100.00	100.00
Toluene/Benzene ratio	2.21	1.09	2.24	2.07

Reaction conditions: Catalyst = 3[Ga]HBeta, W/F = 6.3 h, Reaction temperature = 450 °C, Carrier gas = H_2 or He, Pressure = 1 atm.

It is clear that the *m*-cresol conversion in H_2 is higher than that using He as a carrier gas. The hydrocarbon products, benzene, toluene and xylene, are dominant only in the reaction under H_2 gases (Table 7.9), indicating a dramatic effect of gas-phase H_2 in this reaction. Moreover, the

high toluene/benzene ratio can be obtained in H_2. It indicates that, under H_2, hydrogenolysis of surface pool intermediates (Ar-OH) to form toluene is relative faster than the dealkylation of surface pool intermediates (Ar-CH_3) to form benzene.

The presence of H_2 also shows a marked effect on the catalyst stability (Figure 7.18). A rapid deactivation of the catalyst is observed in the reaction without H_2 suggesting that the surface pool intermediates are retained.

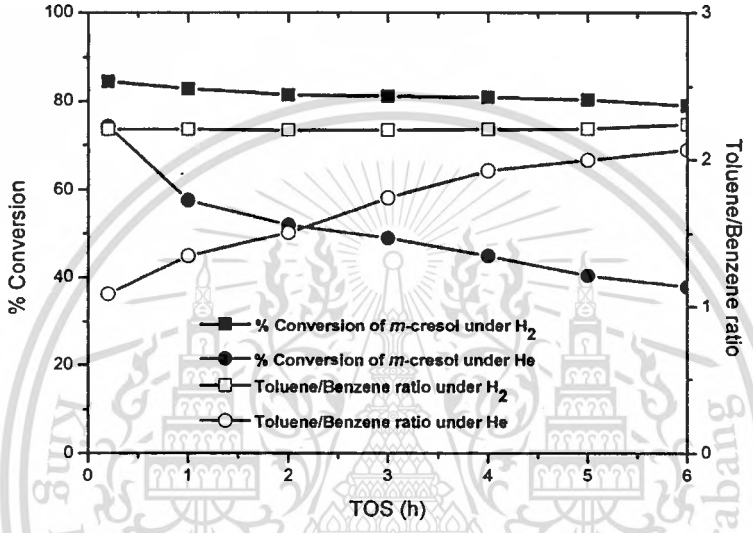

Figure 7.18 Effect of carrier gas.

Reaction conditions: Catalyst = 3[Ga]HBeta, W/F = 6.3 h, Reaction temperature = 450 °C, Carrier gas = H_2 or He, Pressure = 1 atm.

Without H_2 gas, hydrogenolysis activity is readily diminished; however, the condensation of *m*-cresol to surface pool intermediates can be promoted. This allows only the decomposition of surface pool intermediates to form phenol and oxygenated compounds and the catalyst is rapidly deactivated. The surface pool intermediates can be removed by hydrogenolysis to lighter aromatic products (benzene and toluene) when H_2 is present. Accordingly, the catalyst stability can be readily improved only in the reaction using H_2 as a carrier gas.

From Table 7.10, it is clear that lower yield of oxygenated compounds but higher yield of light aromatic can be observed when Ga content is increased.

Table 7.10 Effect of Ga content.

Supported Beta catalyst	H	H	1[Ga]H	3[Ga]H	6[Ga]H
Temperature (°C)	450	400	400	400	400
% Conversion	70.45	55.51	70.76	70.56	71.64
% Yield					
Methane	0.70	0.87	1.43	1.32	1.55
Benzene	0.80	0.68	3.24	3.45	6.12
Toluene	1.59	2.90	8.74	9.45	21.67
Xylene	0.54	1.38	3.56	3.20	5.40
Other hydrocarbons	2.45	2.83	3.75	3.30	4.80
Phenol	18.22	32.00	19.76	23.61	24.66
Oxygenated compounds	46.16	14.83	30.28	26.23	7.44
Total yield	70.45	55.51	70.76	70.56	71.64
% Selectivity					
Methane	0.99	1.58	2.02	1.87	2.17
Benzene	1.14	1.23	4.58	4.89	8.54
Toluene	2.25	5.23	12.35	13.39	30.25
Xylene	0.76	2.49	5.03	4.54	7.53
Other hydrocarbons	3.47	5.10	5.30	4.67	6.70
Phenol	25.86	57.65	27.93	33.45	34.42
Oxygenated compounds	65.51	26.71	42.79	37.18	10.39
Total selectivity	100.00	100.00	100.00	100.00	100.00

Reaction conditions: W/F = 6.3 h, Reaction temperature = 400 and 450 °C, Carrier gas = H_2, Pressure = 1 atm.

It indicates that the Ga active sites can catalyze hydrogenolysis of the surface pool intermediates. Such Ga species are suggested to be the Ga species exist under H_2 system (GaH_2^+), as already discussed over [Ga]HZSM-5 (**section 6.3**). TPR and IPA-TPD (Figure 7.19 and 7.20) suggest that reduction of octahedrally coordination Ga_2O_3 (Ga^{3+} ions) leads to the formation of

reduced univalent Ga^{+} ions [1,9,33,33] which can replace with acidic protons, as discussed earlier (Eq. (1)-(2)).

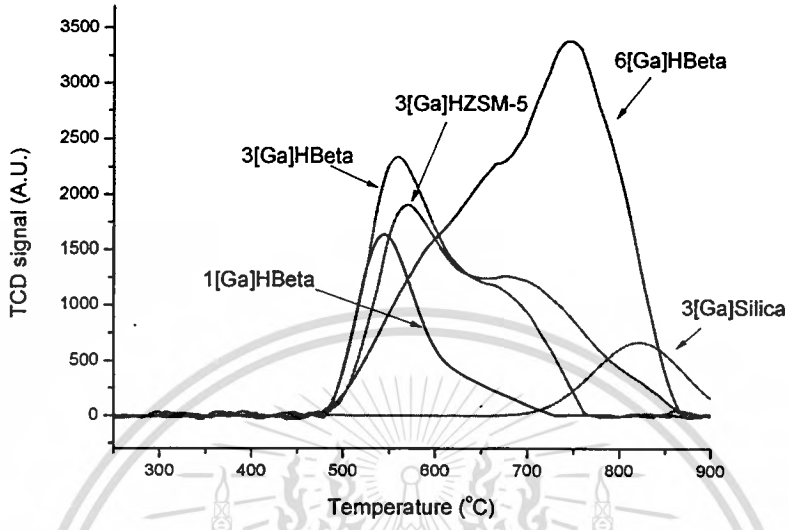

(f)

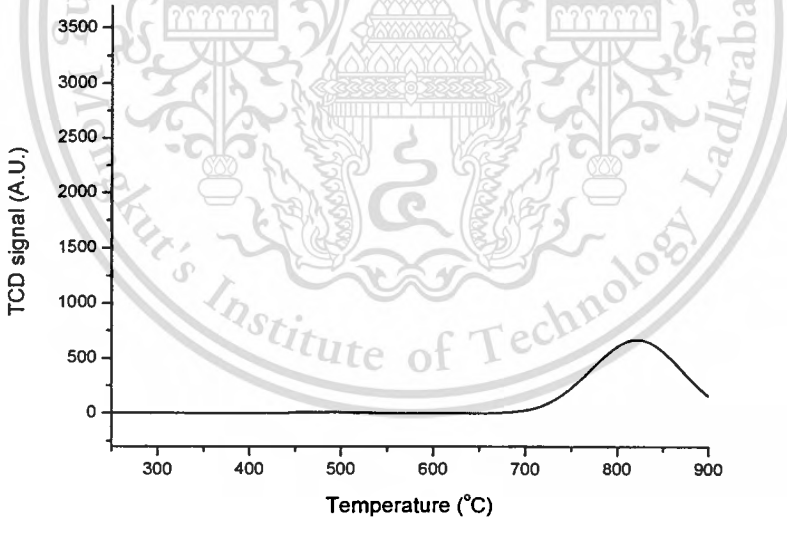

(e)

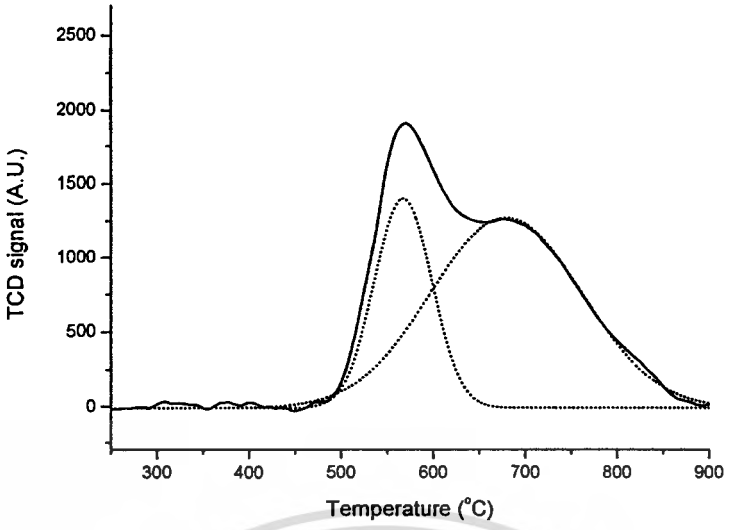

(d)

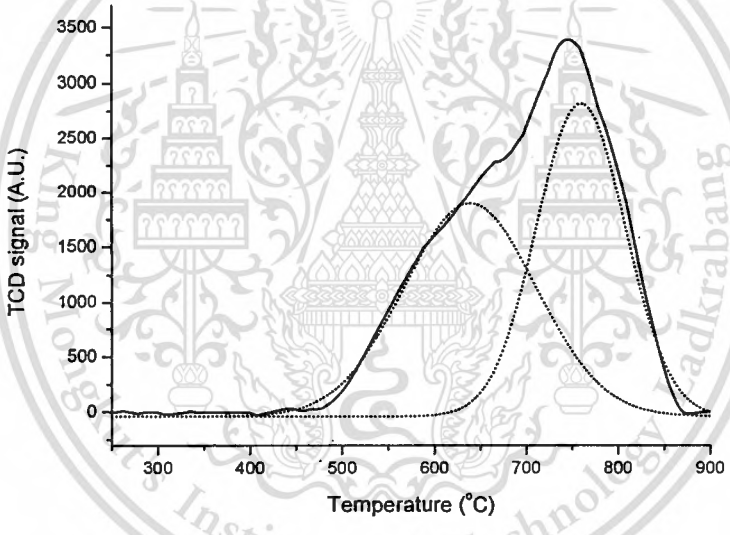

(c)

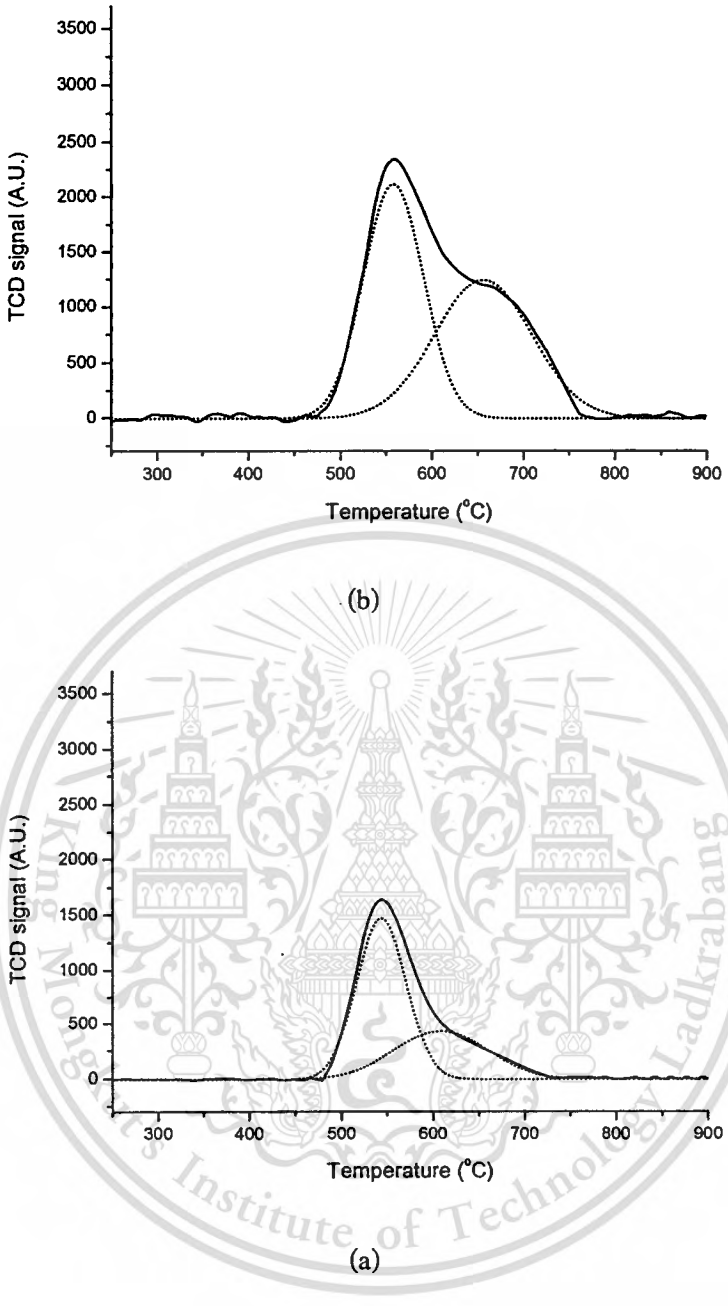

Figure 7.19 TPR profiles of (a) 1[Ga]HBeta, (b) 3[Ga]HBeta, (c) 6[Ga]HBeta, (d) 3[Ga]HZSM-5, (e) 3[Ga]Silica, and (f) comparison data of Ga supported catalyst.

Figure 7.19 shows the TPR curves observed for the calcined catalyst samples. With the Gaussian deconvolution, two major peaks are observed on the Ga supported HBeta zeolite. In the case of 1 and 3[Ga]HBeta, the low temperature peak (T_1) was assigned to the reduction of well-dispersed Ga species such as GaO^+ species or small Ga_2O_3 particles interacting with the zeolite. While, the high temperature peak (T_2) peak was attributed to large, bulk Ga_2O_3 particles separated

from or loosely support on the zeolite matrix [29]. Consistently, the incorporated Ga species can be agglomerated in to a larger Ga_2O_3 cluster, particularly on the outer surface of Beta in the case of 6[Ga]HBeta. The H_2-TPR of 3[Ga]HZSM-5 (Si/Al ~ 45) shows two H_2 consumption peaks in a manner similar to that observed over 3[Ga]HBeta (Si/Al ~ 11) samples. While the TPR curve of 3[Ga]Silica displays only one peak of larger gallium oxide particles at relatively high reduction temperature.

Since the reduction of Ga_2O_3 leads to the formation of Ga exchangeable cation (Ga^+), the Brønsted acid sites of [Ga]HBeta were decreased, as evidenced by IPA-TPD (Figure 7.20).

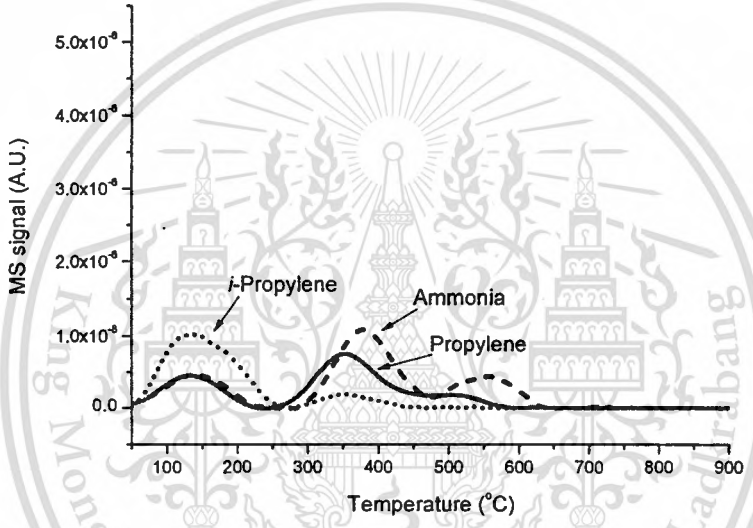

(d)

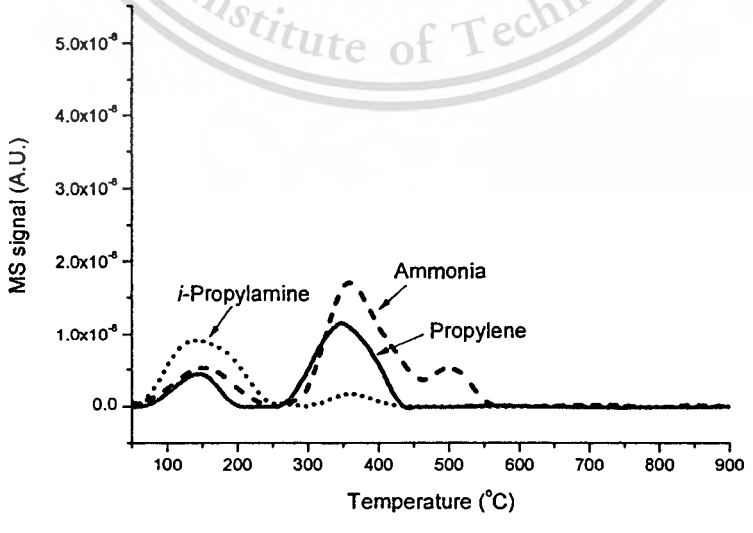

(c)

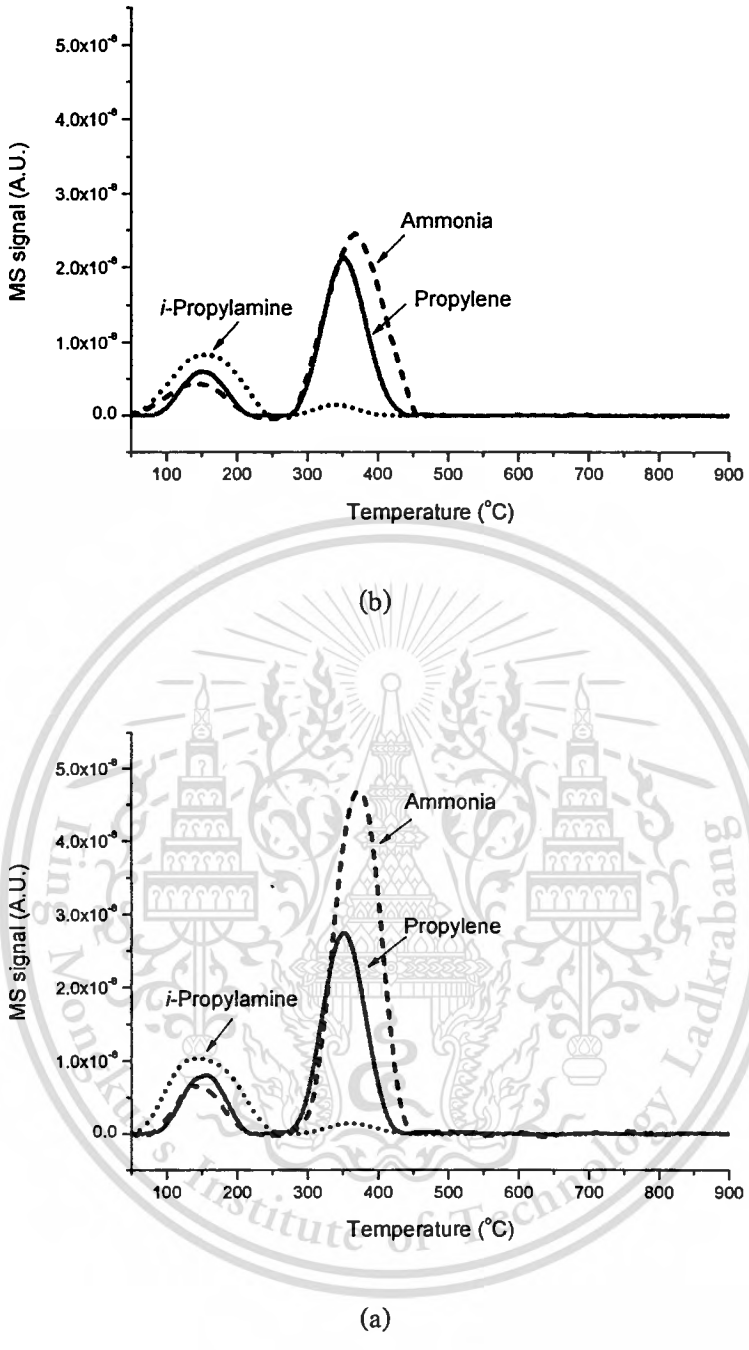

Figure 7.20 IPA-TPD of (a) HBeta, (b) red-1[Ga]HBeta[a], (c) red-3[Ga]HBeta[a], and (d) 6[Ga]HBeta[a].

[a] The Ga supported zeolite was firstly reduced with H_2 at 550 °C for 2 hours and then cool down to 40 °C under He.

The number of bridgingly Brønsted acid site (≡Si-OH-Al≡) can be calculated and shown in Table 7.11.

Table 7.11 Acidity of various catalysts[a].

Catalyst	Acidity of catalyst (mmol/g)		
	High acid strength	**Low acid strength**	**Total acidity**
HBeta	1.20	0	1.20 (*1.39*[b])
red-1[Ga]HBeta	0.94	0	0.94
red-3[Ga]HBeta	0.66	0	0.66
red-6[Ga]HBeta	0.44	0.15	0.59

[a] The data were summarized from IPA-TPD curves.

[b] Theoretical acidity calculated from Si/Al ratio.

It can be seen that a dramatic decrease in Brønsted acid site in the order of 6[Ga]HBeta < 3[Ga]HBeta < 1[Ga]HBeta < HBeta was obtained when the catalyst was treated with H_2. This is consistent with the previous observation when [Ga]HZSM-5 was reduced (**section 7.3**).

Further evidence supporting the hydrogenolysis activity of the H_2 chemisorbed Ga species, GaH_2^+, was shown by the H_2/D_2 exchange (Table 7.12).

Table 7.12 Activity of H_2/D_2 exchange of various catalysts.

Type of catalyst	Temperature (°C)	Area ratio of H-D/D-D
HBeta	400	12.10
	450	12.43
	500	12.63
	550	13.05
3[Ga]HBeta	400	12.48
	450	13.17
	500	13.98
	550	14.58

It is important to note that the observed H_2/D_2 exchange over 3[Ga]HBeta derives from the dissociative adsorption of H_2/D_2 and consecutive recombination of the adsorbed H-D species.

Accordingly, the GaH_2^+ species can possibly transfer the dissociated H_2 to the C-C or C-O of the surface pool intermediates and consecutively hydrogenolyse leading to the formation of light aromatic, as discussed earlier.

It is known that the decomposition/hydrogenolysis activity is thermodynamically favored at high reaction temperature. Consequently, the increase in reaction temperature may largely affect the *m*-cresol conversion to light aromatics (Figure 7.21).

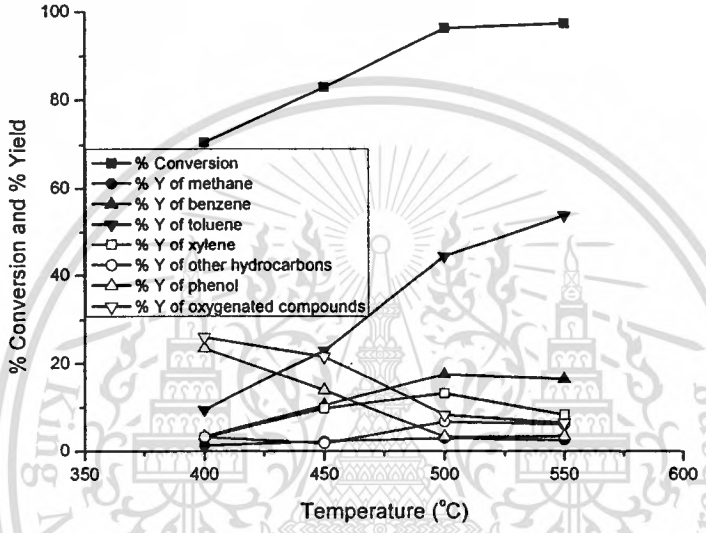

Figure 7.21 Effect of temperature.

Reaction conditions: Catalyst = 3[Ga]HBeta, W/F = 6.3 h, Reaction temperature = 400-550 °C, Carrier gas = H_2, Pressure = 1 atm.

When the reaction temperature is increased, the higher hydrogenolysis activity giving light aromatics can be obtained. This is consistent with an increase in H_2/D_2 exchange with temperature (Table 7.12). High reaction temperature can facilitate the decomposition/ hydrogenolysis of the surface pool intermediates, leaving more available active sites for consecutive *m*-cresol adsorption and activation.

It is also found that the yield of light aromatics is especially increased with temperature. This is due to the increase in rate of decomposition/hydrogenolysis which is favored at high reaction temperature. While a marked drop of the oxygenated compounds as a function of temperature indicates that these heavier compounds tend to be hydrogenolysed/decomposed into lighter hydrocarbons.

In addition, the zeolites support has shown a marked role in preserving the incorporated reduced Ga species (in benzaldehyde conversion (**section 7.3**)). Therefore, in this section, further evidence for the influence of the zeolite Beta support on the catalytic activity of the incorporated Ga catalyst is also provided.

Table 7.13 Effect of supporting material.

Type of catalyst	3[Ga]H Beta	3[Ga] Silica	3[Ga]H ZSM-5	H ZSM-5
% Conversion	82.78	4.49	40.32	41.69
% Yield				
Methane	2.25	0.78	0.34	1.50
Benzene	10.45	0.15	1.24	1.24
Toluene	23.06	0.32	8.90	2.00
Xylene	9.84	0.00	0.86	0.00
Other hydrocarbons (C2-C6)	1.83	0.00	0.90	1.50
Phenol	13.78	2.82	19.91	23.90
Oxygenated compounds	21.57	0.41	8.18	11.55
Total yield	82.78	4.49	40.32	41.69
% Selectivity				
Methane	2.72	17.45	0.84	3.60
Benzene	12.62	3.40	3.08	2.97
Toluene	27.85	7.19	22.06	4.80
Xylene	11.88	0.00	2.13	0.00
Other hydrocarbons (C2-C6)	2.22	0.00	2.23	3.60
Phenol	16.65	62.88	49.38	57.34
Oxygenated compounds	26.06	9.08	20.29	27.70
Total selectivity	100.00	100.00	100.00	100.00

Reaction conditions: Catalysts = 3[Ga]HBeta, 3[Ga]Silica, 3[Ga]HZSM-5, and HZSM-5, W/F = 6.3 h, Reaction temperature = 450 °C, Carrier gas = H_2, Pressure = 1 atm.

From Table 7.13, relatively lower *m*-cresol conversion and light aromatic (benzene, toluene, xylene) selectivity were obtained over 3[Ga]Silica, as compared to Ga supported zeolites. It is clear that the silica support possesses the lower acid strength, non-uniform pore size and no negatively framework charge. Consequently, such silica support cannot facilitate the formation of well-dispersed Ga species. Agglomeration into bulk Ga_2O_3 is expected in 3[Ga]Silica, as evidenced by H_2-TPR (Figure 7.19). Despite, the same Ga content is obtained over 3[Ga]Silica catalyst, toluene yield is exceedingly low (Table 7.13). This is presumably because Ga cationic species cannot be formed in this catalyst, due to the lack of high strength of Brønsted acid site and negative framework charge. However, it is suggested that the observed catalytic activity of 3[Ga]Silica is derived from the interaction of H_2 with gallia (Ga_2O_3) surfaces. It is reported that H_2 can dissociate over Ga_2O_3 surfaces either (i) as homolytic dissociative adsorption to form Ga-H species or (ii) as heterolytic dissociative adsorption to form Ga-OH and Ga-H [44-46]. However, there is relatively less available active Ga species in 3[Ga]Silica, as evidenced by a relatively low H_2 consumption at relatively high reduction temperature in TPR (Figure 7.19). Therefore, the lower activity can be obtained from this catalyst.

Regarding to the selectivity of oxygenated compounds, 3[Ga]Silica provides an exceedingly low selectivity of oxygenated compounds, as compared to 3[Ga]HBeta (Table 7.13). In addition, the relatively higher phenol and methane selectivity are obtained over 3[Ga]Silica catalyst. It is presumably explained that the surface pool intermediates cannot be readily promoted over 3[Ga]Silica catalyst due to the lack of high activity acid sites. Instead, only the direct hydrodealkylation of *m*-cresol can be promoted over 3[Ga]Silica leading to the high methane and phenol selectivity.

The 3[Ga]HZSM-5 possesses lower catalytic activity, as compared to 3[Ga]HBeta (Table 7.13). This is clearly explained by the restrict pore size of ZSM-5 zeolite that can inhibit diffusion of the *m*-cresol. Over 3[Ga]HZSM-5, the active Ga species is also expected, in a manner similar to that of 3[Ga]HBeta (Figure 7.19). However, diffusion of *m*-cresol into the pore size of 3[Ga]HZSM-5 cannot be readily facilitated due to the smaller pore size, as compared to the kinetic diameter of *m*-cresol. Therefore, the relatively lower toluene yield can be obtained over 3[Ga]HZSM-5, as compared to 3[Ga]HBeta.

The observed activity of 3[Ga]HZSM-5 zeolite may be derived from two possibilities; (i) pore mouth catalysis over Ga active sites or (ii) isomerization of *m*-cresol to less restrict isomer of cresol that can readily diffuse into pore and be activated over internal Ga active sites. If the first

possibility (i) is the case, one could be expected a rapid deactivation of 3[Ga]HZSM-5. This is because the surface pool intermediates at the pore mouth would readily lead to the pore blockage. However, only a slightly drop of catalytic activity can be obtained over 3[Ga]HZSM-5 (Figure 7.22).

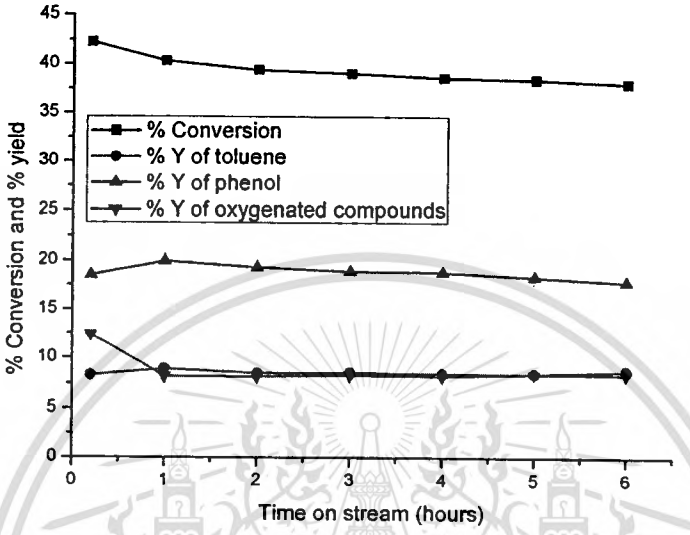

Figure 7.22 Conversion of *m*-cresol over 3[Ga]HZSM-5.
Reaction conditions: Catalyst = 3[Ga]HZSM-5, W/F = 6.3 h, Reaction temperature = 450 °C, Carrier gas = H_2, Pressure = 1 atm.

Hence, the possibility (i) is excluded. The catalytic activity of 3[Ga]HZSM-5 is presumably explained by the isomerization of *m*-cresol to *p*-cresol over the acid sites at the pore mouth [53-58], as observed over HZSM-5 (Table 7.13).

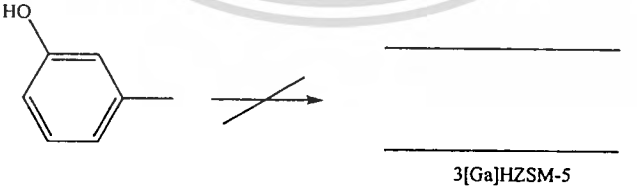

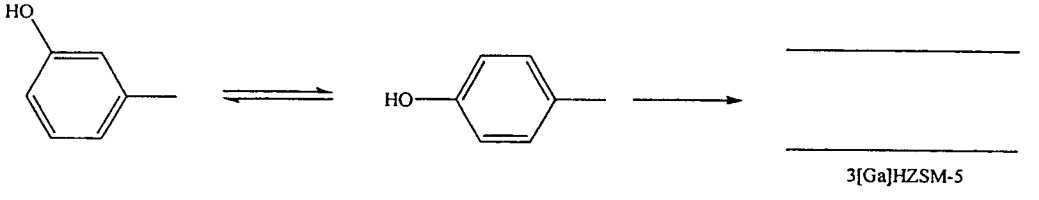

Such less restricted isomers can readily diffuse into the pore of ZSM-5 and be consecutively converted over the incorporated Ga active sites, as discussed earlier. However, the formation of hydrogenolysed products depend largely on the rate of isomerization and diffusion. Therefore, the lower catalytic activity was obtained over the restrict pore size of 3[Ga]HZSM-5, as compared to 3[Ga]HBeta. Accordingly, the control by the pore-opening is one of the key parameter for *m*-cresol conversion.

Although 3[Ga]HZSM-5 provides a lower selectivity of oxygenated compounds with higher selectivity of phenol, the directly hydrodealkylation of *m*-cresol to phenol shall not be the case for 3[Ga]HZSM-5. This is because methane is not proportionally produced over this catalyst (Table 7.13). The surface pool intermediates can be readily promoted over 3[Ga]HZSM-5 catalyst due to the high activity acid sites, as observed over HZSM-5 (Table 7.13). However, the formation of surface pool intermediates can be diminished into the restricted pore size of ZSM-5 leading to the lower substitution of phenolic compounds. Consequently, the stronger of C-O bond of aromatic-hydroxyl group can be obtained, as compared to the high substitution of phenolic compounds formed into Beta zeolite. This leads to the lower activity of hydrogenolysis to cleave Ar-OH. However, the 3[Ga]HZSM-5 catalyst can cleave the weaker of C-C bond of aromatic-alkyl group forming the phenol.

7.7 Conclusions

For *m*-cresol conversion over [Ga]HBeta, the product formation was proposed by the hydrogenolysis and decomposition of the surface pool intermediates produced by the condensation of *m*-cresol over the catalyst. The active Ga species are suggested to be the Ga species exist under H_2 system (GaH_2^+). The *m*-cresol firstly adsorb on the surface of the catalyst forming the high MW oxygenated intermediates. Such intermediates can be decomposed/ hydrogenolysed over Ga active sites forming light aromatic (benzene, toluene, xylene), light hydrocarbons (C2-C6 hydrocarbons), phenol and oxygenated compounds. Without H_2 gas, Brønsted sites still are active for surface pool intermediates decompostion giving mainly the oxygenated compounds. In addition, lack of hydrogenolysis activity leads to a rapid catalyst deactivation and a lower yield of light aromatic. On the other hand, the yield of light aromatics can be enhanced over [Ga]HBeta by the presence of H_2 stream, increasing in Ga content and reaction temperature. However, the light aromatics yield obtained over 3[Ga]Silica and 3[Ga]HZSM-5 catalyst is exceedingly low. This is because such silica support cannot facilitate

the formation of well-dispersed Ga species leading to less available active Ga species in 3[Ga]Silica. While the diffusion of *m*-cresol into the pore size of 3[Ga]HZSM-5 cannot be readily facilitated due to the restrict pore size with respected kinetic diameter of *m*-cresol.

References

[1] Biscardi J.A., Iglesia E. "Structure and Function of Metal Cations in Light Alkane Reactions Catalyzed by Modified H-ZSM5" **Catalysis Today**. vol. 31, 1996. pp. 207-231.

[2] Buckles G.J., Hutchings G.J. "Aromatisation of Propane over Ga/H-ZSM-5: Comments on the Activation of Propane" **Catalysis Today**. vol. 31, 1996. pp. 233-246.

[3] Hart V.I., Bryant M.B., Butler L.G., Wu X. and Dooley K.M. "Proton-poor, gallium- and intium-loaded zeolite dehydrogenation catalysts" **Catalysis Letters**. vol. 53, 1998. pp. 111-118.

[4] Kwak B.S., Sachtler W.M.H. and Haag W.O. "Catalytic Conversion of Propane to Aromatics: Effect of Adding Ga and/or Pt ro HZSM-5" **Journal of Catalysis**. vol. 149, 1994. pp. 465-473.

[5] Kwak B.S., Sachtler W.M.H. "Effect of Ga/Proton Balance in Ga/HZSM-5 Catalysts on C3 Conversion to Aromatics" **Journal of Catalysis**. vol. 145, 1994. pp. 456-463.

[6] Montes A., Giannetto G. "A New Way to Obtain Acid or Bifunctional Catalysts V. Considerations on Bifunctionality of the Propane Aromatization Reaction over [Ga,Al]-ZSM-5 Catalysts" **Applied Catalysis A: General**. vol. 197, 2000. pp. 31-39.

[7] Meriaudeau P., Naccache C. "Further Evidence on the Change of Acid Properties of H-ZSM-5 by Ga and Pt" **Journal of Catalysis**. vol. 157, 1995. pp. 283-288.

[8] Meriaudeau P., Sapaly G., Wicker G. and Naccache C. "Revisiting Ga_2O_3/H-ZSM-5 Propane Aromatization Catalysts" **Catalysis Letters**. vol. 27, 1994. pp. 143-148.

[9] Price G.L., Kanazirev V. "Ga_2O_3/HZSM-5 Propane Aromatization Catalysts: Formation of Active Centers via Solid-State Reaction" **Journal of Catalysis**. vol. 126, 1990. pp. 267-278.

[10] Kanazirev V., Price G.L. and Dooley K.M. "Preparation of Ga-Doped Zeolite Catalysts via Hydrogen Induced Solid State Interaction Between Ga_2O_3 and HZSM-5 Zeolite" **Studies in Surface Science and Catalysis**. vol. 69, 1991. pp. 277-285.

[11] Kazansky V.B., Subbotina I.R., van Santen R.A. and Hensen E.J.M. "DRIFTS Study of the Chemical State of Modifying Gallium Ions in Reduced Ga/ZSM-5 Prepared by Impregnation I. Observation of Gallium Hydrides and Application of CO Adsorption as a Molecular Probe for Reduced Gallium Ions" **Journal of Catalysis**. vol. 227, 2004. pp. 263-269.

[12] Ragauskas A.J., Williams C.K., Davison B.H., Britovsek G., Cairney J., Eckert A., Frederick Jr.W.J., Hallet J.P., Leak D.J., Liotta C.H., Mielenz J.R., Murphy R., Templer R. and Tschaplinski T. "The Path Forward for Biofuels and Biomaterias" **Science**. vol. 311, 2006. pp. 484-489.

[13] Koonin S.E. "Getting Serious About Bifuels" **Science**. vol. 311, 2006. pp. 435.

[14] Huber G.W., Iborra S. and Corma A. "Synthesis of Transportation Fuels from Biomass: Chemistry, Catalysts, and Engineering" **Chemical Reviews**. vol. 106, 2006. pp. 4044-4098.

[15] Corma A., Iborra S. and Velty A. "Chemical Routes for the Transformation of Biomass into Chemicals" **Chemical Reviews**. vol. 107, 2007. pp. 2411-2502.

[16] Huber G.W., Corma A. "Synergies Between Bio- and Oil Refineries for the Production of Fuels from Biomass" **Angewandte Chemie International Edition**. vol. 46, 2007. pp. 7184-7201.

[17] Lynd L.R., Cushman J.H., Nichols R.J. and Wyman C.E. "Fuel Ethanol from Cellulosic Biomass" **Science**. vol. 251, 1991. pp. 1318-1323.

[18] Wyman C.E. "Alternative Fuels from Biomass and Their Impaction on Carbon Dioxide Accumulation" **Applied Biochemistry and Biotechnology**. vol. 45-46, 1994. pp. 897-915.

[19] Mohan D., Pittman Jr. C.U. and Steele P.H. "Pyrolysis of Wood/Biomass for Bio-Oil: A Critical Review" **Energy Fuels**. vol. 20, 2006. pp. 848-889.

[20] Czernik S., Bridgwater A.V. "Overview of Applications of Biomass Fast Pyrolysis Oil" **Energy Fuels**. vol. 18, 2004. pp. 590-598.

[21] Furimsky E. "Catalytic Hydrodeoxygenation" **Applied Catalysis A: General**. vol. 199, 2000. pp. 147-190.

[22] Sooknoi T., Danuthai T., Lobban L.L., Mallinson R.G. and Resascon D.E. "Deoxygenation of Methylesters Over CsNaX" **Journal of Catalysis**. vol. 258, 2008. pp. 199-209.

[23] Arvela P.M., Kubickova I., Snare M., Eranen K. and Murzin D.Y. "Catalytic Deoxygenation of Fatty Acids and Their Derivatives" **Energy & Fuels**. vol. 21, 2007. pp. 30-41.

[24] Snare M., Kubickova I., Arvela P.M., Chichova D., Eranen K. and Murzin D.Y. "Catalytic Deoxygenation of Unsaturated Renewable Feedstocks for Production of Diesel Fuel Hydrocarbons" **Fuel**. vol.87, 2008. pp. 933-945.

[25] Furimsky E. "Catalytic Hydrodeoxygenation" **Applied Catalysis A: General.** vol. 199, 2000. pp. 147-190.

[26] Lukyanov D.B., Vazhnova T. "Aromatization Activity of Gallium Containing MFI and TON Zeolite Catalysts in n-Butane Conversion: Effects of Gallium and Reaction Conditions" **Applied Catalysis A: General.** vol. 316, 2007. pp. 61-67.

[27] Choudhary V.R., Mantri K. and Sivadinarayana C. "Influence of Zeolite Factors Affecting Zeolitic Acidity on the Propane Aromatization Activity and Selectivity of Ga/H-ZSM-5" **Microporous and Mesoporous Materials.** vol. 37, 2000. pp. 1-8.

[28] Gricus Kofke T. J., Gorte R.J. and Kokotailo G.T. "Stoichiometric Adsorption Complexes in H-ZSM-5, H-ZSM-12, and H-Mordenite Zeolites" **Journal of Catalysis.** vol. 115, 1989. pp. 265-272.

[29] Nowak I., Quartararo J., Derouane E.G. and Ve'drine J.C., "Effect of H_2-O_2 Pre-treatments on the State of Gallium in Ga/H-ZSM-5 Propane Aromatisation Catalysts" **Applied Catalysis A: General.** vol. 251, 2003. pp. 107-120.

[30] Southward B.W.L., Nash R.J. and O'Connor C.T., "*In-situ* Drifts Studies of the Activation of Ga/H-ZSM-5 Catalysts for the Aromatization of Propane" **Applied Catalysis A: General.** vol. 135, 1996. pp. 177-191.

[31] Brabec L., Jeschke M., Klik R., Novakova J., Kubelkova L., Freude D., Bosacek V. and Meusinger J., "Various Types of Ga in MFI Metallosilicates: Characterization and Catalytic Activity" **Applied Catalysis A: General.** vol. 167, 1998. pp. 309-320.

[32] Dooley K.M., Chang C. and Price G.L., "Effect of Pretreatments on State of Gallium and Aromatization Activity of Gallium/ZSM-5 Catalysts" **Applied Catalysis A: General.** vol. 84, 1992. pp. 17-30.

[33] Meitzner G.D., Iglesia E., Baumgartner J.E. and Huang E.S., "The Chemical State of Gallium in Working Alkane Dehydrocyclodimerization Catalysis. *In situ* Gallium K-edge X-ray Absorption Spectroscopy" **Journal of Catalysis.** vol. 140, 1993. pp. 209-225.

[34] Meriaudeau P., Naccache C., "H-ZSM-5 Supported Ga_2O_3 Dehydrocyclisation Catalysts Infrared Spectroscopic Evidence of Gallium Oxide Surface Mobility" **Applied Catalysis.** vol. 73, 1991. pp. L13-L18.

[35] Gricus Kofke T. J., Gorte R.J. and Kokotailo G.T. "Determination of framework concentrations of gallium in [Ga]-ZSM-5" **Applied Catalysis.** vol. 54, 1989. pp. 177-188.

[36] Kazansky V.B., Subbotina I.R., van Santen R.A. and Hensen E.J.M. "DRIFTS Study of the Nature and Chemical Reactivity of Gallium Ions in Ga/ZSM-5: II. Oxidation of Reduced Ga Species in ZSM-5 by Nitrous Oxide or Water" **Journal of Catalysis**. vol. 233, 2005. pp. 351-358.

[37] Ausavasukhi A., Sooknoi T., "Additional Brønsted Acid Sites in [Ga]HZSM-5 Formed by the Presence of Water" **Applied Catalysis A: General**. vol. 361, 2009. pp. 93-98.

[38] Sanchez M.G., Magusin P.C.M.M., Hensen E.J.M. and Thune P.C., "Characterization of Ga/HZSM-5 and Ga/HMOR Synthesized by Chemical Vapor Deposition of Trimethylgallium" **Journal of Catalysis**. vol. 219, 2003. pp. 352-361.

[39] Aboul-Gheit A.K., "Hydroconversion of *meta*-Xylene on Catalysts Containing Pt, Re and PtRe on H-Mordenite" **Applied Catalysis A: General**. vol. 105, 1993. pp. L127-L133.

[40] Tsai T.C., Wang I., Huang C.K. and Liu S.D., "Study on Ethylbenzene and Xylene Conversion over Modified ZSM-5" **Applied Catalysis A: General**. vol. 321, 2007. pp. 125-134.

[41] Pokrovski G.S., Schott J., Hazemann J.L., Farges F. and Pokrovsky O.S., "An X-ray Absorption Fine Structure and Nuclear Magnetic Resonance Spectroscopy Study of Gallium-Silica Complexes in Aqueous Solution" **Geochimica et Cosmochimica Acta**. vol. 66, 2002. pp. 4203-4220.

[42] Shpiro E.S., Shevchenko D.P., Tkachenko O.P. and Dmitriev R.V., "Platinum Promotion Effects in Pt/Ga Zeolite Catalysts of Lower Alkane Aromatization. I. Ga and Pt Electronic States, Dispersion and Distribution in Zeolite Crystals in Dependence of Preparation Techniques. Dynamic Effects Caused by Reaction Mixture" **Applied Catalysis A: General**. vol. 107, 1994. pp. 147-164.

[43] Gonzales N.O., Chakraborty A.K. and Bell A.T. "A Density Functional Theory Study of Hydrogen Recombination and Hydrogen-Deuterium Exchange on Ga/H-ZSM-5" **Topics in Catalysis**. vol. 9, 1999. pp. 207-213.

[44] Collins S.E., Baltanas M.A., Fierro J.L.G. and Bonivardi A.L., "Gallium-Hydrogen Bond Formation on Gallium and Gallium-Palladium Silica-Supported Catalysts" **Journal of Catalysis**. vol. 211, 2002. pp. 252-264.

[45] Collins S.E., Baltanas M.A. and Bonivardi A.L., "Hydrogen Chemisorptions on Gallium Oxide Polymorphs" **Langmuir**. vol. 21, 2005. pp. 962-970.

[46] Jochum W., Penner S., Fottinger K., Kramer R., Rupprechter G. and Klotzer B., "Hydrogen on Polycrystalline β-Ga_2O_3: Surface Chemisorptions, Defect Formation, and Reactivity" **Journal of Catalysis**. vol. 256, 2008. pp. 268-277.

[47] Scholze B., Hanser C. and Meier D., "Characterization of the Water-Insoluble Fraction from Fast Pyrolysis Liquids (Pyrolytic Lignin): Part II. GPC, Carbonyl Groups, and ^{13}C-NMR" **Journal of Analytical and Applied Pyrolysis**. vol. 58, 2001. pp. 387-400.

[48] Scholze B., Meier D., "Characterization of the Water-Insoluble Fraction from Pyrolysis Oil (Pyrolytic Lignin). Part I. PY-GC/MS, FTIR and Functional Groups" **Journal of Analytical and Applied Pyrolysis**. vol. 60, 2001. pp. 41-54.

[49] Dooley K.M., Guidry T.F. and Price G.L., "Control of Intrazeolitic Gallium Cation Content and Its Effects on C_2 Dehydrogenation in Ga-MFI Catalysts" **Journal of Catalysis**. vol. 157, 1995. pp. 66-75.

[50] Dooley K.M., Price G.L. and Hart V.I., "Gallium-Loaded Zeolites for Light Paraffin Aromatization: Evidence for Exchanged Gallium Cation Active Centers" **Catalysis Today**. vol. 31, 1996. pp. 305-315.

[51] Meshram N.R., Hegde S.G., Kulkarni S.B. and Ratnasamy P., "Disproportionation of Toluene over HZSM-5 Zeolites" **Applied Catalysis**. vol. 8, 1983. pp. 359-367.

[52] Mavrodinova V., Popova M., "Selective *p*-Xylene upon Toluene Disproportionation over MCM-22 and ZSM-5 Zeolites Modified with Indium" **Catalysis Communications**. vol. 6, 2005. pp. 247-252.

[53] Imbert F.E., Gnep N. and Guisnet M., "Cresol Isomerization on HZSM-5" **Journal of Catalysis**. vol. 172, 1997. pp. 307-313.

[54] Imbert F.E., Guisnet M. and Gnep S., "Comparison of Cresol Transformation on USHY and HZSM-5" **Journal of Catalysis**. vol. 195, 2000. pp. 279-286.

[55] Imbert F.E., Gnep N.S., Ayrault P. and Guisnet M., "Effects of Commercial HFAU Structural Parameters over *m*-Cresol Transformation" **Applied Catalysis A: General**. vol. 215, 2001. pp. 225-234.

[56] Tsai T.C., Wang I., Huang C.K. and Liu S.D., "Study on Ethylbenzene and Xylene Conversion over Modified ZSM-5" **Applied Catalysis A: General**. vol. 321, 2007. pp. 125-134.

[57] Kunieda T., Kim J.H. and Niwa M., "Source of Selectivity of *p*-Xylene Formation in the Toluene Disproportionation over HZSM-5 Zeolites" **Journal of Catalysis.** vol. 188, 1999. pp. 431-433.

[58] Llopis F.J., Sastre G. and Corma A., "Xylene Isomerization and Aromatic Alkylation in Zeolites NU-87, SSZ-33, Beta, and ZSM-5: Molecular Dynamics and Catalytic Studies" **Journal of Catalysis.** vol. 227, 2004. pp. 227-241.

Chapter 8

Conclusions and Suggestions

8.1 Conclusions

This thesis has studied the alteration of various metal species of Ag- and Ga-incorporated zeolite during the preparation and reaction which can readily influence with their catalytic activity and selectivity. The Ag- and Ga-incorporated zeolites are prepared by ion exchange and impregnation method on ZSM-5 and Beta zeolites. These modified zeolites are treated with hydrogen or steam at various temperatures in order to investigate the alteration of metal species.

^{1}H MAS NMR, XRD, TPR, TPHE (temperature-programmed hydrogen evolution) techniques, and catalytic characterization by ethanol conversion were employed to investigate the reducibility and reversible interconversion behavior of Ag species in Ag-modified HZSM-5. In AgHZSM-5, the Si/Al ratio of the host zeolite strongly influences the reducibility of the Ag species and the types of the reduced Ag species formed. It was found that charge-balancing Ag cations in AgHZSM-5 (Si/Al ~ 11) and AgHZSM-5 (Si/Al ~ 28) can be readily reduced to ''cationic Ag clusters'' at ~ 220 °C, while a higher temperature is required for the Ag species in AgHZSM-5(28) to be reduced to ''metallic Ag clusters'', as compared with that for AgHZSM-5(11). Both cationic and metallic Ag clusters formed can be reversibly conversed into charge-balancing Ag cations by the reaction with neighboring Brønsted acid sites (reversible interconversion). The metallic Ag clusters were found to be more resistant to the reversible interconversion, as compared to the cationic Ag clusters. It is presumed that the larger the metal clusters, the less the reactivity with the neighboring Brønsted acid sites. Metallic Ag clusters are readily formed in a low silica sample, AgHZSM-5(11). This is due to the closely proximate sites that allow the reduced Ag species to agglomerate into larger and more stable Ag metal clusters. For AgHZSM-5(28), a higher silica sample, most of the reduced Ag species, formed at 425 °C, are cationic Ag clusters with small amounts of the metallic ones. This may well be due to a better interaction of the softer cationic Ag clusters with the soft framework of high silica zeolites. Under hydrogen stream, the reduced Ag species could be preserved and ''silver hydride'' species were observed by NMR, together with the active Brønsted acid sites. This phenomenon is suggested to play a decisive role on the catalytic activity of AgHZSM-5 towards BTX formation in the presence/absence of hydrogen.

Unlike AgHZSM-5, the incorporation of $Ga(NO_3)_3$ into HZSM-5 zeolite results in additional Brønsted acid sites evidenced by ^1H MAS NMR and FTIR. Such acid sites are proposed to arise from the incorporated Ga extra framework (GaO(OH)) and the insertion of such species into the zeolite framework (GaOHSi) by a reaction with defect hydroxyls. These additional Brønsted acid sites are particularly formed under steaming and may well be responsible for the change in the catalytic behaviour of [Ga]HZSM-5 when water is present in the reaction stream. In the reaction using ethylene as a feed, higher hydrocarbons, namely aromatics, can be produced over ''reduced Ga species''. In contrast, the conversion of ethanol over [Ga]HZSM-5 showed an increased activity in a manner similar to that over a typical HZSM-5, but with higher acidity. The formation of the additional acid sites is readily reversible at high temperature (> 450 °C) and hence the steam treatment can be used for re-dispersing the incorporated Ga species.

In the presence of hydrogen, various gallium species (Ga_2O_3, GaO^+, Ga^+, and GaH_2^+) in [Ga]HZSM-5 catalyst were studied for ethane dehydrogenation by a pulsed reactor and H_2-TPR. It was found that the activity of Ga-modified HZSM-5 depends largely on the Ga species which can be regulated by the H_2 treatment. Among the various Ga species, the GaH_2^+, that is a predominant species under the H_2 system, displays the highest dehydrogenation activity (~ 55 % conversion). However, GaH_2^+ can readily decompose to Ga^+ under a non-reducing gas stream, leading to a lower ethane conversion (~ 30 % conversion). While the Ga oxide species, which are mostly retained as isolated Ga_2O_3 and exchangeable GaO^+, provide low dehydrogenation activity (~ 25 % conversion), particularly for the bulkier Ga_2O_3 cluster. In addition, the hydrogen and steam treatment can facilitate the dispersion of bulk Ga_2O_3 into an exchangeable Ga^+ and GaO^+, respectively. With an increase in the Si/Al ratio of the host zeolite, the activity is decreased. This is because the number of Brønsted acid sites play an important role in determining the number of Ga species.

From above observation, water interacts strongly with Ga species and readily modifies its chemical natures. It is expected that oxygenated compounds would also interact well with Ga-incorporated zeolite which may lead to its application of deoxygenating catalyst. Hence, deoxygenation of benzaldehyde was investigated over Ga-modified ZSM-5 catalysts, as a model for bio-oil upgrading. It was found that [Ga]HZSM-5 catalyst, possessing Brønsted acid sites, can promote benzaldehyde decarbonylation resulting in benzene. While the Ga cationic species generated by H_2 reduction can promote hydrogenation/hydrogenolysis of benzaldehyde to

toluene. No toluene yield can be obtained over [Ga]HZSM-5 under He stream due to the lack of hydrogenation/hydrogenolysis activity. The presence of water as co-feeding provides the additional acid sites that are proposed to arise from the reaction of the incorporated Ga extra-framework with chemisorbed water (GaO(OH)) and/or defect hydroxyls of the zeolite framework (GaOHSi). These Brønsted acid sites lead to relatively higher benzene yield, as compared to the reaction without water. In contrast, the decrease in toluene yield can be observed due to the deterioration of reduced Ga cationic species.

In addition to benzaldehyde, the deoxygenation of *m*-cresol over Ga-modified HBeta catalysts provide further evidence for the role of Ga species and shape selectivity. In this reaction, formation of the various products can be explained by a "surface pool" of condensation products. The *m*-cresol firstly adsorb on the surface of the catalyst forming the high MW oxygenated intermediates. Such intermediates can be decomposed/hydrogenolysed over Ga active sites providing light aromatics (benzene, toluene, xylene), light hydrocarbons (C2-C6 hydrocarbons), phenol and oxygenated compounds. Without H_2 gas, Brønsted sites are still active for surface pool intermediates decompostion giving mainly the oxygenated compounds. However, lack of hydrogenolysis activity leads to a rapid catalyst deactivation and a lower yield of light aromatic. On the other hand, the yield of light aromatics can be enhanced by the presence of H_2 stream, increasing in Ga content and reaction temperature. The light aromatics yield obtained over 3[Ga]Silica catalyst is exceedingly low. This is because such silica support cannot facilitate the formation of well-dispersed Ga species leading to less available active Ga species in 3[Ga]Silica. While the low yield of light aromatics obtained over 3[Ga]HZSM-5 was described by shape selectivity due to the restrict pore size, with respect to the kinetic diameter of *m*-cresol.

Finally, the state of the art of various metal species in zeolite leading to an efficiency for heterogeneous catalysis is now well advanced. The various metal species can occasionally be obtained from incorporated counter-ions or metal oxides that located within the intra-framework zeolite cavities during the post-synthesis step. Such metal species can be achieved either by a control of treatment (steaming or reduction) or by a reaction condition with the feed stream. The microstructure of metal surface evolved during the treatment and/or reaction is due to changes in the local atomic arrangement at the surface (dispersion and/or agglomeration of cluster precursors). Such metal species may well be stabilized by appropriate neighboring-metal (i.e. Ag_n^+, Ag_n), molecular ligand (i.e. Ag_n-H, GaH_2^+, GaO(OH), GaO^+) and/or zeolite framework with

different Si/Al ratio and topology. Such different metal species can affect adsorption and activity of reactants and also catalytic intermediates and products selectivity.

8.2 Suggestions

1. The Si/Al ratio of the host zeolite strongly influences the reducibility of the Ag species and the types of the reduced Ag species formed. The enhancement of ethanol conversion only occurs over the Ag-modified zeolite in which Brønsted acid sites can be recovered bearing metallic Ag cluster after H_2 reduction. The Si/Al ratio of the zeolites would play a marked role in hosting, retaining and even altering the incorporated Ag species. A specified catalysis of Ag-modified zeolites for the various types of reactions such as photo-dimerization of alkane, photocatalytic degradation of malathion, methane activation with ethylene to form propylene and selective catalytic reduction of NO by alkane in the presence of hydrogen should be studied on various Ag species.
2. The additional Brønsted acid sites evidenced by ^{1}H MAS NMR and FTIR was only observed over zeolite possessed Si/Al ~ 28. One could expect that the Si/Al ratio of the zeolites would play a marked role in insertion and retaining the incorporated Ga species. Therefore, the influence of the zeolite Si/Al ratio on the additional of Brønsted acid sites when the incorporation of Ga species should be studied.
3. Despite the pulsed study has attempted to determine the catalytic activity of various Ga species based on the ethane dehydrogenation, there is a lack of *in situ* studies of the Ga-modified HZSM-5 system at the high temperature range. This system can exhibit its local catalytic activity and a true active species may well be revealed. Thus, an *in situ* investigation of the nature of gallium species in the reduced Ga-modified HZSM-5 zeolite obtained at different temperatures should be studied using XPS and EXAFS techniques.
4. The pyrolysis oil is a viscous liquid with a high oxygen content. However, pyrolysis oil as such is not directly suitable as feed for this modified zeolite catalysis. This is because the molecular shape dimension of oil component cannot enter to the zeolite micropore. An upgrading technology should be studied to improve the molecular shape dimension to extend the application range such as fluid catalytic cracking (FCC).

Appendix A

CALCULATIONS

A1. Calculation of theoretical acidity

From the elemental analysis, the theoretical acidity of zeolite is calculated as follows:

The general unit cell of HZSM-5 is $H_nAl_nSi_{96-n}O_{192}$.

In the case of HZSM-5 (Si/Al = 45),

Thus; $Si + Al = 96$ Eq. (1)

$Si/Al = 45$ Eq. (2)

From Eq. (1) and Eq. (2)

$Si = 93.91$

$Al = 2.09$

From the above, the unit cell of HZSM-5 (Si/Al = 45) is therefore $H_{2.09}Al_{2.09}Si_{93.91}O_{192}$. The weight of unit cell of HZSM-5 (U) is

$U = 2.09(1) + 2.09(26.98) + 93.91(28.09) + 192(15.99)$

$U = 5767.86$ g

The theoretical acidity ($[H^+]$) of HZSM-5 is

$[H^+] = 2.09/5767.86$

$[H^+] = 0.362$ mmol/g

The general unit cell of HBeta is $H_nAl_nSi_{64-n}O_{128}$.

In the case of HBeta (Si/Al = 11),

Thus; $Si + Al = 64$ Eq. (1)

$Si/Al = 11$ Eq. (2)

From Eq. (1) and Eq. (2)

Si = 58.67

Al = 5.33

From the above, the unit cell of HBeta (Si/Al = 11) is therefore $H_{5.33}Al_{5.33}Si_{58.67}O_{128}$. The weight of unit cell of HBeta (U) is

U = 5.33(1) + 5.33(26.98) + 58.67(28.09) + 128(15.99)

U = 3844.86 g

The theoretical acidity ($[H^+]$) of HBeta is

$[H^+]$ = 5.33/3844.86

$[H^+]$ = 1.387 mmol/g

A2. Calculation of % Ag ion-exchanged

In the case of 2.80 wt% of AgHZSM-5 (Si/Al = 11),

Thus; Si + Al = 96 Eq. (1)

Si/Al = 11 Eq. (2)

From Eq. (1) and Eq. (2)

Si = 88.00

Al = 8.00

From the above calculation, the unit cell of AgHZSM-5 (Si/Al = 11) is therefore $Ag_nH_{8.00-n}Al_{8.00}Si_{88.00}O_{192}$. The degree of silver ion-exchange in unit cell of 2.80 wt% of AgHZSM-5 (Si/Al = 11) is calculated as follow:

The weight of unit cell of 2.80 wt% of AgHZSM-5 (Si/Al = 11) (U) is

$$U = n(107.87) + (8-n)(1) + 8(26.98) + 88(28.09) + 128(15.99)$$

$$U = 107.87n + (8-n) + 215.84 + 2471.92 + 2046.72 \quad \text{Eq. (1)}$$

The silver content loaded zeolite sample is

$$107.87n/U = 2.80/100 \quad \text{Eq. (2)}$$

From the Eq. (1) and Eq. (2),

n = 1.27 and hence the unit cell of 2.80 wt% of AgHZSM-5 (Si/Al =11) is $Ag_{1.27}H_{6.73}Al_{8.00}Si_{88.00}O_{192}$. The ion exchange of silver into the exchangeable site of the framework is estimated to be 15.83 %.

Similar calculation is used in the case of AgHZSM-5 with different Si/Al ratio and different Ag loading.

A3. Calculation of catalytic parameter

$$W/F = \frac{\text{Weight of catalyst (g)}}{\text{Mole of liquid reactant feed (mol/h)}}$$

In the reaction using 0.01 mol/h of ethanol (or benzaldehyde or *m*-cresol) as feed and using 0.0675 grams of catalyst, the W/F is calculated as follows:

$$W/F = [0.0675\ (g)/0.01\ (mol/h)]$$

$$= 6.75\ g \cdot h/mol$$

In a similar manner; W/F of catalyst with different catalyst weight and different feed rate are calculated.

A4. Calculation of % carbon yield from gas chromatography

From the chromatogram, the peak of samples were identified using of reference standard for comparison. The peak area of hydrocarbon (or oxygenated compounds) which possesses the equal number of carbon was summerized. The summation of the peak area obtained from chromatogram of a mixture hydrocarbon product is shown in Table A1.

Table A1 the summation of the peak area for hydrocarbon products.

Number of carbon	Summation of the peak area
C_1	-
C_2	343.12
C_3	888.76
C_4	999.21
C_5	21.97
C_6	53.83
C_7	128.21
C_8	0.00
B	912.00
T	28.18
X	1970.74
C_9	1959.13
C_{10}	0.00
Total	7305.18

In the normalization method, the areas of all eluted peak were compute after correcting these areas for differences in the detector response to different compound types. After correcting areas, the concentration of the analyte was found from the ratio of its area to the total area of all peaks.

Calculate the percent carbon yield of each component in sample as follows:

$$\text{Corrected \% carbon yield in each product} = \frac{\text{Summation of peak area of } C_n \text{ x } 100}{\text{Total area x RF}}$$

Where RF is the response factor of the analyte sample.

For example;

$$\text{Corrected \% carbon yield of } C_2 = \frac{343.12 \text{ x } 100}{7305.18 \text{ x } 1} = 4.6969$$

The percent carbon yield of each sample which is obtained from above calculation is shown is Table A2.

Table A2 % Carbon yield derived by normalization method.

Number of carbon	% carbon yield of sample
C_1	0.0000
C_2	4.6969
C_3	12.1662
C_4	13.6782
C_5	0.3008
C_6	0.7369
C_7	0.0000
C_8	0.3858
B	1.7551
T	12.4843
X	26.9774
C_9	26.8184
C_{10}	0.0000
Total	100

Appendix B

COLUMN PARAMETERS AND GAS CHROMATOGRAPH CONDITIONS

B1. Column parameter and gas chromatograph condition for ethanol conversion

Column parameter

Type	:	VA-1
Length (meters)	:	15
I.D. (mm)	:	0.53
Film thickness (μm)	:	1.5
Carrier gas	:	Helium
Linear velocity (cm/sec)	:	20
Injector temperature (°C)	:	220
FID detector temperature (°C)	:	220

Gas chromatograph condition

Step	Oven temperature (°C)	Heating rate (°C/min)	Hold time (min)
1	35	-	5.0
2	200	10	-
3	200	-	30.0
		Total time	51.5

B2. Column parameter and gas chromatograph condition for ethane conversion

Column parameter

Type	:	HP-Plot
Length (meters)	:	30
I.D. (mm)	:	0.53
Film thickness (μm)	:	15
Carrier gas	:	Helium
Linear velocity (cm/sec)	:	20
Injector temperature (°C)	:	220
FID detector temperature (°C)	:	220

Gas chromatograph condition

Step	Oven temperature (°C)	Heating rate (°C/min)	Hold time (min)
1	40	-	10.0
		Total time	10.0

B3. Column parameter and gas chromatograph condition for benzaldehyde and *m*-cresol conversion

Column parameter

Type	:	HP-5
Length (meters)	:	30
I.D. (mm)	:	0.25
Film thickness (μm)	:	0.88
Carrier gas	:	Helium
Linear velocity (cm/sec)	:	20
Injector temperature (°C)	:	220
FID detector temperature (°C)	:	220

Gas chromatograph condition

Step	Oven temperature (°C)	Heating rate (°C/min)	Hold time (min)
1	35	-	5.0
2	200	10	-
3	200	-	30.0
		Total time	51.5

AUTHOR BIOGRAPHY

Mr. Artit Ausavasukhi was born on August 8, 1976 in Bangkok. He received a Bachelor Degree in Industrial Chemistry from the Department of Chemistry, Faculty of Science, King Mongkut's Institute of Technology Ladkrabang in 1998 and a Master Degree in Petrochemicals and Hydrocarbon Chemistry from the same institute in 2001. His master's thesis was entitled "The Production of Gasoline and Aromatics from Ethanol".

From 2002 to 2004, he worked at Department of Chemistry, Faculty of Science and Technology, Valaya Alongkorn Rajabhat University, Pathumthanee, as a lecturer. While working at the university, he did research on catalytic oxidation of organic compounds using metal-loaded zeolite.

He has been a graduate student of the program of Applied Chemistry since 2004. While studying, he worked for Rayong Olefins Company Limited, as an assistant researcher. Moreover, he worked at the Phranakhon Rajabhat University, as a lecturer. In 2006, he got a fund from the Thailand Research Funds (TRF) through the Royal Golden Jubilee Ph.D. Program.